Sinusoids with linear frequency shift in time series – precise characterisation and removal

Dissertation

zur Erlangung des Grades eines
Doktors der Naturwissenschaften

der Fakultät Physik
der Technischen Universität Dortmund

vorgelegt von

Felix Gorschlüter

September, 2014

Erster Gutachter	PD Dr. Jürgen Altmann
Zweiter Gutachter	Prof. Dr. Thomas Weis

Kontakt zum Autor felix.gorschlueter@tu-dortmund.de

This work is dedicated to Jan Feldhoff, my long-time friend and physicist colleague who tragically died by poisoning in a fire accident at the age of 32.

Abstract

Cases occur in which the signal, one is interested in, is superposed with periodic noise. This work is motivated by the perspective of supporting the Comprehensive Nuclear-Test-Ban Treaty Organization. During on-site inspections, seismic signals can be measured to detect aftershocks of an underground nuclear explosion in order to locate the hypocentre precisely and allow for instance the taking of samples. Aftershocks are weak and can be masked by signals produced on/above the surface, in particular, periodic ones from engines. Aftershock signals are profoundly non-periodic, whereas many anthropogenic signals are mostly periodic. Therefore, the removal of periodic disturbances will increase the signal-to-noise ratio. We are developing algorithms capable of reducing such disturbances. The Fourier transform can distinguish between period and non-periodic signals. Periodic signals can be represented by sums of monofrequent sinusoids – their characterisation and removal has been proven to work earlier. This work describes and evaluates a procedure which includes linearly in time changing frequencies, processes a time interval of arbitrary length and provides the noise-reduced data.

At first, an analytic function is derived for the Hann-windowed discrete spectrum of a sine with linear frequency shift (LFS), defined by the four parameters amplitude, initial phase, initial frequency and frequency-change rate. This function is fitted to the complex values of the magnitude peaks in the spectrum. If successful, the peaks are removed successively by subtraction of the spectrum of an LFS sine with the corresponding parameters.

The curve progression of (LFS) sines in the spectral domain is illustrated and the influence of the parameters on the complex spectrum is investigated. The revealed dependencies can be reverted in the sense that characteristics of the curve progression are extracted and utilised to estimate the start parameters for the following fitting.

The success of the characterisation and removal is tested with synthetic (LFS) sines, sometimes superposed on pulse signals or Gaussian white noise. In order to quantitatively evaluate the fit results, three measures are introduced: the sum of squared deviations between spectral peak and (LFS) sine, the root-mean-square value of the difference between reconstructed and original signal in the time domain, and the absolute value of a four-component vector containing the deviations between input and fit parameters. However the latter two require the knowledge of the input values, which are not available if processing real data. Combinations of parameters and different levels of Gaussian white

noise are used to define the receiver operating characteristic in the form of thresholds for the first measure.

Then the algorithm is applied to real data. The principal procedure is demonstrated by adding pure synthetic LFS sines to a real seismic event of a coal mine, the resulting peaks in the spectrum are precisely fitted and subtracted resulting in minimal changes between original data and reconstructed ones even if the LFS amplitude is five orders of magnitude stronger than the event.

In a next step synthetic sounds played via a speaker and measured seismically and acoustically are investigated. Fits on narrow peaks are very successful both for acoustic and seismic measurements and the processed spectrum is reduced down to the background noise level. For the monofrequent case the peak magnitude is reduced by at least three orders of magnitude but the reduction factor might be principally unlimited, as indicated for synthetic superpositions. For sines with a strong LFS, the reduction is limited to 1.5 orders of spectral magnitude, probably caused by slight frequency dependencies in the transfer function between played signal and its measurement.

For real signals, all peaks which have been fitted successfully are reduced to the level of the background, but typically several smaller and sometimes even stronger peaks remain. On the basis of the acoustic signal of a propeller aircraft, the limitation of the described algorithm regarding peaks at the very margins of a spectrum is demonstrated. The acoustic data of a main battle tank are processed successfully in the sense of subtracting most of the strongest peaks. The non-periodic contributions remain in the signal – fitting to the goal of the work. The acoustic spectra of a helicopter signal recorded at close distance seem to contain peaks different from the ones of pure sinusoids, probably caused by second peaks at slightly differing frequencies. If a peak shape does not match the one of an (LFS) sine, the fit result is not very convincing; thus, strong (pseudo-)periodic components remain in the signal.

In sum, it is possible to reduce the periodic content of time-series data significantly. However, the signals of the vehicles analysed contain non-periodic components which remain in the signal. The achieved reduction of periodic content can increase the signal-to-noise ratio and therefore the chance to detect aftershock signals in data containing periodic disturbances.

Contents

Abbreviations

ADC	analogue-digital converter
AR	auto-regression
ARMA	autoregressive moving-average
BVP	Bochum Verification Project
CTBT	Comprehensive Nuclear-Test-Ban Treaty
CTBTO	Comprehensive Nuclear-Test-Ban Treaty Organization – Preparatory Commission
DAC	digital-analogue converter
DC	direct current
DFT	discrete Fourier transform
ESPRIT	estimation of signal parameters via rotational invariance techniques
FFT	fast Fourier transform
FIR	finite-impulse response
FWHM	full width at half maximum
GWN	Gaussian white noise
IFFT	inverse fast Fourier transform
IIR	infinite-impulse response
IMS	International Monitoring System
LFS	linear frequency shift
MA	moving average
MUSIC	multiple signal classification

OSI	on-site inspection
RMS	root mean square
SNR	signal-to-noise ratio
UTC	universal time, coordinated

Parameters and variables

A_0	Amplitude of an (LFS) sine function.
b_0	LFS parameter of a an LFS sine function.
$b_{0,r}$	Normalised LFS parameter of an LFS sine function in units of the index, addressing the discrete spectral values.
$\mathrm{d}(t), \mathrm{D}(\nu)$	Dirac comb in the time and frequency domain respectively.
$\mathrm{F}_{\mathrm{Erf}}$	Theoretical error-function expression for a spectrum of an LFS sine. It does not include the convolution with the Dirac comb and comprises exactly two peaks – the one located at positive frequencies and the one located at negative frequencies (Eq. 2.63).
$\mathrm{F}^{n}_{\mathrm{Erf}}$	Theoretical error-function expression for a spectrum of an LFS sine. It is the sum of n $\mathrm{F}_{\mathrm{Erf}}$ functions with shifted frequencies in order to compensate for the omitted convolution with the Dirac comb.
$\mathrm{F}_{\mathrm{Mono}}$	Theoretical expression for a spectrum of a monofrequent sine. It comprises all components and is exact for all parameter ranges (Eq. 2.29).
$\mathrm{F}_{\mathrm{Sum}}$	Theoretical sum expression for a spectrum of an LFS sine. It comprises all components and is exact for all parameter ranges (Eq. 2.95).
GWN_{Level}	Ratio of the magnitude of the highest value of a peak in the spectrum and the GWN amplitude.
GWN_{Seed}	Seed for the pseudo-random phases utilised to generate an interval of GWN.
$\mathrm{h}(t), \mathrm{H}(\nu)$	Hann window function in the time and frequency domain respectively.
i_{Max}	Index of the discrete frequency value at which the strongest spectral magnitude of a peak is located.
N	Number of discrete samples used for one spectrum.
ν	Continuous frequency variable.

n_{Fit}	Number of complex values used in the fit algorithm.
ν_0	(Initial) frequency of an (LFS) sine function.
$\nu_{0,r}$	Normalised (initial) frequency of an (LFS) sine function in units of the index, addressing the discrete spectral values.
ν_{Mean}	Mean frequency of an LFS sine in the time interval T and thus the frequency of the centre of the peak in its spectrum.
ν_{Nyquist}	Nyquist frequency: $\nu_{\text{Nyquist}} = {}^{N}\!/_{2} \cdot \Delta\nu$.
$\Delta\nu$	Interval between two neighbouring discrete frequencies (resolution in the frequency domain).
$\lvert\vec{p}_{\text{Err}}\rvert$	Magnitude of the four-component error vector with the differences between the input signal and the fit result as entries is a mathematical measure for the accuracy of the fit.
$\mathrm{r}(t), \mathrm{R}(\nu)$	Rectangle function in the time and frequency domain respectively.
RMS_{Δ}	RMS value about the time domain differences between the underlying signal without sine (typically pure GWN) and the signal after addition, fitting and subtraction of a sine.
r_{Max}	Position of the peak in the magnitude spectrum in units of the frequency index, but on a continuous scale.
r_{W}	Width of a peak in the magnitude spectrum, defined as the difference between the two frequencies enclosing the peak and fulfilling the condition that the magnitude at the boundary frequencies has dropped by 50% compared to the peak value at i_{max}.
$\mathrm{S}(\nu)$	Fourier spectrum of $\mathrm{s}(t)$. It consists of two δ-functions; if only one of them is utilised, a subscript, S_{pos}, indicates that it is the one located in the positive frequencies (resp. S_{neg} in the negative frequencies).
$\mathrm{s}(t)$	Time-domain signal of a sine: $\mathrm{s}(t) = A_0 \sin(2\pi\nu_0 t + \phi_0)$.
$\hat{\mathrm{S}}(\nu)$	Fourier spectrum of $\hat{\mathrm{s}}(t)$. Similar to $\mathrm{S}(\nu)$, it consists of two summands, which are addressed with $\hat{\mathrm{S}}_{\text{pos}}$ and $\hat{\mathrm{S}}_{\text{neg}}$.
$\hat{\mathrm{s}}(t)$	Time-domain signal of an LFS sine: $\hat{\mathrm{s}}(t) = A_0 \sin\left(2\pi\left(\frac{b_0}{2} \cdot t + \nu_0\right) \cdot t + \phi_0\right)$.
Δt	Time between two samples in a discrete time series (resolution in the time domain).
T	Duration of the time interval for one spectrum.

ν	Continuous time variable.
ϕ_0	Initial phase of an (LFS) sine function.
χ^2	Sum of the n_{Fit} squared deviations between the discrete complex values of the magnitude peak and the values produced by the fit function with the current set of parameters, normalised by the maximum magnitude of the peak.
χ_n^2	Normalised sum of the n_{Fit} squared deviations between the discrete complex values of the magnitude peak and the values produced by the fit function with the current set of parameters, compensates the trend of χ^2 to increase with more summands.
$\chi^2_{\mathrm{Thres}}(n_{\mathrm{Fit}})$	Threshold for χ_n^2, increases with increasing n_{Fit}, if $\chi_n^2 \geq \chi^2_{\mathrm{Thres}}(n_{\mathrm{Fit}})$ the fit is unsuccessful.
$\mathrm{x}(t)$	Time-domain signal.
$\mathrm{X}(\nu)$	Spectrum of $x(t)$

Chapter 1

Introduction

1.1 Motivation

Nuclear weapons are a strong instrument to provoke other states or deter them from threatening the possessing state. But there is the security dilemma: having nuclear weapons might be an advantage for the possessing state but if multiple states possess them, the security is reduced for all because of the disastrous impact of these weapons should a possessing country be assaulted and revert to their launch. To keep the number of nuclear weapon states limited and prepare nuclear disarmament, an international agreement stipulates a stop of the spread of nuclear weapon technology around the globe and even the obligation to negotiate about disarmament of the existing weapons (Treaty on the Non-Proliferation of Nuclear Weapons, 1970). To prevent further weapon development the Comprehensive Nuclear-Test-Ban Treaty was concluded in 1996.

1.1.1 Types of nuclear weapons

The first nuclear weapons used nuclear fission. The next step in qualitative development were fusion (hydrogen) bombs. At all times these thermonuclear weapons have been two-staged: At first a fission process – which is similar to the explosion of a fission bomb – is used to ignite the second stage of a nuclear fusion. Consequently, without being able to produce a fission bomb, fusion bombs are not feasible. The fission material in the nuclear warhead has to have low concentrations of isotopes which either absorb neutrons without producing new ones or have a too high decay activity which could lead to premature ignition. These essential prerequisites, combined with further conditions[1], greatly reduce the number of suitable materials for the fission stage of nuclear warheads. By far the most suitable materials for nuclear fission weapons are certain isotopes of the elements uranium and plutonium:

---

[1] A minimum cross section of fast neutron induced fission, availability or producibility, manageability like reactivity, storage properties etc.

$^{235}_{92}$U is found as a natural resource at low concentrations. Its half-life is $t_{1/2} = 7.0 \cdot 10^8$ yr and therefore lower than the one of the isotope with the longest half-time – $^{238}_{92}$U – with $t_{1/2} = 4.5 \cdot 10^9$ yr, meaning that over the life time of the Earth the isotope concentration decreases. Today, its concentration is only 0.72 % in natural uranium. To use it as fission material for a bomb, it must be enriched to a level of approximately 90 %, which requires sophisticated and energy-intensive processes. The development of enrichment facilities along with the production of significant amounts of highly enriched uranium is said to take decades and it is highly unlikely that this can be achieved clandestinely. However, the bomb design can be comparatively simple.

$^{239}_{94}$Pu has a low half-life ($t_{1/2} = 24{,}000$ yr), it is therefore literally non-existent in nature. Nevertheless, it can be bred from natural uranium by neutron absorption in $^{238}_{92}$U which happens continuously in uranium reactors. For use in weapons the fuel assembly is retained before significant concentrations of $^{240}_{94}$Pu that has a high spontaneous fission rate are bred. The separation can be done chemically by comparatively simple means. The bomb design is challenging[2] and testing absolutely required before such a weapon can be deployed.

$^{233}_{92}$U is a third material rarely used in atomic bombs. It is bred from $^{232}_{90}$Th and has a half-life of 160,000 years. Invariably small amounts of $^{232}_{92}$U are produced which drastically increases the activity (especially γ-decay) making this material hardly utilisable.

Nuclear tests cannot be scaled arbitrarily due to the underlying chain reaction principle. The total fissionable mass is limited because the explosion drives it away before it can be hit by neutrons produced by unpreventable spontaneous fission.[3] Downscaling is challenging because of the exponential energy release with the number of generations before the material is dispersed. The decision on the order of magnitude, with which energy is released during the reaction, lies in the kinetics of the last few fission generations. This makes it extremely difficult to reduce the total energy release by certain factors. A reduction of the mass of fission material close to the critical mass (which is the absolute lowest limit) bears the probability that the energy release is insignificant and the bomb fails as such.

From this it follows that a successful explosion is always accompanied by a minimum amount of nuclear fission reactions, with the production of a minimum of fission products and a minimum of energy release. These products and secondary products can be used

---

[2] The short half-life, a factor 10,000 shorter than of $^{235}_{92}$U, makes it hard to reach criticality before the radiation pressure disperses the material. Low concentrations of impurities and a bomb design based on (hollow sphere) implosion are necessary to overcome these obstacles.

[3] Thermonuclear weapons can be upscaled arbitrarily because the materials used for the fusion of nuclei can be stored densely without a chance of self-ignition of a chain reaction.

to detect nuclear explosions reliably.[4]

1.1.2 The Comprehensive Nuclear-Test-Ban Treaty Organization

Either the extensive enrichment of uranium or the test explosions that are necessary at least for the implosion bomb design can be used for detection of states on their way to nuclear weapons. Since decades international treaties are the means to control testing and non-proliferation; one of them is the Partial Nuclear Test Ban Treaty (PTBT)[5] from 1963, restricting nuclear explosions to underground ones. It was adopted mainly to stop the release of fallout responsible for a significant increase of radiation all over the world. The treaty still allowed underground tests meaning that the advancement of the weapons could continue. For a comprehensive test ban methods and instruments of verification were required because of fears of strong strategic disadvantages if testing would continue clandestinely for one party. It is insufficient to only detect seismic events, but – because of hundreds of small natural earthquakes every day – to discriminate between earthquakes and explosions. Scientists developed convincing procedures[6] to automatically reject most of the natural events and in 1996, after years of intensive efforts, the multilateral Comprehensive Nuclear-Test-Ban Treaty (CTBT) was adopted by the United Nations General Assembly [3]. Since then the Comprehensive Nuclear-Test-Ban Treaty Organization (CTBTO)[7], among other things, builds up and maintains the IMS to ensure that no successful[8] nuclear test is conducted undetected.

The most reliable evidence that an atomic fission took place is the detection of certain radio isotopes or even ratios of isotope concentrations that can be assigned to a small geographical area of release. The strongest challenges are underground tests; the main

---

[4] E.g. the energy release causes high pressures which under ground will create a cavity and excite seismic, acoustic or – in water – hydro-acoustic waves. Additionally, radionuclides transported by wind may be detected. These are not only released from above-ground nuclear explosions but also from underground tests deeply buried – diffusion and barometric pumping often bring isotopes (especially noble gases) to the surface. Once released to the atmosphere, few atoms can be enough to indicate a nuclear explosion [1].

[5] Treaty Banning Nuclear Weapon Tests in the Atmosphere, in Outer Space and Under Water. It was signed and ratified by the governments of the Soviet Union, the United Kingdom and the United States which was the condition for the entry into force on October 10, 1963. Additionally many more states ratified or acceded the treaty.

[6] "[...] comparison of teleseismic body-wave and surface-wave amplitudes has empirically been shown to provide an excellent discriminant. Surface waves from a shallow earthquake with the same body-wave strength as an explosion are typically 6 to 8 times larger than surface waves from the explosion" [2].

[7] To be accurate it is the Preparatory Commission for the CTBTO – the treaty did not yet enter into force since the ratification by China, Egypt, India, Iran, Israel, North Korea, Pakistan and the United States is still pending [4]. Nonetheless, the treaty already has 183 members (May 2014) and the preparation of the International Monitoring System (IMS) is almost complete. The IMS measures non-stop and exercises for on-site inspections (OSIs) are held.

[8] The prescribed detection threshold is 1 kt TNT equivalent anywhere on Earth. Actually it is around 0.1 kt for most areas [5]. It is very elaborate if not impossible to plan a nuclear explosion on a smaller scale especially for newcomers.

method is to detect the explosion via seismic sensors at large distances. Typically multiple measurement stations with multiple sensors each allow the localisation of the source mostly by onset times with an accuracy of 10-20 km on the whole globe [6].To investigate uncertainties, e.g. after a state had announced a strong conventional explosion, an OSI can be conducted in the case of initial suspicion to collect further indications. Using the seismic data of the IMS to locate the origin of the signal results in an error ellipse containing an area up to $1,000\,\mathrm{km}^2$ which is too large to cover it completely with isotope sampling. Several techniques are developed to further reduce this area [7], [8]. The most developed one is to set up local arrays of seismic sensors at the surface in the area of interest (up to $1,000\,\mathrm{km}^2$, Protocol to the CTBT: II.A.3) and to detect and locate aftershock signals coming from the cavity and its vicinity.[9] The problem here is that the signals are weak – for example they can stem from rocks falling 50 m until they hit the bottom of the cavity or from relaxation cracks in the surrounding material – and need to propagate 1 km or more through (different layers of) soil up to the surface where they are to be measured. Because of their low amplitudes, these signals are very susceptible to disturbances which can be either anthropogenic or natural. The former is produced by traffic, construction sites, the mining industry or the like and could even be produced intentionally to mask the signals to hide the test. Furthermore the inspectors themselves produce noise with vehicles and helicopters during measurements and maintenance of their sensors. During the planning of the placement of the seismic sensors, attention is paid to the surrounding noise sources to prevent disturbances in advance, but some disturbances will always reduce the signal-to-noise ratio (SNR) of the data. The reduction of disturbances which have already been measured is the motivation of this work.

1.1.3 Periodic and broadband signals

The Fourier transform gives the spectrum of a given interval of time-domain data [11]. Periodic signals are superpositions of sine waves in which every sine shows up as a peak in the spectrum at the frequency of the sine. Non-periodic signals have a broadband spectrum. Therefore these two classes of signals can be distinguished from each other in the spectral domain. Examples are shown in Figure 1.1. Many anthropogenic signals are mostly periodic: Combustion engines run in cycles whereby periodic vibrations occur by the ignition of the fuel-gas mixture at a certain rate as well as periodic emissions of fumes at the exhaust opening. Especially the latter produces acoustic excitations which is of interest because acoustic signals couple to the ground [12]. Consequently even aircraft signals are measured with seismic sensors buried near-surface. Rotors have a certain revolution rate; they cut through the air and return to the same location after one

---

[9] In solid ground a nuclear explosion will always form a cavity because of the high pressure being the product of the extremely high energy release. It can vary in size and stability. Typical diameters are roughly in the order of 60 m [9] (increases with the the third root of the yield [10]).

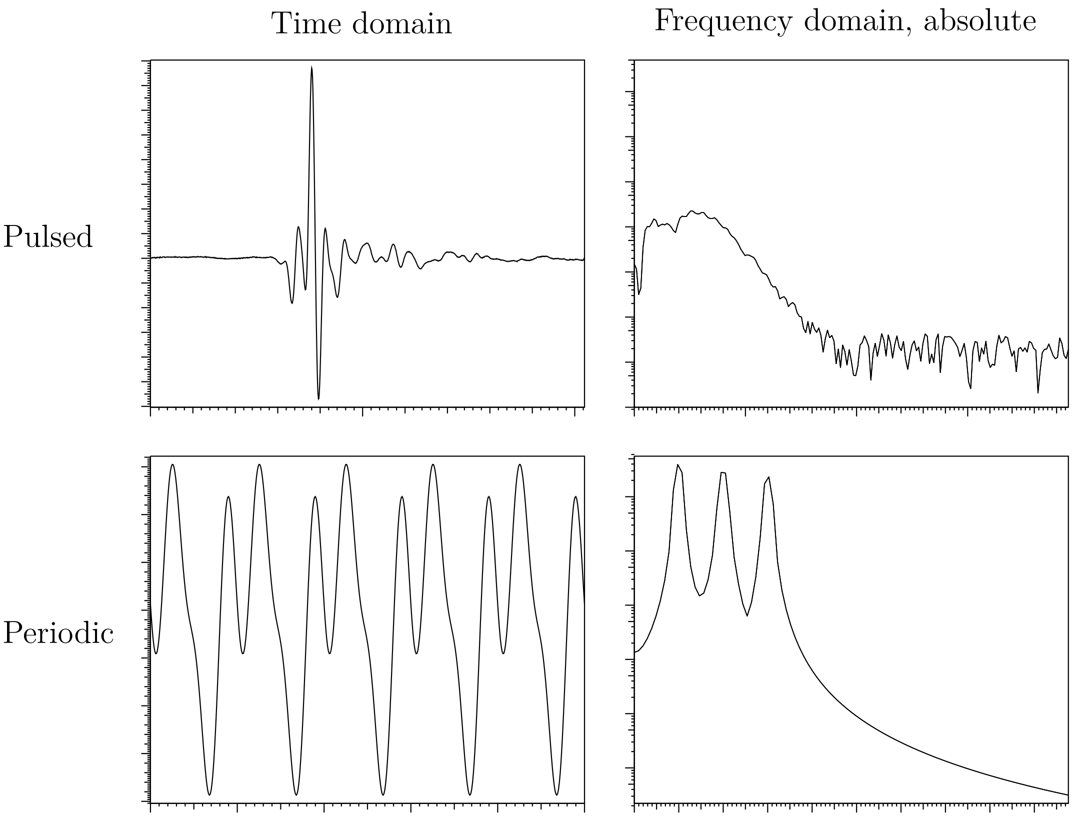

Figure 1.1: Examples for periodic and broadband signals: The pulsed signal stems from a firecracker (seismic); the periodic one is synthetic, to see the periodicity easily, its frequencies are chosen to be integer multiples of each other so they produce the same form for each period of the fundamental frequency in the time domain. Labels for the axes are omitted in order to focus the attention on the curve shapes.

revolution.[10] The signals of helicopters and propeller aircraft in general produce strong periodic signals which are commonly measurable with near-surface velocity or acceleration sensors even in hundreds of meters distance to the source.

1.1.4 Time-varying frequency

A pure sine is a special kind of time-dependent signal. It has a constant amplitude, and a time varying phase angle. This phase angle implies the frequency and the start phase. If a sine changes its frequency sufficiently slowly certain properties of the sine remain in part; for example it still can be distinguished from non-periodic signals in the spectral domain. Main fields for the occurrence of time-shifting sines are changes in revolution rates of engines or the change of Doppler shift of moving engines. Figure 1.2 shows an example for each. The next complexer order of a change to the phase angle is a linear

---

[10] Multi-blade rotors produce frequencies of multiples of their revolution rate (because of their superposable rotation symmetry), then typically the n-th harmonic is the strongest if n is the number of blades. Another reason for the occurrence of harmonics is that the excitation usually is not sinusoid.

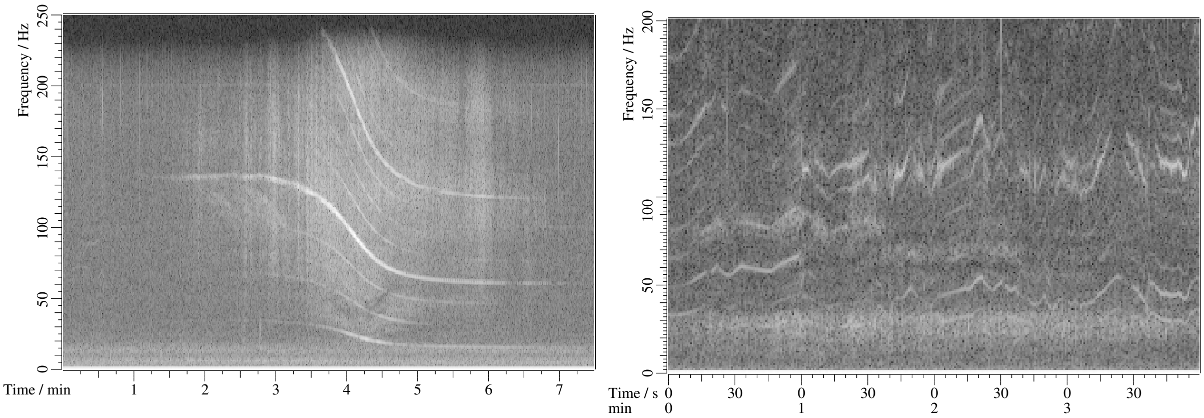

Figure 1.2: Sequences of spectra (quadratic time-frequency representation) to demonstrate changes in periodic signals. The grey scale is logarithmic and proportional to the spectral power density – the brighter the stronger the spectral density. Vertically limited narrow bright regions indicate periodicity at these frequencies; timely persistent, they form horizontal lines. If frequencies change in time, lines are aslant. If a source does not produce perfect sinusoids, harmonics appear, keeping the same relative distance to each other. Left: a propeller aircraft flying towards the sensor, reaching the point of closest approach at approximately 4 min, then the distance increases again so that the frequencies at the sensor appear to be lower. Right: a land vehicle; it is easy to recognise fast changes in the revolution rate of the engine.

frequency change.

1.1.5 About this work

The analysis and subtraction of both the monofrequent sine and the sines with a linear frequency shift are introduced, described and evaluated in this work. The algorithm design and the mathematical expression for the monofrequent sine have been developed before by Jürgen Altmann [13] and during my Diploma thesis [14].

1.2 General usability

The support of OSIs of the CTBTO is only one application. In this work a general method is analysed to improve time-series data in terms of periodic disturbances. For this purpose mathematical expressions are derived allowing a fit routine to precisely determine the parameters representing the disturbances and allowing their subtraction from the data. That is why in Chapter 6 (real-data analysis) for some events seismic data are processed, for others acoustic ones; acoustic data can have some advantages like easier producibility, better SNR or – in older measurements – a higher sampling rate.

1.3 Related work

The techniques to find repetitions of patterns or, in general, intervals between which the autocorrelation does not vanish, are called spectral estimation. Beside the autocorrelation the Fourier transform is a common technique to detect periodicities. The underlying principles are similar (Wiener-Khinchin theorem): The Fourier theory states that every continuous signal can be composed from sinusoidal functions. If the signal is periodic, then these sinusoids have the frequency and harmonics of the repetitions in the original signal. Autocorrelation is the correlation with the input itself. If the signal is regarded as a sum of sinusoids, then autocorrelation becomes similar to the Fourier analysis which yields the likeliness of the presence of each sinusoid in the signal. The pure autocorrelation approach is useful if a signal contains few (periodic) signals (each consisting of one fundamental frequency and possibly its harmonics), otherwise the abundance of peaks is hard to interpret.[11] In this case the autocorrelation function contains one or more peaks at the periods (and their multiples – depending on the number of repetitions) of these signals.

The discrete Fourier transform (DFT) separates sampled signals into sinusoids of equidistant frequencies. If a time-domain signal covers N samples then its discrete spectrum gives one (complex) value each for $N/2$ sinusoids (frequencies). This method is able to handle complexer signals but requires the detection of prominent peaks and their harmonics to assign them to a certain signal.

Main fields of research are techniques to either enhance the autocorrelation approach, making it feasible for real-data applications, or to increase the spectral resolution in Fourier spectra below the step size between two discrete values. Our own work uses the Fourier approach. Nonetheless a short overview on different approaches is given.

1.3.1 Estimators

Estimators are used to provide information about unknown parameters of a statistical population by the evaluation of (generally random) samples. According to [16, p. 98]:

> ”Maximum likelihood is the most important and widespread method of estimation. Many well-known estimators such as the sample mean, and the least-squares estimator in regression are maximum likelihood estimators if the data have a normal distribution. Maximum likelihood estimation generally provides more efficient (less variable) estimators than other techniques of estimation.”

---

[11] The abundance of peaks could be assigned to different signals by a subsequent Fourier transform. This leads to the ”Power Spectral Density”, a common estimation technique similar to the periodogram. Another technique is the cepstrum: the ”Mel Frequency Cepstral Coefficients” can be used for speech processing and music-information-retrieval tasks [15].

In this work the main use is in spectral estimation. At places least-squares regression is used.

1.3.2 Spectral estimators

Periodic or nearly periodic sequences appear in many disciplines, including astronomy, meteorology, sonar, machine diagnosis, speech, music and economics. The task of spectral estimation is to determine the frequencies contained in such sequences. Several spectral estimators have been developed for different applications. Typically and in contrast to what is done in this work the signals to be characterised are of a periodic nature and the noise is the disturbing component. Also usually the phase is of low interest for most applications whereas here a good fit of the phase is essential for a successful subtraction of periodic content.

Once frequencies are located – by whatever method – and suppressed, the method could be repeated until certain requirements are fulfilled or further processing could be applied. On the one hand, this is done in this work, on the other hand, this is, for instance, currently used to detect exoplanets [17].[12]

Techniques for spectral estimation can be classified into two general types [18, p. 195]:

> ”[*Nonparametric* techniques, F.G.] do *not* assume a particular functional form, but allow the form of the estimator to be determined *entirely* by the data. These methods are based on the discrete Fourier transform of either the signal segment or its autocorrelation sequence. In contrast, *parametric* [emphasis added, F.G.] methods assume that the available signal segment has been generated by a specific parametric model (e.g., a pole-zero or harmonic model).”

1.3.2.1 Nonparametric power-spectrum estimation

If the goal is to find and characterise single sinusoids, this is often called frequency estimation. The periodogram[13] may provide a basis, especially if no information about the signal is available a priori. When applying a periodogram, only the number of samples must be chosen, which is typically a compromise between desired spectral resolution and accepted blurring for unstationary signals.

The periodogram is already an estimator for the spectral density and describes a distribution of (poorly calculated [20, Sec. 5.2]) power as a function of frequency. A power estimate over a narrow frequency band can be seen as the output power of a narrow-bandpass filter leading to the filter-bank interpretation of the periodogram [18, p. 213].

---

[12] In this regard the least-squares spectral analysis (Lomb-Scargle periodogram) should be mentioned as a method to handle unevenly spaced samples.

[13] Let T be the length of the time-domain interval of a signal x_T, then the continuous periodogram is given via Fourier transform by: $\frac{1}{T}\left|\mathcal{F}\left\{x_T(t)\right\}\right|^2$ [19].

Aside from problems like spectral leakage, peaks in the periodogram indicate periodic content. Taking the discrete frequency at a local maximum may be imprecise by up to $\pm 0.5\,\Delta\nu$,[14] which is insufficient for many applications. More frequency samples can be gained by zero padding, but this approach requires doubling the number of samples for the fast Fourier transform (FFT) for each doubling of the frequency resolution and can thus greatly increase computation effort.

In order to determine the frequency of a peak more precisely and under the condition that a peak in the magnitude spectrum / periodogram consists of sufficient samples, a function can be fitted to these samples to find a better frequency approximation in the abscissa of its maximum.[15] Whereas in our work the exact mathematical expression is used, earlier research worked with approximate functions. In the literature parabolas are often used [21, 22, 23]; a parabola is the function easiest to calculate, and fitting is unnecessary (Sec. 4.5.1). Since a Gaussian curve is a parabola in the logarithmic scale, the Gaussian interpolation reduces to the parabolic interpolation in this scale. In [24] the two approaches with eleven different window functions are quantitatively compared with respect to the interpolation error. It is shown that the maximum error for the parabolic interpolation ranges from $0.234\,\Delta\nu$ for the pure rectangle window down to $0.0295\,\Delta\nu$ for a Gaussian window of $8\,\sigma$. The Gaussian interpolation has the same ranking order for the different window functions but systematically lower maximum errors: $0.167\,\Delta\nu$ for the rectangle and $8.69 \cdot 10^{-5} \Delta\nu$ for the 8-σ Gaussian window. It should be noted that the errors indicate a dependency on the main lobe width of the window-function spectrum: for the 8-σ Gaussian window it is $11.41\,\Delta\nu$. In general, it can be stressed that the smaller the maximum frequency error is, the worse is the separability of neighbouring peaks. Since the Hann window [11, Chap. 9.5] is used throughout this work, its parameters should be mentioned: the main lobe width is $4\,\Delta\nu$, the maximum error for the parabolic interpolation is $0.0692\,\Delta\nu$ and $0.0160\,\Delta\nu$ for the Gaussian one. In this work a varying number of samples is used for the calculation of parabola parameters to estimate start values for the subsequent fit, which also uses the values of the peak to fit the exact mathematical expression. As a consequence, the frequency (and the other parameters) are without errors.

In [25] the phases of the complex values around the peaks are utilised to determine the frequency. In this work, a similar, extended approach to estimate the sign of the shifting parameter and the initial phase for the subsequent fit procedure is used.[16]

Spectrograms are the visual implementation of a sequence of periodograms. They are

---

[14] $\Delta\nu$ is the frequency resolution. $\Delta\nu = {}^{1}/_{T}$, $T = N \cdot \Delta t$ where N is the number of samples in the time domain and Δt the time between two samples.

[15] Typically this means ≥ 3 samples in a spectrum or periodogram. This can be achieved by moderate zero padding or the application of a window function. In this work the Hann window is used.

[16] We shall see that the initial phase (ϕ_0) is crucial to avoid the fitting routine from getting stuck in secondary minima. Therefore I use the estimated value, but I do not rely on this value being the optimum (Sec. 4.9).

commonly used if the variability in the spectral characteristics of the signal occurs at a time scale much larger than the duration of the time interval for one spectrum (T) [26]. In this work spectrograms are used to show longer intervals of data and to track frequencies visually to verify the algorithm. However, they are not used in the process of peak fitting. In real data small peaks will even occur in noise. Their smoothing or examination and evaluation before or after application of the DFT is the basis of several techniques including the one described in this work. Among others, common types of power-spectrum estimation with smoothing are:

- The Blackman-Tukey approach to smooth a single periodogram: 1. Estimate the autocorrelation sequence from the unwindowed data. 2. Window the obtained autocorrelation samples. 3. Compute the DFT of each segment. The disadvantage is that the resolution is inversely proportional to the maximum lag of the autocorrelation. [18, p. 222ff]

- The Welch-Bartlett approach averages multiple periodograms to reduce variance. 1. Segment the data (with up to 50% overlap). 2. Window each segment. 3. Compute the DFTs. 4. Accumulate the squared magnitude values. 5. Finally, normalise (with respect to the number of segments and their lengths). Again, the disadvantage is that the resolution is inversely proportional to segment length. [18, p. 227ff]

- The Multitaper approach [27]: The same data segment is taken multiple times completely but each time with a different window (= taper); it is important for these windows to form an orthonormal set. The DFT is taken for every segment, afterwards the mean of the power spectra is evaluated. The windowed signals provide statistically independent estimates of the underlying spectrum which reduces the variance by the number of tapers without a reduction of the resolution compared to the pure periodogram. [18, p. 246ff][17]

The said methods are compared in [18, Table 5.3, p. 235]. These approaches – to this point – are not sufficient for the subtraction of sinusoids as no information on the phases is gained.

There are also several techniques to find, group and track fundamentals and harmonics available in the literature (e.g. [13], [28]), which could be interesting for future applications but are beyond this work.

1.3.2.2 Parametric power spectrum estimation

Since they are not used in this work, only a very brief introduction is given on parametric methods [26]:

---

[17] This approach is also used by the widely known Thomson multitaper method (which uses Slepian baseband filters) and the Capon method. [19]

> ”In general, when a parametric model assumption is valid for the data, parametric methods are more accurate and more efficient than nonparametric methods [...].”

[18, p. 195]:

> ”Since the choice of an inappropriate signal model will lead to erroneous results, the successful application of parametric techniques, without sufficient a priori information, is very difficult in practice.”

Parametric approaches assume the underlying stationary stochastic process to have a certain structure which can be described using a small number of parameters. Autocorrelation can be used to estimate the coefficients for auto-regression (AR) and moving average moving average (MA) or the combined ARMA methods which all are kinds of infinite-impulse response (IIR) filters building up a linear combination of previous values of the signal and of already processed values.[18] To whiten the data, ARMA can be used to estimate the IIR filter coefficients for notch filters.

The task is the estimation of model parameters describing the stochastic process. Popular methods of spectrum estimation are based on the linear-algebraic concepts of subspaces and are therefore called "subspace methods". In [29] it is written:

> ”Pisarenko [...] first observed that the zeros of the z-transform of the eigenvector corresponding to the minimum eigenvalue of the covariance matrix lie on the unit circle, and their angular positions correspond to the frequencies of the sinusoids.”

On this basis, the amplitudes are obtained from the autocorrelation relationships of the observations and the noise strength from the last eigenvalue of the same autocorrelation matrix. The phases can be determined from the input data by means of standard least-squares methods after determining the frequencies. According to [19]:

> ”In a later development it was shown that the eigenvectors might be divided into two groups, namely, the eigenvectors spanning the signal space and eigenvectors spanning the orthogonal noise space. The eigenvectors spanning the noise space are the ones whose eigenvalues are the smallest and equal to the noise power. One of the most important techniques, based on the Pisarenko’s approach of separating the data into signal and noise subspaces is the MUSIC method [...] and ESPRIT method [...].”

---

[18] The ARMA approach is also called pole-zero model because of the rational representation of the system function (z-transform: zeros are the roots of the numerator, poles of the denominator). For dynamic modelling also Kalman filters are used [18].

> ”Both methods are similar in the sense that they are both eigendecomposition-based methods which rely on decomposition of the estimated correlation matrix into two subspaces: noise and signal subspace. On the other hand, MUSIC uses the noise subspace to estimate the signal components while ESPRIT uses the signal subspace.”

1.4 Thesis overview

This thesis is structured into the following chapters:

1 This chapter motivates this thesis by describing the reason what the algorithm, developed and evaluated in the following chapters, is meant to be used for.

2 The theory chapter shows ways how usable expressions for the spectrum of sine functions in discrete spectra are derived (zero and first order of frequency shift).

3 The gained, comprehensive expression for sinusoidal functions is demonstrated with different sets of parameters to get the feel of the influence of certain parameters to the curve progression in the magnitude and the phase spectra.

4 The estimation of reasonable start values for the four parameters characterising a linear-frequency-shift (LFS) sine is essential for a good fit performance. Information about the properties of these parameters from the shape of a peak in the magnitude spectrum or from the phase is derived here.

5 In this chapter, fits to artificial spectra are analysed and thresholds for real-data applications are set. Additionally, the fit performance is demonstrated for the data of a real seismic event superposed with an artificial LFS sine.

6 Subsequently, in this chapter real data of different sources are processed and the fit results presented.

7 The final chapter consists of a short summary, a conclusion and an outlook with recommended future research.

A The appendices give additional information in the areas: error-function approach, transition of the exact LFS expression to the monofrequent case for a vanishing LFS parameter, computer run time, and major software extensions.

Chapter 2

Theory

2.1 Introduction

In order to reduce the periodic content in time-series data, sine waves are to be subtracted from the signal if their parameters are known. Because every sine component produces a single peak in the spectrum, this is to be done one by one. The knowledge of the parameters of a single sine is to be gained by fitting them to its peak in the spectral domain. The typical approach is to use a fitting algorithm that fits the continuous, theoretical function to the data with the help of its derivatives with respect to the parameters. In this work the Levenberg-Marquardt algorithm is used and the theoretical function and its first derivatives are developed in this chapter.

Beside the sine function itself, three facts need to be taken into account to calculate the expression for the fit algorithm: [11]

- Real data are gained by analogue-digital converters (ADCs) by sampling the continuous signal with a certain rate;[1] thus the data consist of a sequence of equidistant discrete values. This is represented mathematically by multiplying the continuous sine function with an equidistant Dirac comb.

- Real signals can only be handled for a finite duration. In addition they can change over time, whereas the (continuous) Fourier spectrum has no time resolution. Short-term signals in a long interval of data being transformed will therefore be suppressed, which is a reason to limit the interval durations to small ones. Mathematically this means multiplication with a rectangle function. For real data, the interval will consist of 2^n $(n \in \mathbb{N})$ samples in order to apply the applied FFT [30].

- Because of the first two items mentioned the discrete spectrum of a monofrequent

---

[1] For instance, the CTBTO samples with 500 Hz when performing on-site inspection exercises. In all measurements we performed ourselves during the last years we sampled with 10 kHz. Firstly, because we are interested also in higher frequencies. Secondly, as we usually include microphones, one could listen to the recorded data and even understand human speech.

sine does not necessarily consist of two δ functions at the frequency of the sine and its negative (as would hold for the Fourier transform of the continuous, monofrequent sine) but depends on the difference between the frequency of the sine and the closest frequency of the Dirac comb. The bigger this difference is, the bigger the effect called "spectral leakage" will be. In order to reduce the effect that the small changes of the frequency of the sine have a strong influence on the shape of the peak in the spectrum, window functions are used [31]. Here we use the Hann window by multiplying each interval of data with the corresponding window function before performing the FFT.

2.1.1 The Levenberg-Marquardt algorithm

The implemented version of the Levenberg-Marquardt algorithm originates from [30]. The Pascal code was ported to `C/C++`. In general this fit algorithm changes the parameter vector of a continuous function along its gradient to find a minimum in the sum of squared deviations between input values and function values at the same positions. Strictly speaking, it minimises:

$$\chi^2 = \sum_{i=0}^{n_{\mathrm{Fit}}-1} \frac{(a_i - \mathrm{f}_a(i))^2}{(\mathrm{w}(i))^2}, \tag{2.1}$$

where:

- n_{Fit} is the number of complex values used.
- a_i is the i-th discrete value of the input.
- $\mathrm{f}_a(i)$ is the value of the continuous function, calculated for the current set of parameters and evaluated at the same position as the i-th discrete value.
- $\mathrm{w}(i)$ is a weight for the difference produced by the i-th value.

For this work, two adjustments are made:

- During an adaptation from fits in the magnitude spectra to fits in complex numbers, we decided to handle both – the real and the imaginary part – in the same way like the magnitude values before, by duplicating the number of samples and placing the values of the real part in front (indices 0 to $(n-1)$) of the values of the imaginary part (indices n to $(2n-1)$), when delivering the input to the fit algorithm. The continuous fit function is adjusted accordingly.
- The weights for all values are the same, namely the absolute value at the maximum of the peak in the discrete frequencies.

The Levenberg-Marquardt algorithm adjusts the step length: Each time the new set of parameters decreases χ^2 compared to the last accepted parameter set, the new set replaces the last one and the step length is increased. The other way round, if χ^2 is not decreased, the set of parameters is discarded and the step length is decreased. This approach has the advantage, that the number of iterations is usually manageable while the precision of the fit result is not limited by the procedure itself. Furthermore, because only the gradients are used, no second derivatives are needed.

There are two regular termination conditions:

- If 10 consecutive times the χ^2 value could not be decreased by decreasing the step length. Subsequently the comparison of this minimal χ^2 with a threshold decides whether or not the fit was successful (it is assumed that the peak stems from a sine).
- If 120 iteration steps are reached.[2]

2.2 Variables and general properties

Let Δt be the time between two discrete samples, then N is the number of samples within the time interval T:

$$N = \frac{T}{\Delta t}. \tag{2.2}$$

$\Delta\nu$ is the interval between two neighbouring discrete frequencies (resolution in the frequency domain); it arises from the sampling rate Δt and the number of values used (N):

$$\Delta\nu = \frac{1}{T}. \tag{2.3}$$

The continuous Fourier transform used here is given by [11, Chap. 2.1]:

$$\mathrm{x}(t) \circ\!\!-\!\!\!-\, \mathrm{X}(\nu) = \int_{-\infty}^{\infty} \mathrm{x}(t)\, \mathrm{e}^{-\mathrm{i}2\pi\nu t}\, \mathrm{d}t. \tag{2.4}$$

Therefore the inverse continuous Fourier transform is:

$$\mathrm{x}(t) = \frac{1}{2\pi} \int_{-\infty}^{\infty} \mathrm{X}(\nu)\, \mathrm{e}^{\mathrm{i}2\pi\nu t}\, \mathrm{d}\nu. \tag{2.5}$$

The δ-function is defined as:

$$\delta(\nu) = \int_{-\infty}^{\infty} \mathrm{e}^{\mathrm{i}2\pi\nu t}\, \mathrm{d}t. \tag{2.6}$$

---

[2] This threshold is set to such a high number, that the probability to loose a valid peak is insignificant. It seems that, if the topography of the parameter space is in such a way that many iteration steps are necessary, it is very unlikely that the peak was originated by a sinusoid. For further applications it could be reasonable to reduce the number or to mark the fit as failed if the limit is reached, no matter of the current χ^2.

With Euler's formula, $\mathrm{e}^{\mathrm{i}x} = \cos x + \mathrm{i}\sin x$, one derives:

$$\sin(x) = \frac{\mathrm{e}^{\mathrm{i}x} - \mathrm{e}^{-\mathrm{i}x}}{2\mathrm{i}}. \tag{2.7}$$

2.3 Analytical expression of a monofrequent sine in the frequency domain

The assumption here is that the periodic content does not change during the time interval used for a single spectrum. This can often at least approximately be fulfilled by limiting the number of samples used for the discrete Fourier transform. Four components are required in order to derive the expression needed for the fit algorithm: sine, rectangle, Hann window and Dirac comb.

2.3.1 Sine

Each such sine has an amplitude A_0, a frequency ν_0 and an initial phase ϕ_0, its continuous time course is:

$$\mathrm{s}(t) = A_0 \sin(2\pi\nu_0 t + \phi_0). \tag{2.8}$$

The continuous Fourier transform is gained by insertion of Equation 2.7 into Equation 2.4:

$$\mathrm{s}(t) \circ\!\!-\!\!- \mathrm{S}(\nu) = \frac{A_0}{2\mathrm{i}} \int_{-\infty}^{\infty} \left(\mathrm{e}^{\mathrm{i}(2\pi\nu_0 t + \phi_0)} - \mathrm{e}^{-\mathrm{i}(2\pi\nu_0 t + \phi_0)}\right) \cdot \mathrm{e}^{-\mathrm{i}2\pi\nu t}\,\mathrm{d}t \tag{2.9}$$

$$= \frac{A_0}{2\mathrm{i}} \left(\mathrm{e}^{\mathrm{i}\phi_0} \int_{-\infty}^{\infty} \mathrm{e}^{\mathrm{i}2\pi(\nu_0 - \nu)t}\,\mathrm{d}t - \mathrm{e}^{-\mathrm{i}\phi_0} \int_{-\infty}^{\infty} \mathrm{e}^{-\mathrm{i}2\pi(\nu_0 + \nu)t}\,\mathrm{d}t\right) \tag{2.10}$$

With the definition of the δ-function (Eq. 2.6) and swapped term order, it becomes:

$$\mathrm{S}(\nu) = \mathrm{i}\frac{A_0}{2} \left(\delta(\nu + \nu_0)\mathrm{e}^{-\mathrm{i}\phi_0} - \delta(\nu - \nu_0)\mathrm{e}^{\mathrm{i}\phi_0}\right) \tag{2.11}$$

2.3.1.1 Symmetry

By separation of Equation 2.11 into real and imaginary part, it becomes obvious that the real part has mirror symmetry and the imaginary part point symmetry relating to $\nu = 0$. This is intrinsic to the Fourier transform itself and means that the complete information is given by either the positive or negative frequencies (including zero) for every real time-domain signal.

$\mathrm{s}(t)$ is symmetric under negation of its parameters: $\mathrm{s}(A_0, \nu_0, \phi_0, t) = \mathrm{s}(-A_0, -\nu_0, -\phi_0, t)$, the Fourier transform reflects this by having a second peak at negative frequencies. $\mathrm{S}(\nu)$

can be separated in two terms; one where the peak is at a positive frequency, one where it is at the corresponding negative frequency:

$$\mathrm{S}(\nu) = \underbrace{\mathrm{i}\frac{A_0}{2}\delta(\nu+\nu_0)\mathrm{e}^{-\mathrm{i}\phi_0}}_{\mathrm{S}_{\mathrm{neg}}(\nu)} \underbrace{-\mathrm{i}\frac{A_0}{2}\delta(\nu-\nu_0)\mathrm{e}^{\mathrm{i}\phi_0}}_{\mathrm{S}_{\mathrm{pos}}(\nu)} = \mathrm{S}_{\mathrm{neg}}(\nu)+\mathrm{S}_{\mathrm{pos}}(\nu) \tag{2.12}$$

$$\mathrm{S}_{\mathrm{neg}}(A_0,\nu_0,\phi_0,\nu) = \mathrm{S}_{\mathrm{pos}}(-A_0,-\nu_0,-\phi_0,\nu) \tag{2.13}$$

This means that the negative part of the spectrum can be generated by taking the positive one with negated signs of the parameters. Calculation and implementation effort can be reduced. This is helpful in the following.

2.3.2 Rectangle function

Let $\mathrm{r}(t)$ be the rectangle function from 0 to T, then the Fourier transform can be gained directly by execution of the integration:

$$\mathrm{r}(t) = \Pi\left(\frac{t}{T}-\frac{1}{2}\right) \circ\!\!-\!\!-\; \mathrm{R}(\nu) = \int_0^T \mathrm{e}^{-\mathrm{i}2\pi\nu t}\,\mathrm{d}t \tag{2.14}$$

$$= \frac{1}{\mathrm{i}2\pi\nu}\left(1-\mathrm{e}^{-\mathrm{i}2\pi\nu T}\right) \tag{2.15}$$

2.3.3 Hann window function

The Hann window function consists of one period of a (co-)sine shifted in a way that the it becomes zero at its sides. The continuous Fourier transform can be deduced from the transformation of a general sine (Sec. 2.3.1) as the cosine is a phase shifted sine and the Fourier integral of a constant is the delta function at frequency zero.

$$\mathrm{h}(t) = \frac{1}{2}-\frac{1}{2}\cos\left(\frac{2\pi t}{T}\right) \circ\!\!-\!\!-\; \mathrm{H}(\nu) = \frac{1}{2}\delta(\nu)-\frac{1}{4}\delta(\nu+\Delta\nu)-\frac{1}{4}\delta(\nu-\Delta\nu) \tag{2.16}$$

2.3.4 Dirac comb

Sampling with a certain frequency means that every Δt one sample is taken; thus the continuous signal is multiplied with the Shah function $\mathrm{III} = \sum\limits_{k=-\infty}^{\infty}\delta(t-k\cdot\Delta t)$. The factor Δt can be factored out [31]:

$$\delta(\alpha x) = \frac{\delta(x)}{|\alpha|} \tag{2.17}$$

leading to:

$$\mathrm{d}(t) = \frac{1}{\Delta t}\mathrm{III}\left(\frac{t}{\Delta t}\right) = \frac{1}{\Delta t}\sum_{k=-\infty}^{\infty}\delta\left(\frac{t}{\Delta t}-k\right) \circ\!\!-\!\!-\; \mathrm{D}(\nu) = \mathrm{III}(\Delta t\cdot\nu) = \frac{1}{\Delta t}\sum_{k=-\infty}^{\infty}\delta\left(\nu-\frac{k}{\Delta t}\right) \tag{2.18}$$

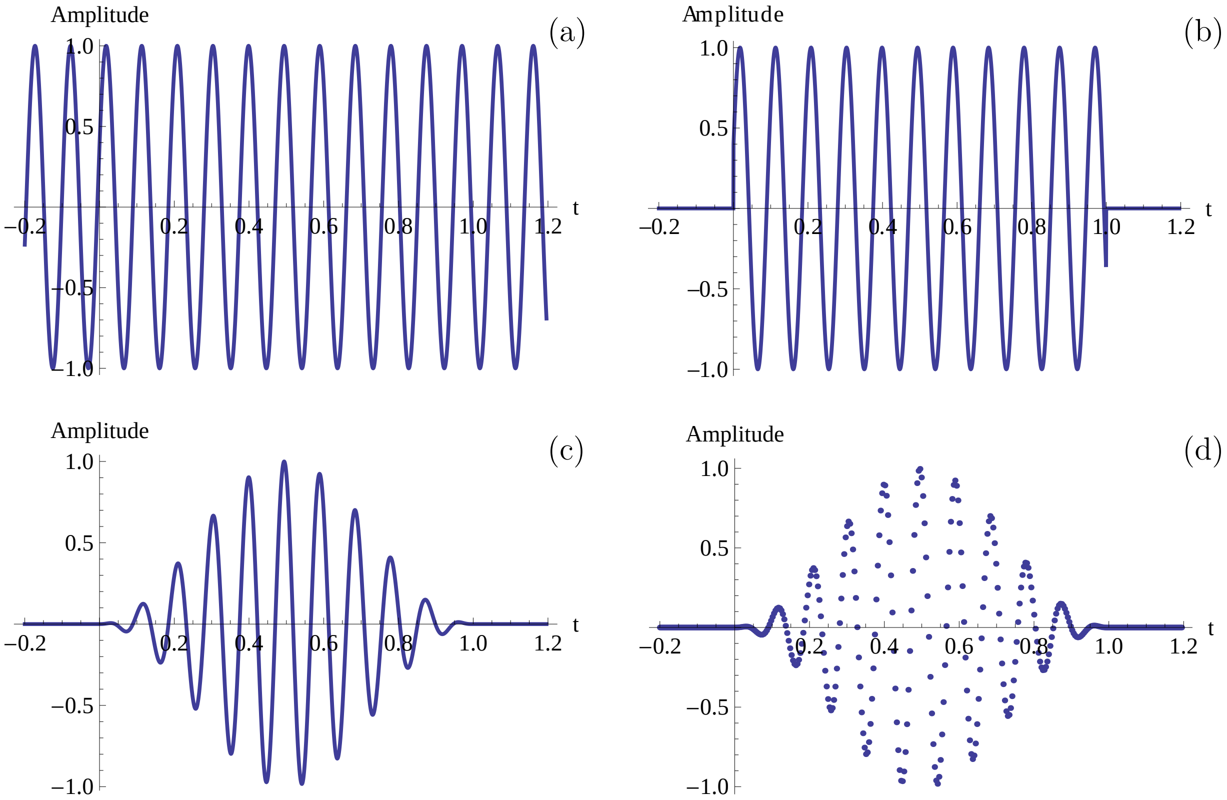

Figure 2.1: Demonstration of the components used before transformation to the spectral domain. (a) shows the continuous function with the parameters: $A_0 = 1.0$, $\nu_0 = 10.5\,\mathrm{Hz}$ and $\phi_0 = \pi/8$; (b) after application of a rectangle with $T = 1.0\,\mathrm{s}$; (c) after application of the Hann window function and finally (d) after discretising with 256 samples in the interval of the rectangle.

With equation 2.3 it is: $\mathrm{III}\left(\Delta t \cdot \nu\right) = \mathrm{III}\left(\frac{\nu}{N\Delta\nu}\right)$; showing that the whole discrete spectrum is repeated forever to both sides as a result of sampling.

2.3.5 Plots for demonstration

Figure 2.1 shows the different steps for the continuous function that occur to real data before its transformation to the spectral domain. Figure 2.2 shows the corresponding spectra. The sign of the real part is the same for the positive and the negative frequencies (mirrored at $\nu = 0$), whereas the imaginary part has an inverted sign (point symmetric with respect to $\nu = 0$).

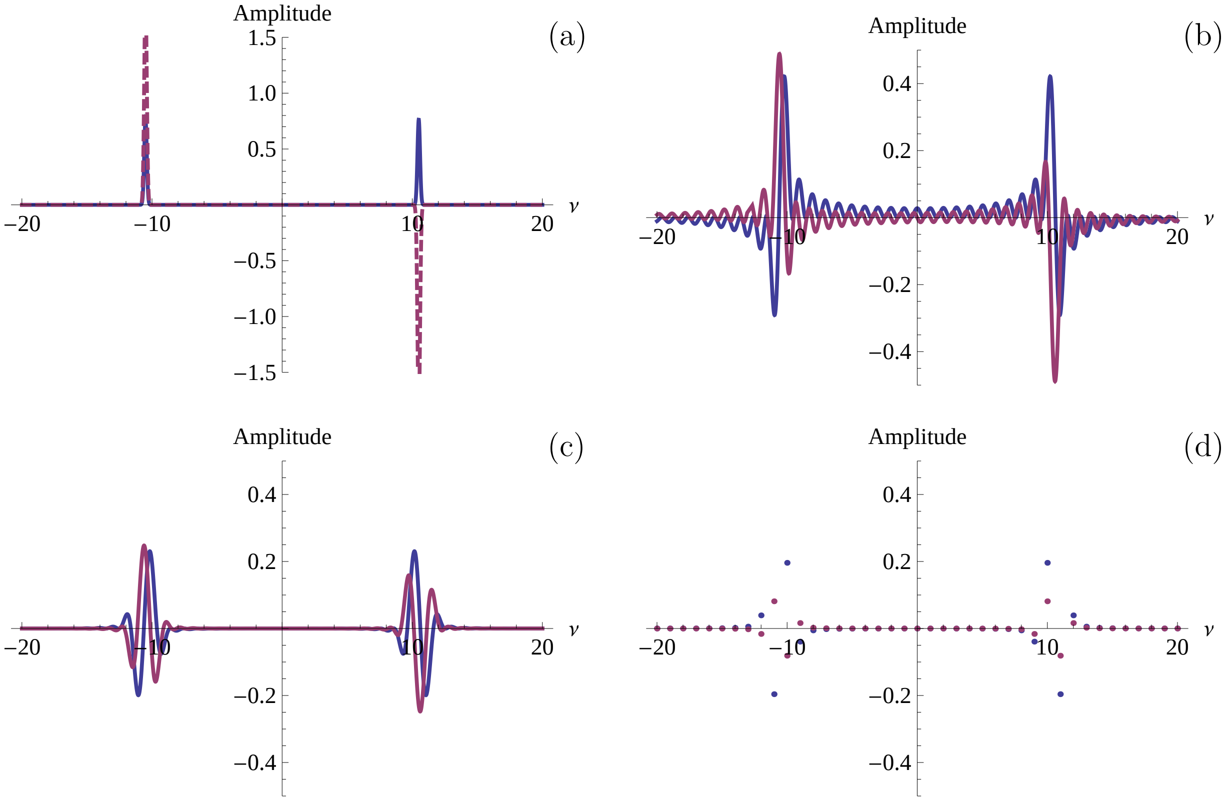

Figure 2.2: The spectra of the plots shown in Figure 2.1 (real part blue, imaginary part red). (a) shows an approximation for the continuous-time Fourier transform of the monofrequent sine wave (the real peak would be infinitely narrow, furthermore the amplitudes of the Dirac delta functions are meaningless as they are irregular distributions and only valid if integrated); (b) after application of a rectangle; (c) after application of the Hann window function (spectral leakage decreased but peak width increased). (d) shows the discrete Fourier transform after the data is sampled (divided by N).

2.3.6 Convolution of the spectral components

[3] The four components introduced above are multiplied in the time domain. To get the spectrum of the product, the Fourier transform has to be applied to it or the Fourier transform of the components is calculated and their results are convolved afterwards [32]. Because the result is the same one can choose the path that is easier to perform. Here the single spectra are convolved.

$$\mathrm{srht}(t)=\mathrm{s}(t)\cdot\mathrm{r}(t)\cdot\mathrm{h}(t)\cdot\mathrm{d}(t)\;\circ\!\!-\!\!\!-\;\mathrm{SRHD}(\nu)=\mathrm{S}(\nu)*\mathrm{R}(\nu)*\mathrm{H}(\nu)*\mathrm{D}(\nu) \tag{2.19}$$

The convolution is defined as:

$$(\mathrm{f}*\mathrm{g})\,(x)\overset{\mathrm{def}}{=}\int_{-\infty}^{\infty}\mathrm{f}(y)\,\mathrm{g}(x-y)\,\mathrm{d}y. \tag{2.20}$$

The convolution of a function consisting of delta functions with a continuous function thus is accomplished by summing up the continuous function with appropriately shifted arguments. As three of the four components only consist of delta functions the result will be a sum of shifted spectra of rectangles $\mathrm{R}(\nu)$. For the implementation into numerical applications, however, the infinite sum of the Dirac comb is not suitable; we will see that the utilisation of summation rules allows the replacement of the sum expression and the further reduction of summands.

2.3.6.1 Convolution of the rectangle with the dirac comb

At first, Equations 2.18 and 2.15 are convolved:

$$\mathrm{RD}(\nu)\,\hat{=}\,\mathrm{R}(\nu)*\mathrm{D}(\nu)=\left[\frac{1}{\Delta t}\sum_{k=-\infty}^{\infty}\delta\left(\nu-\frac{k}{\Delta t}\right)\right]*\left[\frac{1}{\mathrm{i}2\pi\nu}\left(1-\mathrm{e}^{-\mathrm{i}2\pi\nu T}\right)\right] \tag{2.21}$$

$$=\frac{1}{2\pi\mathrm{i}}\sum_{k=-\infty}^{\infty}\frac{1-\mathrm{e}^{-2\mathrm{i}\pi T\left(\nu-\frac{k}{\Delta t}\right)}}{\Delta t\left(\nu-\frac{k}{\Delta t}\right)} \tag{2.22}$$

$$=\frac{1}{2\pi\mathrm{i}}\sum_{k=-\infty}^{\infty}\frac{1-\mathrm{e}^{-2\mathrm{i}\pi T\nu}\mathrm{e}^{2\mathrm{i}\pi Nk}}{\Delta t\left(\nu-\frac{k}{\Delta t}\right)}. \tag{2.23}$$

Because $N,k\in\mathbb{N}$: $\mathrm{e}^{2\mathrm{i}\pi Nk}=1$. As a consequent, the nominator is independent of k. In the denominator $\nu\Delta t=q$ is substituted and can be replaced by a cotangent expression

---

[3] The derivations in the next two subsections (2.3.6 and 2.3.7) are based on the work of Jürgen Altmann. A publication is in preparation.

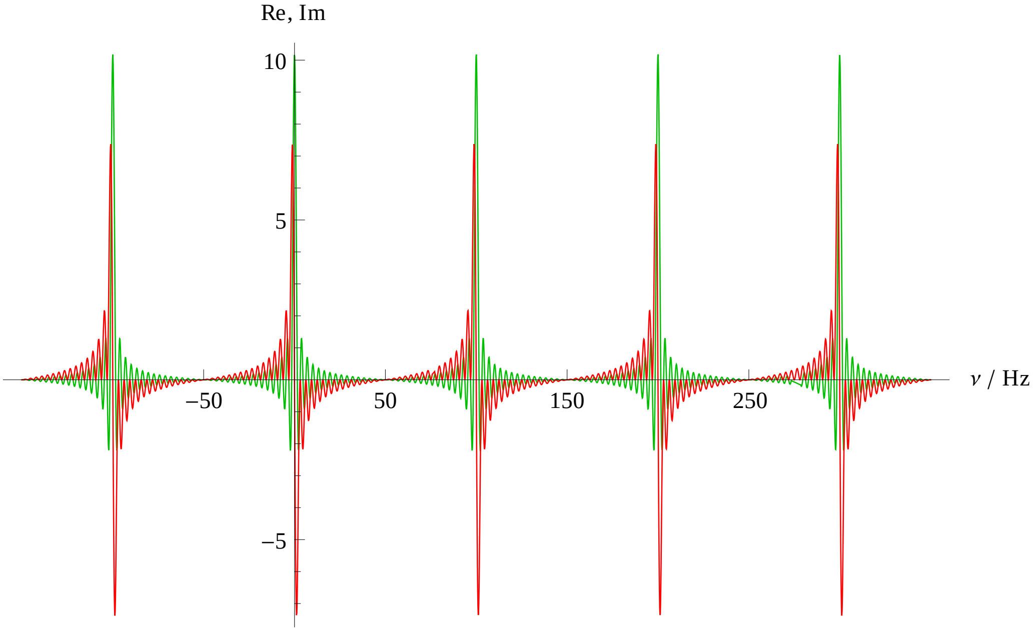

Figure 2.3: Plot of Equation 2.24: The convolution of the rectangle and the Dirac comb. The parameters are: $\Delta t = 0.01\,\mathrm{s}$, therefore the spectrum has a 100 Hz periodicity. $N = 32$, so $T = 0.32\,\mathrm{s}$. N is given a small number to resolve the high frequency modulation. Real part is green, imaginary part red.

(partial fraction decomposition):

$$\begin{aligned}\mathrm{RD}(\nu) &= \frac{1}{2\mathrm{i}\pi}\left(1-\mathrm{e}^{-2\mathrm{i}\pi T\nu}\right)\cdot \underbrace{\sum_{k=-\infty}^{\infty}\frac{1}{(q-k)}}_{\underbrace{\frac{1}{q}+\sum_{k=1}^{\infty}\frac{1}{q-k}+\underbrace{\sum_{k=-\infty}^{-1}\frac{1}{q-k}}_{\sum_{k=1}^{\infty}\frac{1}{q+k}}}_{\pi\cot(\pi q)}} \\ &= \frac{1}{2\mathrm{i}}\left(1-\mathrm{e}^{-2\mathrm{i}\pi T\nu}\right)\cot\left(\pi\nu\Delta t\right). \end{aligned} \tag{2.24}$$

Alternatively this can be written as a product (Eq. 2.7):

$$\mathrm{RD}(\nu) = \frac{1}{2\mathrm{i}}\mathrm{e}^{-\mathrm{i}\pi T\nu}\underbrace{\left(\mathrm{e}^{\mathrm{i}\pi T\nu}-\mathrm{e}^{-\mathrm{i}\pi T\nu}\right)}_{=2\mathrm{i}\sin(\pi T\nu)}\cot\left(\pi\nu\Delta t\right) \tag{2.25}$$

$$= \mathrm{e}^{-\mathrm{i}\pi T\nu}\sin(\pi T\nu)\cot\left(\pi\nu\Delta t\right) \tag{2.26}$$

A plot for demonstration is shown in Figure 2.3.

2.3.6.2 Complete expression for the spectrum of a monofrequent sine

The next step is to convolve the former result (Eq. 2.24) with the spectrum of the sine. Taking the symmetry into account (Sec. 2.3.1.1), it is sufficient to take either $\mathrm{S_{neg}}$ or $\mathrm{S_{pos}}$ (Eq. 2.12):

$$\begin{aligned}
&\mathrm{RDS_{pos}}(\nu) \hat{=} \\
\mathrm{RD}(\nu) * \mathrm{S_{pos}}(\nu) &= \left[\frac{1}{2\mathrm{i}}\left(1-\mathrm{e}^{-2\mathrm{i}\pi T\nu}\right)\cdot\cot\left(\pi\nu\Delta t\right)\right] * \left[-\mathrm{i}\frac{A_0}{2}\delta(\nu-\nu_0)\mathrm{e}^{\mathrm{i}\phi_0}\right] \\
&= -\frac{A_0}{4}\mathrm{e}^{\mathrm{i}\phi_0}\left(1-\mathrm{e}^{-2\mathrm{i}\pi T(\nu-\nu_0)}\right)\cdot\cot\left(\pi\Delta t(\nu-\nu_0)\right) && (2.27) \\
&= -\mathrm{i}\frac{A_0}{2}\sin\left(\pi T(\nu-\nu_0)\right)\cdot\cot\left(\pi\Delta t(\nu-\nu_0)\right)\mathrm{e}^{-\mathrm{i}(\pi T(\nu-\nu_0)-\phi_0)} && (2.28)
\end{aligned}$$

The negative frequencies are gained by negating the signs of the sine parameters. The Hann window component ($\mathrm{H}(\nu)$, Sec. 2.3.3) is taken into account by shifting the frequencies corresponding to Equation 2.19:

$$\begin{aligned}
\mathrm{RDS}*\mathrm{H} \hat{=} \mathrm{RDSH}(A_0,\nu_0,\phi_0,\Delta t,T,\nu) = &\\
&-\frac{1}{4}\mathrm{RDS_{pos}}\left(A_0,\ \nu_0,\ \phi_0,\ \Delta t,\ T,\ \nu-\frac{1}{T}\right)\\
&+\frac{1}{2}\mathrm{RDS_{pos}}\left(A_0,\ \nu_0,\ \phi_0,\ \Delta t,\ T,\ \nu\right)\\
&-\frac{1}{4}\mathrm{RDS_{pos}}\left(A_0,\ \nu_0,\ \phi_0,\ \Delta t,\ T,\ \nu+\frac{1}{T}\right)\\
&-\frac{1}{4}\mathrm{RDS_{pos}}\left(-A_0,-\nu_0,-\phi_0,\ \Delta t,\ T,\ \nu-\frac{1}{T}\right)\\
&+\frac{1}{2}\mathrm{RDS_{pos}}\left(-A_0,-\nu_0,-\phi_0,\ \Delta t,\ T,\ \nu\right)\\
&-\frac{1}{4}\mathrm{RDS_{pos}}\left(-A_0,-\nu_0,-\phi_0,\ \Delta t,\ T,\ \nu+\frac{1}{T}\right) && (2.29)\\
&= \mathrm{F_{Mono}}
\end{aligned}$$

This expression is called $\mathrm{F_{Mono}}$ in order to discriminate between different approaches (namely $\mathrm{F_{Erf}}$ and $\mathrm{F_{Sum}}$). This is how it is implemented in the new version of the evaluation software; it means that only one $\mathrm{RDS_{pos}}$ is implemented and called with different arguments; the derivatives and checks for roots of the cotangent term (following sections) are much more elementary.

The following equation shows the full expression as it is implemented in the previous version of the software (`Eval6`), it results from the insertion of Equation 2.28 into Equation

2.29 and using that $e^{\pm i\pi} = -1$.

$$\begin{aligned}
&\mathrm{RDSH}^{\mathrm{Eval}}(A_0, \nu_0, \phi_0, \Delta t, T, \nu) = && (2.30)\\
&\quad i\frac{A_0}{8}\Bigg[\sin\Big(\pi T(\nu+\nu_0)\Big)\Bigg(-\cot\left(\pi\Big(\Delta t\,(\nu+\nu_0)-\frac{1}{N}\Big)\right)\\
&\qquad\qquad +2\cot\Big(\pi\Delta t\,(\nu+\nu_0)\Big)\\
&\qquad\qquad -\cot\left(\pi\Big(\Delta t\,(\nu+\nu_0)+\frac{1}{N}\Big)\right)\Bigg)\cdot e^{-i\left(\pi T(\nu+\nu_0)+\phi_0\right)}\\
&\quad -\sin\Big(\pi T(\nu-\nu_0)\Big)\Bigg(-\cot\left(\pi\Big(\Delta t\,(\nu-\nu_0)-\frac{1}{N}\Big)\right)\\
&\qquad\qquad +2\cot\Big(\pi\Delta t\,(\nu-\nu_0)\Big)\\
&\qquad\qquad -\cot\left(\pi\Big(\Delta t\,(\nu-\nu_0)+\frac{1}{N}\Big)\right)\Bigg)\cdot e^{-i\left(\pi T(\nu-\nu_0)-\phi_0\right)}\Bigg] && (2.31)
\end{aligned}$$

2.3.7 Implementation

There are some facts that need to be taken into account:

- Whereas in highest-level programming languages (such as `Mathematica`), the removable singularity ($\sin(nx)\cot(x)$, Eq. 2.28) can be handled, in C/C++ the function has to be expanded for arguments very close to that position.
- The Levenberg-Marquardt algorithm needs the first derivatives with respect to the parameters for the fitting.

2.3.7.1 Taylor-expansion around the cotangent pole

With $x = \pi\Delta t(\nu - \nu_0)$, the term: $\cot(x) = \frac{\cos(x)}{\sin(x)}$ has a pole at $x = 0$.[4] This is cancelled by the multiplication with $\sin(Nx)$; nevertheless it crashes implementations in `C/C++` and needs to be expanded. It is ([33], p. 81):

$$\sin(Nx) = N\sin(x)\cos^{N-1}(x) - \binom{N}{3}\sin^3(x)\cos^{N-3}(x) + \binom{N}{5}\sin^5(x)\cos^{N-5}(x) \mp \cdots \tag{2.32}$$

Combining it with the fraction for the cotangent term, $\sin(x)$ can be reduced and the exponent of the $\cos(x)$ term is increased by one in every summand.

$$\cos(x)\frac{\sin(Nx)}{\sin(x)} = N\cos^N(x) - \binom{N}{3}\sin^2(x)\cos^{N-2}(x) + \binom{N}{5}\sin^4(x)\cos^{N-4}(x) \mp \cdots \tag{2.33}$$

---

[4] Actually, this singularity is 2π periodical, but for the interval of one spectrum – the interval used in the implementation – it appears only once.

The trigonometric functions can then be developed up to second order:[5]

$$\cos(x)\frac{\sin(Nx)}{\sin(x)} = N\left(1-\frac{x^2}{2}\right)^N - \frac{N(N-1)(N-2)}{6}x^2\left(1-\frac{x^2}{2}\right)^{N-2} + \mathcal{O}(x^4) \tag{2.34}$$

The first summand contains beside the constant expression also N times $1\cdot\frac{x^2}{2}$:[6]

$$\cos(x)\frac{\sin(Nx)}{\sin(x)} \approx N\left(1-\frac{x^2 N}{2}\right) - N\frac{N^2-3N+2}{6}x^2 \tag{2.35}$$

$$\approx N - \frac{1}{6}N\left(N^2+2\right)x^2 \tag{2.36}$$

$$\mathrm{RDS}_{\mathrm{pos}}(\nu) \underset{\nu\to\nu_0}{\approx} \frac{1}{2\mathrm{i}}A_0\mathrm{e}^{-\mathrm{i}(\pi T(\nu-\nu_0)-\phi_0)}\left(N-\frac{1}{6}N\left(N^2+2\right)(\pi\Delta t(\nu-\nu_0))^2\right) \tag{2.37}$$

This replacement is used if the magnitude of the argument of the cotangent is smaller than 10^{-7}.

Taylor series and derivation calculations are all uncomplicated and can easily be calculated by hand or with programmes like `Mathematica`. In the following these calculations are not shown in detail.

2.3.7.2 Derivatives with respect to the parameters

Because of the linearity of the derivatives the same partition (positive and negative frequencies) is valid. ξ is a wild-card variable; this is valid for all parameters:

$$\frac{\mathrm{d}}{\mathrm{d}\xi}\mathrm{RDS}(\nu) = \frac{\mathrm{d}}{\mathrm{d}\xi}\mathrm{RDS}_{\mathrm{pos}}(\nu) + \frac{\mathrm{d}}{\mathrm{d}\xi}\mathrm{RDS}_{\mathrm{neg}}(\nu) \tag{2.38}$$

where analogously to Equation 2.13, $\mathrm{RDS}_{\mathrm{neg}}$ is equal to $\mathrm{RDS}_{\mathrm{pos}}$ with negated signs for the sine parameters. But because of the inner derivatives of the parameters a sign is generated for negative frequencies:

$$\frac{\mathrm{d}}{\mathrm{d}\xi}\mathrm{RDS}_{\mathrm{pos}}(A_0,\nu_0,\phi_0,T,\Delta t,\nu) = -\frac{\mathrm{d}}{\mathrm{d}\xi}\mathrm{RDS}_{\mathrm{neg}}(-A_0,-\nu_0,-\phi_0,T,\Delta t,\nu) \tag{2.39}$$

If the parameters for the negative frequencies are inserted after the derivation, the negation of the derived factors must be ensured.

---

[5] $\sin(x) \underset{x\to 0}{\approx} x$, $\cos(x) \underset{x\to 0}{\approx} \left(1-\frac{x^2}{2}\right)$.

[6] The first summand is $\left(1-\frac{x^2}{2}\right)\cdot\left(1-\frac{x^2}{2}\right)\cdot\left(1-\frac{x^2}{2}\right)\cdot\cdots$. All combinations are permuted, but as soon as more than one time the $\left(\frac{x^2}{2}\right)$ term is chosen the order of the x dependency will be of x^4 or higher. The second summand is a priori of order x^2 therefore only the $1\cdot 1\cdot 1\cdots$ case needs to be taken into account here.

For the derivative with respect to the frequency this substitute is used:

$$x = \pi\Delta t(\nu - \nu_0) \tag{2.40}$$

$$\frac{\mathrm{d}}{\mathrm{d}\nu_0}\mathrm{RDS}_{\mathrm{pos}}(x) = \frac{1}{2}A_0\pi T\mathrm{e}^{\mathrm{i}\phi_0}\left(\mathrm{ie}^{-\mathrm{i}2xN}\cot(x) - \frac{1-\mathrm{e}^{-\mathrm{i}2xN}}{2N\sin^2(x)}\right) \tag{2.41}$$

$$\frac{\mathrm{d}}{\mathrm{d}\nu_0}\mathrm{RDS}_{\mathrm{pos}}(x) \underset{x\to 0}{=} -\frac{1}{6}A_0\pi T\mathrm{e}^{\mathrm{i}\phi_0}(-3N + \mathrm{i}2(1+2N^2)x + 3(N+N^2)x^2) \tag{2.42}$$

$$\frac{\mathrm{d}}{\mathrm{d}A_0}\mathrm{RDS}_{\mathrm{pos}}(\nu) = \frac{1}{A_0}\,\mathrm{RDS}_{\mathrm{pos}}(\nu) \tag{2.43}$$

$$\frac{\mathrm{d}}{\mathrm{d}\phi_0}\mathrm{RDS}_{\mathrm{pos}}(\nu) = \mathrm{i}\,\mathrm{RDS}_{\mathrm{pos}}(\nu) \tag{2.44}$$

In Equation 2.41 both the cotangent and the squared reciprocal sine diverge in the same order but with opposed signs for small arguments. Therefore, their sum forms a removable singularity which is dealt with by Taylor series expansion. By feeding the derivative to `Mathematica, Series[]`, $x \to 0$ and limiting it to the second order, an equivalent to the approximation given is gained.

2.4 Advancing to the spectrum of a sine with linear frequency shift

The calculations to be done are the same as for a monofrequent sine except for the sine term itself; $\mathrm{s}(t)$ is expanded by a term changing the frequency linearly in time:

$$\hat{\mathrm{s}}(A_0, b_0, \nu_0, \phi_0, t) = A_0 \sin\left(2\pi\left(\frac{b_0}{2}\cdot t + \nu_0\right)\cdot t + \phi_0\right). \tag{2.45}$$

An example is shown in Figure 2.4. The spectrum of the continuous time-domain signal is not shown because it obviously runs through all frequencies if the time interval is not limited to a certain interval. Analogously to Equation 2.19, the wanted expression $\hat{\mathrm{S}}\mathrm{RHD}(\nu)$ is therefore assembled as:

$$\hat{\mathrm{s}}\mathrm{rhd}(t) = \hat{\mathrm{s}}(t)\cdot\mathrm{r}(t)\cdot\mathrm{h}(t)\cdot\mathrm{d}(t) \circ\!\!-\!\!\!-\; \hat{\mathrm{S}}\mathrm{RHD}(\nu) = \hat{\mathrm{S}}(\nu) * \mathrm{R}(\nu) * \mathrm{H}(\nu) * \mathrm{D}(\nu). \tag{2.46}$$

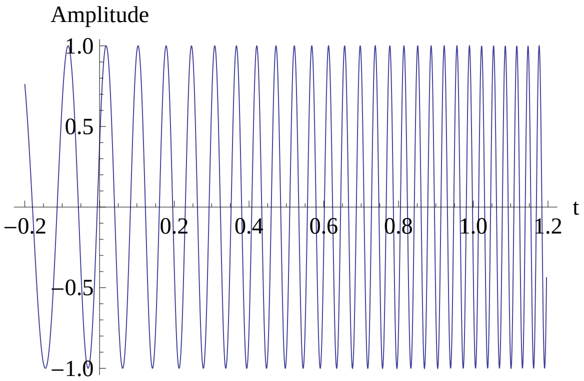

Figure 2.4: Demonstration of a section of an LFS sine in the time domain with the parameters: $A_0 = 1.0$, $\nu_0 = 10.5\,\mathrm{Hz}$, $b_0 = 20.0\,{}^{\mathrm{Hz}}/_{\mathrm{s}}$, $\phi_0 = {}^{\pi}/_{8}$.

2.4.1 Spectrum of an LFS sine limited by a rectangle

The consideration of the rectangle function can be done by adaptation of the limits of the Fourier integral (Eq. 2.4). The spectrum of the sine (Eq. 2.45) limited to the rectangle from 0 to T (Sec. 2.3.2) is:

$$\hat{\mathrm{S}}\mathrm{R}(\nu) \mathrel{\hat{=}} \hat{\mathrm{S}}(\nu) * \mathrm{R}(\nu) \circ\!\!-\!\!-\, \hat{\mathrm{s}}(t) \cdot \Pi\left(\frac{t}{T} - \frac{1}{2}\right) \tag{2.47}$$

$$\hat{\mathrm{S}}\mathrm{R}(\nu) = \int_0^T A_0 \sin\left(\pi b_0 t^2 + 2\pi\nu_0 t + \phi_0\right) \mathrm{e}^{-\mathrm{i}2\pi\nu t}\,\mathrm{d}t. \tag{2.48}$$

With Equation 2.7 the sine is written as a sum of two exponential functions and analogously to Section 2.3.1.1 each of the summands can be assigned to form a peak which is located at positive or negative frequencies. The symmetry allows the calculation to be done with either the positive or the negative term. In this case it is shown for the positive one. Because of a slightly different way of calculation the negative one is also shown in the appendix (Sec. A.1.1).

$$\hat{\mathrm{S}}\mathrm{R}(\nu) = \underbrace{\frac{A_0}{2\mathrm{i}} \int_0^T \mathrm{e}^{\mathrm{i}\left(\pi b_0 t^2 + 2\pi(\nu_0 - \nu)t + \phi_0\right)} \mathrm{d}t}_{\hat{\mathrm{S}}\mathrm{R}_{\mathrm{pos}}(\nu)} \underbrace{- \frac{A_0}{2\mathrm{i}} \int_0^T \mathrm{e}^{-\mathrm{i}\left(\pi b_0 t^2 + 2\pi(\nu_0 + \nu)t + \phi_0\right)} \mathrm{d}t}_{\hat{\mathrm{S}}\mathrm{R}_{\mathrm{neg}}(\nu)} \tag{2.49}$$

$$\hat{\mathrm{S}}\mathrm{R}_{\mathrm{pos}}(\nu) = \frac{A_0}{2\mathrm{i}} \int_0^T \cos\left(\pi b_0 t^2 + 2\pi(\nu_0 - \nu)t + \phi_0\right) + \mathrm{i}\sin\left(\pi b_0 t^2 + 2\pi(\nu_0 - \nu)t + \phi_0\right) \mathrm{d}t \tag{2.50}$$

With $a = \pi b_0$, $b = \pi(\nu_0 - \nu)$, $c = \phi_0$:

$$\hat{\mathrm{S}}\mathrm{R}_{\mathrm{pos}}(\nu) = \frac{A_0}{2\mathrm{i}} \int_0^T \cos\left(at^2 + 2bt + c\right) + \mathrm{i}\sin\left(at^2 + 2bt + c\right) \mathrm{d}t \tag{2.51}$$

These are Fresnel integrals. In [34] helpful solutions are given: Equation 7.4.38:

$$\begin{aligned}\int \cos\left(ax^2+2bx+c\right)\mathrm{d}x \\ =\sqrt{\frac{\pi}{2a}}\Bigg(\cos\left(\frac{b^2-ac}{a}\right)\mathrm{C}\left[\sqrt{\frac{2}{a\pi}}(ax+b)\right] \\ +\sin\left(\frac{b^2-ac}{a}\right)\mathrm{S}\left[\sqrt{\frac{2}{a\pi}}(ax+b)\right]\Bigg)+\text{const}\end{aligned} \tag{2.52}$$

c can be shifted by $\frac{\pi}{2}$ or [34, Eq. 7.4.39] can be used directly:

$$\begin{aligned}\int \sin\left(ax^2+2bx+c\right)\mathrm{d}x \\ =\sqrt{\frac{\pi}{2a}}\Bigg(\cos\left(\frac{b^2-ac}{a}\right)\mathrm{S}\left[\sqrt{\frac{2}{a\pi}}(ax+b)\right] \\ -\sin\left(\frac{b^2-ac}{a}\right)\mathrm{C}\left[\sqrt{\frac{2}{a\pi}}(ax+b)\right]\Bigg)+\text{const}\end{aligned} \tag{2.53}$$

in which [34, Eq. 7.3.1]:

$$\mathrm{C}[z]=\int_0^z \cos\left(\frac{\pi}{2}t^2\right)\mathrm{d}t \tag{2.54}$$

and [34, Eq. 7.3.2]:

$$\mathrm{S}[z]=\int_0^z \sin\left(\frac{\pi}{2}t^2\right)\mathrm{d}t. \tag{2.55}$$

These can be combined into an error-function expression [34, Eq. 7.3.22]:

$$\mathrm{C}[z]+\mathrm{i}\mathrm{S}[z]=\frac{1+\mathrm{i}}{2}\mathrm{Erf}\left[\frac{\sqrt{\pi}}{2}(1-\mathrm{i})\,z\right]. \tag{2.56}$$

The insertion of the solutions for the integrals (Equations 2.52 and 2.53) converts Equation 2.51 into:

$$\begin{aligned}\hat{\mathrm{S}}\mathrm{R}_{\mathrm{pos}}(\nu)=\frac{A_0}{2\mathrm{i}}\sqrt{\frac{\pi}{2a}}\Bigg(\\ \cos\left(\frac{b^2-ac}{a}\right)\mathrm{C}\left[\sqrt{\frac{2}{a\pi}}(ax+b)\right]_0^T+\sin\left(\frac{b^2-ac}{a}\right)\mathrm{S}\left[\sqrt{\frac{2}{a\pi}}(ax+b)\right]_0^T \\ +\mathrm{i}\cos\left(\frac{b^2-ac}{a}\right)\mathrm{S}\left[\sqrt{\frac{2}{a\pi}}(ax+b)\right]_0^T-\mathrm{i}\sin\left(\frac{b^2-ac}{a}\right)\mathrm{C}\left[\sqrt{\frac{2}{a\pi}}(ax+b)\right]_0^T\Bigg),\end{aligned} \tag{2.57}$$

$$
\begin{aligned}
\hat{\mathrm{S}}\mathrm{R}_{\mathrm{pos}}(\nu) = & \frac{A_0}{2\mathrm{i}}\sqrt{\frac{\pi}{2a}}\Bigg(\\
& \cos\left(\frac{b^2-ac}{a}\right)\left(\mathrm{C}\left[\sqrt{\frac{2}{a\pi}}(aT+b)\right]-\mathrm{C}\left[\sqrt{\frac{2}{a\pi}}b\right]+\mathrm{iS}\left[\sqrt{\frac{2}{a\pi}}(aT+b)\right]-\mathrm{iS}\left[\sqrt{\frac{2}{a\pi}}b\right]\right) \\
& +\sin\left(\frac{b^2-ac}{a}\right)\left(\mathrm{S}\left[\sqrt{\frac{2}{a\pi}}(aT+b)\right]-\mathrm{S}\left[\sqrt{\frac{2}{a\pi}}b\right]-\mathrm{iC}\left[\sqrt{\frac{2}{a\pi}}(aT+b)\right]+\mathrm{iC}\left[\sqrt{\frac{2}{a\pi}}b\right]\right)\Bigg).
\end{aligned}
\tag{2.58}
$$

Using Equation 2.56:

$$
\begin{aligned}
\hat{\mathrm{S}}\mathrm{R}_{\mathrm{pos}}(\nu) = & \frac{A_0}{2\mathrm{i}}\sqrt{\frac{\pi}{2a}}\Bigg(\\
& \cos\left(\frac{b^2-ac}{a}\right)\left(\frac{1+\mathrm{i}}{2}\mathrm{Erf}\left[\frac{\sqrt{\pi}}{2}(1-\mathrm{i})\sqrt{\frac{2}{a\pi}}(aT+b)\right]-\frac{1+\mathrm{i}}{2}\mathrm{Erf}\left[\frac{\sqrt{\pi}}{2}(1-\mathrm{i})\sqrt{\frac{2}{a\pi}}b\right]\right) \\
& -\mathrm{i}\sin\left(\frac{b^2-ac}{a}\right)\left(\frac{1+\mathrm{i}}{2}\mathrm{Erf}\left[\frac{\sqrt{\pi}}{2}(1-\mathrm{i})\sqrt{\frac{2}{a\pi}}(aT+b)\right]-\frac{1+\mathrm{i}}{2}\mathrm{Erf}\left[\frac{\sqrt{\pi}}{2}(1-\mathrm{i})\sqrt{\frac{2}{a\pi}}b\right]\right)\Bigg).
\end{aligned}
\tag{2.59}
$$

The arguments of cosine and sine function are negated, then they can be combined to an exponential expression:

$$
\hat{\mathrm{S}}\mathrm{R}_{\mathrm{pos}}(\nu) = \frac{A_0}{2\mathrm{i}}\sqrt{\frac{\pi}{2a}}\frac{1+\mathrm{i}}{2}\mathrm{e}^{\mathrm{i}\frac{ac-b^2}{a}}\left(\mathrm{Erf}\left[(1-\mathrm{i})\sqrt{\frac{1}{2a}}(aT+b)\right]-\mathrm{Erf}\left[(1-\mathrm{i})\sqrt{\frac{1}{2a}}b\right]\right).
\tag{2.60}
$$

The substitutes are inserted:

$$
\begin{aligned}
\hat{\mathrm{S}}\mathrm{R}_{\mathrm{pos}}(\nu) = & \frac{A_0}{4}\sqrt{\frac{1}{2b_0}}(1-\mathrm{i})\,\mathrm{e}^{\frac{-\mathrm{i}\pi(\nu_0-\nu)^2}{b_0}+\mathrm{i}\phi_0} \\
& \left(\mathrm{Erf}\left[(1-\mathrm{i})\sqrt{\frac{\pi}{2b_0}}(b_0T+\nu_0-\nu)\right]-\mathrm{Erf}\left[(1-\mathrm{i})\sqrt{\frac{\pi}{2b_0}}(\nu_0-\nu)\right]\right).
\end{aligned}
\tag{2.61}
$$

The complete expression without Hann window function and Dirac comb is:

$$
\begin{aligned}
\hat{\mathrm{S}}\mathrm{R}(\nu) = \hat{\mathrm{S}}\mathrm{R}_{\mathrm{pos}}(\nu)+\hat{\mathrm{S}}\mathrm{R}_{\mathrm{neg}}(\nu) = & \frac{A_0}{4}\sqrt{\frac{1}{2b_0}}(1-\mathrm{i})\Bigg(\\
& \mathrm{e}^{\frac{-\mathrm{i}\pi(\nu_0-\nu)^2}{b_0}+\mathrm{i}\phi_0}\left(\mathrm{Erf}\left[(1-\mathrm{i})\sqrt{\frac{\pi}{2b_0}}(b_0T+\nu_0-\nu)\right]-\mathrm{Erf}\left[(1-\mathrm{i})\sqrt{\frac{\pi}{2b_0}}(\nu_0-\nu)\right]\right) \\
& -\mathrm{e}^{\frac{\mathrm{i}\pi(\nu_0+\nu)^2}{b_0}-\mathrm{i}\phi_0}\left(\mathrm{Erfi}\left[(1-\mathrm{i})\sqrt{\frac{\pi}{2b_0}}(b_0T+\nu_0+\nu)\right]-\mathrm{Erfi}\left[(1-\mathrm{i})\sqrt{\frac{\pi}{2b_0}}(\nu_0+\nu)\right]\right)\Bigg).
\end{aligned}
\tag{2.62}
$$

$\hat{\mathrm{S}}\mathrm{R}_{\mathrm{neg}}$ can also be gained by the symmetry (similar to Sec. 2.3.1.1, a proof is given in Sec. A.1.2):

$$\hat{\mathrm{S}}\mathrm{R}_{\mathrm{neg}}\left(A_0,\nu_0,\phi_0,b_0,T,\Delta t,\nu\right)=\hat{\mathrm{S}}\mathrm{R}_{\mathrm{pos}}\left(-A_0,-\nu_0,-\phi_0,-b_0,T,\Delta t,\nu\right).$$

The convolution with the spectrum of the Hann window function ($\mathrm{H}(\nu)$, Sec. 2.3.3) is conducted by shifts of the ν argument:

$$\begin{aligned}\hat{\mathrm{S}}\mathrm{R}*\mathrm{H}\mathrel{\hat{=}}\hat{\mathrm{S}}\mathrm{RH}(A_0,\nu_0,\phi_0,b_0,T,\Delta t,\nu)=&\\ &-\frac{1}{4}\,\hat{\mathrm{S}}\mathrm{R}\left(A_0,\nu_0,\phi_0,b_0,T,\Delta t,\nu-\frac{1}{T}\right)\\ &+\frac{1}{2}\,\hat{\mathrm{S}}\mathrm{R}\left(A_0,\nu_0,\phi_0,b_0,T,\Delta t,\nu\right)\\ &-\frac{1}{4}\,\hat{\mathrm{S}}\mathrm{R}\left(A_0,\nu_0,\phi_0,b_0,T,\Delta t,\nu+\frac{1}{T}\right)\\ =\mathrm{F}_{\mathrm{Erf}}.&\end{aligned}\tag{2.63}$$

$\mathrm{F}_{\mathrm{Erf}}$ is a name used in the next chapters, it is to be distinguished from $\mathrm{F}_{\mathrm{Sum}}$. The missing convolution with the spectrum of the Dirac comb is not conducted as the infinite sum would remain in the result making it unfeasible to implement in numerical procedures. As an approximation arbitrary numbers of summands according to this infinite sum can be added making this equation arbitrarily precise. A short discussion is given in the appendix (Sec. A.1).

2.4.1.1 Derivatives for the implementation

Similar to Section 2.3.7.2 the derivatives are calculated. This is straightforward usage of the chain rule. The derivative of the Erf function is:

$$\frac{\mathrm{d}}{\mathrm{d}x}\mathrm{Erf}[c\cdot x]=\frac{2}{\sqrt{\pi}}x\mathrm{e}^{-c^2x^2}\tag{2.64}$$

$$
\begin{aligned}
\frac{\mathrm{d}}{\mathrm{d}b_0}\hat{\mathrm{S}}\mathrm{R}_{\mathrm{pos}}(\nu) = \mathrm{i}\,\frac{1}{4}A_0\frac{1}{b_0^2}\mathrm{e}^{\mathrm{i}\phi_0}\left((\nu-\nu_0)-\mathrm{e}^{-\mathrm{i}\pi T(2\nu-2\nu_0-b_0T)}(\nu-\nu_0+b_0T)\right)\\
-\frac{1}{2}\frac{1}{b_0^2}\left(b_0-2\mathrm{i}\pi(\nu-\nu_0)^2\right)\hat{\mathrm{S}}\mathrm{R}_{\mathrm{pos}}(\nu)
\end{aligned}
\tag{2.65}
$$

$$
\frac{\mathrm{d}}{\mathrm{d}\nu_0}\hat{\mathrm{S}}\mathrm{R}_{\mathrm{pos}}(\nu) = \mathrm{i}\frac{A_0}{2b_0}\mathrm{e}^{\mathrm{i}\phi_0}(1-\mathrm{e}^{-\mathrm{i}\pi T(2\nu-2\nu_0-b_0T)})+\mathrm{i}\frac{2\pi}{b_0}(\nu-\nu_0)\,\hat{\mathrm{S}}\mathrm{R}_{\mathrm{pos}}(\nu) \tag{2.66}
$$

$$
\frac{\mathrm{d}}{\mathrm{d}\phi_0}\hat{\mathrm{S}}\mathrm{R}_{\mathrm{pos}}(\nu) = \mathrm{i}\,\hat{\mathrm{S}}\mathrm{R}_{\mathrm{pos}}(\nu) \tag{2.67}
$$

$$
\frac{\mathrm{d}}{\mathrm{d}A_0}\hat{\mathrm{S}}\mathrm{R}_{\mathrm{pos}}(\nu) = \frac{1}{A_0}\hat{\mathrm{S}}\mathrm{R}_{\mathrm{pos}}(\nu) \tag{2.68}
$$

Regarding an implementation, factoring out $\hat{\mathrm{S}}\mathrm{R}_{\mathrm{pos}}$ which is already evaluated brings an advantage regarding the calculation effort.

2.4.1.2 Summary for this approach

The presented results are suitable to fit and subtract sines with linearly changing frequencies. Two major disadvantages should be mentioned:

- At this point the convolution with the Dirac comb is missing because its infinite repetitions of its content would lead to a infinite sum expression (see Sec. 2.3.4) making it inappropriate for applications. However, the single expression converges to zero at its sides so as an approximation one could add some of these repetitions manually in an arbitrary number to compensate the ignored component. A systematic analysis of the rate of convergence and its dependencies on the parameters would be necessary to predict how many repetitions are needed to achieve a certain precision (a brief introduction is given in Sec. A.1.3).

- For $b_0 \to 0$ the differences between the error functions for the peaks at the positive and the negative frequencies (e.g. see Eq. 2.61) also tend to zero and therefore the complete expression does. This is non-physical and an implementation would be necessary to switch to the usage of the monofrequent expression if $b_{0,r}$ is below a certain threshold.

An advantage could be a fast runtime (depending on the added number of repetitions for the Dirac comb).

In the following section an expression is derived that is complete (including the Dirac comb) and is valid for all parameter ranges. In comparison to the runtime, an easier approach is rated as much more important. This expression is used for all applications shown later on this work. Nevertheless the $\mathrm{F}_{\mathrm{Erf}}$ approach could outmatch the complete but slow expression for real applications. An introduction to its application and some plots demonstrating the mentioned disadvantages are given in the appendix (Sec. A.1 incl. subsections).

2.4.2 Complete expression for the LFS sine

This approach changes the order of calculation for $\hat{\mathrm{S}}$RHD (Eq. 2.46). The convolution of the rectangle and the Dirac comb is performed first: $\mathrm{R}(\nu) * \mathrm{D}(\nu) = \mathrm{RD}(\nu)$, this is already described for the monofrequent sine, Equation 2.24. Like in the approaches above, the convolution with the spectrum of the Hann window, $\mathrm{H}(\nu)$, is regarded by summing up shifted arguments at the very end. We will see that the continuous spectrum of the sine ($\hat{\mathrm{S}}(\nu)$, Eq. 2.78) does not exclusively consist of Dirac delta functions (in comparison to $\mathrm{S}(\nu)$, Eq. 2.11) so its convolution with the also continuous function $\mathrm{RD}(\nu)$ has to be performed by solving the integral (Eq. 2.20).

2.4.2.1 The continuous spectrum of an LFS sine

Equation 2.57 can be used with different limits: Instead of a rectangle from 0 to T the general Fourier transform covers the complete real axis. Again the substitutes $a = \pi b_0$, $b = \pi(\nu_0 - \nu)$ and $c = \phi_0$ are used and the evaluation is restricted to positive frequencies:

$$\begin{aligned}\hat{\mathrm{S}}_{\mathrm{pos}}(\nu) = & \frac{A_0}{2\mathrm{i}}\sqrt{\frac{\pi}{2a}}\Bigg(\\ & \cos\left(\frac{b^2-ac}{a}\right)\mathrm{C}\left[\sqrt{\frac{2}{a\pi}}(ax+b)\right]_{-\infty}^{\infty} + \sin\left(\frac{b^2-ac}{a}\right)\mathrm{S}\left[\sqrt{\frac{2}{a\pi}}(ax+b)\right]_{-\infty}^{\infty} \\ & +\mathrm{i}\cos\left(\frac{b^2-ac}{a}\right)\mathrm{S}\left[\sqrt{\frac{2}{a\pi}}(ax+b)\right]_{-\infty}^{\infty} - \mathrm{i}\sin\left(\frac{b^2-ac}{a}\right)\mathrm{C}\left[\sqrt{\frac{2}{a\pi}}(ax+b)\right]_{-\infty}^{\infty}\Bigg).\end{aligned} \tag{2.69}$$

The values at infinity are also given in [34]; Equation 7.3.20:

$$\mathrm{C}(x) \xrightarrow{x\to\infty} \frac{1}{2},\ \mathrm{S}(x) \xrightarrow{x\to\infty} \frac{1}{2} \tag{2.70}$$

and the symmetry relations [34] Equation 7.3.17 are useful:

$$\mathrm{C}[-z] = -\mathrm{C}[z], \mathrm{S}[-z] = -\mathrm{S}[z] \tag{2.71}$$

leading to:

$$\begin{aligned}\hat{\mathrm{S}}_{\mathrm{pos}}(\nu) = & \frac{A_0}{2\mathrm{i}}\sqrt{\frac{\pi}{2a}}\Bigg(\\ & \cos\left(\frac{b^2-ac}{a}\right)\left(\mathrm{C}[\infty]-\mathrm{C}[-\infty]+\mathrm{i}\mathrm{S}[\infty]-\mathrm{i}\mathrm{S}[-\infty]\right) \\ & +\sin\left(\frac{b^2-ac}{a}\right)\left(\mathrm{S}[\infty]-\mathrm{S}[-\infty]-\mathrm{i}\mathrm{C}[\infty]+\mathrm{i}\mathrm{C}[-\infty]\right)\Bigg) \qquad (2.72)\end{aligned}$$

$$= \frac{A_0}{2\mathrm{i}}\sqrt{\frac{\pi}{2a}}\left(\cos\left(\frac{b^2-ac}{a}\right)(1+\mathrm{i})+\sin\left(\frac{b^2-ac}{a}\right)(1-\mathrm{i})\right). \qquad (2.73)$$

The arguments of the trigonometric functions are negated and the imaginary unit i is factored out for the term with the sine in order to combine them to an exponential expression:

$$\hat{\mathrm{S}}_{\mathrm{pos}}(\nu) = \frac{A_0}{2\mathrm{i}}\sqrt{\frac{\pi}{2a}}\left(\cos\left(\frac{ac-b^2}{a}\right)(1+\mathrm{i})+\mathrm{i}\sin\left(\frac{ac-b^2}{a}\right)(1+\mathrm{i})\right) \qquad (2.74)$$

$$= \frac{A_0}{2\mathrm{i}}\sqrt{\frac{\pi}{2a}}(1+\mathrm{i})\,\mathrm{e}^{\mathrm{i}\left(\frac{-b^2}{a}+c\right)}. \qquad (2.75)$$

The expression for the spectrum of a continuous LFS sine for the positive frequencies is gained by insertion of the substitutes:

$$\hat{\mathrm{S}}_{\mathrm{pos}}(\nu) = \frac{A_0}{2}(1-\mathrm{i})\sqrt{\frac{1}{2b_0}}\mathrm{e}^{-\mathrm{i}\frac{\pi(\nu_0-\nu)^2}{b_0}+\mathrm{i}\phi_0}. \qquad (2.76)$$

The calculation for the negative frequencies is very similar. The result is:

$$\hat{\mathrm{S}}_{\mathrm{neg}}(\nu) = \frac{A_0}{2}(1+\mathrm{i})\sqrt{\frac{1}{2b_0}}\mathrm{e}^{\mathrm{i}\frac{\pi(\nu_0+\nu)^2}{b_0}-\mathrm{i}\phi}. \qquad (2.77)$$

$$\hat{\mathrm{S}}(\nu) = \hat{\mathrm{S}}_{\mathrm{neg}}(\nu)+\hat{\mathrm{S}}_{\mathrm{pos}}(\nu) = \frac{A_0}{2}\sqrt{\frac{1}{2b_0}}(1+\mathrm{i})\left(\mathrm{e}^{\mathrm{i}\frac{\pi(\nu_0+\nu)^2}{b_0}-\mathrm{i}\phi}-\mathrm{i}\mathrm{e}^{-\mathrm{i}\frac{\pi(\nu_0-\nu)^2}{b_0}+\mathrm{i}\phi_0}\right) \qquad (2.78)$$

is the spectrum of a general, LFS sine.

2.4.2.2 Sine with rectangle and Dirac comb

Equation 2.78 has to be convolved with the rectangle and the Dirac comb (Eq. 2.24). Again either the positive or negative frequencies can be used:

$$\mathrm{RD}(\nu)*\hat{\mathrm{S}}_{\mathrm{neg}}(\nu) = \left[\frac{1}{2\mathrm{i}}\left(1-\mathrm{e}^{-2\mathrm{i}\pi T\nu}\right)\cdot\cot(\pi\nu\Delta t)\right]*\left[\frac{A_0}{2}\sqrt{\frac{1}{2b_0}}(1+\mathrm{i})\,\mathrm{e}^{\mathrm{i}\frac{\pi(\nu+\nu_0)^2}{b_0}}\mathrm{e}^{-\mathrm{i}\phi_0}\right]. \qquad (2.79)$$

To avoid the later convolution with the cotangent, it is replaced by:

$$\cot(z) = \frac{\cos(z)}{\sin(z)} = \frac{\frac{1}{2}\left(\mathrm{e}^{\mathrm{i}z} + \mathrm{e}^{-\mathrm{i}z}\right)}{\frac{1}{2\mathrm{i}}\left(\mathrm{e}^{\mathrm{i}z} - \mathrm{e}^{-\mathrm{i}z}\right)} = \mathrm{i}\frac{1+\mathrm{e}^{-2\mathrm{i}z}}{1-\mathrm{e}^{-2\mathrm{i}z}}, \tag{2.80}$$

which leads to:

$$\mathrm{RD}(\nu) = \frac{1}{2\mathrm{i}}\left(1-\mathrm{e}^{-2\mathrm{i}\pi T\nu}\right) \cdot \cot\left(\pi\nu\Delta t\right) = \frac{1}{2}\left(1-\mathrm{e}^{-2\mathrm{i}\pi N\Delta t\nu}\right) \cdot \frac{1+\mathrm{e}^{-2\mathrm{i}\pi\nu\Delta t}}{1-\mathrm{e}^{-2\mathrm{i}\pi\nu\Delta t}}. \tag{2.81}$$

The bracket in combination with the denominator forms the geometric series ([33], p. 19):

$$\frac{1-z^N}{1-z} = \sum_{k=0}^{N-1} z^k. \tag{2.82}$$

Temporarily $z = \mathrm{e}^{-2\mathrm{i}\pi\nu\Delta t}$ is substituted:

$$\begin{aligned}
\mathrm{RD}(\nu) = \frac{1}{2}\left(1-z^N\right) \cdot \frac{1+\mathrm{e}^{-2\mathrm{i}\pi\nu\Delta t}}{1-z} &= \frac{1}{2}\left(1+\mathrm{e}^{-2\mathrm{i}\pi\nu\Delta t}\right)\sum_{k=0}^{N-1}\mathrm{e}^{-2\mathrm{i}k\pi\nu\Delta t} \\
&= \frac{1}{2}\left(\sum_{k=0}^{N-1}\mathrm{e}^{-2\mathrm{i}k\pi\nu\Delta t} + \sum_{k=0}^{N-1}\mathrm{e}^{-2\mathrm{i}(k+1)\pi\nu\Delta t}\right) \\
&= \frac{1}{2}\sum_{k=0}^{N-1}\sum_{l=k}^{k+1}\mathrm{e}^{-2\mathrm{i}l\pi\nu\Delta t} && (2.83) \\
&= \frac{1}{2}\left(\sum_{k=0}^{N-1}\mathrm{e}^{-2\mathrm{i}k\pi\nu\Delta t} + \sum_{k=1}^{N}\mathrm{e}^{-2\mathrm{i}k\pi\nu\Delta t}\right) \\
&= \frac{1}{2}\left(1+\mathrm{e}^{-\mathrm{i}2\pi N\nu\Delta t} + 2\sum_{k=1}^{N-1}\mathrm{e}^{-\mathrm{i}2\pi k\nu\Delta t}\right). && (2.84)
\end{aligned}$$

Because it is less computational work to do, Equation 2.84 will be used in the implementation section. For the convolution to be done here, it is reasonable to reduce the terms with ν dependencies (Eq. 2.83).

With $C = \frac{A_0}{4}\sqrt{\frac{1}{2b_0}}(1+\mathrm{i})$ the convolution (Eq. 2.79) is performed:

$$\hat{\mathrm{S}}\mathrm{RD}_{\mathrm{neg}}(\nu) = C \cdot \left[\sum_{k=0}^{N-1}\sum_{l=k}^{k+1} \mathrm{e}^{-2\mathrm{i}l\pi\nu\Delta t}\right] * \left[\mathrm{e}^{\mathrm{i}\frac{\pi(\nu+\nu_0)^2}{b_0}-\mathrm{i}\phi_0}\right] \tag{2.85}$$

$$= \int_{-\infty}^{\infty}\sum_{k=0}^{N-1}\sum_{l=k}^{k+1} C\mathrm{e}^{-2\mathrm{i}l\pi\mu\Delta t+\mathrm{i}\frac{\pi(\nu-\mu+\nu_0)^2}{b_0}-\mathrm{i}\phi_0}\,\mathrm{d}\mu \tag{2.86}$$

$$= \int_{-\infty}^{\infty}\sum_{k=0}^{N-1}\sum_{l=k}^{k+1} C\mathrm{e}^{\mathrm{i}\frac{\pi}{b_0}\left(\mu^2+(-2l\Delta t b_0-2\nu-2\nu_0)\mu\right)}\mathrm{e}^{\mathrm{i}\frac{\pi}{b_0}\left(\nu^2+\nu_0^2+2\nu\nu_0\right)-\mathrm{i}\phi_0}\,\mathrm{d}\mu. \tag{2.87}$$

The last exponential factor is μ independent. Completing the square and substituting $\rho = (-l\Delta t b_0 - \nu - \nu_0)$ leads to:

$$\hat{\mathrm{S}}\mathrm{RD}_{\mathrm{neg}}(\nu) = \sum_{k=0}^{N-1}\sum_{l=k}^{k+1} C\mathrm{e}^{\mathrm{i}\frac{\pi}{b_0}\left(\nu^2+\nu_0^2+2\nu\nu_0-\rho^2\right)-\mathrm{i}\phi_0} \cdot \int_{-\infty}^{\infty}\mathrm{e}^{\mathrm{i}\frac{\pi}{b_0}(\mu+\rho)^2}\,\mathrm{d}\mu \tag{2.88}$$

It is the complex Gaussian integral $(b, c \in \mathbb{R})$:[7]

$$\int_{-\infty}^{\infty} a\mathrm{e}^{\mathrm{i}b(x-c)^2}\,\mathrm{d}x = \frac{(-1)^{\frac{1}{4}}a\sqrt{\pi}}{\sqrt{b}} \tag{2.89}$$

and thus:

$$\hat{\mathrm{S}}\mathrm{RD}_{\mathrm{neg}}(\nu) = \sum_{k=0}^{N-1}\sum_{l=k}^{k+1} C\mathrm{e}^{\mathrm{i}\frac{\pi}{b_0}\left(\nu^2+\nu_0^2+2\nu\nu_0-\rho^2\right)-\mathrm{i}\phi_0} \cdot \sqrt{ib_0}. \tag{2.90}$$

C and ρ are inserted, $\hat{\mathrm{S}}\mathrm{RD}_{\mathrm{neg}}(\nu)$ can be calculated similarly:

$$\hat{\mathrm{S}}\mathrm{RD}_{\mathrm{neg}}(\nu) = \mathrm{i}\frac{1}{4}\cdot A_0 \cdot \mathrm{e}^{-\mathrm{i}\phi_0} \cdot \sum_{k=0}^{N-1}\sum_{l=k}^{k+1} \mathrm{e}^{-\mathrm{i}\pi l\Delta t(l\Delta t b_0+2\nu+2\nu_0)} \tag{2.91}$$

$$\hat{\mathrm{S}}\mathrm{RD}_{\mathrm{pos}}(\nu) = -\mathrm{i}\frac{1}{4}\cdot A_0 \cdot \mathrm{e}^{\ \mathrm{i}\phi_0} \cdot \sum_{k=0}^{N-1}\sum_{l=k}^{k+1} \mathrm{e}^{\ \mathrm{i}\pi l\Delta t(l\Delta t b_0-2\nu+2\nu_0)} \tag{2.92}$$

$$\hat{\mathrm{S}}\mathrm{RD}(\nu) = \hat{\mathrm{S}}\mathrm{RD}_{\mathrm{pos}}(\nu) + \hat{\mathrm{S}}\mathrm{RD}_{\mathrm{neg}}(\nu) \tag{2.93}$$

where

$$\hat{\mathrm{S}}\mathrm{RD}_{\mathrm{neg}}(A_0, \nu_0, b_0, \phi_0, \nu) \mathrel{\hat{=}} \hat{\mathrm{S}}\mathrm{RD}_{\mathrm{pos}}(-A_0, -\nu_0, -b_0, -\phi_0, \nu). \tag{2.94}$$

The complete spectrum results by convolving this result with the spectrum of the Hann window (Eq. 2.19); an example for single summands and the complex sum is given in Figure 2.5.

---

[7] Can also be solved if represented as combination of Fresnel integrals; [33, p. 718]

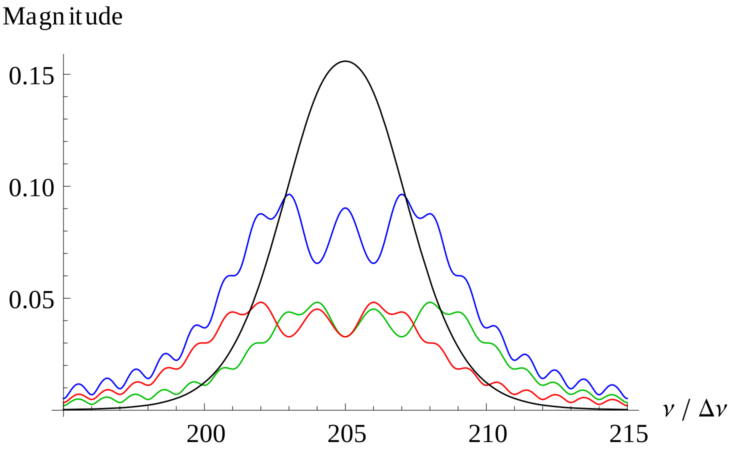

Figure 2.5: Example plot of the summands and the sum corresponding to the application of the Hann window function, shown are the respective magnitudes. $N = 512$, $\Delta t = (1/N)\,\mathrm{s}$, thus $T = 1.0\,\mathrm{s}$ and $\Delta\nu = 1.0\,\mathrm{Hz}$; $A_0 = 1.0$, $\nu_0 = 200.0\,\mathrm{Hz}$, $\phi_0 = 0.0$ and $b_0 = 10.0\,\mathrm{Hz/s}$. Colour codes for the summands: green: $\nu - 1/T$, red: $\nu + 1/T$, blue: ν. The sum of the three complex summands is given in black.

$$
\begin{aligned}
\hat{\mathrm{S}}\mathrm{RD} * \mathrm{H} \mathrel{\hat{=}} \hat{\mathrm{S}}\mathrm{RDH}(A_0,\nu_0,\phi_0,b_0,T,\Delta t,\nu) = \\
&-\frac{1}{4}\,\hat{\mathrm{S}}\mathrm{RD}_{\mathrm{pos}}\left(\ A_0,\ \ \nu_0,\ \ \phi_0,\ \ b_0,\ \ \Delta t,\ \ T,\ \ \nu-\frac{1}{T}\ \right)\\
&+\frac{1}{2}\,\hat{\mathrm{S}}\mathrm{RD}_{\mathrm{pos}}\left(\ A_0,\ \ \nu_0,\ \ \phi_0,\ \ b_0,\ \ \Delta t,\ \ T,\ \ \nu\ \right)\\
&-\frac{1}{4}\,\hat{\mathrm{S}}\mathrm{RD}_{\mathrm{pos}}\left(\ A_0,\ \ \nu_0,\ \ \phi_0,\ \ b_0,\ \ \Delta t,\ \ T,\ \ \nu+\frac{1}{T}\ \right)\\
&-\frac{1}{4}\,\hat{\mathrm{S}}\mathrm{RD}_{\mathrm{pos}}\left(-A_0,-\nu_0,-\phi_0,-b_0,\ \ \Delta t,\ \ T,\ \ \nu-\frac{1}{T}\ \right)\\
&+\frac{1}{2}\,\hat{\mathrm{S}}\mathrm{RD}_{\mathrm{pos}}\left(-A_0,-\nu_0,-\phi_0,-b_0,\ \ \Delta t,\ \ T,\ \ \nu\ \right)\\
&-\frac{1}{4}\,\hat{\mathrm{S}}\mathrm{RD}_{\mathrm{pos}}\left(-A_0,-\nu_0,-\phi_0,-b_0,\ \ \Delta t,\ \ T,\ \ \nu+\frac{1}{T}\ \right)\\
&= \mathrm{F}_{\mathrm{Sum}}
\end{aligned}
\tag{2.95}
$$

This expression contains all components of the theoretical function thus it is perfectly accurate and precise. For large N it takes some computational effort especially if numerous values (for bigger b_0) are fitted or a complete theoretical spectrum with some 1,000 values is calculated. For the implementation used for this work, the latter is accelerated by calculating the FFT of the time-domain signal of that sine.

2.4.3 Implementation

As mentioned above computation effort can be reduced by avoiding the same calculation done multiple times; it is reasonable to solve the inner sum of Equation 2.92 analogously to Equation 2.84 by extracting the summands occurring twice:

$$\hat{\mathrm{S}}\mathrm{RD}_{\mathrm{pos}} = -\mathrm{i}\frac{1}{4}\cdot A_0 \mathrm{e}^{\mathrm{i}\phi_0} \sum_{k=0}^{N-1} \left(\mathrm{e}^{\mathrm{i}\pi k\Delta t(k\Delta t b_0 - 2\nu + 2\nu_0)} + \mathrm{e}^{\mathrm{i}\pi (k+1)\Delta t((k+1)\Delta t b_0 - 2\nu + 2\nu_0)} \right) \tag{2.96}$$

$$= -\mathrm{i}\frac{1}{4}\cdot A_0 \mathrm{e}^{\mathrm{i}\phi_0} \left(1 + 2\sum_{k=1}^{N-1} \mathrm{e}^{\mathrm{i}\pi k\Delta t(k\Delta t b_0 - 2\nu + 2\nu_0)} + \mathrm{e}^{\mathrm{i}\pi N\Delta t(N\Delta t b_0 - 2\nu + 2\nu_0)} \right). \tag{2.97}$$

2.4.3.1 Derivatives

As mentioned above (Sec. 2.3.7.2): When using the expressions for the positive frequencies to calculate the derivatives and then utilise the symmetry to gain the ones for the negative frequencies, the sign must be changed because of the inner derivative of the parameter (which is always -1).

$$\frac{\mathrm{d}}{\mathrm{d}A_0}\hat{\mathrm{S}}\mathrm{RD}_{\mathrm{pos}} = \frac{\hat{\mathrm{S}}\mathrm{RD}_{\mathrm{pos}}}{A_0} \tag{2.98}$$

$$\frac{\mathrm{d}}{\mathrm{d}\nu_0}\hat{\mathrm{S}}\mathrm{RD}_{\mathrm{pos}} = \pi\Delta t A_0 \mathrm{e}^{\mathrm{i}\phi_0} \left(\sum_{k=1}^{N-1} k\mathrm{e}^{\mathrm{i}\pi k\Delta t(k\Delta t b_0 - 2\nu + 2\nu_0)} + \frac{N}{2}\mathrm{e}^{\mathrm{i}\pi N\Delta t(N\Delta t b_0 - 2\nu + 2\nu_0)} \right) \tag{2.99}$$

$$\frac{\mathrm{d}}{\mathrm{d}b_0}\hat{\mathrm{S}}\mathrm{RD}_{\mathrm{pos}} = \frac{1}{4}\pi\Delta t^2 A_0 \mathrm{e}^{\mathrm{i}\phi_0} \left(2\sum_{k=1}^{N-1} k^2\Delta t^2\mathrm{e}^{\mathrm{i}\pi k\Delta t(k\Delta t b_0 - 2\nu + 2\nu_0)} + N^2\mathrm{e}^{\mathrm{i}\pi N\Delta t(N\Delta t b_0 - 2\nu + 2\nu_0)} \right) \tag{2.100}$$

$$\frac{\mathrm{d}}{\mathrm{d}\phi_0}\hat{\mathrm{S}}\mathrm{RD}_{\mathrm{pos}} = \mathrm{i}\,\hat{\mathrm{S}}\mathrm{RD}_{\mathrm{pos}} \tag{2.101}$$

2.4.3.2 Substitutes for an efficient implementation

Every expression used more than once should be calculated in advance.[8]

The colours mark different levels where a certain value can be calculated; green is a marker for values that need to be calculated only once per spectrum: $\tau = \pi\Delta t$, blue marks parameter dependency: $d = 2(\nu_0 - \nu)$, $\beta = \Delta t b_0$, $r = \frac{1}{4}A_0\mathrm{e}^{\mathrm{i}\phi_0}$ and red values have to be calculated every summation step: $\kappa = \mathrm{e}^{\mathrm{i}k\tau(k\beta + d)}$. In a second step the following

---

[8] i is not treated as a factor, as its implementation consists of setting the value as imaginary part of a number.

parameters are calculated: $\epsilon = \mathrm{e}^{\mathrm{i}N\tau(N\beta+d)}$, $q = 2\tau$, $p = \tau\Delta t$, leading to:

$$\hat{\mathrm{S}}\mathrm{RD}_{\mathrm{pos}} = -\mathrm{i}\, r \left(1 + 2\sum_{k=1}^{N-1} \kappa + \epsilon\right) \tag{2.102}$$

$$\frac{\mathrm{d}}{\mathrm{d}A_0}\hat{\mathrm{S}}\mathrm{RD}_{\mathrm{pos}} = \frac{\hat{\mathrm{S}}\mathrm{RD}_{\mathrm{pos}}}{A_0} \tag{2.103}$$

$$\frac{\mathrm{d}}{\mathrm{d}\nu_0}\hat{\mathrm{S}}\mathrm{RD}_{\mathrm{pos}} = r\left(2q\sum_{k=1}^{N-1} k\kappa + Nq\epsilon\right) \tag{2.104}$$

$$\frac{\mathrm{d}}{\mathrm{d}b_0}\hat{\mathrm{S}}\mathrm{RD}_{\mathrm{pos}} = r\left(2p\sum_{k=1}^{N-1} k^2\kappa + N^2 p\epsilon\right) \tag{2.105}$$

$$\frac{\mathrm{d}}{\mathrm{d}\phi_0}\hat{\mathrm{S}}\mathrm{RD}_{\mathrm{pos}} = \mathrm{i}\,\hat{\mathrm{S}}\mathrm{RD}_{\mathrm{pos}}. \tag{2.106}$$

2.5 Further Remarks

Beneath the monofrequent approach (Sec. 2.3.7), the equations given in the last section (Sec. 2.4.3.2) are the ones implemented and used for any application described in the following chapters. Nevertheless some additional insights in these calculations are informative – like alternative representations or the limit case for $b_0 \to 0$ – and given in the appendix (Sec. A.2).

Chapter 3

Evaluation of the expressions

3.1 Introduction

3.1.1 Number of samples per spectrum

In this work a very easy implementation of the Fast Fourier Transform is used ([30], ported from Pascal to C/C++) requiring the number of samples used to calculate a spectrum to be $N = 2^n$ with $n \in \mathbb{N}_+$. For this work a few hundred up to several thousand samples are typically used. The number must not be too small: The following considerations will fail if N is chosen to be ≤ 2 for example.

3.1.2 Periodogram and Hann window normalisation

The peak height in a spectrum should represent the power in a certain frequency band. In particular, for a stationary signal it should be independent of N. A representation fulfilling this requirement is called periodogram [18, p. 212ff]. Additionally the multiplication with the Hann window function decreases the time domain values. This "energy loss" is approximately compensated by dividing the values (in the time domain before or in the frequency domain after the FFT) by the area under the Hann function. Therefore, all functions derived in Chapter 2 are multiplied with

$$f_{\text{Norm}} = \frac{\sqrt{\frac{3}{8}}}{N} \tag{3.1}$$

in the implemented procedure.

3.1.3 Coordinate transformation to unitless numbers

In general the curve progression in a spectrum (resp. the values in the array of the discrete Fourier transform) depends on the number of discrete values used for the DFT and the density of samples with respect to the progression of the signal in the time domain but is independent of the absolute time and sampling rate.[1] This means that scaling in the time domain is allowed as long as the frequency domain is adapted accordingly. For the next sections it is reasonable to divide all frequency variables by $\Delta\nu$ and thus all time variables by T, the proof that this scaling combination is allowed is done in Equation 3.2. The major advantage is that the parameters ν_0 and b_0 become independent of the DFT specific parameter $\Delta\nu$. Another advantage is that dependencies with respect to the discrete raster become easily observable.

Let r be the "continuous index" in the frequency domain. The available discrete values are located at $r = i \cdot \Delta\nu$ with $i \in \mathbb{N} \mid 0 \leq i < N$.[2] A certain frequency can be located anywhere between two discrete values: The digits before the decimal point now give the information between which ones it is located exactly. The digits after the decimal point describe how far it is to the closest discrete frequency.

The following transformed variables are used (it is: $\Delta\nu \cdot T = 1$ (Eq. 2.3)):

- $\nu_{0,r} = \frac{\nu_0}{\Delta\nu}$
- Because the unit of b_0 is frequency per time it has to be divided by $\frac{\Delta\nu}{T} = (\Delta\nu)^2 \rightarrow b_{0,r} = \frac{b_0}{(\Delta\nu)^2}$.
- Division of the comb of discrete frequencies by $\Delta\nu$ leads to: $i \cdot \Delta\nu / \Delta\nu = i$ so the scale of the index becomes identical to the one of the frequency ($r \equiv \nu$).
- The time $t_q = \frac{t}{T}$ generally runs from 0 to 1.

The transformation is shown for the sine (Eq. 2.45) and the rectangle (Eq. 2.15); the Hann window function (Eq. 2.16) and the Dirac comb (Eq. 2.18) are transformed analogously to the rectangle – all their t dependencies are divided by T, transforming to t_q.

$$\begin{aligned}
\mathrm{s} \cdot \mathrm{h} \mathrel{\widehat{=}} \mathrm{sh}\left(A_0, b_0, \nu_0, \phi_0, T, t\right) &= A_0 \sin\left(2\pi\left(\nu_0 + \frac{b_0}{2} \cdot t\right) \cdot t + \phi_0\right) \cdot \Pi\left(\frac{t}{T} - \frac{1}{2}\right) \\
&= A_0 \sin\left(2\pi\left(\nu_{0,r} + \frac{b_{0,r}}{2} \cdot t_q\right) t_q + \phi_0\right) \cdot \Pi\left(t_q - \frac{1}{2}\right) \\
&= \mathrm{sh}\left(A_0, b_{0,r}, \nu_{0,r}, \phi_0, 1, t_q\right) \qquad (3.2)
\end{aligned}$$

The mean frequency (and consequently the maximum of the peak in the continuous spectrum) is located at $r_{\mathrm{Max}} = (\nu_{0,r} + {}^{b_{0,r}}/_{2})$. We shall see that peaks in the magnitude spectra are symmetric with respect to the values left and right if $r_{\mathrm{Max}} \in \mathbb{N}$.

---

[1] E.g. the pure values (the amplitudes in a time series) are the same both if a sine with 10 Hz is sampled with 100 Hz and if a sine with 1 MHz is sampled with 10 MHz. Therefore the same applies to its spectrum as long as it is transformed with the same number of samples.

[2] In this work an implementation of the DFT from [30] is used. The negative frequencies are located above the positive ones (indices run from 0 to $\frac{N}{2}$ for the positive frequencies; from $\frac{N}{2}+1$ to $N-1$ for the negative frequencies).

For artificial signals such as the ones in this chapter the DFT parameters can be chosen in such a way that $\Delta\nu = 1\,\text{Hz}$ by setting $\Delta t = \frac{1}{N}\,\text{s}$, in this case the values of the transformed and untransformed parameters are the same anyway.

3.2 Curve progression and parameter dependencies

3.2.1 Some plots for demonstration

Some examples are shown to demonstrate the continuous curve progression of the F_{Sum} expression and the values that are available if the DFT is performed on an array of values calculated from an LFS sine with the same parameters. The plots are limited to the peak in the magnitude spectrum (at positive frequencies) and the surrounding.[3] Figure 3.1 illustrates the magnitude spectrum of a sine fulfilling the property for a symmetric peak ($\nu_{0,r} + b_{0,r}/2 \in \mathbb{N}$). The ordinate presents the magnitude values $|A|$ of the spectrum, the division by N clarifies that the proportionality to the number of samples used for the DFT is cancelled (Parsevals' theorem). Figure 3.2 shows phase spectra:[4] The topmost one belongs to the magnitude spectrum of the previous figure. But also the one in the middle has the same magnitude spectrum because swapping the begin and end frequencies of a time interval keeps the mean frequency the same and does not even change the spectral magnitude. Because of the strong progression between two neighbouring discrete values in the phase spectrum, the symmetry in the discrete values is clearly visible here (compared to the magnitude spectrum, Fig. 3.3). The sine of the last plot is shifted by 0.5 Hz to the right; the discrete points are no longer symmetric.

Figure 3.3 shows two examples demonstrating the influence of b_0 on the spectra. The bigger $|b_0|$ gets, the broader the peak in the magnitude spectrum becomes and the smaller the oscillations caused by spectral leakage become. In the phase spectra, bigger $|b_0|$ make the blue line to be wrapped more often because of the standardisation to $[\pi; -\pi[$.

The phases of the complex spectral values bear valuable information e.g. about the sign of the start value for b_0 (will be used in Sec. 4.6.2) and to estimate the start value for ϕ_0 (Sec. 4.9) but it is very sensitive to small changes of ν_0 and b_0 (e.g. see Fig. 3.2). The next two sections (Sec. 3.2.2 and 3.2.3) show a few systematic plots revealing useful dependencies for the subsequent start parameter estimation.

---

[3] ν_0 is the frequency at the beginning of the time interval. For $b_0 \neq 0\,\text{Hz/s}$ the end frequency after the time interval T is different. The peak has its maximum at the mean frequency in T. As mentioned in Section 3.1.3, in these examples $\Delta\nu$ is chosen to be 1 Hz. Because $T = \frac{1}{\Delta\nu}$ it is 1 s and the mean frequency simply is $\nu_0 + 0.5\,b_0$.

[4] Note that the phases of the complex values vary – there are N phase values in a spectrum with N samples – and are not identical to the initial phase ϕ_0 of the sine. In the following sections the influence of the initial phase parameter ϕ_0 on the phases of the complex values is demonstrated and used for start value estimation later on.

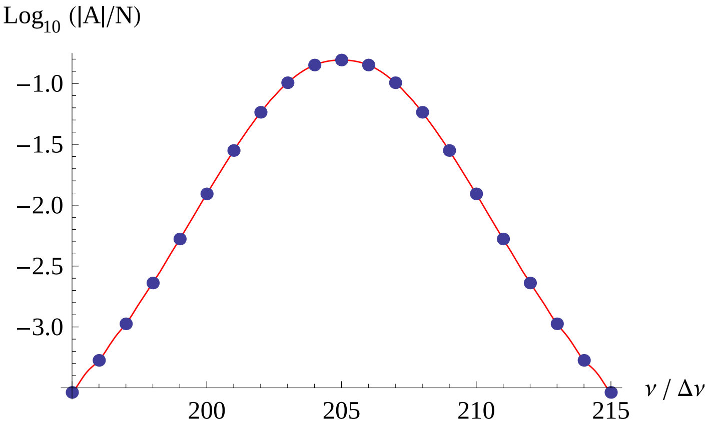

A_0	1.0	
ν_0	200.0	Hz
ϕ_0	0.0	rad
b_0	10.0	$^{\mathrm{Hz}}/_{\mathrm{s}}$
$\Delta\nu$	1.0	Hz

Figure 3.1: Magnitude spectrum of $\mathrm{F}_{\mathrm{Sum}}$ with the given parameters. Here and in the following figures the blue dots show the values known by DFT, the red line shows the continuous function $\mathrm{F}_{\mathrm{Sum}}$.

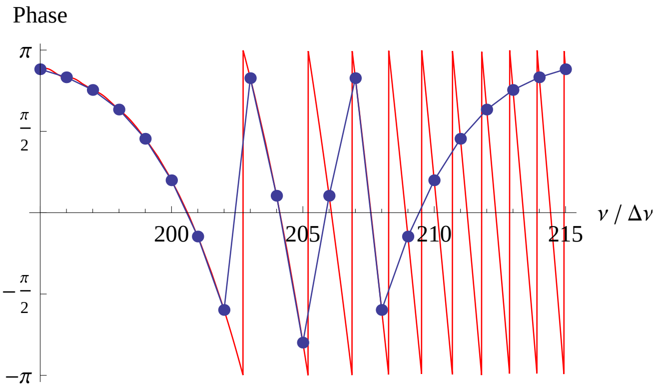

Left: the phase of the complex values of the previous plot (Fig. 3.1). One can recognise that the continuous function decreases monotonously with increasing steepness, but the discrete values (at integer multiples of $\Delta\nu$) are symmetric with regard to the sides of the maximum in the magnitude spectrum at 205.

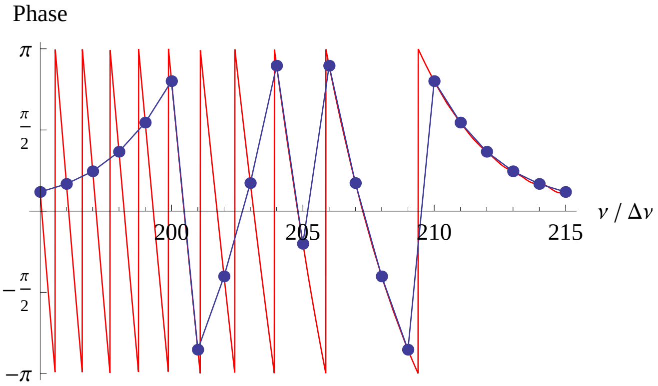

Left: the spectrum after time inversion (not exactly: the ϕ_0 is not set to the end phase of the previous example, but this would only give a constant offset):

A_0	1.0	
ν_0	210.0	Hz
ϕ_0	0.0	rad
b_0	-10.0	$^{\text{Hz}}/_{\text{s}}$
$\Delta\nu$	1.0	Hz

The magnitude spectrum is the same as in Figure 3.1.

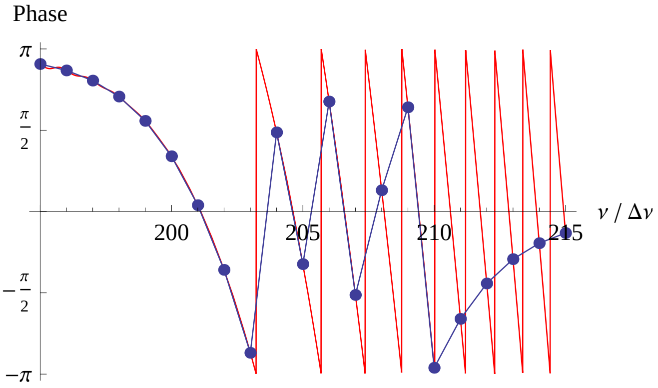

Left: spectrum with slightly different start frequency ν_0 is 200.5 Hz, the other parameters stay the same (b_0 is positive).

Figure 3.2: Plots of the phases of complex spectra.

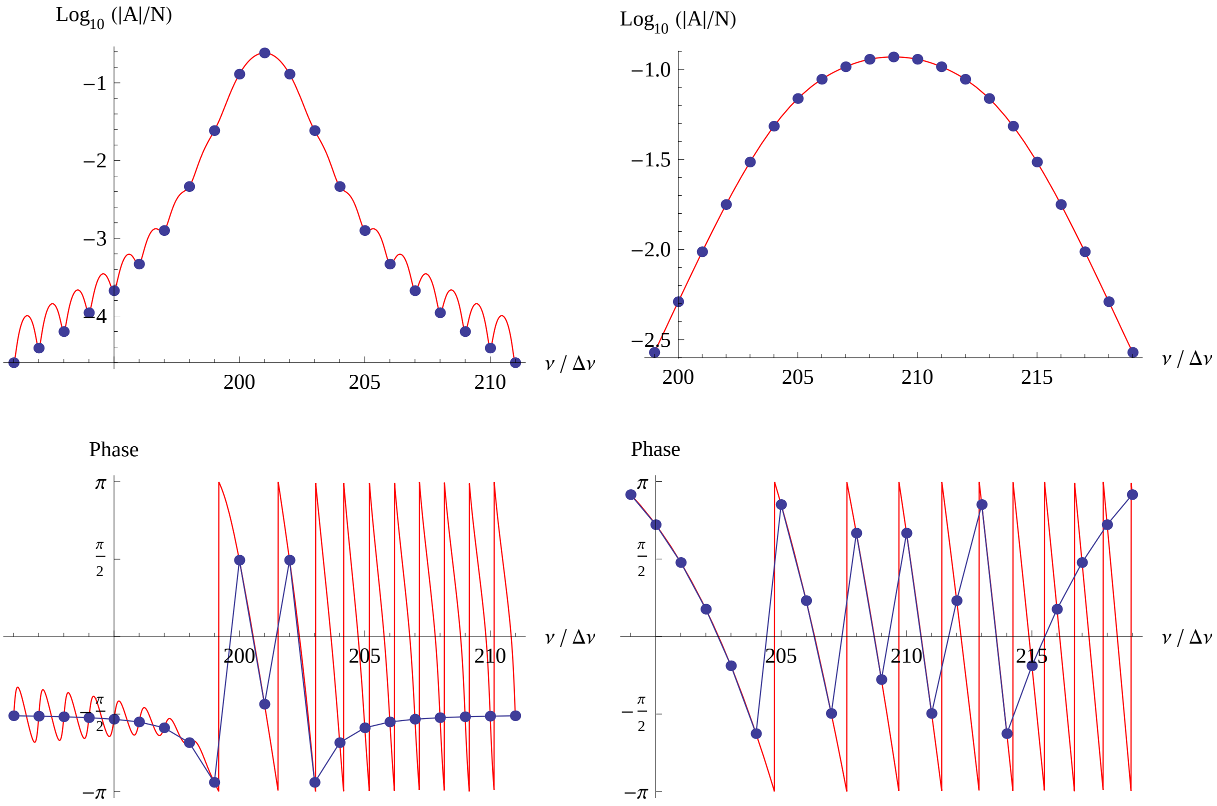

Figure 3.3: Magnitude and phase spectra with two more peak widths. Left column: $A_0 = 1.0$, $\nu_0 = 200.0\,\mathrm{Hz}$, $\phi_0 = 0.5\,\pi$, $b_0 = 2.0\,{}^{\mathrm{Hz}}\!/\mathrm{s}$, $\Delta\nu = 1.0\,\mathrm{Hz}$. Right column: the same but with $b_0 = 18.0\,{}^{\mathrm{Hz}}\!/\mathrm{s}$.

3.2.2 Details on the spectrum of monofrequent sines

Like before, in the following figures parameters are chosen in such a way that $\Delta\nu = 1\,\mathrm{Hz}$, so the discrete frequencies lie exactly on integer values of ν (see Sec. 3.1.3). This also means that the frequency with a value of $(N/2)\,\mathrm{Hz}$ is also the Nyquist frequency ν_{Nyquist}, behind which the negative frequencies begin; further behind $2\cdot\nu_{\mathrm{Nyquist}} = N$ the spectrum is repeated completely. A few more frequencies behind that point are shown here for clarity.

Figure 3.4 shows some interesting facts:

- At the positions of the peak (a), the phases flip three times with exactly π (b)-(d). This behaviour is unique for $b_0 = 0$, for broader peaks the phase changes between two discrete values become smaller (or broader which is the same because of the wrapping to a 2π wide range), see the following section.

- (c) and (d) show the spectrum corresponding to peak located at the positive respectively negative frequencies; their sum is (b). In the separated plots the phases are constant except for the three values at the peak itself and a single π jump exactly $N/2$ points (half of a spectrum) behind the peak.

- The initial phase of the sine, ϕ_0, contributes linearly to the phases of the complex values:[5] Because ν_0 is chosen to be exactly between two discrete values, the phase spectrum (c) does only consist of the values ϕ_0 and $\phi_0 + \pi$ (resp. $-\phi_0$ and $-\phi_0 + \pi$ for (d)).

- (c) and (d) merge smoothly into (b) corresponding to their magnitude spectra: Each magnitude peak is symmetric with monotonous increase/decrease meaning that its weight in the superposition decreases. From some point the weight of the neighbouring peak gets stronger. At the frequencies: $16 \pm n\cdot 32\,\mathrm{Hz}$ and $0 \pm n\cdot 32\,\mathrm{Hz}$ the magnitudes are equal and so the resulting phase is zero because the phase angles have inverted signs at the same absolute value.

Figure 3.5 (a), (b) shows the behaviour of the spectrum if ν_0 is exactly on a discrete frequency. (a) shows the magnitude spectrum with a linear ordinate scale (for reasons of comparability to Fig. 3.4 (a), the following figures have a logarithmic scale), so spectral leakage is hard to see here in general. Anyway, the discrete values (except for the three values of the peaks) lie in the zeros, which is the reason for the random phases (numerical errors) shown in (b).[6] Generally changes in ν_0 shift the continuous curve through the

---

[5] Equations 2.91 and 2.92 show that ϕ_0 does only rotate the spectrum in the complex plane linearly.

[6] The samples for plotting the continuous function are obviously gained without ever hitting $\nu_{\mathrm{Plot\ sample}} = n\cdot\Delta\nu$, where discontinuities occur. Otherwise, the phase of the complex value $0 + \mathrm{i}\cdot 0$ would show the same noisy behaviour at frequencies on the raster like the discrete values that are taken exactly at the points meeting this condition. This could have happened already for the plots on the last figure (Fig. 3.4) as the curve progression is the same (shifted by $0.5\,\Delta\nu$).

raster of discrete frequencies: A comparison of Figure 3.4 (b), and 3.5 (c) shows that the progression of the continuous phase (red curve) has the same progression but is shifted by 0.5 $\Delta\nu$. Figure 3.5 shows a plot done for ν_0 very slightly shifted off the raster making the phases of the discrete values balancing right on a drop by π.

(d) is a demonstration of the influence of N on the phase spectrum; the curve progression is very similar. The Nyquist frequency is half of the spectrum above (c) so the distance to the right between the peak at positive and negative frequencies is reduced. The difference to the left remains the same because the spectral resolution and the frequency of the peak remain. This results in periodic repetitions of regions looking the same as before (e.g. 25-39 Hz).

Note that the height of the highest discrete value of a peak in the magnitude spectrum depends considerably on the distance between ν_0 and the closest frequency of the raster. This fact will be picked up in the upcoming chapters.

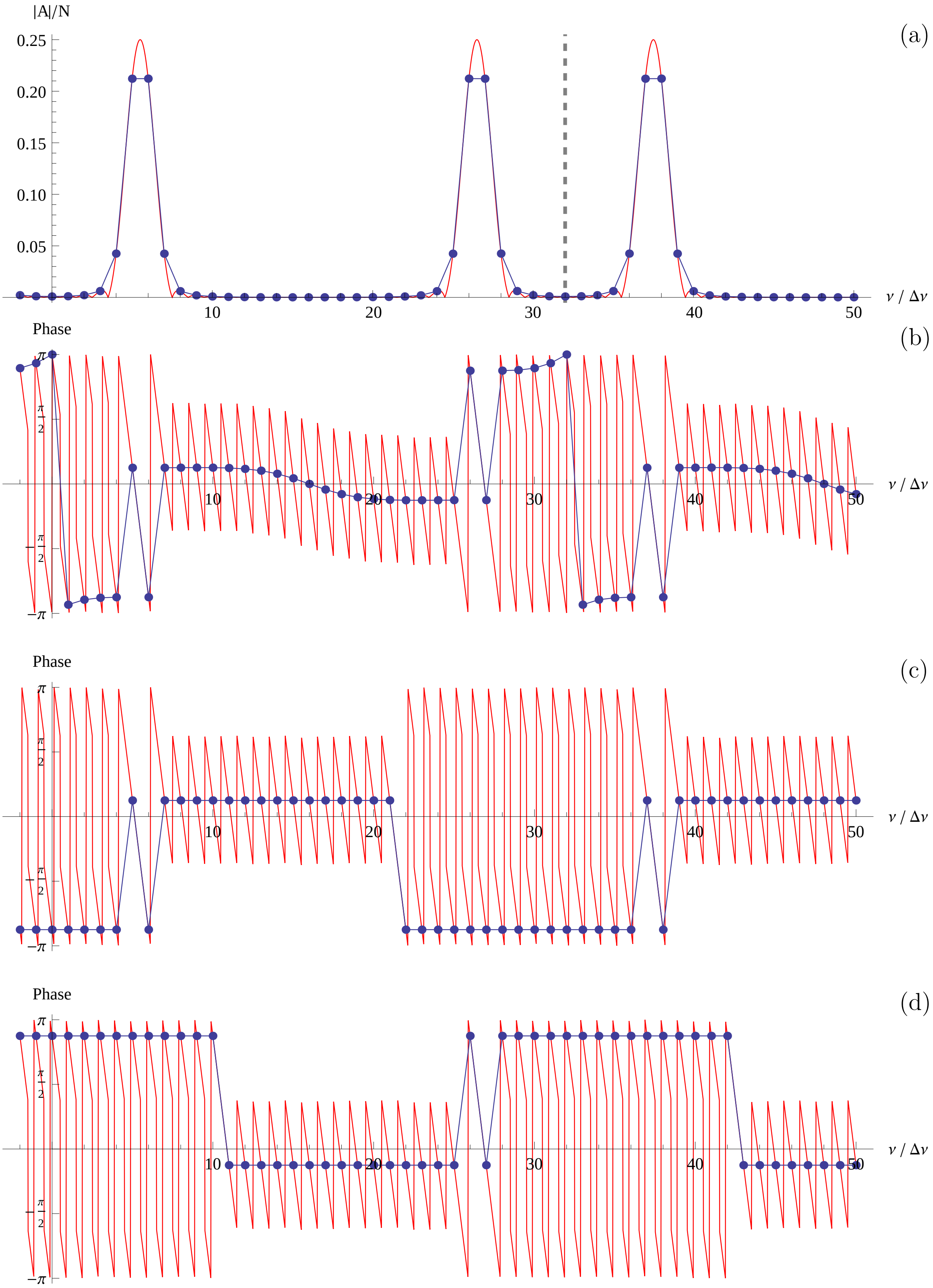

Figure 3.4: (a) gives the absolute values of $\mathrm{F}_{\mathrm{Sum}}$ with the parameters: $A_0 = 1.0$, $\nu_0 = 5.5\,\mathrm{Hz}$, $\phi_0 = {}^{\pi}\!/_{8}$, $b_0 = 0.0\,{}^{\mathrm{Hz}}\!/_{\mathrm{s}}$, $N = 32$, $\Delta t = ({}^{1}\!/_{N})\,\mathrm{s}$; (b) the phase, (c) the phase if only the peak for positive frequencies is taken, (d) respectively with negative frequencies. Note that the spectrum is periodic with period $32\,\Delta\nu$.

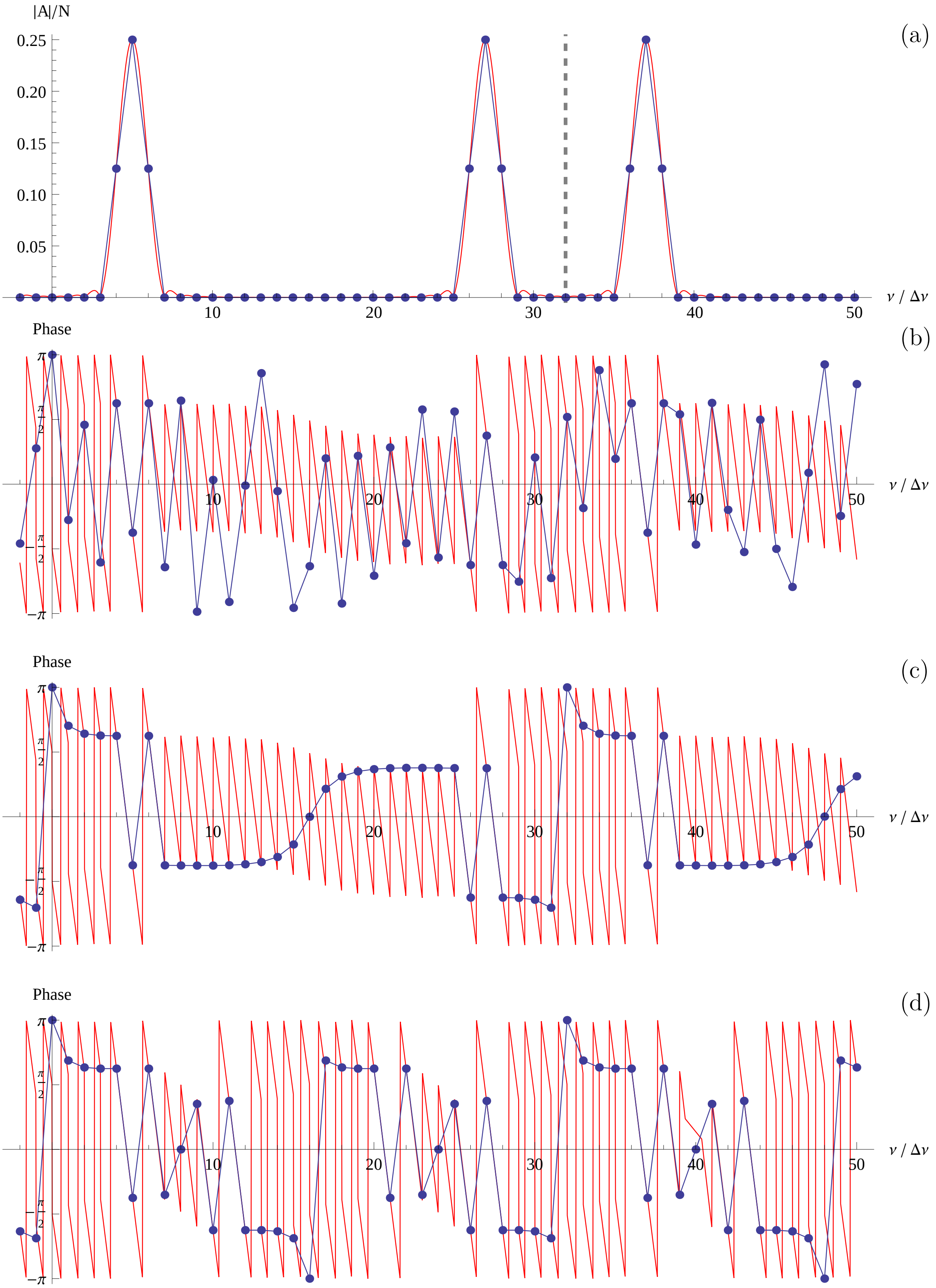

Figure 3.5: (a) gives the absolute values of $\mathrm{F}_{\mathrm{Sum}}$ with the parameters: $A_0 = 1.0$, $\nu_0 = 5.0\,\mathrm{Hz}$, $\phi_0 = {}^{\pi}/_{8}$, $b_0 = 0.0\,{}^{\mathrm{Hz}}/_{\mathrm{s}}$, $N = 32$, $\Delta t = ({}^{1}/_{N})\,\mathrm{s}$; (b) the phase, (c) the phase if $\nu_0 = 5.000000001$, (d) is like (c) with $N = 16$. Note that in (b) the values are caused by numerical noise for magnitudes that should be exactly zero.

3.2.3 Linear frequency shift

In this section only positive b_0 are shown, which simplifies the pairwise comparison. Inverting the sign of b_0 just inverts the curve progression with respect to ν (see Fig. 3.2; the peak in the negative frequencies has inverted signs for the parameters, so every plot shown here for a complete spectrum is also an example for a negative b_0).

Figure 3.6 shows the spectrum of an LFS sine ($\mathrm{F}_{\mathrm{Sum}}$) for symmetric peaks (because $\Delta\nu = 1\,\mathrm{Hz}$, the mean frequency $\nu_0 + {}^1\!/\!{}_2 \cdot b_0/\Delta\nu$ is integer and thus on the raster of discrete frequencies: $n \cdot \Delta\nu$; $n \in \mathbb{N}$). (a) shows its magnitude spectrum. First of all one can observe that the magnitudes never become zero (in contrast to the case when $b_0 = 0$, for $\nu_0 = n \cdot \Delta\nu$, Fig. 3.5 (a)). However, the continuous spectrum indicates that spectral leakage is significant (with growing b_0 the sidelobe peaks get relatively smaller while the peak itself broadens, see magnitude spectra in Fig. 3.3). (b) shows the phase spectrum, the spectra at the bottom are shown for reasons of clarity: (c) contains only the peak at positive frequencies, (d) has a different phase in order to shift most of the values closer to zero to avoid the wrapping at $\pm\pi$. It is important to notice that the phase is never really constant, behind the three peak values the phase smoothly merges into a plateau. Comparing (c) and (d) also illustrates that the progression does not change if the phase parameter is changed; ϕ_0 acts just like an offset to the phases (already mentioned in the last section).

Figure 3.7 shows two more examples of phase spectra for larger b_0. Because of the small N ($= 32$) one can easily recognise how the phase spectra superpose: The phases are weighted with their magnitudes; no matter whether the surrounding peaks of the negative spectrum are present or not, the curve progression close to the peak at positive frequencies looks very similar (compare e.g. (a) and (b) at $\pm 6\,\mathrm{Hz}$).

The larger b_0 becomes the slower the decrease in the change of the phases gets (see Fig. 3.7 (c), (d)). Because the phases are 2π periodic, one can add or subtract an arbitrary integer multiple of 2π. Thus, in (a), one can take the three phases of the discrete values around the first peak (5.0, 6.0, 7.0 Hz) and subtract 2π, analogously 2π can be added to the phases around the peak in the negative frequencies (behind $N/2$); the result is shown in Figure 3.8 (a). The phase spectrum below (fig. 3.7 (c)) is treated in the same manner and is shown in Figure 3.8 (b). If the peaks become broader, multiples of $2\,\pi$ are required to unfold the peak in the phase spectra and the following rule is applied for positive b_0: Subtract multiples of $2\,\pi$ as long as it is smaller than the previous value and as long as the difference to the previous value is smaller than π. For negative b_0 all signs are negated. For the subsequent values the complete rule can be inverted meaning that with differences $\leq \pi$ the phase unfolds similar until it asymptotically reaches the same constant value as previous to the peak. In this way the broad peek, which was already shown in Figure 3.3, is unfolded (c). (d) includes the same spectrum, but here the inversion is omitted – no matter the actual value, (for positive b_0) multiples of $2\,\pi$ are subtracted as long as the current value is smaller than its precursor. The phase continues to drop monotonously to reach asymptotically the constant slope: 2π per $\Delta\nu$.[7] The property, that the phase spectrum (of a peak in the magnitude spectrum) can be unfolded to form a single peak whose direction depends on the sign of the b_0 and that grows with increasing $|b_0|$ will be important to gain the start values (Chap. 4).

---

[7] This means that (for a pure LFS sine signal) around a peak in the magnitude spectrum two neighbouring values never have small phase differences. Note that in magnitude spectra, even equal values can occur by the combination of $\nu_{0,r}$ and $b_{0,r}$ if the theoretical maximum of the peak is exactly between two discrete frequencies.

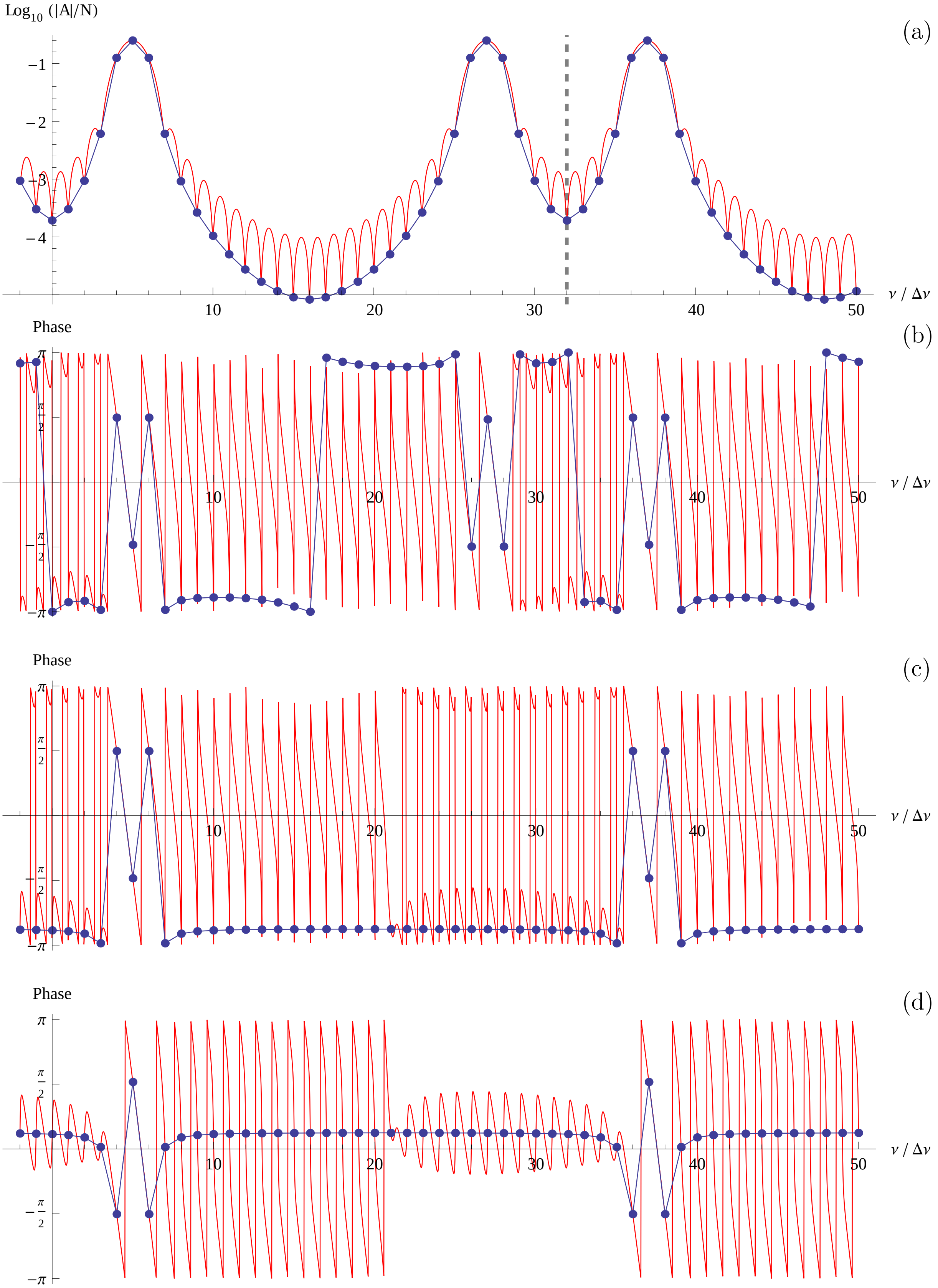

Figure 3.6: (a) gives the absolute values of $\mathrm{F}_{\mathrm{Sum}}$ with the parameters: $A_0 = 1.0$, $\nu_0 = 4.75\,\mathrm{Hz}$, $\phi_0 = {}^{\pi}/_{8}$, $b_0 = 0.5\,{}^{\mathrm{Hz}}/_{\mathrm{s}}$, $N = 32$, $\Delta t = ({}^{1}/_{N})\,\mathrm{s}$; (b) the phase, (c) the phase if only the peak at positive frequencies is used, (d) is like (c) but with $\phi_0 = {}^{9}/_{8}\pi$.

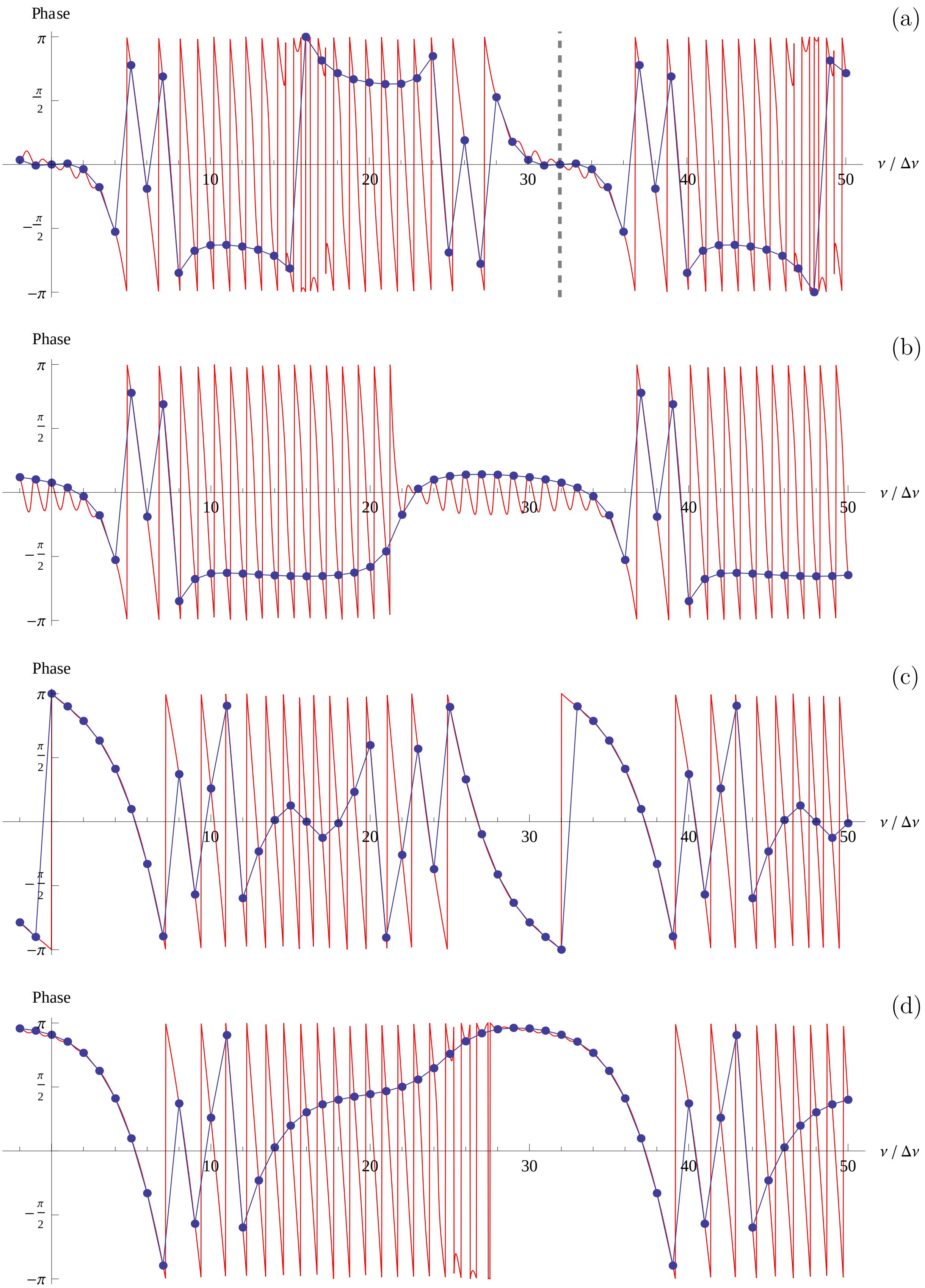

Figure 3.7: (a) gives the phase of $\mathrm{F}_{\mathrm{Sum}}$ with the parameters: $A_0 = 1.0$, $\nu_0 = 4.75\,\mathrm{Hz}$, $\phi_0 = \pi$, $b_0 = 2.0\,{}^{\mathrm{Hz}}\!/_{\mathrm{s}}$, $N = 32$, $\Delta t = ({}^{1}\!/_{N})\,\mathrm{s}$; (b) the phase if only the peak at positive frequencies is used, (c) and (d) are the same but with $b_0 = 8.0\,{}^{\mathrm{Hz}}\!/_{\mathrm{s}}$.

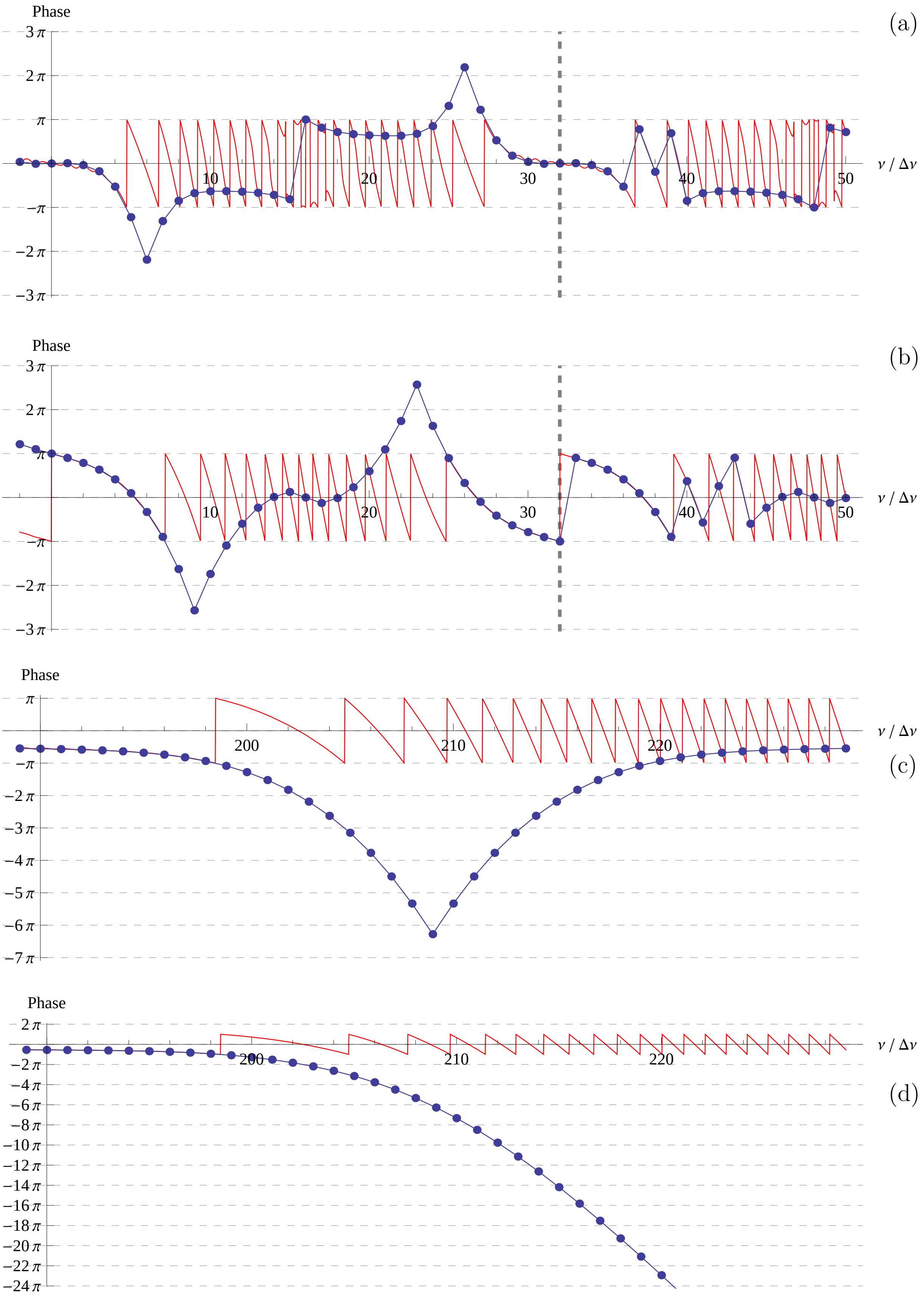

Figure 3.8: Utilisation of the 2π periodicity of the phases of complex values; partially unwrapped phases of the first N values (dashed lines): (a) and (b) is equivalent to (a) and (c) in Figure 3.7. (c) is an example of the phase spectrum with a large b_0 $(= 18\,{}^{\mathrm{Hz}}\!/\mathrm{s},\ A_0 = 1.0,\ \nu_0 = 200.0\,\mathrm{Hz},\ \phi_0 = 0.5\,\pi,\ N = 512,\ \Delta t = ({}^{1}\!/N)\,\mathrm{s})$ shown in Figure 3.3. (d) shows what it looks like if the phase is not reversed at the frequency of the peak in the magnitude spectrum.

Chapter 4

Start values for the sine fitting

4.1 Introduction

For a successful fit good start values for the parameters of the sine expression are required. These have to be estimated from the (complex) spectrum. In the same way as time-domain signals superpose linearly, spectra do. Assuming a typical spectrum, the highest values of a peak are the least influenced by noise or the tails of other peaks, so it is reasonable to evaluate the strongest values of the strongest peaks first. This must be balanced against the fact that the influence of noise statistically becomes less the more values are included in the evaluation.

It is reasonable to begin with the start value for b_0, because all the other parameters depend on this one: The amplitude corresponds to the power in a peak; the peak width is needed to estimate the spectral values contributing to the peak and therefore need to be summed up. By construction, the frequency is taken at the beginning of the interval, whereas the maximum of the peak is at the mean frequency, so again the width is necessary to determine ν_0. Finally, the phase strongly depends on the parameters, as shown in the preceding chapter (Chap. 3).

In order to systematically construct test data Gaussian white noise (GWN) will be utilised. Its implementation is described at first.

4.2 Gaussian white noise

Later on, the start value estimation must be proven to be stable with respect to noise. For this reason, different levels of Gaussian white noise GWN will be added to the data of a pure sine. The fit will be performed to the strongest values of the peak. In this section it will be shown that the magnitude of a peak is not only proportional to the amplitude of the sine, A_0, but is also a function of the linear frequency shift b_0 (and on a small scale even of ν_0). It is reasonable to conduct the evaluation with frequency independent noise that is roughly adjustable to a certain magnitude with respect to the peak height of the sine.

The GWN for the time domain is created by filling an array with complex values of the same magnitude but random phases and transforming it via inverse fast Fourier transform (IFFT) without subsequent multiplication with an inverse window function. Consequently, the spectral density is constant but the phases are random.

For all signals in this work the FFT is applied after multiplication with a window function. In order to get a comparable spectrum of the GWN, the time domain array is multiplied with the Hann window function before the application of the FFT. Because the application of the Hann window function causes each spectral value to become a weighted sum including its direct neighbours (Sec. 2.3.3), the resulting magnitude for this value depends on the phase relations among these three summands. Therefore, the resulting magnitude spectrum is not perfectly flat but fluctuates with a fixed maximum magnitude.[1]

4.2.1 Adaptation of the noise level to achieve a fixed ratio to the peak height

In order to analyse the influence of noise, its strength should be adjusted relatively to the peak magnitude of the spectrum of an LFS sine. For this the dependency of the peak height on the various parameters has to be estimated at least.

The peak height in the magnitude spectrum is obviously proportional to A_0 (cf. Eq. 2.95). Thus, as the dependency on this parameter is known, it does not need to be analysed any further. The same argument is valid for the initial phase ϕ_0: For a single peak, ϕ_0 causes rotations of the values in the complex plane and does not change the magnitude spectrum (cf. Eq. 2.11). The N dependency is removed by the periodogram normalisation. The dependencies on the parameters $b_{0,r}$ and $\nu_{0,r}$ are shown in Figure 4.1 (a). Larger values for $|b_{0,r}|$ cause the power of a sine to be spread over more spectral values, reducing the height of each. $\nu_{0,r}$ determines the peak position on the raster of discrete frequencies, causing the spectral leakage to distribute more or less power into side lobes. Its influence is reduced with increasing $|b_{0,r}|$ (Sec. 3.2.3). Because of the symmetry with respect to the sign of $b_{0,r}$, the negative values can be joined to the positive ones, resulting in plot (b). The adaptation does not need to be of high quality which is why a function for a rough compensation is gained from a simple exponential fit:

$$A(b_{0,r}) = A_0 \cdot 0.32 \cdot \mathrm{Exp}[-0.061 \cdot |b_{0,r}|] + 0.091. \tag{4.1}$$

---

[1] One could be confused by the way the spectrum of GWN is gained here: An artificial spectrum is created and transformed to the time domain, only to transform it back to the frequency domain. The detail is: Only for the second application of the FFT a window function is used, therefore the two transformations do not cancel each other.

This equation gives a roughly adjusted amplitude for the GWN. In the $b_{0,r}$ range shown here, the adjustment reduces the variation of the peak magnitudes from a ratio of around 6.0 to 1.3.[2] The compensation is implemented in such a way that the noise amplitude can be adjusted for each value of the linear frequency shift so that the factor between the highest value of the peak and the noise background is roughly constant.[3]

The adaptation is demonstrated in Figure 4.2. Here, three examples are given; the ratio between the level of the GWN and the highest value of the peak is roughly the same, independent of the number of samples used or the amount of the linear frequency shift.[4] The initially mentioned influence of the Hann window function on the GWN is clearly visible; without the Hann window, the level of the GWN would be constant (except for regions with significant overlap with the values of the peak).

---

[2] The value of 6.0 results from a comparison of a spectrum with $|b_{0,r}| = 100$ (magnitude of 0.07) with $b_{0,r} = 0$ (magnitude of 0.42). 1.3 is the strongest quotient of the fit function and the values ($|b_{0,r}| = 100$: 0.09/0.07).

[3] A detail to keep the statement given in this work consistent with the implementation in our evaluation software: To get the real amplitude of the GWN, the function $A(b_{0,r})$, Equation 4.1, is additionally divided by $\sqrt{\frac{8}{3N}}$. This includes two factors: Firstly, the general normalisation used in this work (namely the periodogram and the Hann window, Sec. 3.1.2). Secondly, the inversion of an additional normalisation (by the division by $\sqrt{N}$, in the function `SetGWN()`).

[4] The magnitude of the generator spectrum is constant at a certain value A. The resulting spectrum is the same but convolved with the spectrum of the Hann window function, meaning that each spectral value is divided by 2.0 and becomes superposed with a quarter of each of its two neighbouring values. Depending on the three phases, the resulting magnitude value is in the range $[0.0; A]$. Therefore, the upper limit A can still be used to describe the level of noise.

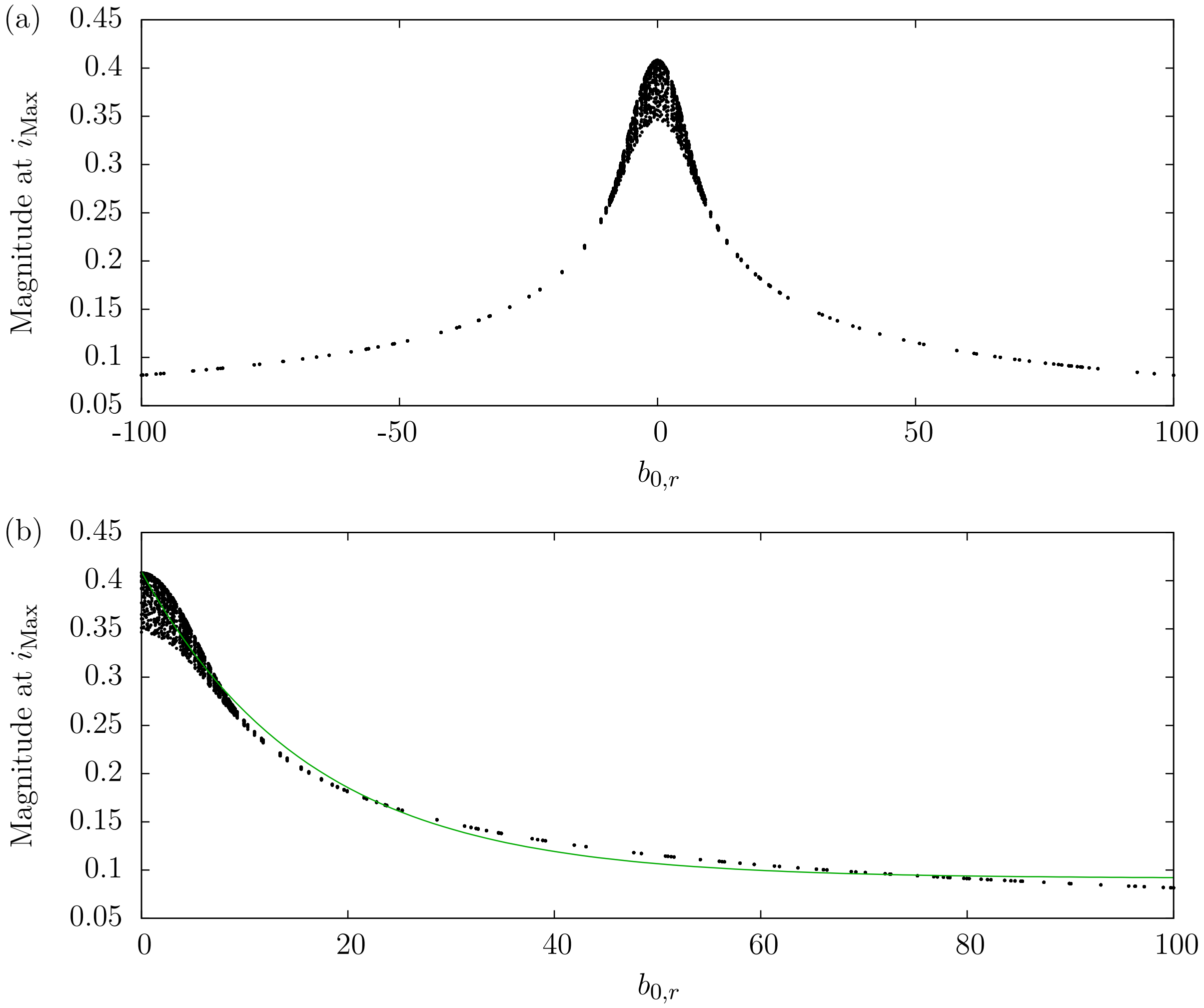

	N	Δt	$\Delta\nu$	A_0	ν_0	b_0	ϕ_0
(a), (b)	1,024	$1/N$	1.0	1.0	var.	var.	$\pi/2$

ν_0	b_0
200.0 Hz	0.0 Hz/s
200.5 Hz	1.0 Hz/s
200.25 Hz	−2.0 Hz/s
200.125 Hz	100.0 Hz/s
	−100.0 Hz/s
+10 from [200.0 Hz; 201.0 Hz]	+100 from [−100.0 Hz/s; 100.0 Hz/s]
	+100 from [−10.0 Hz/s; 10.0 Hz/s]

Figure 4.1: Spectra of pure sine functions are generated with the given parameters. 14 values for the frequency (4 fixed, 10 random) and 205 values for the linear frequency shift (5 fixed, 200 random) are combined, resulting in 2,870 plot points. The scattering for small values of $|b_{0,r}|$ is the result of spectral leakage. (a) depicts the magnitude of the spectral value at i_{Max} (the highest value of a peak) as a function of the linear frequency shift $b_{0,r}$. (b): The symmetry allows the forming of the absolute value for $b_{0,r}$. The fitted function (Eq. 4.1) is illustrated in green.

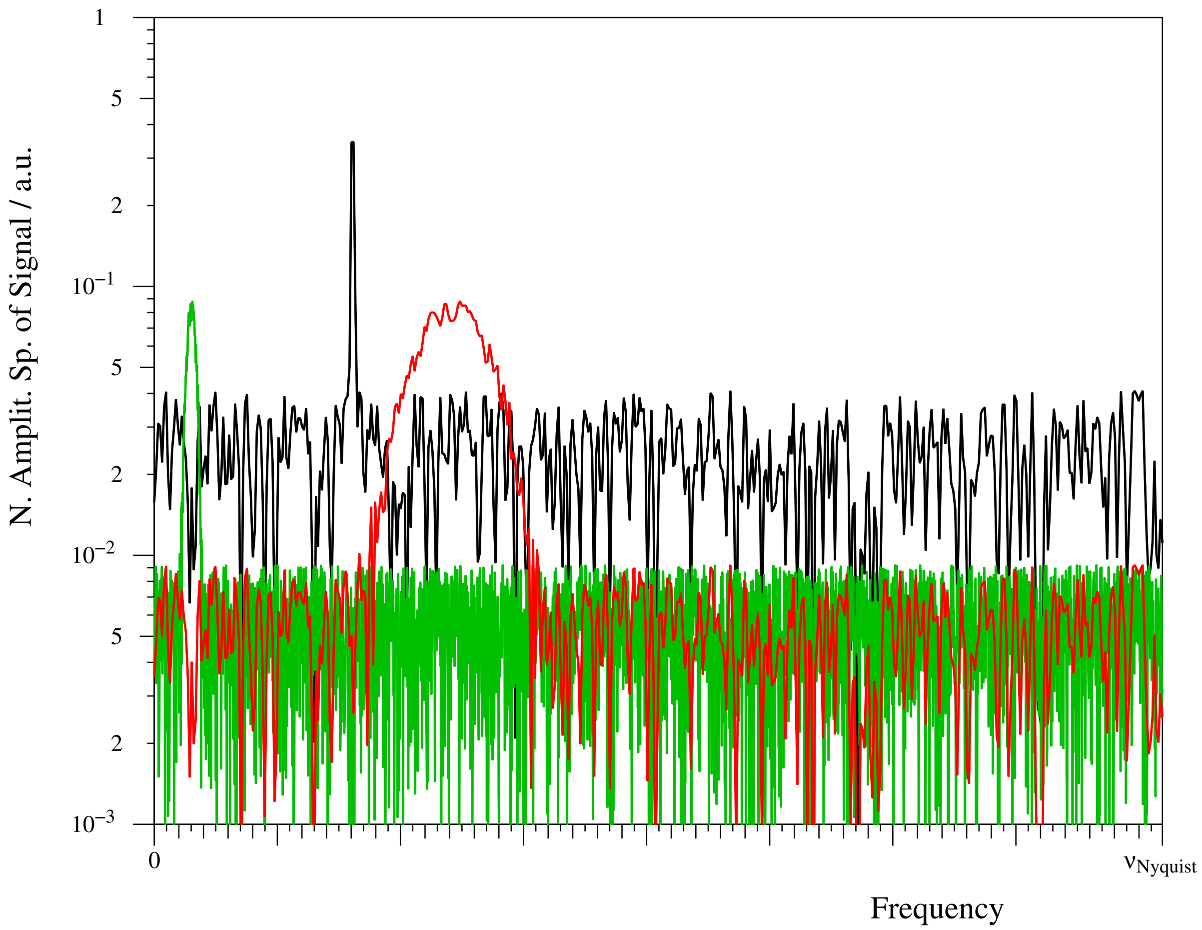

N	Δt	$\Delta\nu$	A_0	ν_0	b_0	ϕ_0
1,024	$(1/N)$ s	1.0 Hz	1.0	100.5 Hz	0.0 Hz/s	0.0
1,024	$(1/N)$ s	1.0 Hz	1.0	100.5 Hz	100.0 Hz/s	0.0
8,192	$(1/N)$ s	1.0 Hz	1.0	100.5 Hz	100.0 Hz/s	0.0

Figure 4.2: Demonstration of the magnitude adaption for Gaussian white noise added to the LFS sine: The level parameter is set to 10 %, which means that the strongest magnitude values of the noise should roughly be $0.1 \cdot |A[i_{\mathrm{Max}}]|$. The mantissa holds no frequency values because for all the plots the data is illustrated to ν_{Nyquist}, that is 512 Hz for the black and the red lines and 4,096 Hz for the green line. The green and the red line have the same linear frequency shift so their peak height is the same; nonetheless the green peak appears to be narrower because of the increased frequency density. A comparison of the red and black line demonstrates that the same seed for the random numbers is used.

4.3 The peak width

There is no obvious definition for the width of a peak as it stretches infinitely; nevertheless it is a fundamental property of a peak, which will be used repeatedly. In this work, the peak width is defined as the difference between the two frequencies enclosing the peak and fulfilling the condition that the magnitude at the boundary frequencies has dropped by 50% compared to the peak value at i_{max}. This choice of the full width at half maximum is relatively arbitrary. The function will be fitted to the spectral values in this range. Setting this threshold to lower levels would increase the number of values for the fit, possibly increasing its quality. But the additional values are of lower magnitude and will be more strongly influenced by noise and potential neighbouring peaks, thereby reducing the fit quality.

Typically, in the discrete magnitude spectrum, the frequency values at which the magnitude has dropped below 50% have to be interpolated. A linear interpolation between the value below and above this threshold gives the virtual continuous index values (r, Sec. 3.1.3) for the left ($r_{0.5\text{ left}}$) as well as the right ($r_{0.5\text{ right}}$) passages through the threshold value. The peak width is:

$$r_{\text{W}} = r_{0.5\text{ right}} - r_{0.5\text{ left}} \tag{4.2}$$

In addition to the inaccuracy produced by the linear interpolation, another error occurs when determining the 50% level: The magnitude at i_{max} depends on $\nu_{0,r}$; this dependency is illustrated in Figure 4.3. Its strong influence on narrow peaks suggests a compensation for a b_0 estimation from the peak width, whereas its decrease with increasing $|b_{0,r}|$ allows a simpler approach for broader peaks.

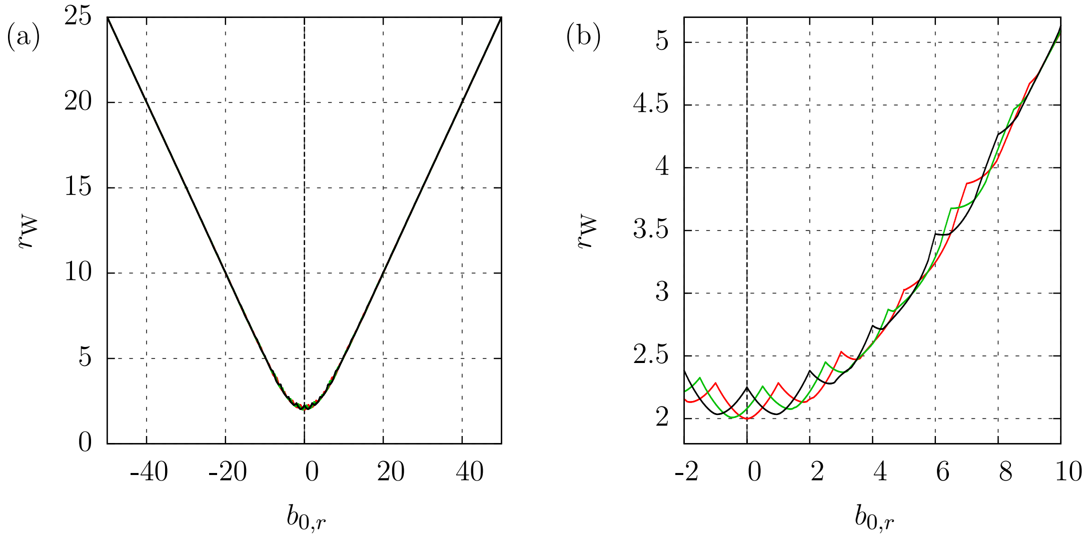

Figure 4.3: Plots demonstrating the peak width (Eq. 4.2) as a function of $b_{0,r}$. (b) is a detail of (a) illustrating that for small $|b_{0,r}|$ the peak width depends on its position with respect to the raster of discrete frequencies. Variation of $\nu_{0,r}$ shifts the magnitude peak linearly on the frequency axis, leading to periodically fulfilled symmetry relations which is clarified by the demonstration of three examples: Red: $\nu_{0,r} = 256.0$, green: $\nu_{0,r} = 256.25$ and black: $\nu_{0,r} = 256.5$ (for $b_{0,r} = 0$, the two extreme cases have already been shown: Fig. 3.4 (a) demonstrates the broadest possible peak with its maximal influence of the spectral leakage (black), whereas Fig. 3.5 (a) comprises the narrowest peak with vanishing sidelobes (red)).

4.4 Interim remark on start value determination

During the development of this algorithm a sign flaw occurred in a deviation, leading to a more unstable behaviour of the fit routine. This could be compensated by using exceptionally good estimates for the start values. For this reason, additional effort was invested, making the start-value estimation much complexer. As we shall see later, the fit – assuming the correct equations are implemented – is very stable and most of this additional effort is of reduced usefulness. Additionally, the old approach estimates the parameters by evaluating only the strongest three values of a peak; approaches using a flexible number of values are much more robust when applied to noisy data. For real data, the old and complexer approach performs better only for small values of $|b_{0,r}|$, that is for narrow peaks. Nevertheless, since these complexer procedures were already implemented and since they increase the accuracy, they are still used in the final algorithm. Considering that the description of the procedures is interminable and they are at the same time only used for narrow peaks, they are briefly explained in subsections where needed.

4.5 The parabola approach

Figure 4.4 shows three examples with different values of b_0. A Gaussian function and a parabola are fitted to the highest magnitude values. One can see that the Gaussian fit models the highest magnitude values significantly better. Nonetheless, the parabola is used in the following because a direct calculation of its parameters – without another non-linear fit – is possible and the deviation is compensated for afterwards.

4.5.1 Parabola calculation

The parameters are calculated with the objective of minimising the sum of squared deviation.[5] The expression for the parabola is:

$$y = \alpha \cdot x^2 + \beta \cdot x + \gamma \tag{4.3}$$

Then the error of the i-th value is:

$$e_i = y_i - (\alpha \cdot x_i^2 + \beta \cdot x_i + \gamma) \tag{4.4}$$

The latter expression is squared and summed up for all values. The derivatives with respect to the parameters must be zero (minimise deviation) so three equations with three parameters can be used to calculate the best values easily.[6] For most of the upcoming applications, the transformation to the vertex form is advantageous, providing the appropriate parameters:

$$y = a\,(x + b)^2 + c \tag{4.5}$$

Applied to data in Figure 4.4, $-b$ represents the frequency of the vertex and c its value; a is a measure of the width of the parabola.

---

[5] The template for the implementation can be found in [35].

[6] Squaring causes summands with powers of x up to four which can become big for high frequencies (x is the frequency, or to be exact it is the frequency in units of $\Delta\nu$ as the fit is done in the index space). To avoid summing up values with strongly different magnitudes, in this approach an offset is added in the form of a reduction of each frequency value (by the frequency of the maximum i_{Max}) and therefore this calculation is centred around zero. Concluding, the result is transformed into the vertex form and the offset is added.

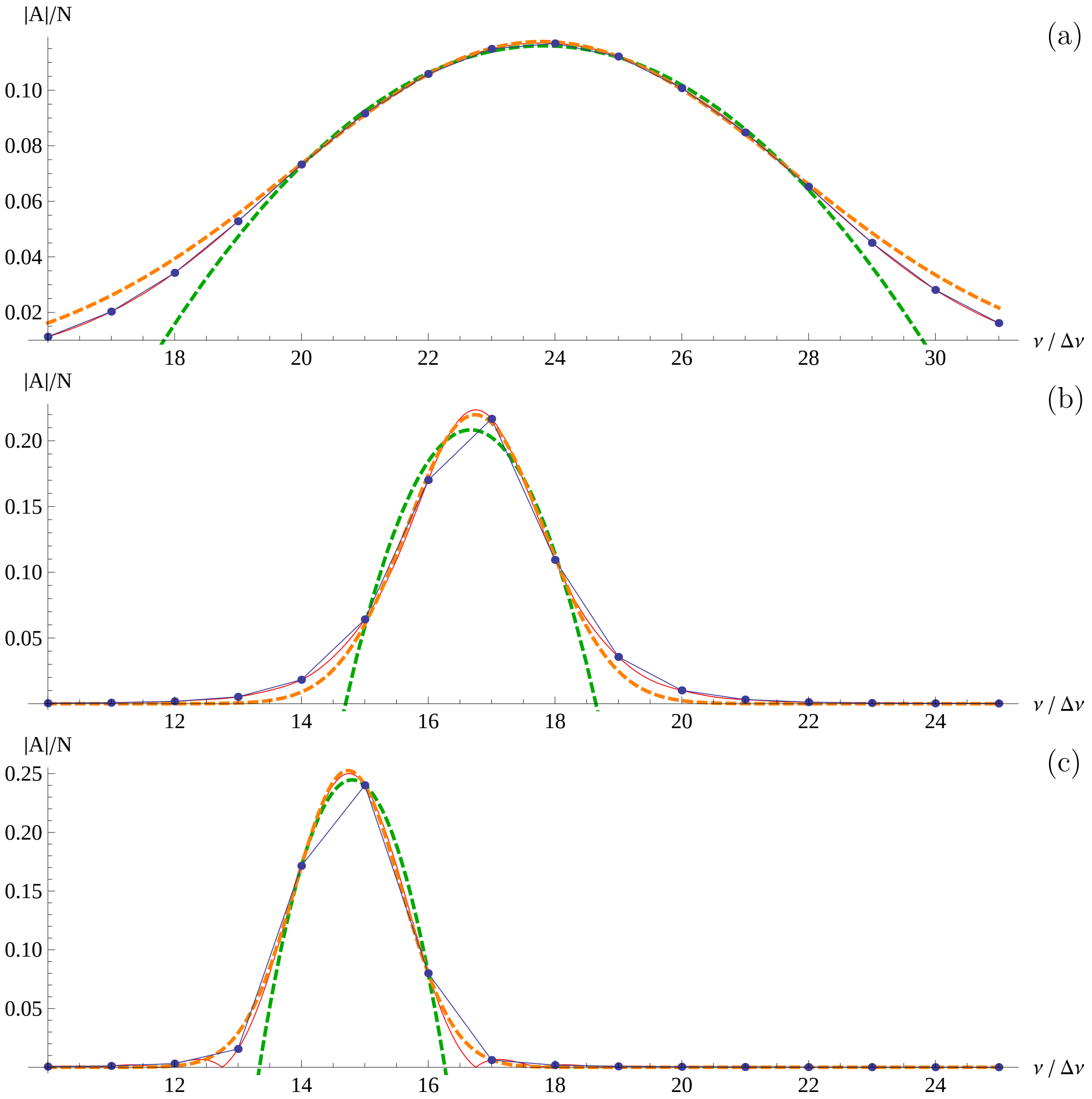

	N	Δt	$\Delta\nu$	A_0	ν_0	b_0	ϕ_0	# Fit values
(a)	128	$1/N$	1.0	1.0	14.75 Hz	18.105 $^{\mathrm{Hz}}/_{\mathrm{s}}$	$^{\pi}/_{8}$	9
(b)	128	$1/N$	1.0	1.0	14.75 Hz	4.000 $^{\mathrm{Hz}}/_{\mathrm{s}}$	$^{\pi}/_{8}$	4
(c)	128	$1/N$	1.0	1.0	14.75 Hz	0.000 $^{\mathrm{Hz}}/_{\mathrm{s}}$	$^{\pi}/_{8}$	3

Figure 4.4: Magnitude spectra: Fit of a Gaussian function (orange, dashed) and a parabola (green, dashed). Red: The continuous function $\mathrm{F}_{\mathrm{Sum}}$, blue: the discrete points. Especially in (b) the Gaussian curve fits significantly better to the data.

4.6 Start value for b_0

According to the definition of the peak width (Sec. 4.3), the range of magnitude values at discrete frequencies within r_{W} is chosen and the parabola parameters a, b and c are determined. $a_c = a/c$ can be understood as the "normalised curvature" and is used to estimate $|b_{0,r}|$.[7] Figure 4.5 shows a_c as a function of the input $|b_{0,r}|$ for synthetic data without noise. For $|b_{0,r}| \leq 5.0$ a parabola is fitted to the data, for larger $|b_{0,r}|$ an exponential fit is done with the objective of minimising the deviation for the logarithmic values, in order to get a good result, especially for small values of a_c. This is reasonable because of the small slope for big $|b_{0,r}|$ and the small absolute value for a_c in that region. Since a_c is known and the start parameter for $|b_{0,r}|$ is to be estimated, the equations in Figure 4.5 are inverted, including the threshold values distinguishing the equations used:

$$|b_{0,r}| = \begin{cases} 0.0 & a_c > 0.4509 \\ \pm\sqrt{\frac{a_c-\gamma}{\alpha}+\frac{\beta^2}{4\alpha^2}}-\frac{\beta}{2\alpha} = \sqrt{64.50-143.05\cdot a_c}+0.11302 & 0.4509 \geq a_c > 0.2840 \\ \exp\left(\frac{\ln a_c-d}{g}\right) = \exp\left(-0.5001\cdot\ln a_c+1.0596\right) & a_c \leq 0.2840 \end{cases}$$

The value of 0.2840 is used as the inverted threshold ($|b_{0,r}| = 5.0$, Fig. 4.5) to decide which curve is to be used.[8] This approach is appropriate for broad peaks because it includes all spectral values within the peak width and thus should be reasonably robust with respect to noise. It was demonstrated, that the influence of the peak position on the raster of discrete frequencies on the peak width increases with decreasing $|b_{0,r}|$ (Fig. 4.3). The next section describes an approach for compensating this effect.

4.6.1 A more accurate approach for small peak widths

If r_{W} (Eq. 4.2) is ≤ 4.0, a different approach to estimate the start value for $|b_{0,r}|$ is used in order to compensate the increasing influence of the spectral leakage for decreasing $|b_{0,r}|$. For narrow peaks, Figure 4.3 (b) shows that two curves are modulated: Mainly, a quadratic increase of the peak width with $|b_{0,r}|$ is observable. Additionally, a modulation with a triangle wave of decreasing amplitude is visible. The latter (as opposed to the former) depends on the position of the peak on the raster of discrete frequencies (see the

---

[7] The parabola parameter a is proportional to the amplitude, which is not useful. A norm height would be more suitable. As this is not available, the vertex height of the parabola proves to be the best alternative. Therefore a is divided by c for this application.

[8] It shall be described that for narrow peaks a different approach is used but just in case that $a_c > 0.4509$ occurs, $b_{0,r}$ is set to zero to avoid invalid solutions (negative value under the square root in the middle equation) within the implementation. This case could occur since the two calculations are different: if the peak width is so wide that the parabola approach is used, the subsequent determination of parabola parameters could principally produce a big value for a_c.

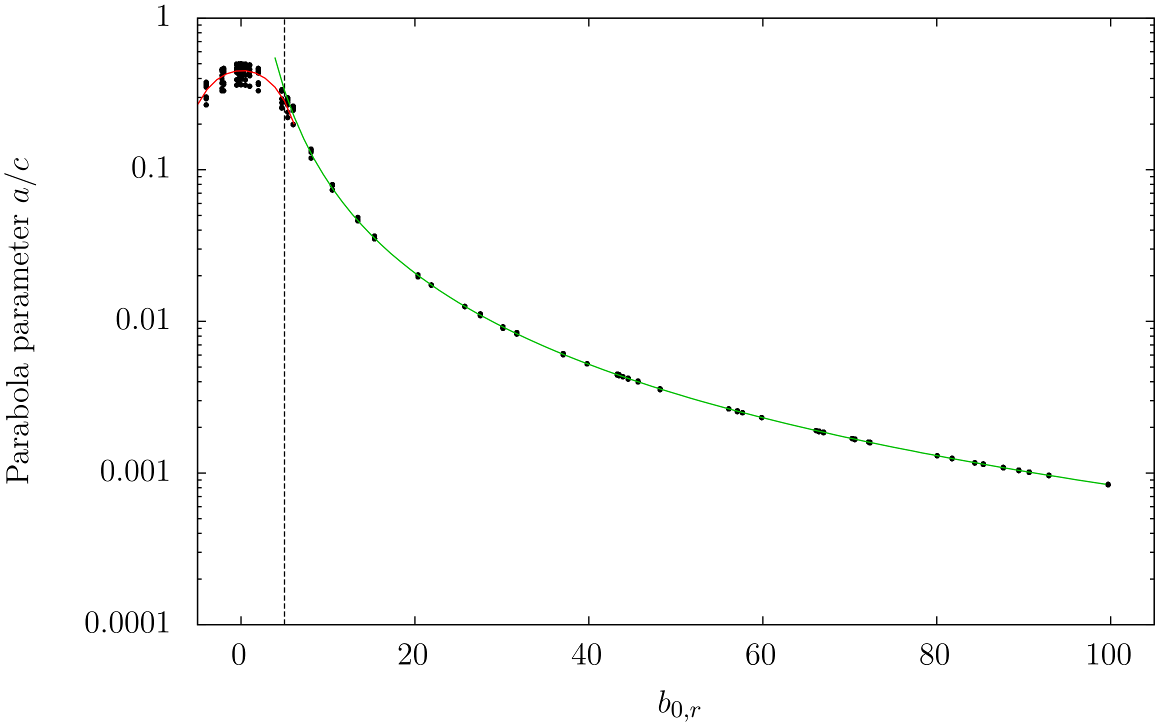

$$\text{If } |b_{0,r}| \leq 5.0\text{:} \quad a_c^{\text{Poly}} = \alpha \cdot |b_{0,r}|^2 + \beta \cdot |b_{0,r}| + \gamma$$

$$\begin{array}{llll} \alpha & = -0.0069906 & \pm 2.274 \cdot 10^{-4} & (3.253\%) \\ \beta & = 0.00158009 & \pm 7.594 \cdot 10^{-4} & (48.06\%) \\ \gamma & = 0.450834 & \pm 1.761 \cdot 10^{-3} & (0.3905\%) \end{array}$$

$$\text{If } |b_{0,r}| > 5.0\text{:} \quad \ln(a_c^{\text{Exp}}) = d + g \cdot (\ln(|b_{0,r}|))$$

$$\begin{array}{llll} d & = 2.11879 & \pm 2.995 \cdot 10^{-3} & (0.1414\%) \\ g & = -1.99964 & \pm 7.950 \cdot 10^{-4} & (0.03976\%) \end{array}$$

$$a_c^{\text{Exp}} = \mathrm{e}^d \cdot |b_{0,r}|^g$$

Figure 4.5: Normalised parabola curvature versus normalised LFS parameter. 3,564 spectra of sines are generated by combination of $11 \times \nu_{0,r} \in [199.5; 201.0]$, $54 \times b_{0,r} \in [-100.0; 100.0]$ and $6 \times \phi_0 \in [0; 2\pi]$. $A_0 = 1.0$, $N = 1{,}024$, $T = (1/N)\,\mathrm{s} \rightarrow \Delta\nu = 1.0\,\mathrm{Hz}$. According to the peak width (Sec. 4.3), the magnitude values of each peak are evaluated to obtain the parameters of a parabola (Sec. 4.5.1). The continuous coloured lines belong to the two functions which are fitted to the curve progression. The errors of the fit parameters are gained by `GnuPlot` (standard error of the regression).

Parameter	Fit results		
m	33.503	± 0.255	(0.76%)
a	-64.792	± 0.416	(0.64%)
b	-0.39657	± 0.03252	(8.2%)

Table 4.1: Fit results for the function: $|b_{0,r}|(r_{\mathrm{W}}^{\mathrm{corr}}) = \sqrt{m \cdot r_{\mathrm{W}}^{\mathrm{corr}} + a} + b$.

different curves in Fig. 4.3 (b)). By evaluating the degree of asymmetry of a peak, a correction to the real position of the peak (r_{Max}) can be estimated.

The difference between the magnitude values of the two neighbours closest to the peak is calculated and normalised by a division by the magnitude of the maximum value itself:

$$d_{\mathrm{Mag}}^{\mathrm{Norm}} = \frac{|A[i_{\mathrm{max}-1}]| - |A[i_{\mathrm{max}+1}]|}{|A[i_{\mathrm{max}}]|}. \tag{4.6}$$

Since the positions on the discrete raster lie equidistantly, $d_{\mathrm{Mag}}^{\mathrm{Norm}}$ is a periodic function with respect to shifting the peak on the frequency axis. Furthermore, with an increasing peak width the two neighbours tend to become equal – meaning that

$$d_{\mathrm{Mag}}^{\mathrm{Norm}} \xrightarrow[|b_{0,r}| \to \infty]{} 0. \tag{4.7}$$

These two properties are exactly the ones needed to approximately compensate the triangle modulation by linear addition of the correction:

$$r_{\mathrm{W}}^{\mathrm{corr}} = r_{\mathrm{W}} \left(1.0 - x_{\mathrm{Scale}} \cdot |d_{\mathrm{Mag}}^{\mathrm{Norm}}|\right). \tag{4.8}$$

For synthetic data, all parameters except for x_{Scale} are known and thus it can be determined by rewriting the Equation 4.8: $x_{\mathrm{Scale}} = 5.9746$.[9]

Finally, the quadratic increase of $|b_{0,r}|$ with increasing $r_{\mathrm{W}}^{\mathrm{corr}}$ has to be handled. For real data the $|b_{0,r}|$ parameter is unknown, so – compared to Figure 4.3 – the axes are swapped and a square-root function is fitted. Table 4.1 gives the fit results. Consequently, $|b_{0,r}|$ is set to

$$|b_{0,r}| = \sqrt{33.503\, r_{\mathrm{W}}^{\mathrm{corr}} - 64.792} - 0.39657 \tag{4.9}$$

if $r_{\mathrm{W}}^{\mathrm{corr}} > 1.9386$ or, if otherwise, to $|b_{0,r}| = 0.0$ in order to avoid imaginary solutions.[10]

---

[9] The scaling is independent of the parameters, but for the sake of completeness, the following parameters are used: $N = 1{,}024$, $\Delta t = 0.1 \cdot (1/N)\,\mathrm{s}$, therefore: $\Delta\nu = 10.0\,\mathrm{Hz}$, $\nu_0 = 100.25 \cdot \Delta\nu$, $\phi_0 = 0.0$, $A_0 = 50.0$, b_0 is systematically varied in steps of $2.0\,\mathrm{Hz/s}$, in the range of $[0.0\,\mathrm{Hz/s}; 1{,}000.0\,\mathrm{Hz/s}]$. The value of x_{Scale} was gained before the analysis was performed with transformed coordinates (Sec. 3.1.3), for $b_{0,r}$, this corresponds to a step size of 0.02 and a range of $[0.0; 10.0]$. For the 501 values the mean value for x_{Scale} (according to Equation 4.8) is gained.

[10] This is an additional case demanding $|b_{0,r}| = 0.0$. This is not in conflict with the description given in the last section (Sec. 4.6): there, the parabola parameters are analysed, whereas here, the peak width (Sec. 4.3) is evaluated. Typically, both follow the same trend, but to avoid invalid solutions or even software crashes, this condition is double-checked.

Figure 4.4 indicates that the parabola fit in order to estimate the mean frequency of a peak is imprecise for narrow peaks. With the estimated value for $|b_{0,r}|$ and a quantitative measure for the symmetry of the peak $d_{\mathrm{Mag}}^{\mathrm{Norm}}$, a corrected position of the peak is gained by a parabola fit:[11]

$$r_{\mathrm{Max}}^{\mathrm{corr}} = (-0.026793\,|b_{0,r}|^2 + 0.055348\,|b_{0,r}| - 0.63619)\,d_{\mathrm{Mag}}^{\mathrm{Norm}} + i_{\mathrm{Max}}, \tag{4.10}$$

which will be useful when estimating the start value for $\nu_{0,r}$. The correction to the discrete i_{Max} amounts to tenths of $\Delta\nu$.

4.6.2 The sign of b_0

In Section 3.2.3 (p. 67), it was described that the slope of the phase as a function of frequency is exactly $\pi/\Delta\nu$ at the mean frequency of the LFS sine. Furthermore, it was demonstrated that the slope of the surrounding values deviates the more from that value, the bigger $|b_{0,r}|$ gets. And finally, that the sign of $b_{0,r}$ determines the sign of the deviation of the slope. Because the phases are 2π periodic, it is somehow absurd to discuss whether the slope is greater than π. But, assuming the slope is always in the range of π, π can be subtracted, leading to a rather flat curve, where it is meaningful to analyse its progression. This is demonstrated in Figure 4.6: Starting with the phase of the strongest value in the magnitude spectrum (at i_{max}), the two differences to the neighbouring values are taken and averaged. π is subtracted and the result is a point-symmetric curve with the important property that the sign of the value is the same as the sign of the b_0 used to create the spectrum. Random parameter combinations are used; (a) is without noise and limited to a range of $b_{0,r} = \pm 30$. For this case, this works reliably. In (b), 20% GWN is added; the spreading of the values can lead to the wrong sign: The black dots have a low absolute value by themselves, especially for large values of $|b_{0,r}|$, and thus a relatively small amount of noise can change the three phases of the spectral values at the maximum in such a way that the wrong sign would be assumed (the cloud of black dots extends to both sides of the zero line). In the section referred to above and especially in Figure 3.8, one can see: The farther one veers away from the maximum, the greater the difference in the slope of $\pi/\Delta\nu$ becomes. Thus, for broader peaks, it is absolutely advisable to include more values. In the same way, differences between the neighbour and the following next-neighbour values are taken: π is subtracted and the average is plotted. This yields the red and finally the green values in (b).

Since a correct estimation of the sign for b_0 is crucial for the fitting, relatively more effort is put into its reliability. In order to estimate the most probable sign of b_0, all values in the range of the peak width r_{W} (Sec. 4.3) are taken into account. Each phase difference between two neighbouring values is weighted by division by the magnitude of

---

[11] The relative errors are: quadratic term: ±0.025%, linear term: ±0.39%, constant term: ±0.23%.

the respective outermost value. These differences are added (with inverted signs for the results gained from the right side of the peak) and finally, the sign of this sum is used as a reliable estimation of the sign of b_0.

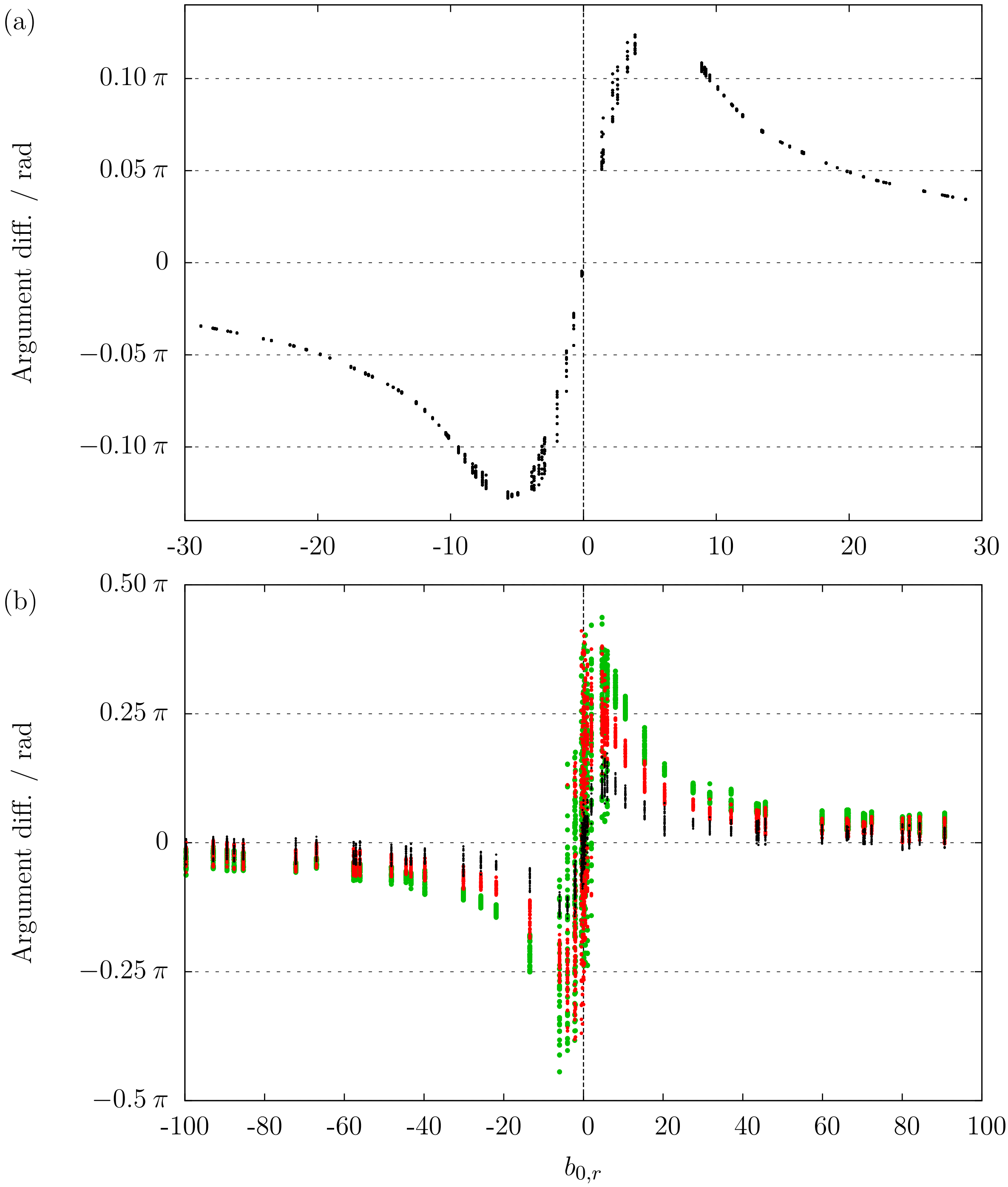

Figure 4.6: (a) demonstrates the mean of the two differences between the phases at $i_{\mathrm{Max}-1}$ and i_{Max} as well as between i_{Max} and $i_{\mathrm{Max}+1}$ as a function of the input $b_{0,r}$. 10 random frequencies ($100.0 \leq \nu_{0,r} \leq 120.0$) × 10 random phases ($0 \leq \phi_0 < 2\pi$) × 100 random linear shifts ($-30 \leq b_{0,r} \leq 30$) are combined (10,000 dots). The sign of their values is the same as the sign of $b_{0,r}$. Analogously, the values for (b) are generated. Here the range for 54 random $|b_{0,r}|$ is enlarged to ($-100 \leq b_{0,r} \leq 100$), additionally, Gaussian white noise with a relative level of 0.2 is superposed. The black dots are similar values to the ones in (a). If one more step to each side is taken into account (namely the phase difference between neighbours of the maximum and their neighbours) and the mean is taken, the red dots occur. Green is again one step further and therefore the mean value from six differences. For narrow peaks this means too many values are evaluated – the outer values are dominated by noise – which is why the green points spread greatly for small values of $b_{0,r}$.

4.7 Start value for ν_0

If the condition allowing for the employment of the parabola parameters is met ($r_{\mathrm{W}} > 4.0$), then the vertex of the parabola (parameter b) is utilised as an estimation for the maximum of the peak in the magnitude spectrum and r_{Max} is set to $-b$ (Sec. 4.5.1). Otherwise, for narrow peaks, the spectral-leakage corrected $r_{\mathrm{Max}}^{\mathrm{corr}}$ (Eq. 4.10) is used to estimate the start value for the frequency:

$$\nu_{0,r}^{\mathrm{Start}} = r_{\mathrm{Max}} - \frac{1}{2} b_{0,r}^{\mathrm{Start}} \tag{4.11}$$

4.8 Start value for A_0

Parseval's theorem can be interpreted as: the total energy contained in the time-domain signal summed across all of time T is equal to the total energy of its spectrum summed across all of its frequency components [11, Sec. 8.12].[12] Consequently, all magnitude values in the spectrum should be considered ideally. But if the data consist of more input than just a single sine, the lower the magnitude of a value is, the more will noise and other signals contribute. Like before, it makes sense to focus on the highest values. In this work, the magnitudes of the highest three values are summed up as a basis for the spectral power of a peak.[13] The broader the peak is, the relatively less of its power is considered in this approach. 30 $\nu_0 \times 500$ b_0 values (up to $|b_{0,r}| = 300$) were calculated and used to fit expressions to their progress (similar to Fig. 4.5). In Figure 4.7 a small fraction of these values and the fitted function are illustrated.[14]

Figure 4.8 depicts the corrected values versus the real $b_{0,r}$ values. Ideally, all values are 1.0, instead the error is less +3 % or -5 %. However, this is absolutely sufficient for the robust fit parameter A_0.

---

[12] If a window function is used, this holds at least approximately if the spectrum is additionally normalised by the window integral, see Section 3.1.2.

[13] Due to the character of the Hann window, there are always at least three high values (Sec. 2.3.3 or Fig. 3.2.2). The estimation accuracy for broader peaks could probably be increased if more values were included. The parabola parameter c (Eq. 4.5) seems to be particularly promising. But since no single case could be found in which an improved start value for the amplitude improved the fit result and (at most) only a few iteration steps could be avoided, a further optimization is not pursued.

[14] Firstly, the range for $|b_{0,r}|$ is limited to 30, secondly, only every seventh value is represented in order to limit the amount of dots in the figure. (Seven is chosen because it is coprime to 30 and 300. Thus, one can be sure that every b_0 and ν_0 value shows up if it is combined systematically)

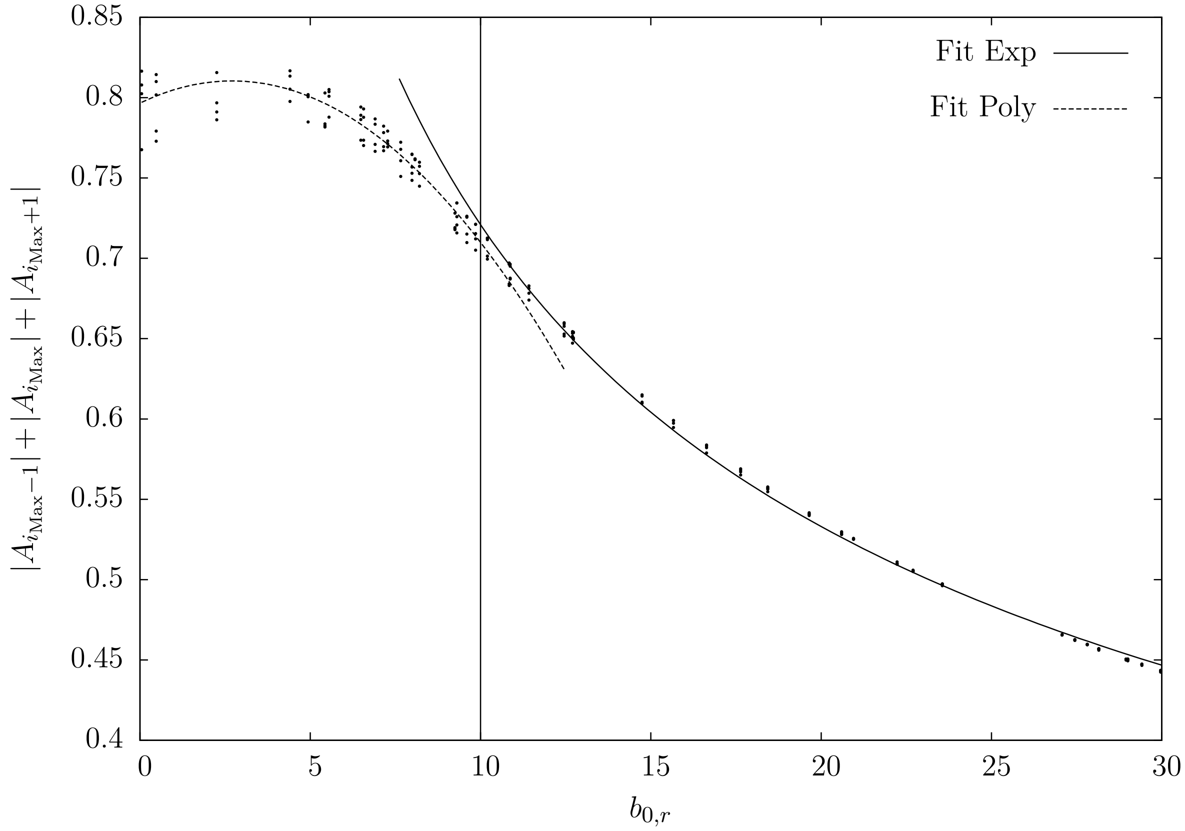

If $b_{0,r} \leq 10.0$: $A^{\mathrm{Start}}_{0,\mathrm{Poly}} = a \cdot |b_{0,r}|^2 + b \cdot |b_{0,r}| + c$

$a = -0.00188999 \quad \pm 4.733 \cdot 10^{-5} \quad (2.505\%)$

$b = 0.0102338 \quad \pm 4.997 \cdot 10^{-4} \quad (4.883\%)$

$c = 0.796579 \quad \pm 1.255 \cdot 10^{-3} \quad (0.1576\%)$

If $b_{0,r} > 10.0$: $A^{\mathrm{Start}}_{0,\mathrm{Exp}} = d \cdot |b_{0,r}|^g$

$d = 1.96502 \quad \pm 3.978 \cdot 10^{-3} \quad (0.2024\%)$

$g = -0.435508 \quad \pm 7.114 \cdot 10^{-4} \quad (0.1634\%)$

Figure 4.7: The sum of the magnitudes of the three highest values $|A_{i_{\mathrm{Max}}-1}| + |A_{i_{\mathrm{Max}}}| + |A_{i_{\mathrm{Max}}+1}|$ is plotted versus the input parameter $b_{0,r}$. 500 $b_{0,r}$ values ($\in [0.0; 300.0]$) and 30 $\nu_{0,r}$ values ($\in [100.0; 120.0]$) are combined for the fit (for all combinations, the sine input $A_0 = 1.0$ and $\phi_0 = \pi/2$, $N = 1{,}024$). For $b_{0,r} \leq 10.0$ a polynomial of second degree is fitted, for greater values an exponential decline.

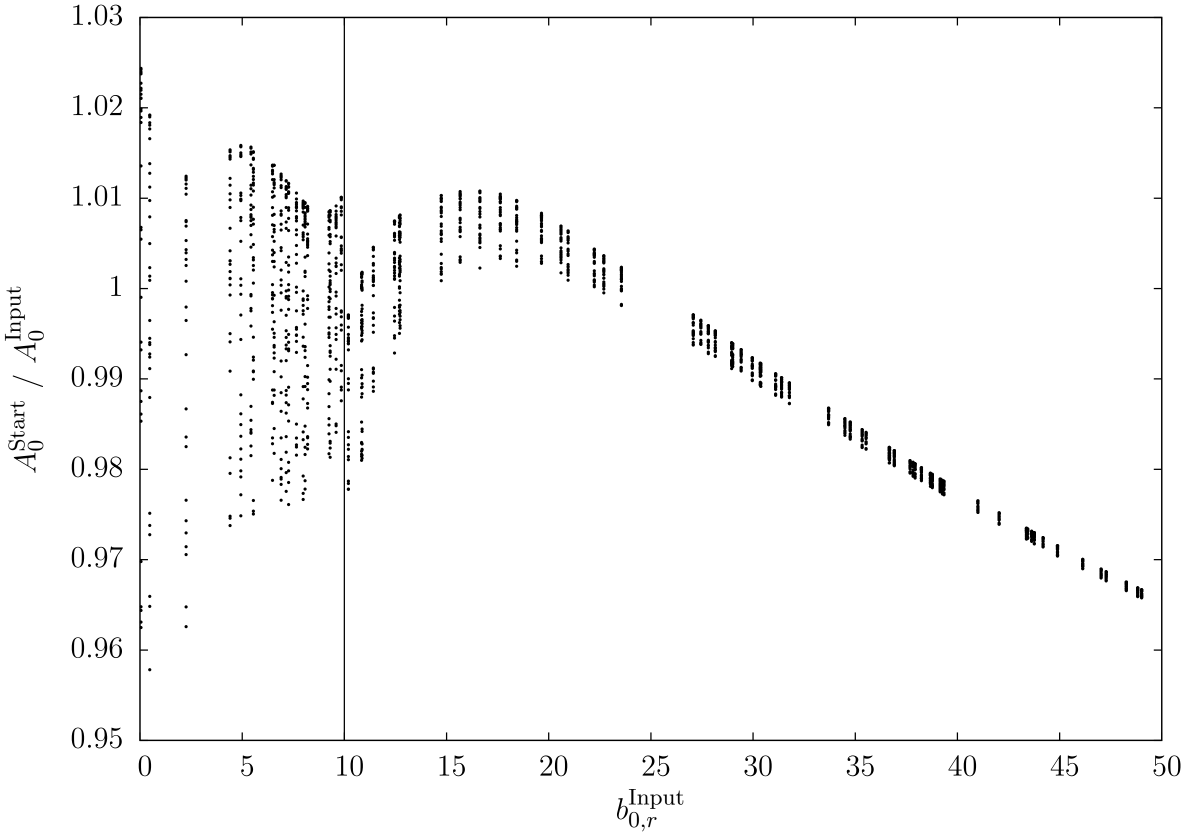

Figure 4.8: This plot demonstrates the estimated start parameter A_0^{Start} as a function of $|b_{0,r}|$. The corrected start values for A_0^{Start} (Fig. 4.7) are normalised by division by their corresponding input A_0.

4.9 Start value for ϕ_0

4.9.1 Parabolic phase fit

In Chapter 3 (esp. Fig. 3.8 (d)) it was demonstrated that a realignment of the phases can lead to a monotonous, smooth progression with the slope continuously changing from 0 to $2\pi/\Delta\nu$ (or vice versa, depending on the sign of b_0). At the point where the frequency is exactly ν_0, the slope is $1\pi/\Delta\nu$. An example in which a straight line with the slope $1\pi/\Delta\nu$ is subtracted from the phase spectrum is given in Figure 4.9. The easiest way how this can be achieved is by adding (or subtracting) π to every second value. In this figure the phase at i_{Max} is subtracted from the phase spectrum for clarity.[15] Beginning with the value for i_{Max}, the nearest values to the sides are decreased by 2π if the difference is bigger than π (resp. increased by 2π if smaller than $-\pi$). This is represented by the blue lines. By comparing the altered values with the original phase progression one can see that the altered curve is smooth. For bigger values of $b_{0,r}$ the smooth interval can be used to fit a parabola to it: The position of the vertex may be used to determine ν_0, its width to determine b_0 (see also 4.6.2). The phase may be determined by the height of the vertex. Therefore, the slope of the phases may also be appropriate to find all the start parameters except for A_0.

In this work, only the phase is estimated by the above mentioned approach because fitting a parabola to the magnitude values is more reliable; the phases are very susceptible to noise and other superposed signals and, in particular, this approach fails for $b_0 \approx 0$ (see Fig. 4.9 (c)).[16]

A parabola cannot represent the real shape of the curve progression: for positive b_0 the slope of the phases increases from 0 to $2\pi/\Delta\nu$ (vice versa for neg. b_0), so to the left and right of the peak it becomes asymptotically constant (e.g. see Fig. 3.8 (d)). Subtraction of a line with with the slope $1\pi/\Delta\nu$ does not change this behaviour. Per definition, a parabola has a linear increase of the slope. Therefore, the fit will contain a systematic error; its suppression is described in the following.

1. A line may be added to a parabola only to result in another parabola. Therefore, the addition of π to every second phase value is omitted. This was done only for the plots in Figure 4.9 to clarify the ansatz.

2. Beginning with the phase closest to r_{Max} (usually close to or exactly the same as i_{Max}: the location of the local magnitude maximum in the given spectrum) the

---

[15] In doing so the ϕ_0 dependency is eliminated. The phase parameter ϕ_0 contributes linearly to all phases in a peak (if the peak at negative frequencies is neglected, otherwise they superpose, Fig. 3.4 (b)).

[16] The mentioned approach could be used as a second, very sensitive way to estimate the start parameters. In the future multiple approaches may be implemented in parallel to increase the start parameter quality, potentially reducing computational effort during the fitting.

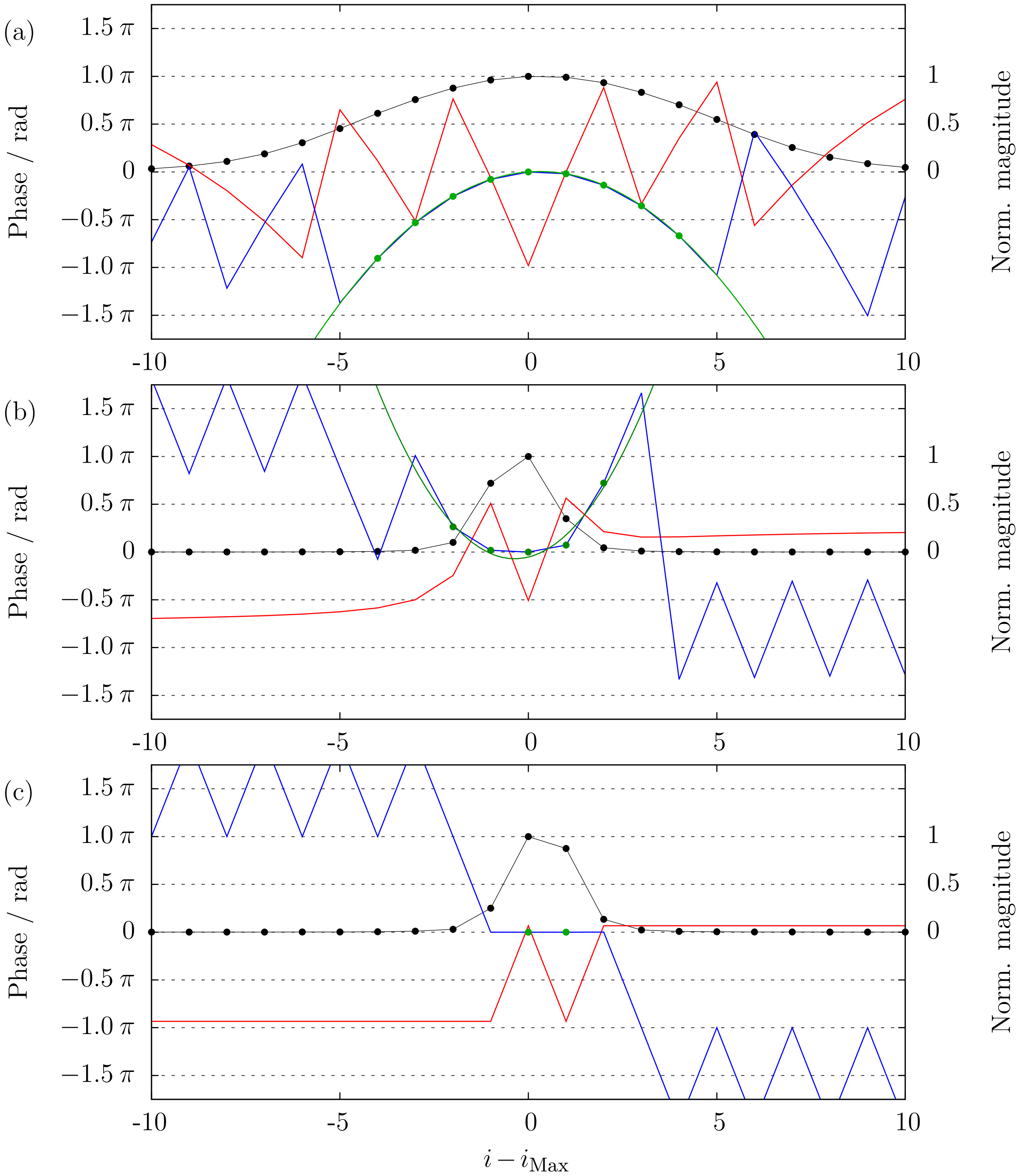

Plot	A_0	ν_0/Hz	$b_0/(\mathrm{Hz}/\mathrm{s})$	$\phi_0/°$	$\Delta\nu$/Hz	Δt/ms
(a)	1.0	30.3	20.0	0.0	1.0000	0.9766
(b)	1.0	30.3	−1.1	0.0	1.0000	0.9766
(c)	1.0	100.0	0.0	30.0	0.9766	1.0000

Figure 4.9: Spectra with $N = 1{,}024$ samples; the abscissa depicts the frequencies in units of the value index after subtraction of i_{Max}. The magnitude (right axis) is illustrated in black, it is normalised to the magnitude at i_{Max}. The red lines represent the phase (left axis); the blue lines represent the phase after the application of the realignment as described in the text. The green dots show the phase, with the phase at the magnitude maximum subtracted, in the region without phase jumps, where admissible (in (a) and (b)), a parabola is fitted.

phases to the sides are aligned by addition of $\pm n\,2\pi$ ($n \in \mathbb{N}$) in such a way that they monotonously rise to the sides.[17]

3. The fit is done as described in Section 4.5.1. The line with a slope of $1\pi/\Delta\nu$ ignored (item 1.) is now considered by adding π in Equation 4.3 to the linear progression: $\beta \to \mathrm{Norm}[\beta+\pi]$.[18] Subsequently, it is transformed to the vertex form $y = a\,(x+b)^2 + c$.

4. Assuming the slope in the direct vicinity to r_{Max} is at a constant $1\pi/\Delta\nu$, the adaptation to the raster is done by linear interpolation:[19]

$$\phi_{\mathrm{Temp}} = c - (r_{\mathrm{Max}} - \lfloor r_{\mathrm{Max}} + 0.5 \rfloor)\cdot\pi \tag{4.12}$$

5. Finally, a linear b_0 dependency is compensated. The derivation of the following equation is shown in Figure 4.10. Corresponding to the freedom to add $n\cdot 2\pi$ to the phase, the axis intercept is reduced to smaller values:[20]

$$\phi_0^{\mathrm{Start}} = \begin{cases} \phi_{\mathrm{Temp}} + 0.784523\cdot b_{0,r}^{\mathrm{Start}} + 0.878841 & \text{if} \quad b_{0,r}^{\mathrm{Start}} > 0 \\ \\ \phi_{\mathrm{Temp}} + 0.784221\cdot b_{0,r}^{\mathrm{Start}} + 2.255041 & \text{if} \quad b_{0,r}^{\mathrm{Start}} \leq 0 \end{cases} \tag{4.13}$$

The axis intercept for either one of the cases results in approximately π minus the axis intercept of the other one.

For signals without noise, this works well as demonstrated in Figure 4.11. In the ideal case, the points would lie on a line through the origin with slope 1.0.

4.9.2 An approach for small $|b_{0,r}|$

In Figure 4.9 it is demonstrated that the parabola approach as described above (Sec. 4.9.1) fails for narrow peak widths. This subsection gives a brief description of the procedure used in this case.

One can use the phase at i_{Max} to estimate the one at r_{Max}, using the slope of the phase here. Especially for small $|b_{0,r}|$ values, the slope (phase shift per $\Delta\nu$) varies and a parabola

---

[17] They can also be aligned to monotonously falling. However, this does not change the result.

[18] Arbitrary multiples of $\pm 2\pi$ can be added to the phase without changing the mathematical meaning. In this context the Norm[ϕ] function limits the range of ϕ to $]-\pi;\pi]$.

[19] The Gaussian bracket (or "floor") gives the largest previous integer to r_{Max} (0.5 is added to round off correctly, the common "rounding" function includes this correction). This is subtracted from r_{Max} itself, meaning that only the digits after the decimal point remain. As r is the "continuous index" of the frequency scale, this is the direct measure for the deviation of the r_{Max} from the raster of discrete frequencies.

[20] When looking at figure 4.10, the y-intercepts appear to be identical or at most have an insignificant difference. However, the phase values of the ordinate may be limited to a range of 2π, thus, in relation, the difference in the y-intercepts is not at all insignificant.

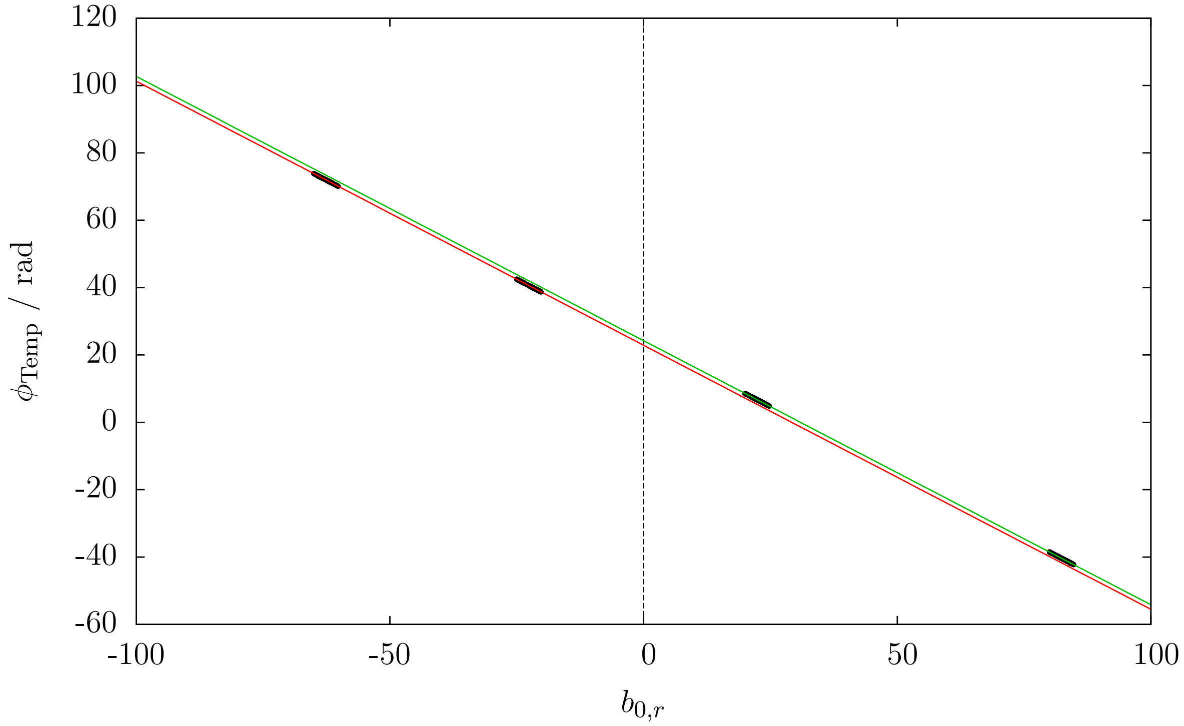

If $b_{0,r} < 0.0$: $\phi_0^{\text{Start}} = \phi_{\text{Temp}} - (m \cdot b_{0,r}^{\text{Start}} + b)$

$m = -0.784523 \pm 5.679 \cdot 10^{-5}$ $(0.007239\,\%)$

$b = 24.2539 \pm 3.437 \cdot 10^{-3}$ $(0.01417\,\%)$

If $b_{0,r} > 0.0$: $\phi_0^{\text{Start}} = \phi_{\text{Temp}} - (k \cdot b_{0,r}^{\text{Start}} + l)$

$k = -0.784221 \pm 8.541 \cdot 10^{-5}$ $(0.01089\,\%)$

$l = 22.8777 \pm 4.011 \cdot 10^{-3}$ $(0.01753\,\%)$

Figure 4.10: Plot demonstrating the linear dependency of ϕ_{Temp} on $b_{0,r}$. $A_0 = 1.0$, $\phi_0 = 0.0$, $\Delta\nu = 1.0\,\text{Hz}$, $N = 1,024$; 8 $\nu_{0,r}$ values are combined with 50 $b_{0,r}$ values within intervals of a width of 5.0 at four different regions. Because of the freedom to add $n \cdot 2\pi$ to ϕ_{Temp}, the right alignment of these values would be a lengthy process. One could write a procedure for this task but I rely on the linearity. Firstly, the $b_{0,r}$ values were chosen so contiguous that no hidden dependency should remain unrecognised. Secondly, a second package for each linear fit was used, exhibiting excellent correspondence to the fit curve progression. Thirdly, subsequent tests confirmed the correctness. Utilising packages allows the usage of few different alignments for several values. Both lines are plotted in both fit intervals to demonstrate their parallel curve progression. In this representation the intercepts appear to be similar, but their difference is significant.

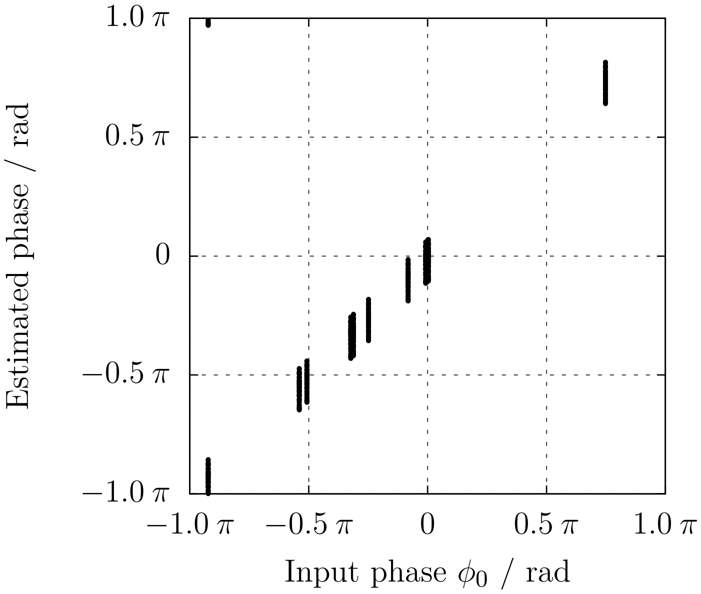

Figure 4.11: The estimated phases are plotted versus the input ϕ_0. For this purpose, 11 ϕ_0, 18 $b_{0,r}$ ($|b_{0,r}| \leq 100.0$) and 11 $\nu_{0,r}$ values are combined to generate 2,178 spectra of sines. If the peak width (Sec. 4.3) results in more than four values representing a peak, the described parabola approach is used to estimate the phase.

can be fitted to this progression (see Fig. 4.6 for small positive or negative $b_{0,r}$ values). Due to the symmetry, only positive values are evaluated, the fit ranges from $0 < b_{0,r} < 8$. The result is a function for the local slope m_{loc}:

$$m_{\text{loc}}(|b_{0,r}|) = a \cdot |b_{0,r}|^2 + b \cdot |b_{0,r}| + c \text{ with:}$$

$$\begin{array}{llll} a & = -0.0114008 & \pm 8.113 \cdot 10^{-6} & (0.07116\%) \\ b & = 0.137131 & \pm 6.478 \cdot 10^{-5} & (0.04724\%) \\ c & = -3.14773 & \pm 1.176 \cdot 10^{-4} & (0.003736\%) \end{array}$$

The deviation between the closest discrete frequency and the estimated peak location is (analogous to Eq. 4.12)

$$r_{\text{diff}} = r_{\text{Max}} - \lfloor r_{\text{Max}} + 0.5 \rfloor \tag{4.14}$$

The phase at r_{Max} can be estimated by linear interpolation:

$$\phi_{r_{\text{Max}}} = \phi_{i_{\text{Max}}} + r_{\text{diff}} \cdot m_{\text{loc}}. \tag{4.15}$$

Analogously to Equation 4.13, the start value for ϕ_0 is gained by compensating for the linear dependency on $b_{0,r}$:

$$\phi_{\text{Temp2}} = m \cdot b_{0,r} + b \tag{4.16}$$

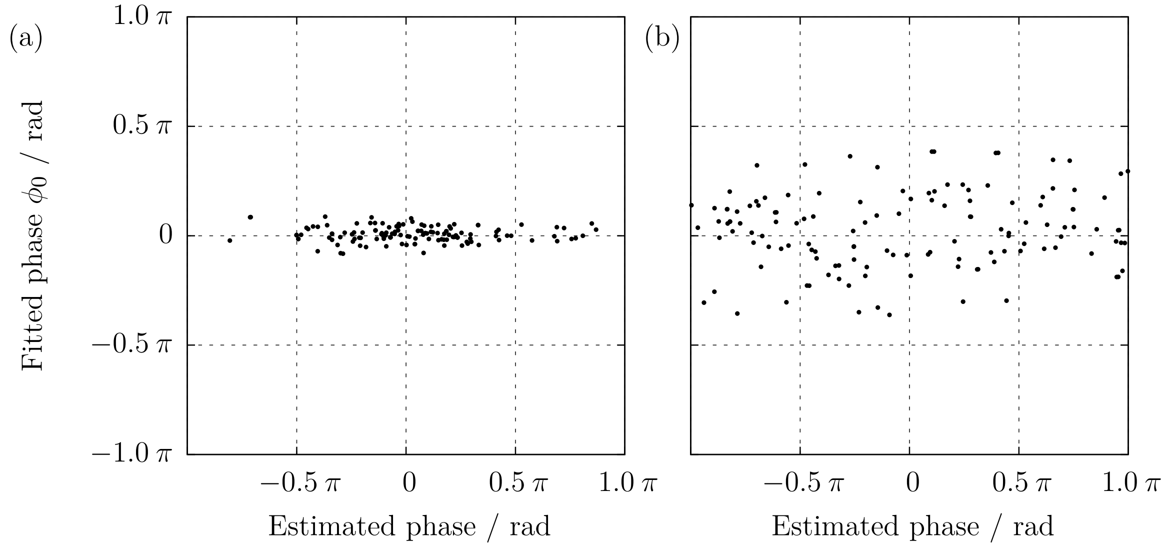

Figure 4.12: Plots demonstrating the estimation and fitting behaviour for the phase parameter under the influence of noise. The input value is fixed at $\phi_0 = 0.0$, 15 values for $b_{0,r}$ and 11 values for $\nu_{0,r}$ are chosen randomly and combined (resulting in 132 dots). (a) 5 % Gaussian white noise; (b): 20 %.

with

$$\begin{aligned} m &= -0.768408 \quad \pm 1.157 \cdot 10^{-3} \quad (0.1506\%) \\ b &= 23.4881 \quad \pm 2.019 \cdot 10^{-2} \quad (0.08596\%). \end{aligned}$$

This approach was developed before the parabola one (Sec. 4.9.1) in which two linear fits are applied depending on the sign of $b_{0,r}$. Here, one common fit is conducted and a correction with respect to the sign of b_0 is performed subsequently. This is less accurate but sufficient for the small range of $|b_{0,r}|$ this approach covers.

$$\phi_0^{\text{Start}} = \phi_{r_{\text{Max}}} - \phi_{\text{Temp2}} + \begin{cases} -0.428352 & \text{if} \quad b_{0,r}^{\text{Start}} > 0 \\ 0.286399 & \text{if} \quad b_{0,r}^{\text{Start}} \leq 0 \end{cases} \tag{4.17}$$

4.9.3 Subsequent phase adaptation

Figure 4.12 shows examples for the start parameter estimation and results of actual fitting of ϕ_0 with two levels of Gaussian white noise. One can see that this approach is highly vulnerable to noise. Ideally, all values should be centred at (0.0; 0.0), because the phases of all input sines are zero. Two results should be pointed out: Firstly, even for low levels of noise the estimated phases are likely to differ from the input ones and these differences seem to have no impact on the fit result (if the fitted ϕ_0 is $\neq 0.0$, one could expect an alignment along the line through the origin with slope 1.0). Secondly, the fitted values are likely to be remarkably different from the input values.

The parameter ϕ_0 is the initial phase of the sine function in the time domain, whereas the start parameter estimation can only be performed in the spectral domain, which includes the complete data interval. Small changes of either ν_0 or b_0 will hardly change the first period in the time domain, but, if the spectral domain is fitted, especially the peripheric regions in the time domain will change. The higher the level of noise, the less precise these parameters will be estimated and therefore the more the phase is going to change during the fitting process, regardless of how well the start value fits to the estimated set of the other start parameters.

To better understand this this behaviour, it was analysed how the start phase influences the fit result by taking a GWN level of 20 % and the estimated start values as described in this chapter. Additionally, the fixed phases $n \cdot \frac{2\pi}{8}$, $n \in \mathbb{N}$, $[0 \leq n \leq 7]$ are also used as start phases. $56,144$ fits were analysed and the estimated phase did not perform any better than the equidistantly distributed ones. Figure 4.13 includes three examples for fitting and LFS-sine removal, demonstrating different effects: (a) shows the fit with the least difference with respect to the RMS_Δ value of the pure noise before the sine has been added and the RMS_Δ value after the sine has been added, fitted and subtracted.[21] This is desirable for all fit results. (b) illustrates a very common behaviour: The complex values of the noise add to the ones of the sine in such a way that the sum is similar to a sine with different parameters. The fit algorithm cannot discriminate between the contributions from the LFS sine and the GWN and, by minimising χ^2, will result in the parameters for their superposition to produce the corresponding spectral peak. Consequently, if a sine with these parameters is subtracted, it will leave a notch in the spectrum (particulars of notches are given in Sec. 5.6). Finally, (c) reveals the reason for these plots being shown in the section about start phase estimation: The fit result is very different from the start parameters:[22]

A_0^{Input}	A_0^{Start}	A_0^{Result}	ν_0^{Input}	ν_0^{Start}	ν_0^{Result}	b_0^{Input}	b_0^{Start}	b_0^{Result}
1.0	0.84496	−0.62886	200.500	199.764	171.198	66.124	70.984	132.931

---

[21] In order to quantify the influence of the LFS-sine subtraction on the data (in anticipation of Section 5.2.1.1) the RMS_Δ value is used as a measure for the energy difference between the original signal and the signal after subtraction of a (LFS) sine. For artificial signals, the signal without (LFS) is known and can be compared with the signal after a (LFS) sine is added, fitted and subtracted. These two signal are subtracted and the root mean square (RMS) value is determined in the time domain; ideally it would be zero.

[22] For the sake of completeness, but with little usefulness: $\phi_0^{\text{Fit}} = 4.2112$, $\phi_0^{\text{Input}} = 5.2679$, $\phi_0^{\text{Start}} = 0.9457$. Because of the difference between input parameters and fit results, the statement that the phase is wrong by only $\phi_0^{\text{Input}} - \phi_0^{\text{Fit}} = 1.0567$ is wrong; multiples of 2π lie between them (compare phase swapping for broad peaks, e.g. Fig. 3.3). A_0 has become negative; this indicates, that the poorly estimated phase is compensated for by decreasing the amplitude through zero and up to its negative value. It also demonstrates the ability of the algorithm to evolve parameters systematically to values far from the starting ones.

Figure 4.13 and, in addition, Figure 4.14 show the LFS sine components for these fits and demonstrate what a wrong start phase can induce:[23] If the phase is close to being maximally wrong, then the χ^2 (Sec. 2.1.1) value at the first iterations is very high, even higher than without any sine function at all. Whatever parameters the gradient drives the algorithm to, they will most likely be accepted as an improvement because the χ^2 value is likely to decrease. Multiple acceptances in a row increase the step size of the algorithm by orders of magnitude. Therefore, the algorithm may perform long steps in the four-dimensional parameter space and subsequently end up in a secondary minimum – with very different parameters from the estimated ones.

A solution is to pin down the fitting algorithm at the best local χ^2 minimum which can be found with reasonable effort. For this, a first step is introduced in which four phases are tested: The first is the one that is estimated like before; furthermore, successively $\pi/2$, π and $3/2\,\pi$ are added. Within the peak width, the complex values for sines with these phases (and the conventionally estimated other three parameters) are calculated and subtracted from the spectrum at hand. The sine producing the lowest sum of squared values, ϕ_{best}, in this range should have the best set of parameters of the four sets. Assuming a smooth topology, the resolution is improved by repeating this procedure with additional phase variations: Centred between this best phase so far and its two neighbours (in this case the ones at $\phi_{\text{best}} \pm \pi/2$) two additional nodes are calculated and again ϕ_{best} is set to the phase producing the lowest sum of squared values. With each repetition two sets of parameters need to be calculated for each duplication of the resolution. In this work the process stops after two more halvings so that the best 16th part of the phase cycle is selected.[24] In sum, the additional effort yields the need to calculate F_{Sum} for all discrete values within the peak width r_{W} (Sec. 4.3) for eight phases.[25] The calculation of the pure values is less computational effort than if the derivatives are included. According to a rough estimate this additional effort is in the range of six iteration steps and thus quite high.[26]

---

[23] Note that, in opposition to the statement in Sec. 2.1.1, the maximum number of iterations is 400 here.

[24] Showing another plot with e.g. ϕ_0^{Start} versus ϕ_0^{Input} is dispensable: the differences between the input and the start values of ν_0 and b_0 are typically big enough to alter the phase spectrum of the input values compared to the start values significantly (the phase shift per $\Delta\nu$ is up to π, e.g. Sec. 3.2). It is important for the start phase to fit to the other start parameters in order to begin the fit procedure with a low χ^2. The potentially big difference between ϕ_0^{Start} and ϕ_0^{Input} is unproblematic and gets cancelled out during iteration.

[25] Four steps on the whole circle yields a resolution of a $1/4$ circle, then twice with halved angles each further doubling the resolution.

[26] For future applications, one could introduce a parameter to decide whether this phase testing is reasonable; e.g. for low levels of noise the introduced estimation approach works very well, therefore a peak-height-above-noise level could be estimated and used with a threshold. Another approach could include the evaluation of the parabola fit quality in the phase spectrum (presumably based on a threshold for the RMS value of the difference between the parabola and the real values).

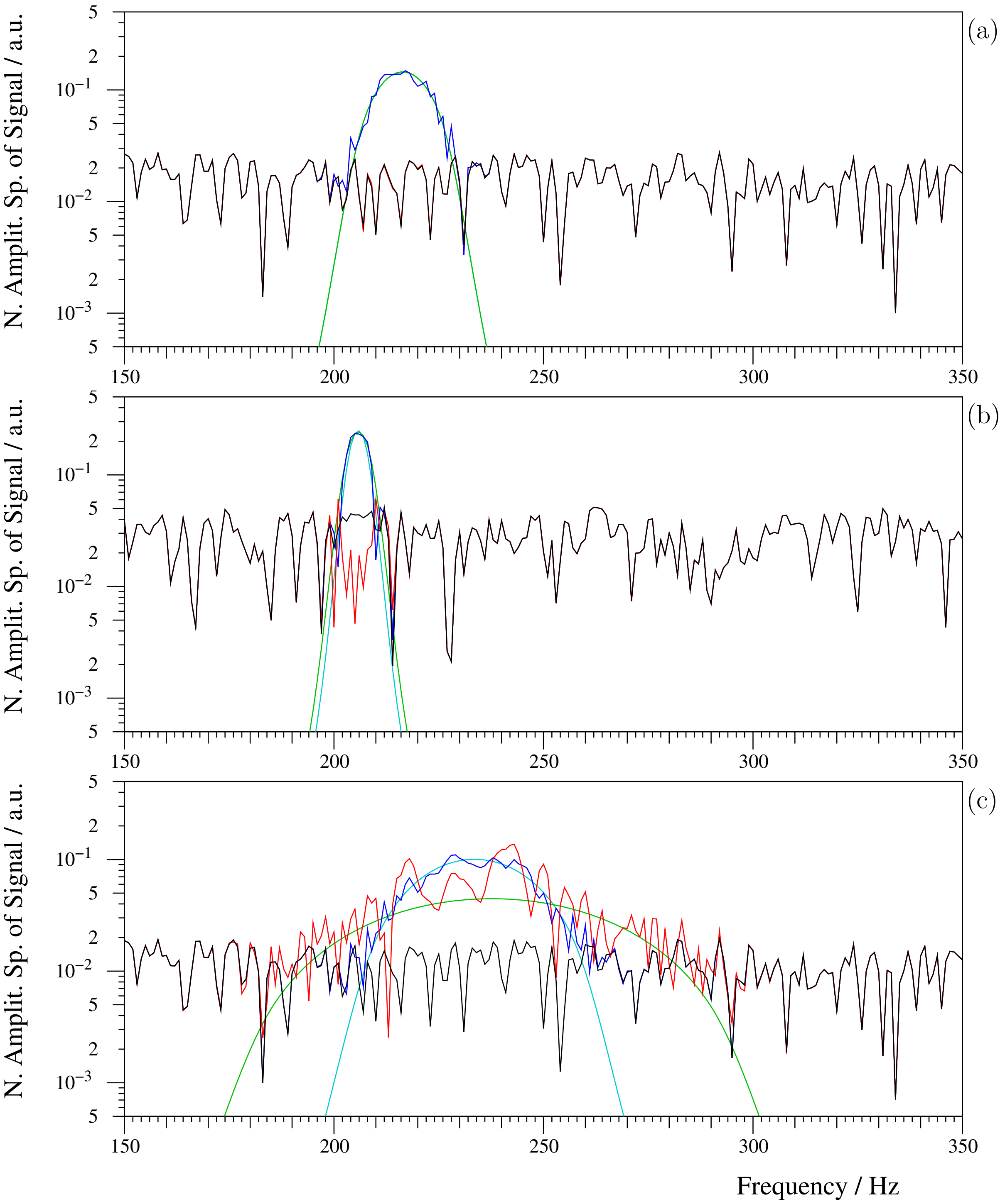

Figure 4.13: LFS sines superposed with GWN (20 %) in the spectral domain. Turquoise: underlying sine, green: fitted sine, blue: input data (sum of noise and sine), red: data after peak subtraction, black: pure noise. (a) shows the best fit with the lowest RMS_Δ value (0.0116) of the difference between the pure noise (black) and the data after addition, fitting and subtraction of a sine (red), indicating that the data remains highly unchanged. (b) is still successfully fitted, but the manipulation of the underlying data is quite strong. By comparing the red and the black curve progression, one can see obvious deviations: The fitting procedure leaves a deep notch in the spectrum, ($RMS_\Delta = 0.531$). (c) shows the most improper of all fits, its RMS_Δ value is 0.785 when the fit is stopped unsuccessful after 400 iterations (Fig. 4.14 shows additional plots).

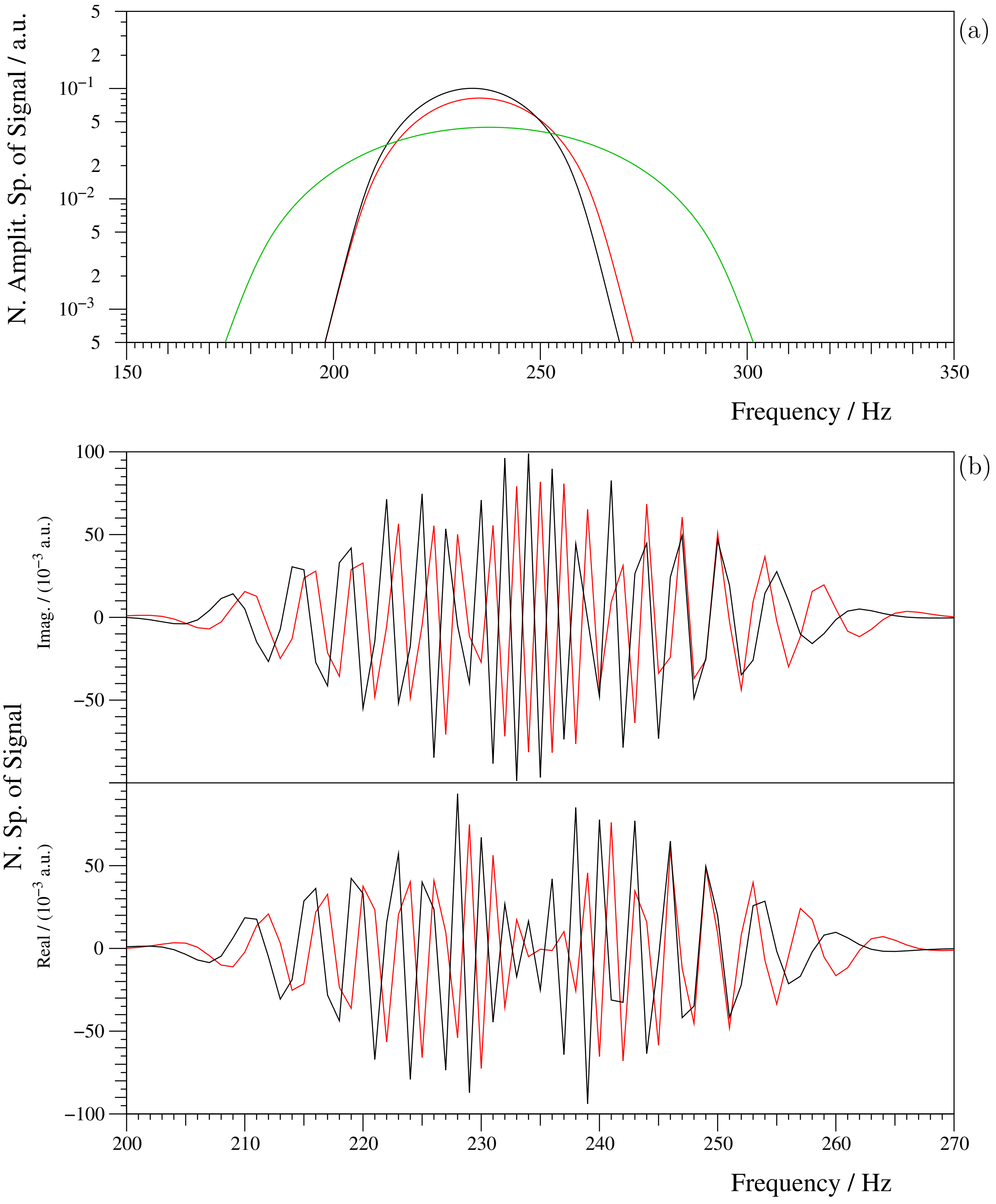

Figure 4.14: Additional plots to the spectra exhibited in Figure 4.13 (c). (a) illustrates the three sine functions: the start values are represented by the red line, the fit results by the green and the input values are given in black. The three start values for A_0, ν_0 and b_0 are neither good, nor exceedingly bad. (b) shows the complex spectrum (zoomed in): For the sake of clarity only the start and input curves are given, pointing out the reason for a very high χ^2 at the beginning of the fit. The start value for ϕ_0 causes most of the values to have negated signs in comparison to the input spectrum.

4.10 Conditions for failure

The correct estimation of the width of a peak is the more challenging, the higher the level of noise becomes in combination with big values of $|b_{0,r}|$. Figure 4.15 shows one example where the start-value-estimation algorithm fails completely: Because of the high level of GWN, the superposed signal shows deep notches and the algorithm sets the borders of the peak width (Sec. 4.3, 50% decrease in magnitude to the sides of i_{Max}) very close to the maximum (see red marked region in (b)). Additionally, the extreme peak width induces a very small slope. Combined with an unfortunate superposition with the noise, the parabola calculation (Sec. 4.6) results in an inverted sign for the parabola orientation a_c for b_0. When the parabola opens upward the peak is per se skipped in the sense that no attempt to fit is done.

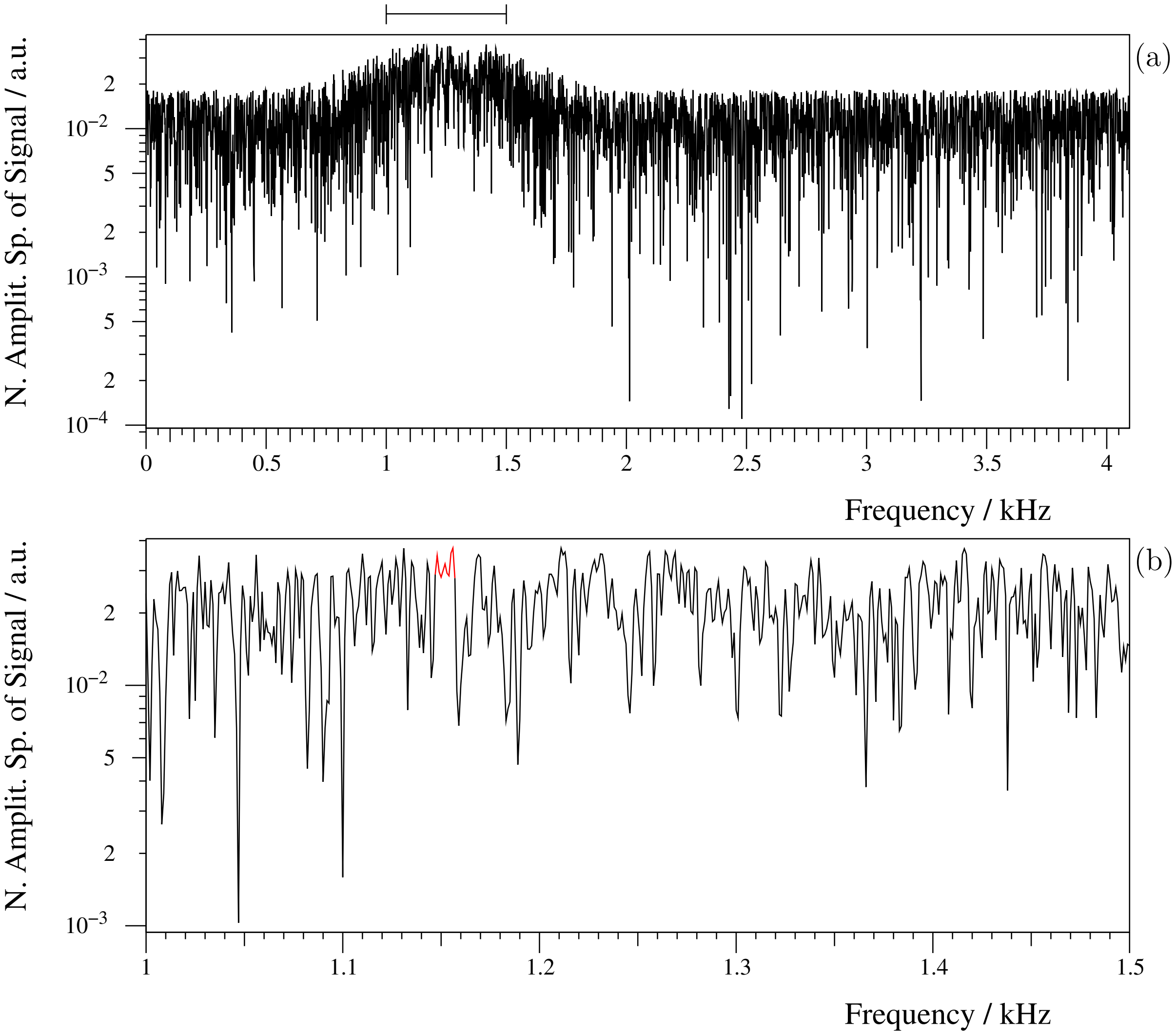

N	Δt	$\Delta\nu$	A_0	ν_0	b_0	ϕ_0
$8{,}192$	$1/N$	1.0	1.0	$2{,}000.125\,\mathrm{Hz}$	$-1{,}495.605\,\mathrm{Hz/s}$	0.0

Figure 4.15: Example for a spectrum where the start parameter estimation fails. (a) shows the complete spectrum, (b) is zoomed to the peak (interval marked with a bar), eleven complex values were used around the absolute maximum (the rightmost peak of the red values). The values given are the input parameters. Due to the fact that the start value estimation fails, no fit results are shown.

Chapter 5

Fit results with synthetic sines

5.1 Introduction

This chapter quantitatively evaluates the performance of the Levenberg-Marquardt algorithm (Sec. 2.1.1) fitting the parameters of the derived continuous equation for an LFS sine ($\mathrm{F_{Sum}}$, Eq. 2.95) with the start parameters as described in the last chapter. Real signals tend to be complex and the exact parameters of supposed LFS sines are unknown. One cannot but rely on the parameters returned by the algorithm and has to accept that some peaks remain in a spectrum and others, such as small peaks which look like noise, are subtracted. Real signals will be treated in Chapter 6. In order to allow a quantitative analysis of fits with comparison of the fitted with the original parameters and a statistical evaluation, this chapter uses synthetic signals. Their input parameters are varied (systematically and randomly) and the fit performance is documented. A spectrum of a LFS sine superposed with GWN (Sec. 4.2) is defined by many parameters:

- In general, the spectral parameters are: T, Δt and N, for which $T = N \cdot \Delta t$. For synthetic signals, the Δt can be chosen to be $({}^{1}\!/_{N})\,\mathrm{s}$ according to the coordinate transform (Sec. 3.1.3). Therefore, the number of parameters can be reduced to a single one, here N is chosen. It stipulates the number of values of a spectrum without influencing any general property. The smaller the N, the more likely it is to find a peak located at a region where the corresponding peak located within the negative frequencies contributes significantly, which cannot be handled by the start parameter estimation procedure and therefore can indeed influence the fitting performance.[1]

- The GWN parameters are: The level (relative to the amplitude of a LFS sine, Sec. 4.2.1) and the seed number of the pseudo-random noise for the phase.

---

[1] The $\mathrm{F_{Sum}}$ expression includes both types of contribution, the one from the peak located within the negative frequencies, as well as the one from the infinite repetitions of peaks. The issue described here exclusively applies to the start-value estimation.

- The LFS sine parameters are: A_0, $\nu_{0,r}$, $b_{0,r}$ and ϕ_0. A_0 can be neglected and is mainly set to 1.0 in this work. ϕ_0 is the initial phase of the LFS sine and contributes linearly to the rotation angle of the complex values in the spectrum of this LFS sine. In a signal with GWN it determines whether the values of the peak superpose constructively or destructively. Therefore, varying the ϕ_0 is somewhat similar to varying the seed of the GWN.[2] Thus, if the phase dependency of superpositions of (LFS) sines and GWN is to be analysed, it is reasonable to combine both, the seed and the ϕ_0, although in limited numbers.

→ In order to keep the number of calculations manageable, for most of the evaluations shown in this chapter, the parameters $\nu_{0,r}$, $b_{0,r}$, ϕ_0 and GWN seeds are combined systematically.

5.2 Parameters for the quantitative evaluation

5.2.1 For known input parameters

5.2.1.1 The RMS_Δ value

This measure was used in the last sections to sort the examples. RMS_Δ is the RMS value of the difference between the underlying signal without LFS sine (here the GWN) and the signal after addition, fitting and subtraction of an LFS sine in the time domain. This is reasonable as it represents exactly what the intention of this work is: The subtraction of an LFS sine without the manipulation of the underlying signal.[3]

5.2.1.2 The four-component error vector

The error vector consists of the four differences between the parameters of the fit result and the ones of the input signal as components. Its magnitude is a mathematical measure for the accuracy of the fit: How close are the values, reproduced by the fit algorithm, to the input values? Rough scale factors have to be identified to render comparable

---

[2] For a certain GWN seed, all values of the noise are determined; changing the seed (pseudo-) randomly sets completely new phases. The GWN can show combinations of neighbouring phases which – in combination with different LFS sines with similar peak positions – produce superpositions, which are more often hard to fit for the algorithm than other combinations no matter the ϕ_0 parameter. In contrast, ϕ_0 acts like an offset to the phases of the LFS sine spectrum; changing its value does not necessarily influence the quality of the superposition with the underlying signal.

[3] The disadvantage of the RMS_Δ measure is its dependencies on the LFS parameters. Firstly, it is proportional to A_0, which is cancelled here by setting $A_0 = 1.0$. Secondly, for a fixed GWN level, the actual amplitude of the GWN is a function of $|b_{0,r}|$ (Sec. 4.2.1). For increasing values of $|b_{0,r}|$, the absolute power in the signal decreases, resulting in lower RMS_Δ values and leading to a superior evaluation to fits of smaller $|b_{0,r}|$ and similar quality. In principle, an additional division by the RMS value of the pure GWN signal could be used to avoid a scaling with the peak width. Instead of excluding these dependencies, the following plot shows this elementary measure; the upcoming plots will use the more suitable one: $|\vec{p}_{\text{Err}}|$.

Difference	Factor
$\Delta A_0 = A_0^{\text{Fit}} - A_0^{\text{Input}}$	$5.0/A_0^{\text{Input}}$
$\Delta\phi_0 = \text{Norm}[\phi_0^{\text{Fit}} - \phi_0^{\text{Input}}]$	$2/\pi$
$\Delta\nu_0 = \nu_0^{\text{Fit}} - \nu_0^{\text{Input}}$	1.0
$\Delta b_0 = b_0^{\text{Fit}} - b_0^{\text{Input}}$	0.5

Table 5.1: Calculation specifications for the components of the error vector. The factors weight the components in order to adapt the influence of each component on the overall result equally. $\Delta\phi_0$ is normalised to the range $]-\pi;\pi]$, otherwise the subtraction of similar values could lead to big results (e.g. for $\phi_0^{\text{Fit}} = 0.99\pi$ and $\phi_0^{\text{Input}} = -0.99\pi$).

parameters (e.g. the amplitude may have any order of magnitude – therefore the same is true for the difference – whereas the phase is always on the same scale). Figure 5.1 shows the input values subtracted from the resulting fit values; the sorting is from bad to good with respect to the RMS_Δ.[4] One can see the ranges of the deviations; the derived scaling factors are given in Table 5.1. The factors are chosen in such a way that most of the values are below 1.0. The accuracy of a single fit can be described with the Euclidean norm of the difference vector:

$$|\vec{p}_{\text{Err}}| = 0.5\sqrt{\left(\frac{5.0\cdot\Delta A_0}{A_0^{\text{Input}}}\right)^2 + (2/\pi\cdot\Delta\phi_0)^2 + (\Delta\nu_{0,r})^2 + (2.0\cdot\Delta b_{0,r})^2} \tag{5.1}$$

The factor 0.5 provides for the mean of the values under the root. Therefore, the result should be as small as possible and, in case it approaches 1.0, the fitting might have failed.

5.2.2 For unknown input parameters: χ^2_n

In real applications, one does not know the pure underlying signal and the approaches described above are not available. Instead, the only information available on the peak lies in the (complex spectral) values that are used to perform the fit. As described in Section 2.1.1, χ^2 is the value used internally by the Levenberg-Marquardt algorithm to evaluate whether or not an iteration step improves the parameters. χ^2 is evaluated in the spectral range comprising the values the fitting is applied to; for very small peaks these are only three or four complex values, for broad peaks their number can be in the order of 100. Because χ^2 (already normalised by the spectral magnitudes) consists of a sum, it

---

[4] An annotation to this figure: The plots (b) to (d) show a split, meaning that (at least for these 51,040 combinations) as soon as one of these parameters evolves to far the others will follow. This behaviour makes sense: At this GWN level (20 %), the peak is still pretty well located at the mean frequency. If e.g. b_0 increases, the peak gets broader, making the ν_0 decrease to keep the mean frequency. For ϕ_0 one can assume that the phase at the begin of the time interval changes if the other parameters change, in order to retain the best fit.

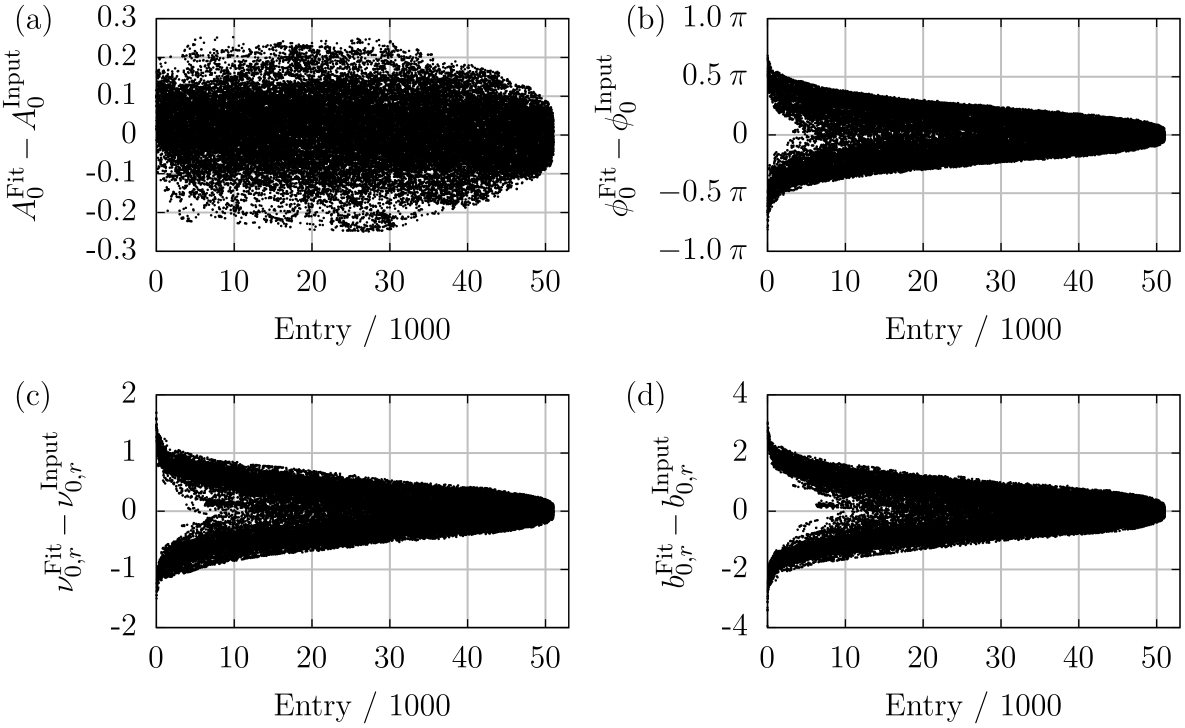

N	Δt	$\Delta\nu$	A_0	ν_0	b_0	ϕ_0	GWN_{Seed}	GWN_{Level}
128	$(1/N)$ s	1.0 Hz	1.0	var.	var.	var.	var.	0.2

Figure 5.1: : Deviations (fit result minus input value) for the four parameters. $16 \times \nu_0$, $29 \times b_0$ ($|b_{0,r}| \leq 20.0$), $11 \times \phi_0$, $10 \times GWN_{\mathrm{Seed}}$ are combined, resulting in 51,040 points. The entries are sorted by RMS_Δ; from left to right the fitting results improve. On the ordinates the deviations (fit result minus input value) for the four parameters are plotted.

is reasonable to divide it by the number of complex values n in order yield comparable results for different fits:

$$\frac{\chi^2}{n} = \chi_n^2 \tag{5.2}$$

The probability of the fit producing quite a good χ^2 value if the underlying signal does not contain an LFS sine is noteworthy. The distinction between false-positive and false-negative is crucial; adjusting the receiver-operating characteristic is an important task and described later on.

5.2.3 Comparison of the parameters

Figure 5.2 (a) shows a histogram comparing the RMS_Δ with the $|\vec{p}_\mathrm{Err}|$ (for all input LFS sines: $A_0 = 1.0$): In the lower left both parameters indicate a successful fit; if the fitted LFS sine parameters were exactly the same as the input parameters the result would inevitably be $|\vec{p}_\mathrm{Err}| = RMS_\Delta = 0.0$. For most fits both parameters are similar, therefore a kind of diagonal line from the zero point to the right top is formed by the data. Nonetheless, the deviation can be quite significant.[5] Two groups of parameter constellations are interesting: A high RMS_Δ and, at the same time, a low $|\vec{p}_\mathrm{Err}|$ (right, bottom) and vice versa. The former consists of cases where parameters are reproduced well while even small parameter changes produce significant signal variation.[6] The latter is the other way around.

Figure 5.2 (b) contains the same data as (a), but compares $|\vec{p}_\mathrm{Err}|$ with χ_n^2, the parameter which will also be available for real data. Both parameters tend to correspond to each other, but with a high variance. Two cases are likely to occur: short vectors (good reproduction of the input parameters) and quite bad χ_n^2 (conformity of data and fit function) at the same time and vice versa. Figure 5.3 includes similar plots for different levels of noise and with double-logarithmic scale in order to give an overview about the ranges of the parameters. Additionally, N was changed, without noteworthy influence on the outcome. (a) demonstrates that the fit always ends in the right minimum and that the subtraction removes the LFS sine completely. The procedure is implemented with double precision in floating-point variables. The deviations of the results are in the same order of magnitude as the numerical resolution (≈ 16 decimal digits).[7] Figure 5.4

---

[5] Two examples: For a given $|\vec{p}_\mathrm{Err}|$ of 0.5, the RMS_Δ value can be in the range of $0.2 - 0.5$ or for a given $RMS_\Delta = 0.2$ the $|\vec{p}_\mathrm{Err}|$ can be anything between close to perfect and up to 0.5, which indicates a poor result.

[6] One could ask whether one parameter is particularly responsible and whether a different scaling of the components of error vector would lead to more consistency. But there are indications that constant factors could be insufficient to describe the parameter dependencies. For example: if b_0 or ν_0 are slightly different from the input ones, the period lengths in the time domain do not match with the ones of the input signal. If the T is long or the local frequency is high, the phase deviation can locally lead to constructive superpositions instead of reductions of amplitudes which can result in significantly high values of RMS_Δ.

[7] The horizontal lines which are visible in Figure 5.3 (a), in all probability, stem from the numerical

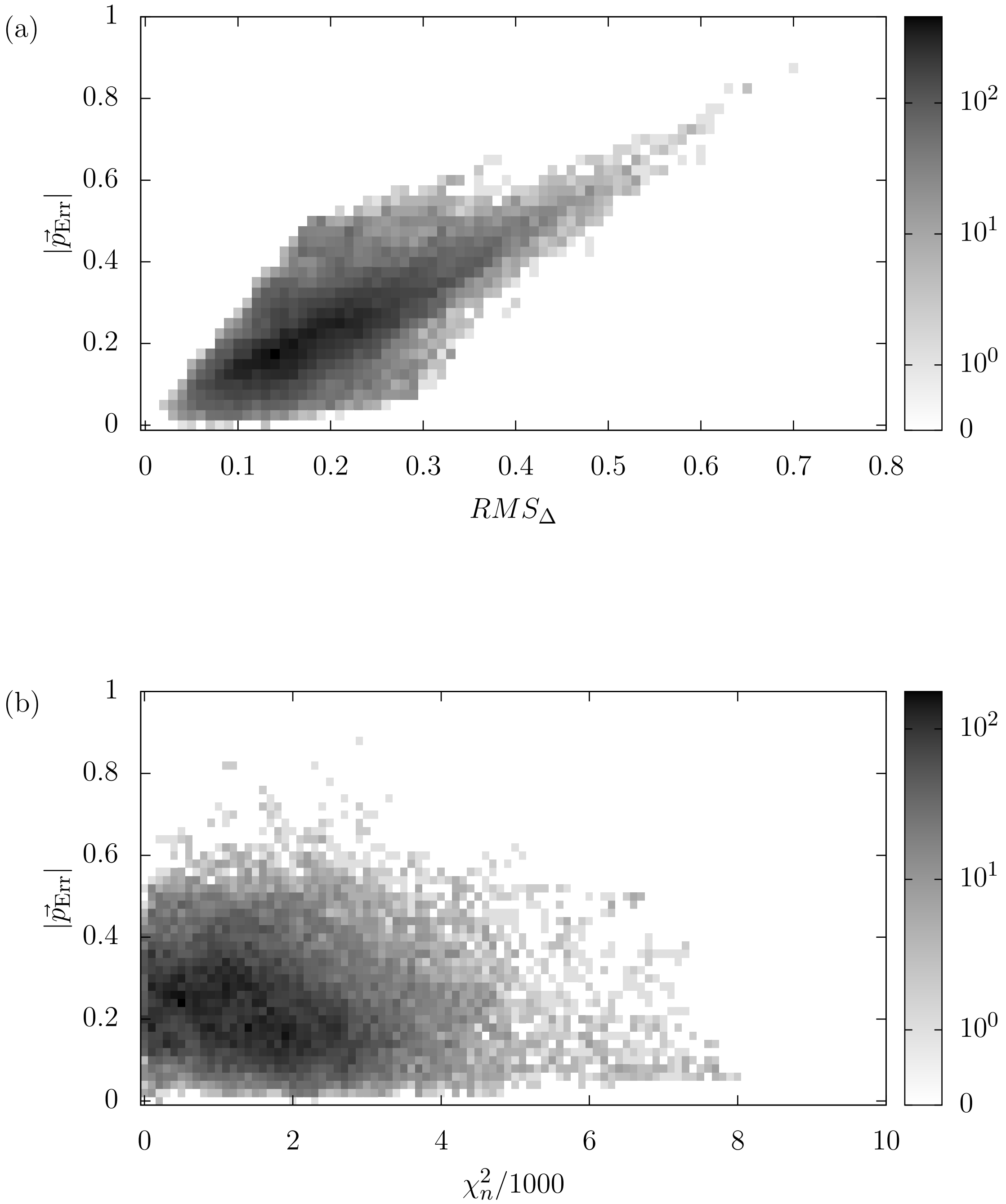

N	Δt	$\Delta\nu$	A_0	ν_0	b_0	ϕ_0	GWN_{Seed}	GWN_{Level}
128	$1/N$	1.0	1.0	var.	var.	var.	var.	0.2

Figure 5.2: Comparison of evaluation parameters. The same data as in Figure 5.1 are plotted in the form of two dimensional histogram over 51,040 values. Grey scale: The number of entries in a certain $\chi_n^2/|\vec{p}_{\mathrm{Err}}|$ bin. Ordinate: $|\vec{p}_{\mathrm{Err}}|$ (Eq. 5.1), Abscissa: (a) RMS_Δ, (b) χ_n^2. E.g. the worst result in (a) ($RMS_\Delta = 0.70$, ordinate: $|\vec{p}_{\mathrm{Err}}| = 0.88$) occurs once, the highest number of occurrences is 455 at $RMS_\Delta = 0.14$, $|\vec{p}_{\mathrm{Err}}| = 0.175$.

illustrates a typical fit for a pure LFS sine. Beyond the sixteenth digit of the fit result basically random digits follow. For non-pure LFS sine signals several examples of spectra are demonstrated in the upcoming sections.

The given plots provide an insight in the typical range of χ_n^2 values if an LFS sine with different levels of noise is fitted. Before the receiver operating characteristic can be set, the false-positive rate needs to be analysed as well.

---

resolution, that is they represent the steps between two values of a certain parameter.

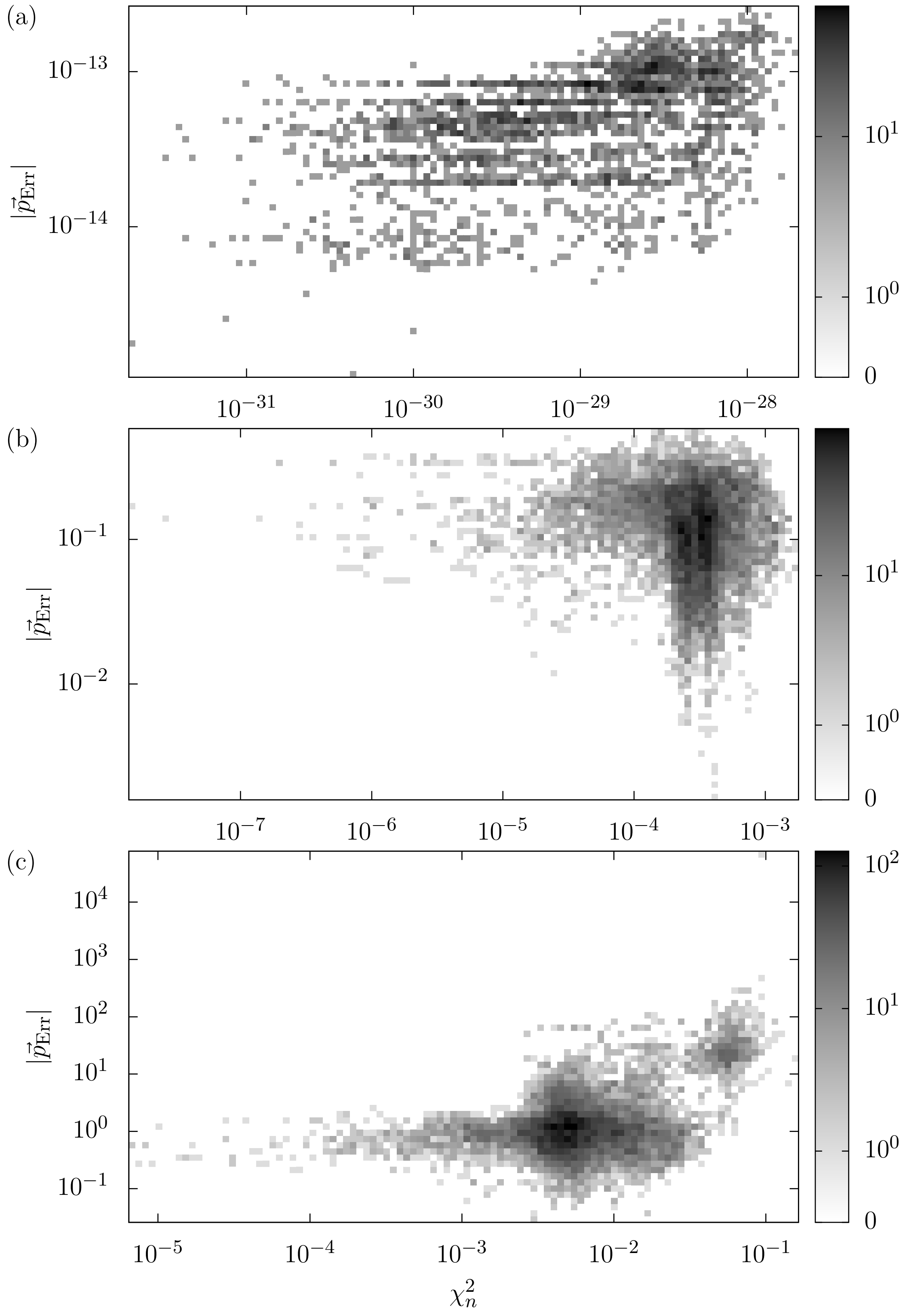

Figure 5.3: For three different GWN_{Level}: (a): 0.0, (b): 0.1, (c): 0.5, the combinations of $16 \times \nu_0$, $29 \times b_0$, $6 \times \phi_0$, $5 \times GWN_{\mathrm{Seed}}$ values are illustrated for $N = 1{,}024$ samples (for $GWN_{\mathrm{Level}} = 0$ the seed variation is replaced by a quintupling of each entry to keep the plot comparable to the other ones), resulting in $13{,}920$ samples each. Grey scale: The number of entries in a certain $\chi_N^2 / |\vec{p}_{\mathrm{Err}}|$ bin. For (c), 642 values are discarded because no reasonable start values could be gained.

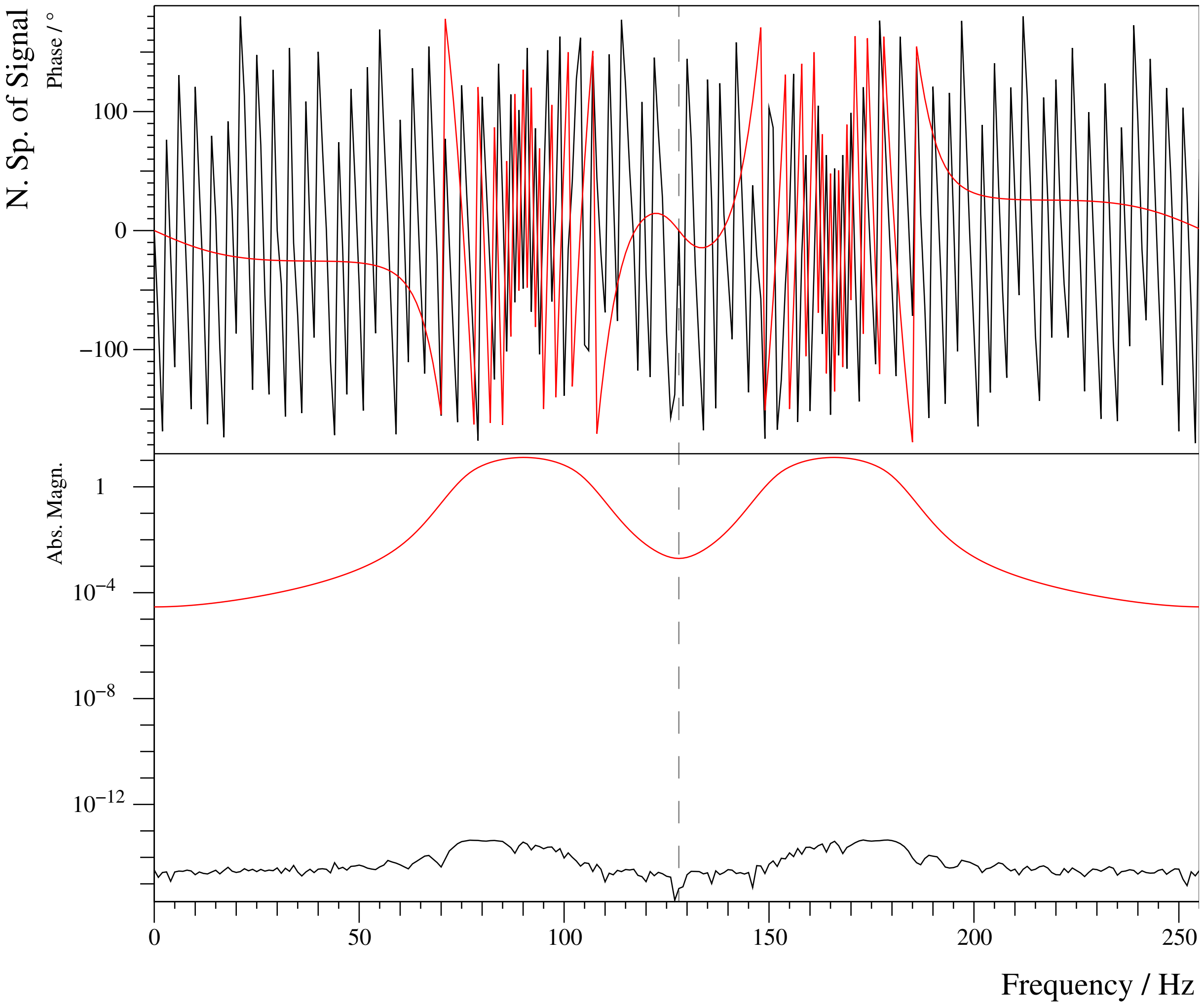

	ν_0 / Hz	b_0 / (Hz/s)	ϕ_0 / °	A_0
Input:	70.1	40.1	160.1	100.0
Start:	69.93	40.41	177.2	98.1
Fit:	70.099999999999994	40.100000000000001	160.09999999999983	100.00000000000021

Figure 5.4: Magnitude (bottom) and phase (top) spectrum of a pure LFS sine (red) and the same after a LFS sine ($\mathrm{F_{Sum}}$ Eq. 2.95) fit and subtraction (black), $N = 256$, $\Delta t = (1/N)\,\mathrm{s} \rightarrow \Delta\nu = 1.0\,\mathrm{Hz}$ (it follows that $\nu_0 \mathrel{\widehat{=}} \nu_{0,r}$ and $b_0 \mathrel{\widehat{=}} b_{0,r}$). The start-value-estimation procedure decided that 21 complex values lie within the peak width; the fitting ends after 53 iterations with $\chi^2_n = 7.92 \cdot 10^{-29}$. Beyond the Nyquist frequency (128 Hz) the negative frequencies are arranged. Especially the phase spectrum (top) suggests that the remaining signal mainly consists of random numbers.

5.3 Receiver operating characteristic

In order to investigate the problem of false positives, the algorithm is applied to spectra generated from pure, Hann-windowed Gaussian white noise.[8] The analysis of the fit results will allow for the determination of thresholds or conditions if a certain proportion of false positives is to be allowed. Figure 5.5 shows the proportion of false positives as a function of χ_n^2. In order to obtain comparable statistics the results of different numbers of spectra (with varying GWN seed numbers) are merged in such a way that the same number of spectral values (in each case $4{,}096$ for the positive frequencies) are taken into account in the form of one set. Five sets for each N are generated to demonstrate the degree of variation. This plot provides an overview of the progression. The table shows how many local maxima were evaluated and gives an insight on the spreading of numbers. It also shows that approximately $N/8$ local maxima occur.[9] Keeping in mind that only $N/2$ values form the positive-frequency spectrum analysed, this means on average every fourth spectral magnitude value is counted as a local maximum.

Figure 5.6 illustrates that the threshold for χ_n^2 should be chosen based on the number of values used for the fit; for example: If the threshold for χ_n^2 is chosen to be 0.01, then 7 % of all fits with 4 values are counted as successfully fitted, but also 43 % of all local maxima with 3 values. Thus, for big values literally no false positives would occur. For three different percentages of allowed false positives the dependency of χ_n^2 thresholds on the number of used complex values is given in Figure 5.7. Using this curve progression one can set different thresholds for every number (or range of numbers) of values used; the corresponding function is called $\chi^2_{\text{Thres}}(n_{\text{Fit}})$. In the program code, this is implemented as a lookup table with the values shown in Figure 5.7. For bigger numbers, the values in between two points are interpolated linearly.

Analogously, thresholds are set for the monofrequent approach (Sec. 2.3.7). Because of the limited peak width, single values are sufficient:

False-positive proportion	$\chi^2_{\text{Thres}}(n_{\text{Fit}})$
1 %	0.00356
2 %	0.00610
5 %	0.01173

Plots similar to the ones in Figure 5.5 are given in appendix A.3.

---

[8] This analysis lives on the effect, that using a window function on GWN values results in local maxima in the spectrum due to superposition of sines: Every value in the spectrum without a window function could be considered as the spectrum of a sine function. Applying the Hann-window function implies a convolution with three δ functions at the same and the direct neighbouring positions, so every single resulting spectral value is influenced by its direct neighbours, resulting in a spiky magnitude spectrum. Without the window function the GWN magnitude spectrum would be perfectly even without any local maxima‘and therefore useless for this approach.

[9] A maximum is counted as valid if the magnitude drops below 50% to both sides (Sec. 4.3); the smaller the N, the relatively more spectral values are close to the borders of the spectrum where this condition may not be fulfilled.

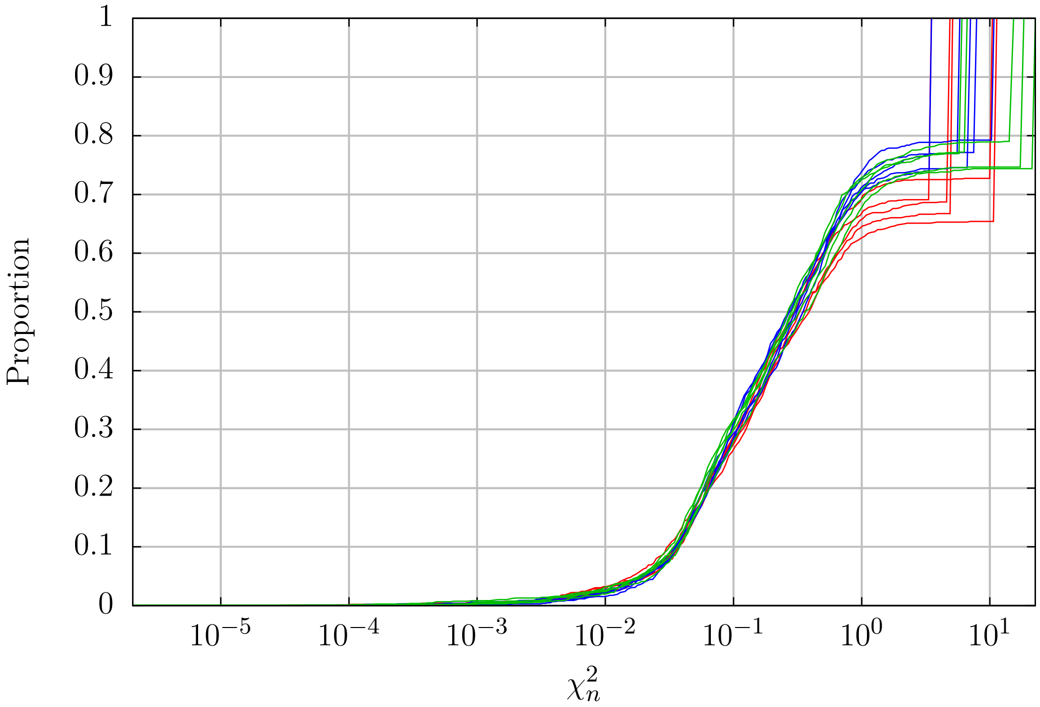

N	Number of spectra per set	Number of local maxima per set				
128	64	998	994	1,023	988	997
$1,024$	8	1,041	1,037	1,036	1,030	1,023
$8,192$	1	1,050	1,053	1,068	1,073	1,054

Figure 5.5: Summed histogram of the χ_n^2 outcome from fits to local maxima in spectra of pure Gaussian white noise (for each spectrum the GWN seed is changed): Green: 5 sets, each consisting of a single spectrum with $8,192$ samples, blue: 5 sets, each consisting of 8 spectra with $1,024$ samples, red: 5 sets, each consisting of 64 spectra with 128 samples. The abscissa shows the quality of the fit: χ_n^2 discretised into 200 steps between the extremes. The ordinate holds the proportion of how many fits have a certain χ_n^2 or better, normalised to the number of local maxima. E.g. one can see that 30% of the local maxima are fitted with a $\chi_n^2 = 0.1$ or better. Local maxima where the algorithm failed to estimate start values are assigned an artificial χ_n^2: The maximum value plus one increment step, therefore the proportion value jumps to 1 right after the biggest valid χ_n^2 value, indicating the proportion of non-fitted maxima.

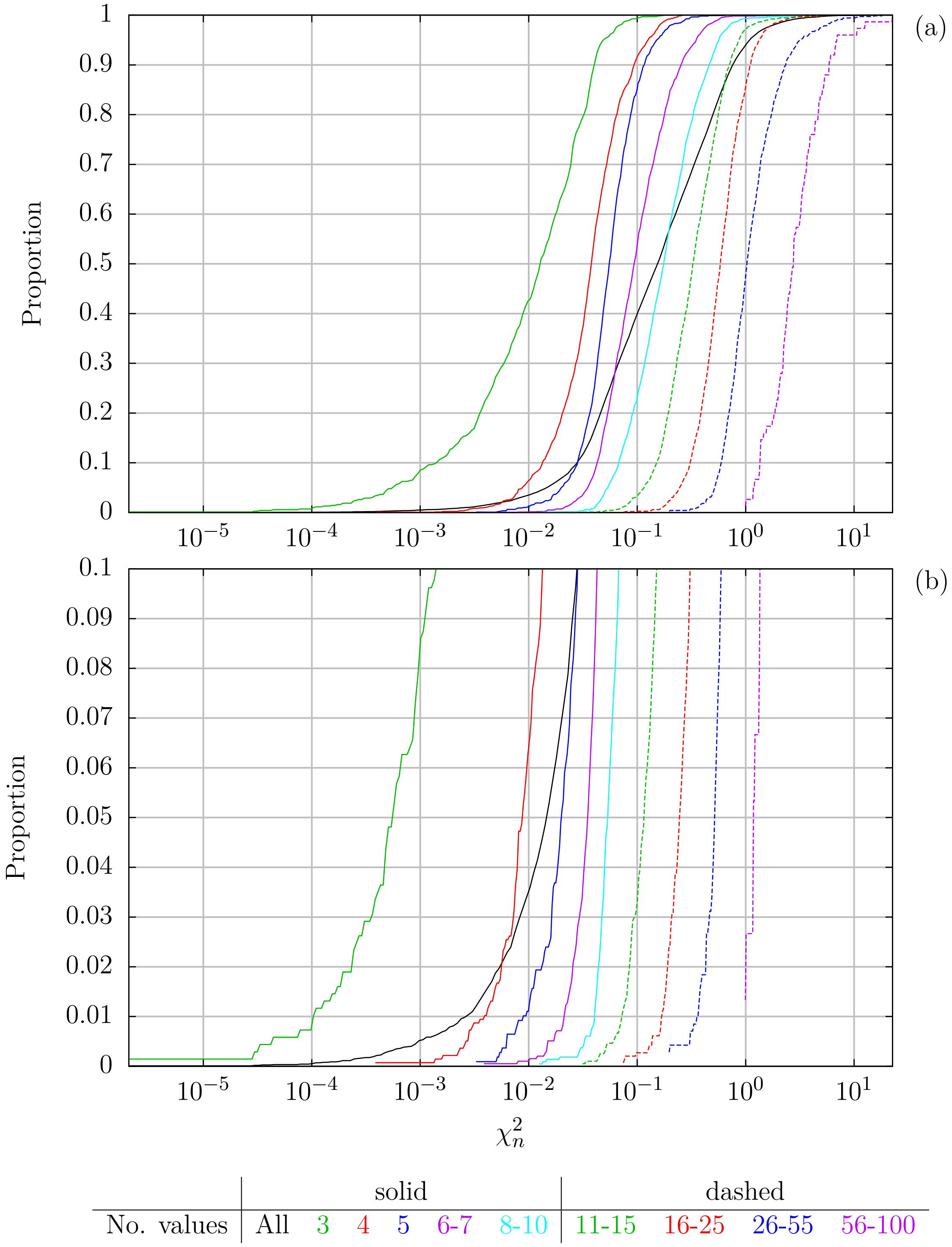

Figure 5.6: This plot shows the same data as Figure 5.5, but here the 15 sets are combined to a single input and separated respectively classified by the number of complex values that are taken into account for the fits. The proportion refers to the overall number of fits performed within e respective class. (a) full scale, (b) zoomed in to the lowest 10 %. Intercepts with horizontal lines give reasonable χ_n^2 thresholds to allow a certain rate of false positives for each line width. E.g. for an intended proportion of 0.02, these thresholds are: For three complex values: $2.3 \cdot 10^{-4}$, four: $5.6 \cdot 10^{-3}$, five: 0.0132 and so forth. The three curves implemented in the software are plotted in Figure 5.7.

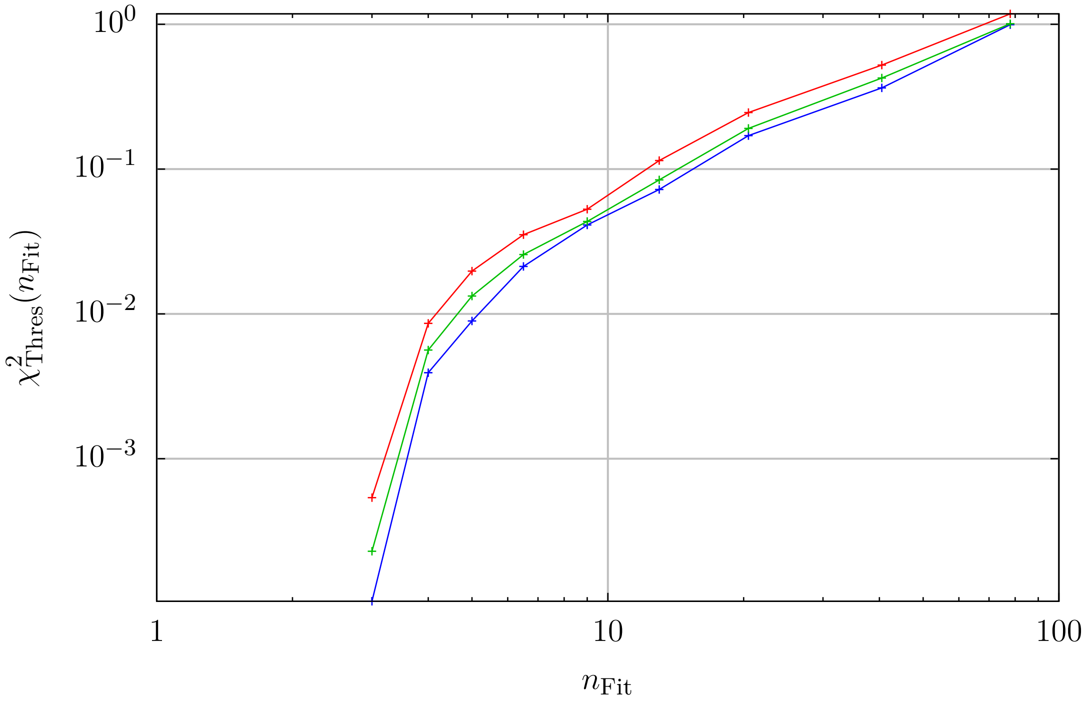

Figure 5.7: For three different proportions of false-positive fits (1%, 2%, 5%) in pure noise, the corresponding χ^2_n values are demonstrated (see Fig. 5.6).

5.4 Further potential issues

5.4.1 The LFS sine spectrum modified by underlying signals

We have seen that, as soon as there is more than one (LFS) sine in the data, the spectral values are superposed. It is likely that this superposition with the underlying signal modifies the sine in a way that the fitted sine parameters are slightly different from the original ones. As described (Sec. 4.9.3), the subtraction is likely to leave a notch in the underlying signal.The more complex values are used for the fit, the smaller is the chance that the sum with the underlying signal forms a fittable sine (consistent with monotonically increase of $\chi^2_{\mathrm{Thres}}(n_{\mathrm{Fit}})$, Fig. 5.7). Therefore, a bigger number of values used in a fit reduces the mean power taken from the signal by mistake.

5.4.1.1 The sine spectrum modified by neighbouring sines

The spectrum of a sine typically has contributions not only at its mean frequency but spreads infinitely to both sides.[10] As soon as there is more than one sine in the data the spectral values are superposed as described above. The algorithm fits (and subtracts) multiple sines one by one starting with the one with the highest magnitude. So the

---

[10] The only exception is: $b_0 = 0$ and ν_0 is an integer multiple of $\Delta\nu$ (see Figure 3.5 (a), (b)).

current fit can be superposed with contributions of other sines (plus remains from non-ideal fits/subtractions of higher peaks done before). In general, this problem is the same as above (sines superposed with GWN noise) but peaks of other sines are typically in the same order of magnitude and if they get too close the peaks merge completely. As described in Section 2.3.3, the Hann-window function causes even the smallest peaks to have a maximum consisting of at least three high values. Therefore, any other sine within approximately 3 $\Delta\nu$ influences a peak significantly. A reasonable solution to this problem is fitting the sum of multiple sines to such superposed peaks. First steps could be done relatively easily by starting with two monofrequent sines.[11] This could be sufficient for a case that appears frequently: A spectrum consists mainly of two series of sines and a few of the respective harmonics lie close to each other. As this work is mainly about the linearly time-shifting sine, this is not treated here. In contrast, the case of two LFS sines is most probable very complicated: At least two more parameters ($2 \times b_0$) need to be fitted and the start value estimation is expected to be intractable as the slopes of the phases are functions of b_0, so an approach with a relative phase as fit parameter should not work out. This seems to be a complicated field for additional research.
Just as an example, one special case is introduced in the following.

5.4.1.2 Opposing sines

The magnitude spectrum is the same whether a sine with a certain start frequency and shift, ending at a certain frequency (after interval time T), or a sine with exactly this end frequency and the inverted shift is used; the difference exists exclusively in the phase (Fig. 3.2). Figure 5.8 shows a superposition of two opposing sines in the time domain (a) and the resulting magnitude spectrum (b); for comparison the spectrum of the single sines is shown in red. By construction, both the time-domain signal and the peak in the spectral domain, are symmetric; the smooth single spectra add up to a rippled combined spectrum due to the phase. The sine parameters are chosen in such a way so that the time domain has a point symmetry in the origin, therefore the spectrum has to be purely real (Fig. 5.9). By this construction, the sines have the same real part and negated imaginary part. As the combined spectrum shows a (rippled) peak similar to a single one it is interesting to see how the peak-fitting algorithm behaves here. Figure 5.10 shows the results. Due to the point symmetry the original curve (black) approaches zero at 0 Hz and at the Nyquist frequency (512 Hz). Note that the ripples cause the algorithm to fit

---

[11] The fitting of two monofrequent sines at once has been pioneered by Jürgen Altmann ([36]). Monofrequent-sine fits were performed in the magnitude spectra, implying that only two parameters (A_0 and ν_0) were fitted. The two phase parameters were gained later by evaluation of the phase at $i_{\max}$ and the degree of asymmetry of the neighbouring magnitude values (to some extent similar to Sec. 4.9.2). In order to fit two peaks at once, a relative phase difference is needed, because the magnitude spectrum depends strongly on the phases, as the superposition can be from constructive to destructive. Therefore, the fitting required five values in the magnitude spectrum, potentially bearing issues concerning the number of degrees of freedom versus the number of values.

only 17 complex values (according to r_{W}, Sec. 4.3). Nonetheless, the algorithm has no chance to find a satisfactory result due to the fact that the imaginary part vanishes which cannot be achieved by $\mathrm{F}_{\mathrm{Sum}}$with $b_0 \neq 0$.[12] Regardlessly of the invalidity of the fit result the subtraction is done for demonstration with the expected bad result (red curve).

---

[12] The real part of the spectrum of a single sine vanishes if, and only if the time-domain signal is point symmetric. This is the case if the frequency is a multiple of $\Delta\nu$ and the phase is $n \cdot \pi$. If the phase is shifted by $\pi/2$ then the signal becomes mirror symmetric and the imaginary part of the spectrum vanishes. As described in Section 3.2.3, a $b_0 \neq 0$ results in phase changes per $\Delta\nu$ different than π, which in turn means that it is impossible to create a single spectrum with either real or imaginary part equals zero. Consequently, a broad peak in one single complex plane is not fittable by a single sine in principle. However, in this section two sines are added, both have non-vanishing real parts but exactly negated ones.

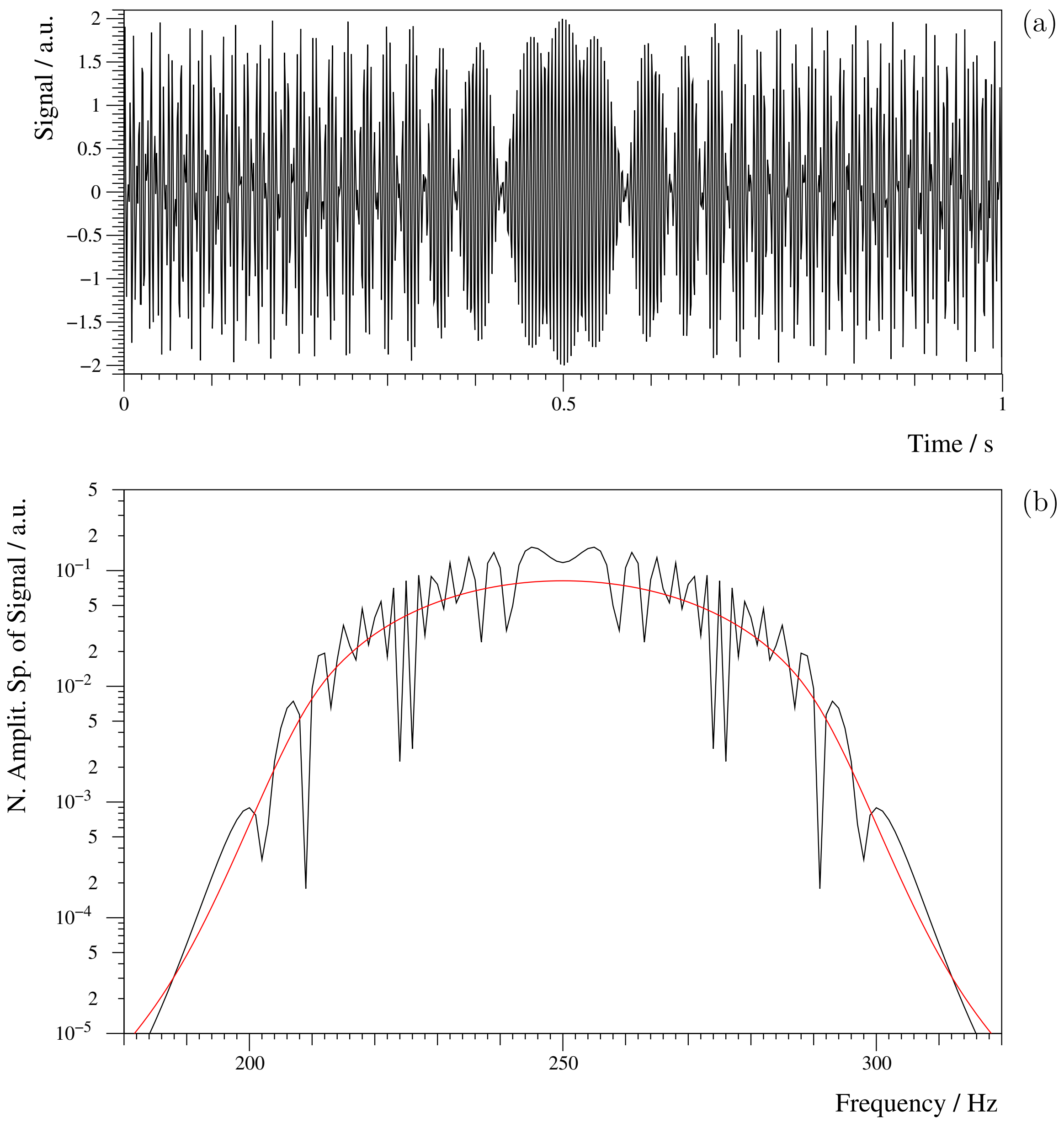

A_0	ν_0	b_0	ϕ_0
1.0	300 Hz	-100 Hz/s	0.0
1.0	200 Hz	100 Hz/s	0.0

Figure 5.8: Sum of two opposing LFS sines. Parameters: $N = 1{,}024$, $\Delta t = (1/N)$s, from this follows that $\Delta\nu = 1$ Hz and $T = 1$ s. (a): The complete interval in the time domain. (b): Middle part of the magnitude spectrum, the red curve shows the spectra of the single sines for comparison.

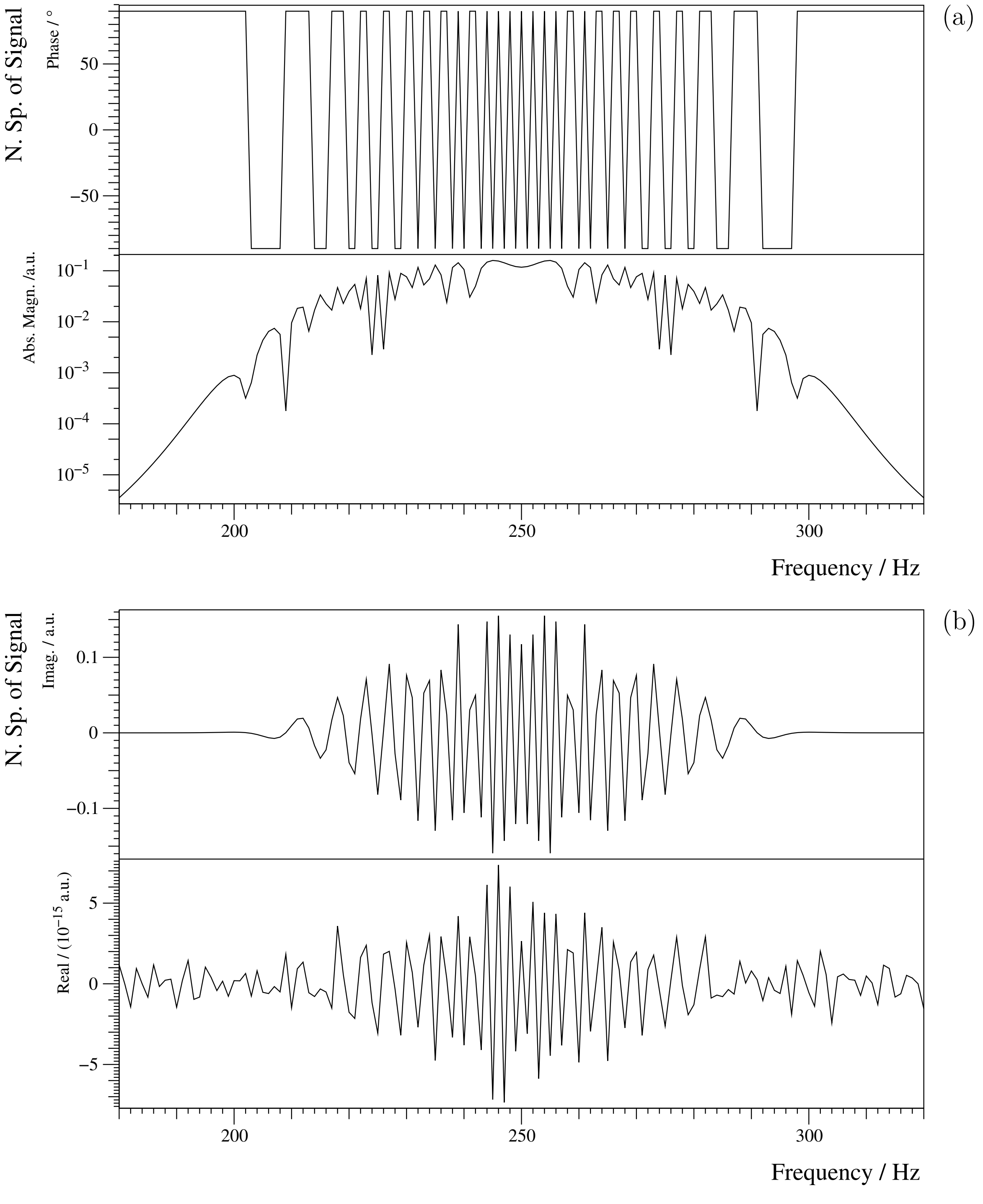

Figure 5.9: (a) Phase and magnitude spectrum of the signal shown in Figure 5.8, (b) shows the same signal but by real and imagniary part; the real part is in the order of numerical errors (64 bit, double precision).

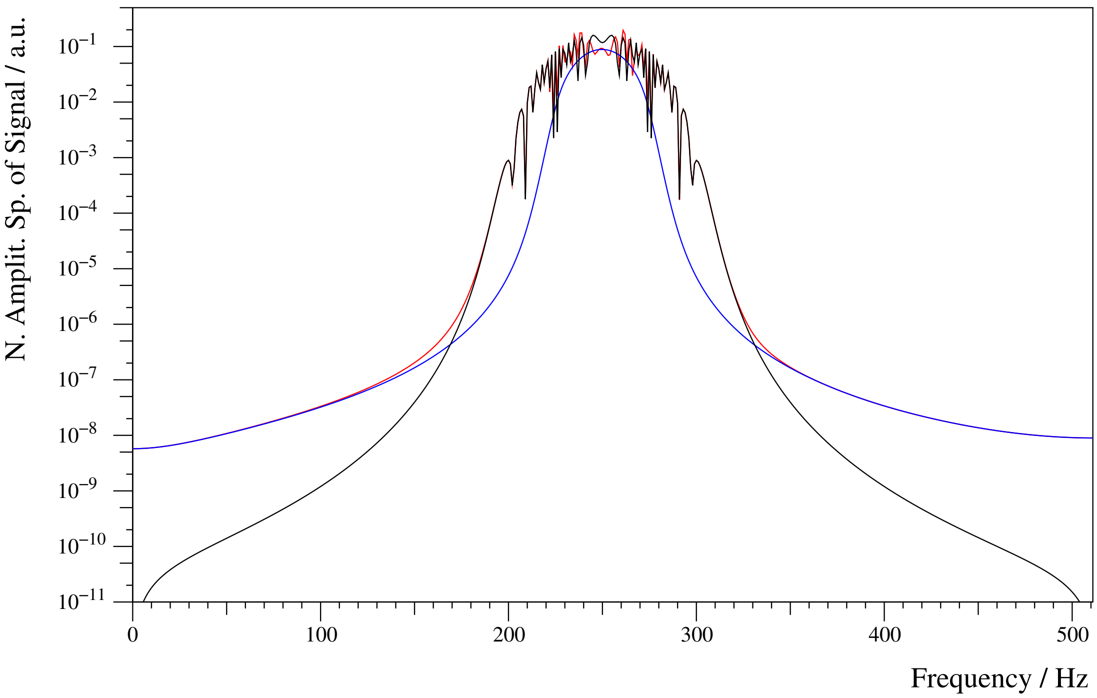

	A_0	ν_0	b_0	ϕ_0
Start	0.8812	268.591 Hz	-37.183 $^{\mathrm{Hz}}/_{\mathrm{s}}$	$-56.54°$
Fit	0.8467	280.264 Hz	-61.006 $^{\mathrm{Hz}}/_{\mathrm{s}}$	$-10.02°$

Figure 5.10: Fit attempt for two opposing LFS sines, magnitude spectra. Due to the notches close to the maximum, only $n_{\mathrm{Fit}} = 17$ complex values are fitted. The algorithm stopped after reaching the limit of 120 iterations. $\chi^2_n = 0.397$ at $\chi^2_{\mathrm{Thres}}(17) = 0.172$. The black line is the original spectrum, blue is the theoretical curve of the fit result, red is the spectrum after subtraction.

5.5 A real signal superposed with synthetic sines

Before analysing completely real signals with periodic disturbances, synthetic sines are superposed with a real signal: This signal is a coal-mine-induced event in the area of Hamm-Herringen, Germany ([37])[13] acting as a model for a substantially non-periodic aftershock signal (Fig. 5.11). It is superposed with artificial sine functions of different frequencies, amplitudes and phases as an example for periodic disturbances. The sampling rate for these data is 200 Hz and the segment length is 15 s; all examples will be performed with 1,024 samples containing the centre part of the signal.

5.5.1 First example

The signal of Figure 5.11 is superposed with a single sine;[14] the input parameters and fit results are shown in Figure 5.12. 1,024 samples are used for the FFT, then a sine is fitted to the highest maximum. In this example, the algorithm stops after 39 iterations with: $\chi_n^2 = 7.646 \cdot 10^{-4}$, the number of complex values used for this fit is $N = 28$.

By applying the inverse FFT, the signal is restored with very few changes (b); the strongest changes occur at the beginning of the time interval in the order of 5 % peak-to-peak, referred to the maximum of the event. In this case a few more plots are given: Figure 5.13 (a) shows the deviation between the original signal and the signal after the sine is added, fitted and subtracted in the time domain. By performing the subtraction, everything of the original signal disappears: What remains is an added sine and a subtracted one with slightly differing parameters, where a subtraction is nothing else than an addition with a phase-shifted sine. However, the result can only consist of the sum of two pure LFS sines. The magnitude spectrum is shown in (b); real and imaginary part in (c). A test is performed:[15] The green line shows the result when another fit is applied to the remaining spectrum; as expected this fit fails completely. Nonetheless, it is subtracted here for demonstration; the result is shown in red.

5.5.2 Bigger amplitudes

The sine of the example above is increased in amplitude, while the procedure remains the same. Two examples for the factors 100 and 10^4 are demonstrated in Figure 5.14. In the spectra one can see fluctuations in the regions where the spectra of the LFS sine and

---

[13] Data kindly provided by Monika Bischoff and Sebastian Wehling-Benatelli (Institut für Geologie, Mineralogie und Geophysik; Ruhr-Universität Bochum). Measured: 1. February 2007, 19:18:28 UTC during the "HAMNET" acquisition period. Location depth is 1,056 m, distance between source and sensor 1,441 m, Mercalli intensity: -0.48, vertical component of a 3D-velocity sensor.

[14] An example of a real signal containing a seismic event and mains hum is briefly described and published on a poster [38].

[15] The spectrum (b) looks similar to other spectra with a broad peak; unique though is the pronounced asymmetry of its flanks. The question arises: What happens if the algorithm is run on these data?

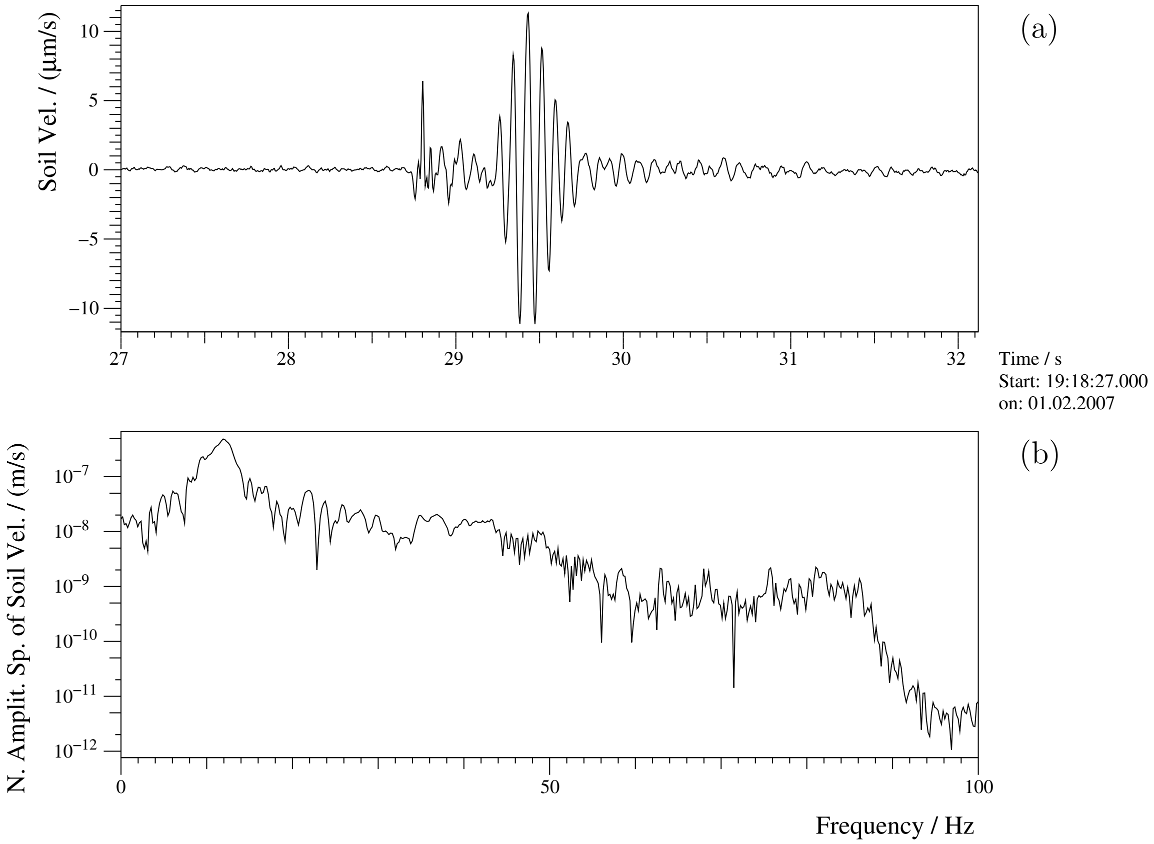

Figure 5.11: Test signal from a coal-mine-induced event. (a) shows the time-domain signal of the $1,024$ samples which will be superposed with artificial sines to test the algorithm. (b) is the magnitude spectrum of the same signal.

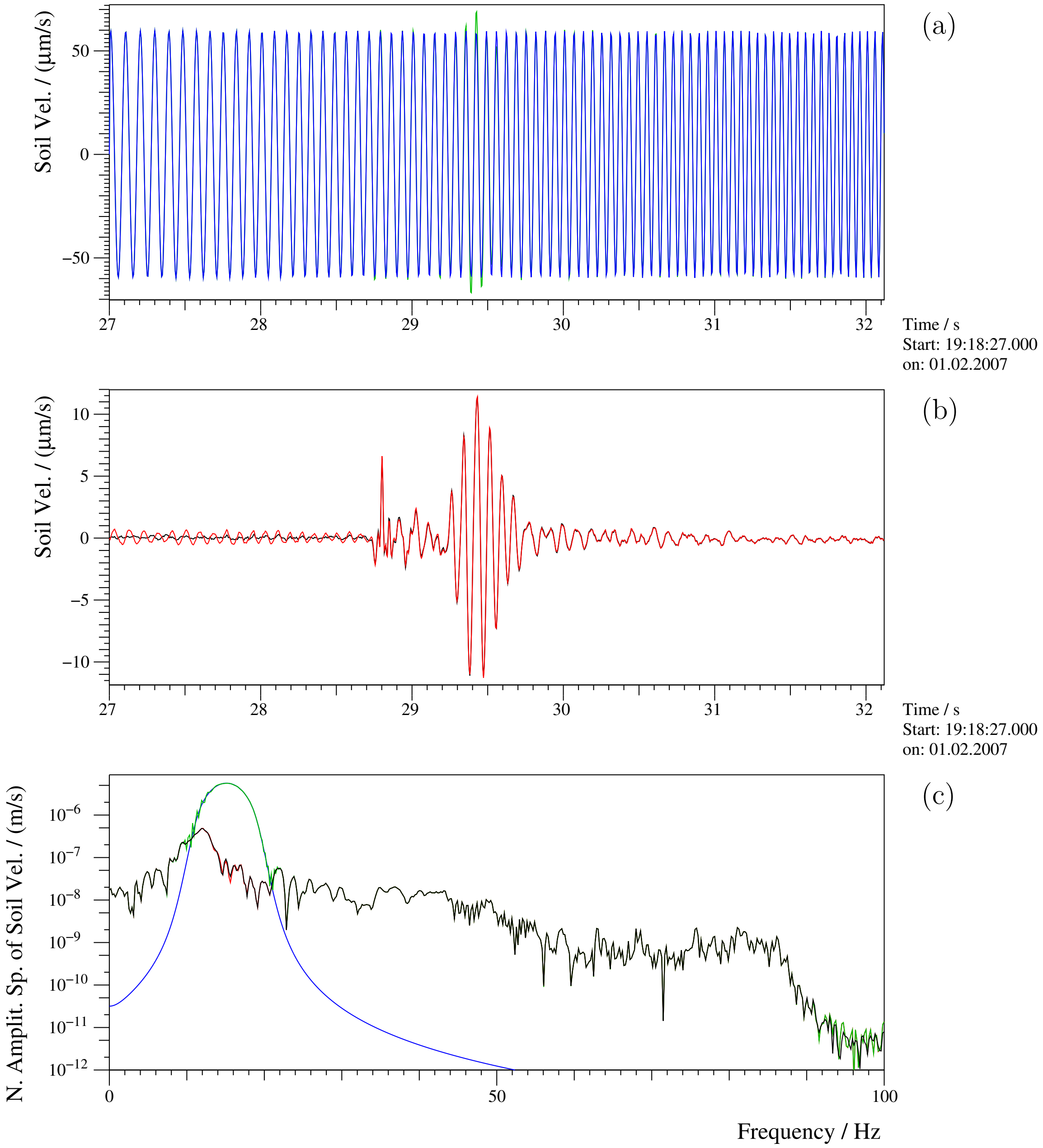

	A_0	ν_0	b_0	ϕ_0
Input	$50.0\,{}^{\mu\mathrm{m}}/_{\mathrm{s}}$	10.0 Hz	$2.0\,{}^{\mathrm{Hz}}/_{\mathrm{s}}$	1.0 rad
Fit result	$49.9964\,{}^{\mu\mathrm{m}}/_{\mathrm{s}}$	9.999311 Hz	$2.000154\,{}^{\mathrm{Hz}}/_{\mathrm{s}}$	1.01019 rad

black	Original signal
green	Signal superposed with sine
red	After subtraction of the sine
blue	Sine with the parameters of the fit result

Figure 5.12: Test signal from a coal-mine-induced event superposed with an artificial LFS sine. (a) and (b) illustrate the time domain; both plots contain two signals according to their scale. (c) shows all four spectra in a logarithmic plot.

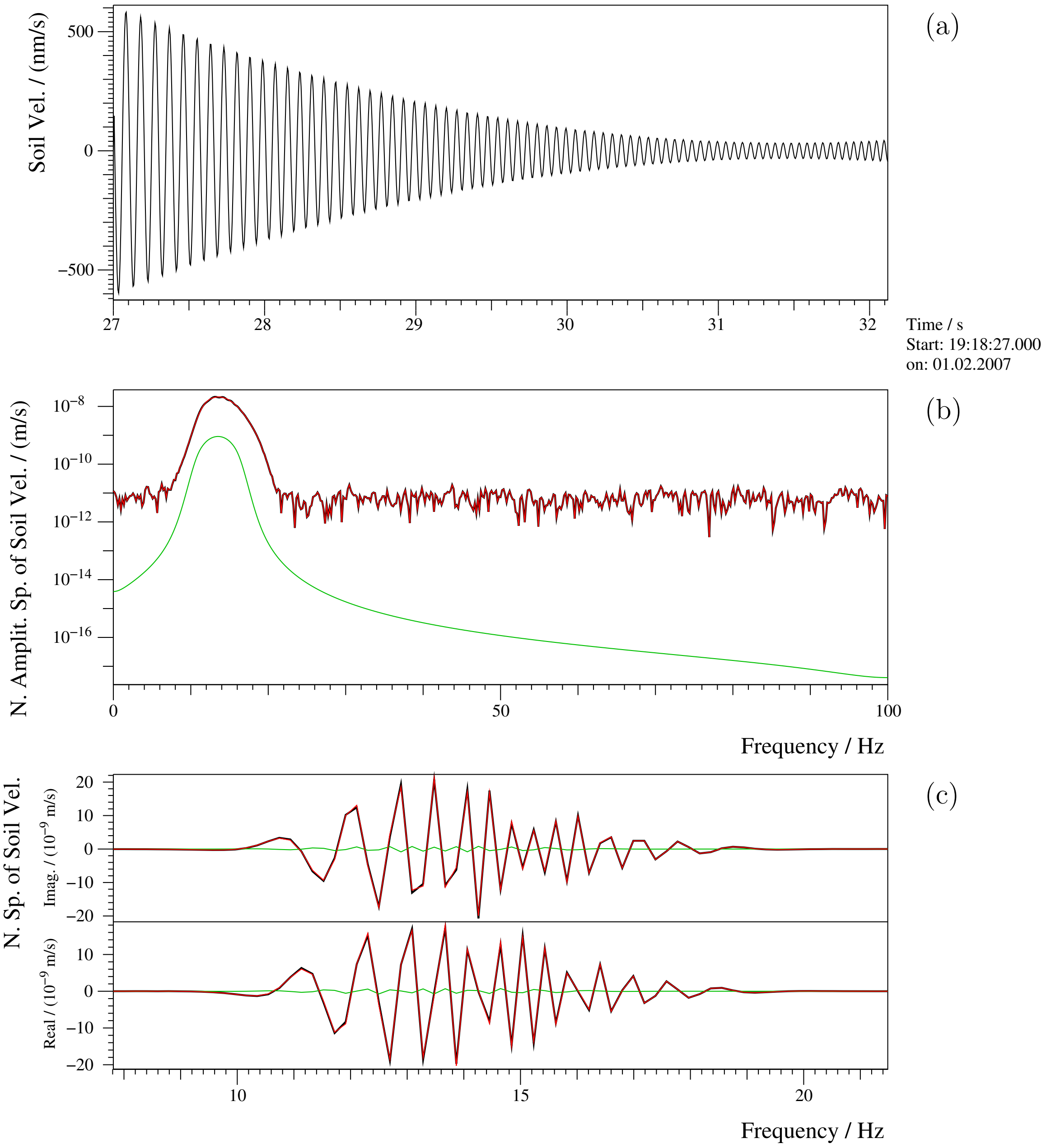

Figure 5.13: Test signal from a coal-mine-induced event superposed with an artificial LFS sine. (a) shows the difference of the time-domain signals: The original data minus the data after sine addition, fitting and subtraction (the difference between the two curves is given in Fig. 5.12 (b)). The black curve in (b) and (c) is the corresponding spectrum. Additionally, the green curve is the result of a peak fit to this result, red is the difference (black curve minus green one).

the underlying signal are in the same order of magnitude. Although both curves have a smooth magnitude spectrum, their phases fluctuate strongly, causing ripples if added. In all other regions the spectrum of the signal dominates, so the sum spectrum shows the respective smoothness.

The superposition is achieved by adding two complex values: As long as the sine is considerably stronger than the other signal, a further amplitude increase does not change the phase significantly. Therefore, no significant changes of the shape of the difference signal can be expected, as long as the fitting and subtraction quality is sufficient to lower the sine peak below the level of the superposed signal. Figure 5.15 compares three examples of different amplitudes: The χ_n^2 becomes better – pretty much in the same way the amplitude increases: χ_n^2 contains the squared differences; for every amplitude increase by a factor 100, χ_n^2 decreases approximately by a factor of 10^4. On the one hand the fit quality increases, on the other hand relatively more has to be subtracted to reach the same level of remaining signal.

To conclude: There is no such thing as a proportionality of the amplitude of the sine and the error that remains in the data. As long as the peak of the sine is clearly higher than the underlying signal, the deviation is more or less the same. Instead, the biggest contribution to RMS_Δ stems from a notch which is likely to remain in the spectrum after subtraction of the sine. Its ”size” depends mainly on the phase spectrum of the underlying signal (in the range of the fitted values, Sec. 4.3) in combination with the sine parameters – with very little influence of the amplitude (as shown in Fig. 5.15).

5.5.3 Bigger linear frequency shift

5.5.3.1 Positive shift

This example demonstrates the performance of the algorithm, if the added sine has a very strong linear frequency shift. The parameters and results are given in Figure 5.16; further fit properties are: $\chi_n^2 = 1.6530 \cdot 10^{-9}$ after 38 iterations; 211 complex values are used, centred at index 261. As described, the sampling rate is 200 Hz, 1,024 samples are used in the FFT, therefore the frequency increases from 10 Hz to $10\,\mathrm{Hz} + 16.0\,\mathrm{Hz/s} \cdot 5.12\,\mathrm{s} = 91.92\,\mathrm{Hz}$ in the chosen time interval. (a) and (b) demonstrate that the deviations from the original signal are low and in the same order as the narrower peaks in the last section ($RMS_\Delta = 1.48781 \cdot 10^{-7}$). By this procedure, smaller magnitude values are altered relatively more than big ones; this is reasonable as for the χ^2 parameter in the fit procedure, the squared differences, which are all weighted the same, are minimised.

5.5.3.2 Negative shift

As a last example, the former one is shown with an inverted time course of the sine: The frequency decreases from 91.92 Hz to $91.92\,\mathrm{Hz} - 16.0\,\mathrm{Hz/s} \cdot 5.12\,\mathrm{s} = 10.0\,\mathrm{Hz}$ in the chosen

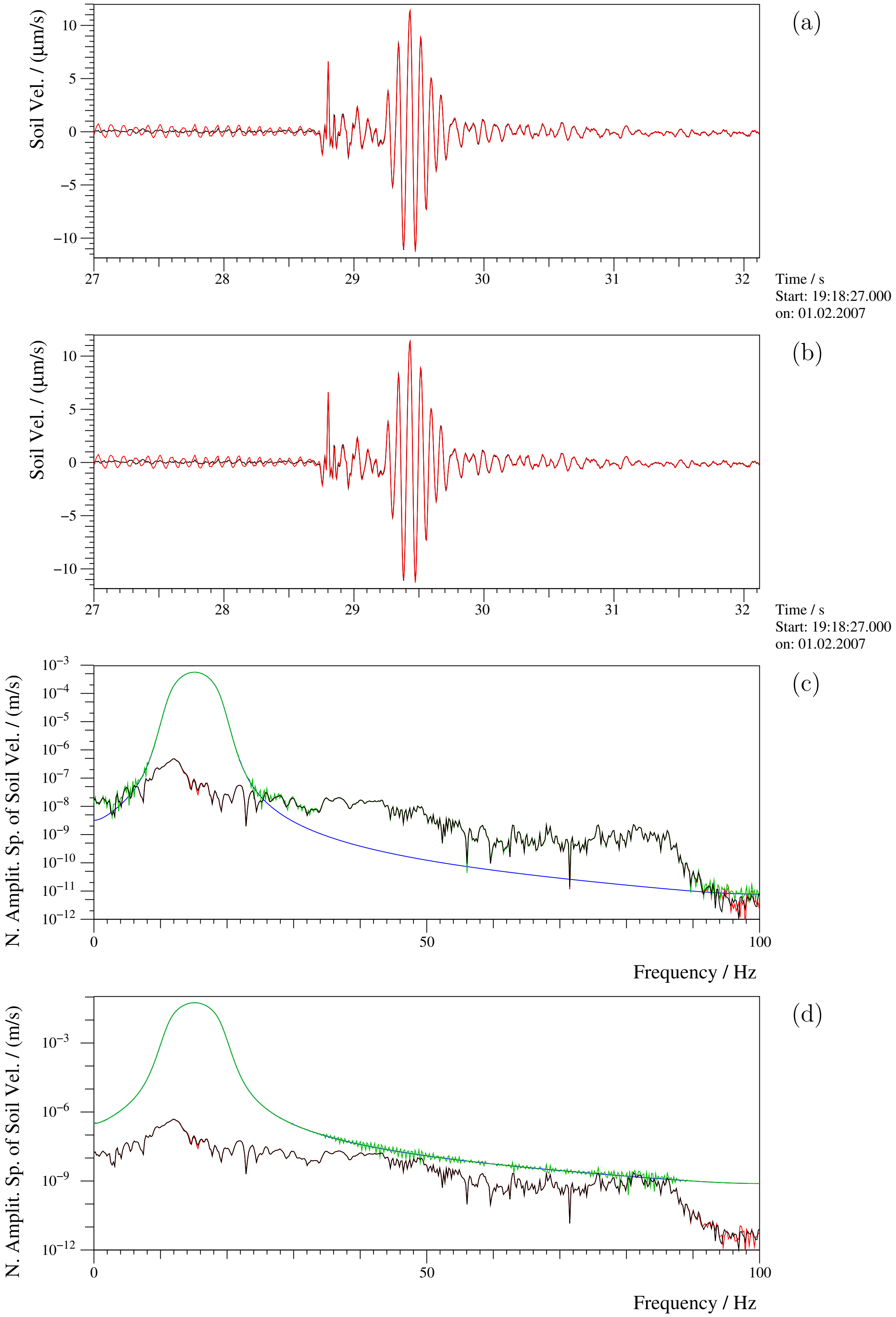

Figure 5.14: Test signal from a coal-mine-induced event superposed with an artificial LFS sine. (a) and (b) illustrate the same original and restored signal as Figure 5.12 (b) but with the sine amplitude increased by a factor of 100 resp. 10^4. (c) and (d) show the corresponding spectra (similar to Fig. 5.12 (c)).

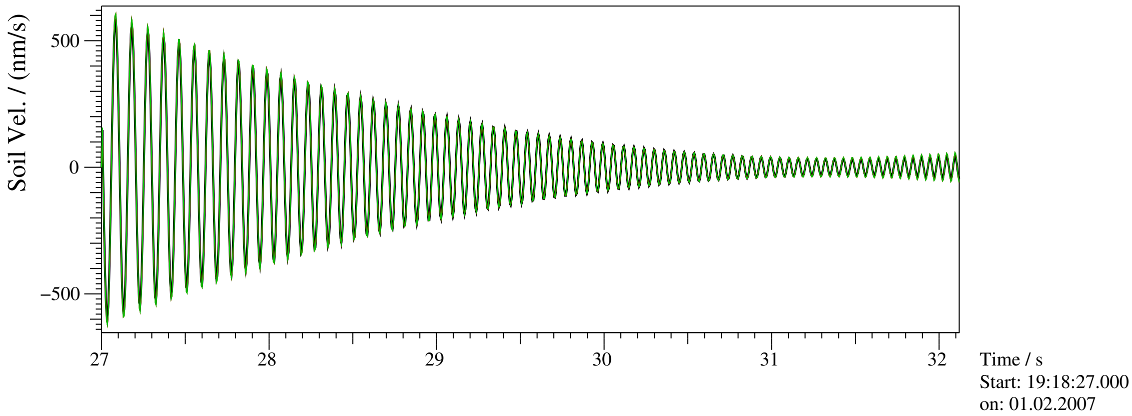

Amplitude factor	#Iterations	#Compl. values	χ_n^2	RMS_Δ
1	39	28	$7.6462 \cdot 10^{-4}$	$1.85684 \cdot 10^{-7}$
100	39	28	$7.5283 \cdot 10^{-8}$	$1.91219 \cdot 10^{-7}$
10^4	32	28	$7.5271 \cdot 10^{-12}$	$1.91246 \cdot 10^{-7}$

Figure 5.15: Similar to Figure 5.13 (a) the deviations between the reconstructed and the original signal are shown. The curves are pretty much the same.

time interval. The parameters and results are given in Figure 5.17, further fit properties are: $\chi_n^2 = 1.7713 \cdot 10^{-9}$ after 37 iterations; again 211 complex values are used, centred at index 261. The deviations from the original signal ($RMS_\Delta = 9.7122 \cdot 10^{-9}$) are significantly lower than in the inverted case, even though the χ_n^2 value is slightly worse. This variation depends on the current superposition with respect to the phase spectra (Sec. 5.2).

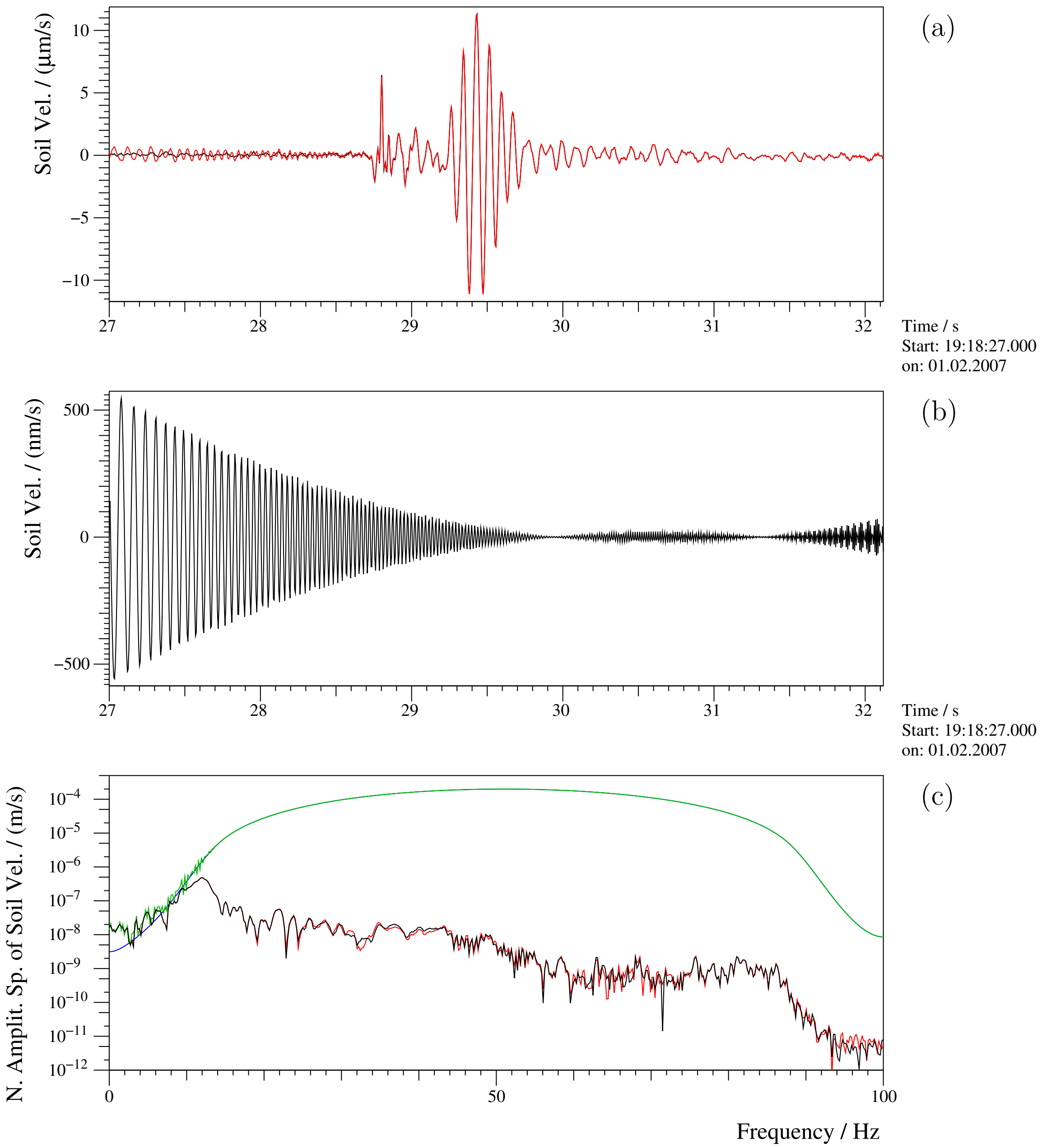

	A_0	ν_0	b_0	ϕ_0
Input	5.0 mm/s	10.0 Hz	16.0 Hz/s	1.0 rad
Fit result	4.9999981 mm/s	9.9999912 Hz	16.000002413 Hz/s	1.000096 rad

black	Original signal
green	Signal superposed with sine
red	After subtraction of the sine
blue	Sine with the parameters of the fit result

Figure 5.16: (a) shows the time-domain signal of the original signal and after sine addition, fitting and subtraction. (b) shows the difference between the two signals. (c) shows all four spectra, just like in the former example.

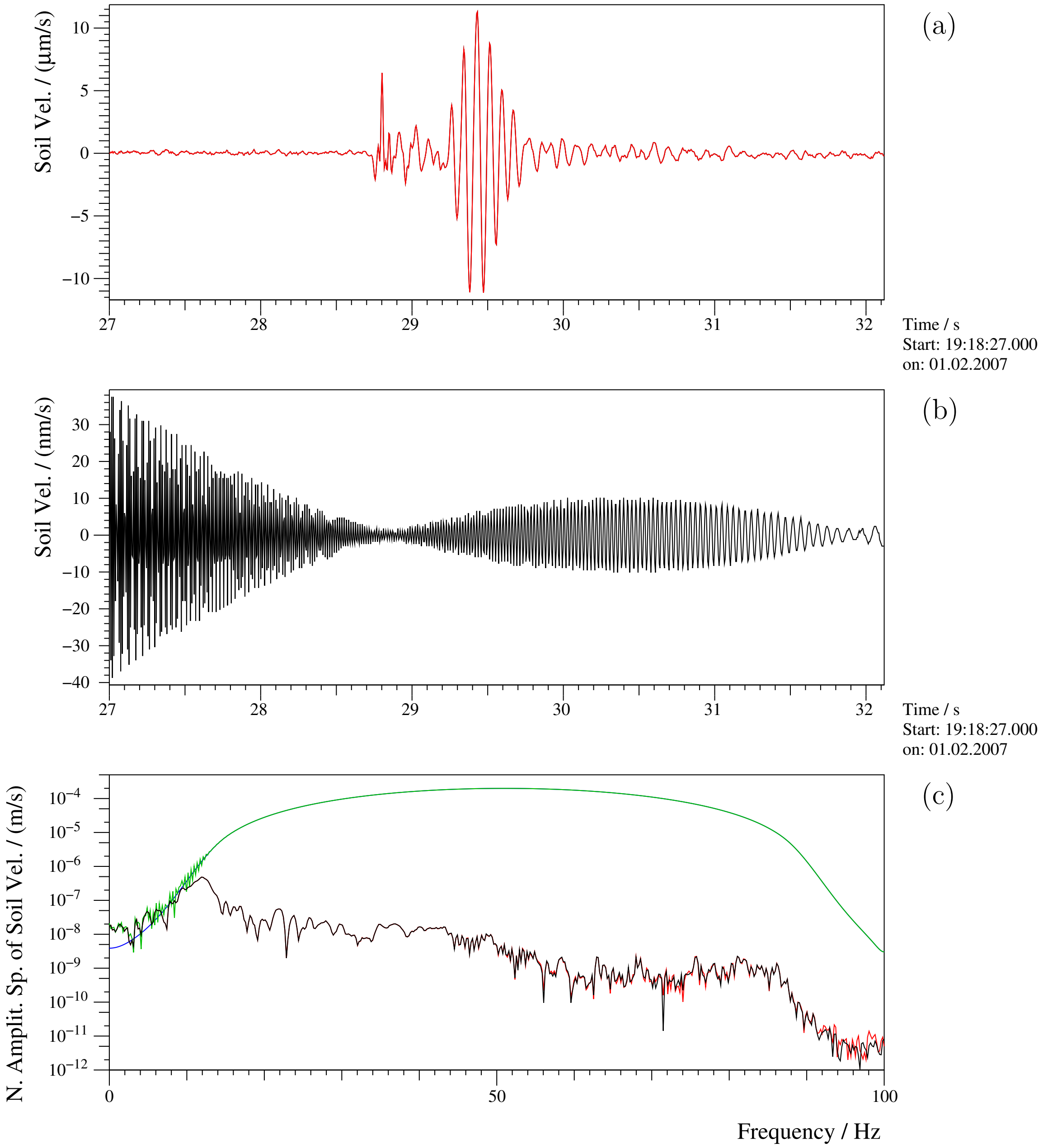

	A_0	ν_0	b_0	ϕ_0
Input	5.0 mm/s	91.92 Hz	-16.0 Hz/s	1.0 rad
Fit result	5.00000114 mm/s	91.920000779 Hz	-16.000000231 Hz/s	0.99999343 rad

black	Original signal
green	Signal superposed with sine
red	After subtraction of the sine
blue	Sine with the parameters of the fit result

Figure 5.17: (a) shows the time-domain signal of the original signal and after sine addition, fitting and subtraction. (b) shows the difference between the two signals. (c) shows all four spectra, just like in the former example.

5.6 Notches and sums of sinusoids with the same frequency

In multiple situations in this and the last chapter, an effect termed ”notches” occurred in the remaining spectra after sine subtractions. Here an analysis of this phenomenon is given.[16]

By fitting sine parameters to superposed spectra, the algorithm tends to subtract more power (not mandatorily equal to a bigger A_0) than the power of the pure sine contained. As a consequence, notches show up in the remaining spectrum. These notches can be interpreted as missing frequencies, needed to compose the original spectrum.[17] If the fit is ”very” successful[18] notches appear in the spectrum but never spikes. The reason comes from the nature of superposing a sine, i.e. every signal in the time interval can be interpreted as a sum of sines, and one can imagine that one of these sines has the same frequency as the sine which was added to the signal. Sines with the same frequency, but possibly of different amplitude and phase, are summed up to another sine with this frequency, but with a different amplitude and phase. No matter if the sines sum up constructively or destructively, it will be their sum that is handed over to the fit function. If the superposition is destructive, the fit algorithm converges to a set of parameters with an A_0 which is smaller than the one of the sine, which was added to the signal, and produces a notch in the spectrum. The other way round, for a constructive superposition, the fitted A_0 is bigger than the input one – likewise producing a notch in the spectrum.

The fact that multiple sines with the same frequency sum up to another sine with this frequency is important because signals are often reflected and interfere with themselves.[19] If the conditions for the superposition change over T, the signal may exhibit strong frequency dependencies for the investigated magnitudes, which can complicate the general

---

[16] It turned out that this phenomenon may be unintuitive and people may think that these notches are errors of the fitting algorithm and that there should be equivalent ”spikes” remaining in the spectra in other cases. In order to clear up this misconception, this small section describes the problem in detail and with more examples.

[17] Imagine the spectrum of a sequence of equal rectangular pulses. The spectrum would consist of a fundamental frequency and its harmonics. In order to match the constant parts of the rectangle, each higher harmonic is used to suppress the sine shape of the lower ones. If one harmonic would be removed, of course its frequency goes missing. As a consequence, this wave would not suppress the shapes of the lower frequency sines and higher harmonics would be adjusted to suppress oscillations not present in the signal. As a result, these oscillations would be visible in the time-domain signal – in form of a sine with exactly the missing frequency. That is what happens with the notches: They produce the wavy shape of the inverse-transformed data (e.g. Fig. 5.15) and typically slightly reduce the peak-to-peak value of the underlying event.

[18] A fit is successful mainly if $\chi^2_n < \chi^2_{\text{Thres}}(n_{\text{Fit}})$. If the sine has a big amplitude and the χ^2_n value is barely sufficient but not superb, it can happen that not the complete power of the peak is subtracted and thus, a peak at this frequency can remain in the spectrum. This is different from the notch phenomenon which occurs even for ”perfect” fits.

[19] E.g. a microphone in a certain height over the ground used to measure air-vehicle sound also records the waves that were reflected from the surface. For seismic measurements additional superpositions occur: E.g. the boundary surfaces of different soil layers can cause reflections.

analysis of the signal. However for this work it is important to note that the peak shape does not change by interference with itself, the algorithm would be applied to this sum signal and return the resulting amplitude and phase. On the contrary, in the next section (Sec. 6.5) cases are discussed which can negatively influence the fit progression.

Notches become apparent especially for narrow peaks. Figure 5.18 shows the fit results when a monofrequent sine is added to a flat region in the "HammNet" spectrum and ϕ_0 is varied. It can be observed that the notches proceed similarly if π is added to ϕ_0. In this case, the signals are superposed very similarly – a phase shift by π is the same as an inverted sign of A_0 – this, in turn, can be interpreted as a sine addition in the one case, in the other it is a subtraction. Because of the high amplitude of the sine, the underlying broad-band signal can be neglected in the region of the peak and so both fits are virtually the same. This results in very similar χ^2_n values as well as in the cases where one fitted amplitude is slightly higher or slightly lower than the input amplitude of 5.0000000 mm/s. In every case a notch is produced.[20]

If this procedure leaves notches in the spectra, one could raise the question whether common notch filters can perform comparably in removing certain peaks. In [39] we demonstrate an example in which the result of the application of highly adjusted Blackman finite-impulse response (FIR) filters is compared with the one the fit procedure for monofrequent sines produces. It seems that both approaches produce suitable results, in which the $\mathrm{F}_{\mathrm{Mono}}$ approach reconstructs the spectrum better, but as we are not trained in analysing seismic signals, we do not want to assess the changes done to the time-domain signal.[21] One has to keep in mind that, in order to manipulate the underlying signal as little as possible, the peak width and its location need to be estimated as accurately as possible. Additionally it might be reasonable the adjust the "amplitude" of the filter. This indicates that – without the phase – well estimated parameters are required for a precise filter application. Filtering cannot replace the fit algorithm, at most it is a kind of substitute for the subtraction part: without precise characterization the removal will be in- or overcomplete.

---

[20] If the correct parameters were set by hand, no notch would occur because the spectra of signals sum up linearly and therefore, a subtraction of exactly the same signal, which was input before, would perfectly reconstruct the underlying signal.

[21] For broader peaks, the notch filters would have to suppress wider frequency bands, increasing the width of the notches, whereas, for the $\mathrm{F}_{\mathrm{Sum}}$ approach, the notch depths are typically reduced (e.g. in comparison of Fig. 5.12 (c) with the plots in Fig. 5.18). The probability for the complex values within the peak width of the LFS sine to superpose consistently with the ones of the underlying signal is smaller when more values are taken into account. In the future, systematic parameter variations could be evaluated in order to quantify the mean power loss of a signal per subtracted sine. Figure 5.15 indicates that (at least for strong peaks) it is essentially independent from A_0. The examples given in Fig. 5.18 show narrow notches with depths of $0.5 - 1.0$ orders of magnitude.

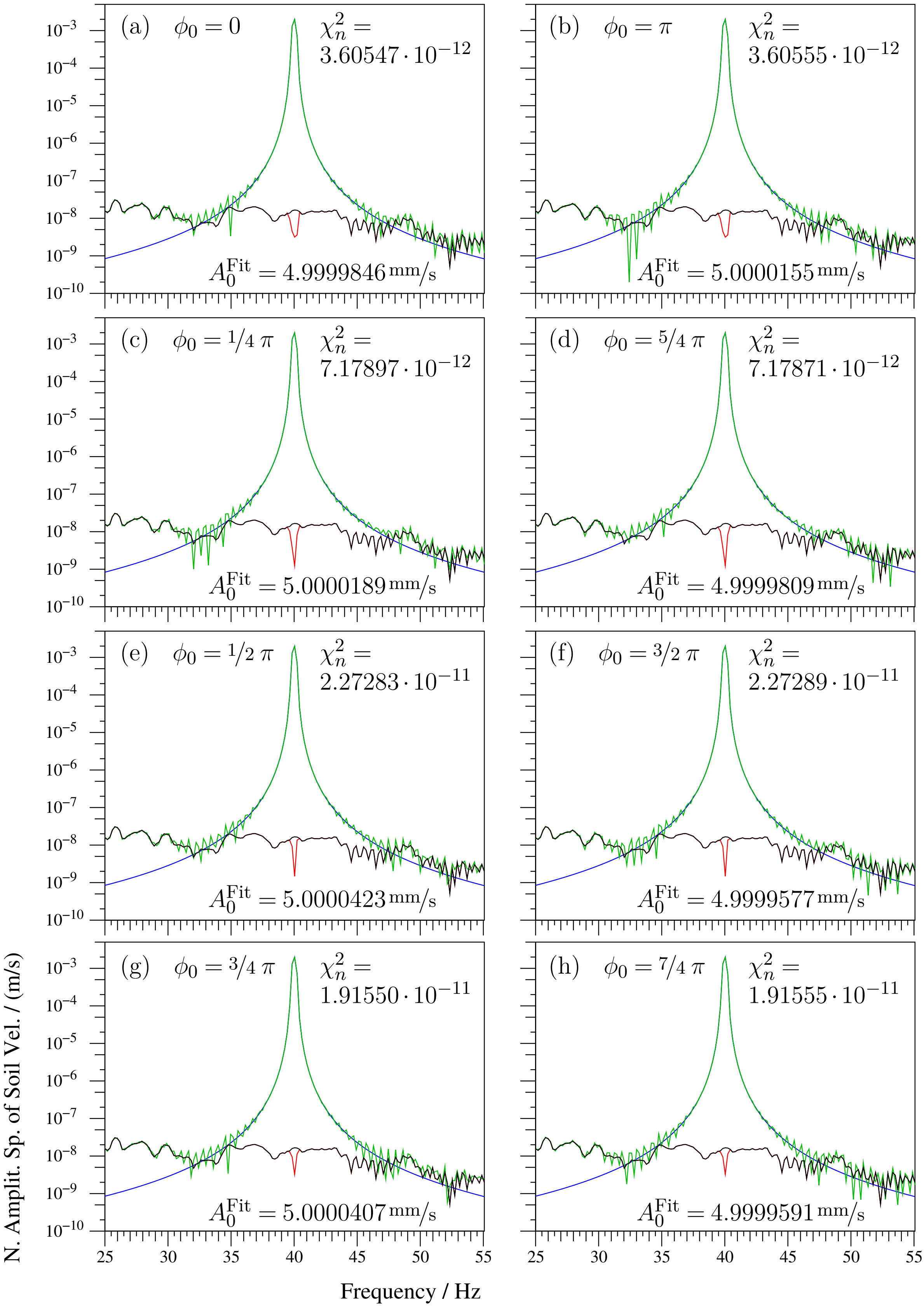

Figure 5.18: Part of the HammNet spectrum superposed with monofrequent sines ($\nu_0 = 40.0\,\mathrm{Hz}$) with different phases (top left in the plots). The phases in the right column are shifted by π compared to the left ones; each peak produces a similar notch.

Chapter 6

Analysis of real data

6.1 Introduction

In this chapter, sine subtractions from longer time intervals of data are demonstrated. For this purpose, sequences of complex spectra are generated from the data that shall be cleaned from periodic disturbances. Yet, no spectra-overarching analysis is provided, and the single spectra are processed separately.[1] For each time interval, the spectrum is calculated and the locations of the local maxima (the peaks) of the magnitude are extracted. These are sorted by amplitude (in decreasing order) and again processed one by one: the start values are estimated and if the subsequent fit is successful, an (LFS) sine with the fit parameters is subtracted from the single, complex spectrum.[2] If all peaks in all spectra are processed, the sequence can be transformed back into the time domain. Much effort was spent to make the processing run automatically and provide clear presentations of the outcomes.

6.1.1 Description of the final algorithm for removal of (LFS) sines

In the implementation some measures have been taken. It turned out that for sequences of real spectra additional constraints are productive and have been implemented. For instance, if the mean frequency ($\nu_{\mathrm{Mean}} = \nu_{0,r} + b_{0,r}/2$) of the fitted parameters is located outside the interval of fitted data (the peak width, Sec. 4.3), the result is categorically marked as failed fit and no sine is subtracted.

---

[1] An optimised algorithm should use fit results of at least one spectrum and expect a similar sine in the neighbouring time intervals. Checking for consistency can also help to discard false positives that occur in just one spectrum.

[2] For the generation of a complete spectrum via $\mathrm{F}_{\mathrm{Sum}}$ (Eq. 2.95) the computation effort is quite high: A spectrum consists of N values and each one is calculated by summing up approximately $6N$ trigonometric terms. Instead, a sine with the corresponding parameters is generated in the time domain and in the usual way transformed with Hann window via FFT.

For the sake of completeness it should be mentioned, that in this chapter, the maximum peak width is limited to $r_\mathrm{W} \leq 100$; peaks estimated to be even broader are excluded.[3]
Beside these rarely occurring, easily handled cases, four important, additional measures are described in this section.

6.1.1.1 A special approach for small peak widths

Admittedly, the F_Sum expression can handle monofrequent sines but it has one parameter (b_0) more than the F_Mono expression. The probability, that the underlying signal / the noise fits well to the spectrum of a certain sine by chance if very few spectral values are used, is considerably higher if one more fit parameter is available. This fact leads to an increased rate of false positives for the F_Sum expression compared to F_Mono (see also Sec. A.3). Lowering the $\chi^2_\mathrm{Thres}(n_\mathrm{Fit})$ (Fig. 5.6), however, leads to an increased false-negative rate; the better approach is to use F_Mono in the case of narrow peaks. On the other hand, small values of $|b_{0,r}|$ can also produce narrow peaks.[4] Therefore a categorical approach, namely the usage of F_Mono for each narrow peak, is not reasonable. Instead, in the case where the start-parameter estimation suggests to use three complex values for the fit, the following sequence is carried out:

- The F_Mono fit is done.
- The F_Sum fit with three parameters is done with its strict $\chi^2_\mathrm{Thres}(n_\mathrm{Fit} = 3)$.
- The F_Sum fit with one added value to the right is done with the weaker threshold for $n_\mathrm{Fit} = 4$.
- This is done with an additional value to the left analogously.

For any fit fulfilling its specific threshold criterion, the resulting χ^2_n value is divided by its individual threshold. The lowest value indicates the best result and an LFS or monofrequent sine with these parameters is subtracted.
As described in Section 3.2.2, depending on the position of the ν_0 on the raster of discrete frequencies, a monofrequent sine can have three or four strong magnitude values. Therefore, if four complex values are chosen by the start parameter estimator both – the monofrequent as well as the F_Sum– expressions are fitted to these four points. Again, the one with the better relative ratio $(\chi^2_n/\chi^2_\mathrm{Thres}(n_\mathrm{Fit}))$ is chosen.

---

[3] This is not a hard limit for b_0; instead it excludes really flat regions in the spectra. This condition means: If a local maximum is detected within a region, where it takes more than 100 spectral values for the magnitude to drop below 50 %, then this region is not expected to be a valid peak. This case occurred in very few spectra in regions of pure noise. Its computation time for a single peak was in the order of 2 min (same hardware as in Sec. A.4).

[4] The peak width of narrow peaks depends not only on $b_{0,r}$ but also on the position of the mean frequency of the peak on the raster of discrete frequencies (Fig. 4.1 shows that the narrowest peak for $|b_{0,r}| = 5$ has approximately the same width as the broadest monofrequent peak).

6.1.1.2 Avoidance of fit results for much broader peaks than expected

In rare cases, the fit was performed successfully starting with few complex values – which suggests a narrow peak – but ends up with a very high value for $|b_0|$. With increasing $|b_{0,r}|$ the magnitude of the peak drops (Sec. 4.2.1), thus sets of parameters with high values for A_0 and $|b_{0,r}|$ can be observed. The subtraction of the corresponding broad and strong peaks from the spectrum, in which only few data points fit, causes the surrounding values to increase in magnitude much above the original ones, yielding a marked increase of power in the spectrum. Such a case should be avoided by all means. If this fit result was correct, its peak should fit on its whole width. Therefore, if the fitted b_0 does not fit to the estimated peak width, the fit is rerun with a higher number of complex values.[5] An example of a broad peak, where a narrow peak width is estimated, was shown in Figure 4.15; if the start value estimation did not fail, then this case would have been a typical example of the described situation. If this fit was successful, it would have been repeated with a corrected peak width corresponding to the fitted b_0.[6]

6.1.1.3 Uncovering of hidden peaks

If a peak is subtracted, its complete spectrum is subtracted. Significant changes occur for the values of the peak and the surrounding. Within these values new peaks might occur or peaks, which could not be fitted successfully before, might now be subtractable. The safest way is to restart the complete procedure for the remaining spectrum after the subtraction of the single peak has been performed. This approach is very time consuming.[7] Due to the monotonous decrease of magnitude of an LFS-sine peak, its subtraction manipulates the values of the spectrum the less, the more distantly they lie from the centre of the peak. Assuming that this manipulation becomes insignificant at a certain (relative) magnitude, it is more sensible to analyse only a small spectral interval again. It was presented (Sec. 4.3) that the strength of the decrease of magnitude is basically a function of $|b_{0,r}|$. Briefly, the following steps are performed to roughly estimate the interval of spectral values in which the peak analysis should be repeated – this is similar to the estimation of

---

[5] The implementation is: if: $|b_{0,r}| > 2.5 \cdot n_{\mathrm{Fit}}$, then: overwrite the left (L_l) and right (L_r) limits of the peak with $L_{l,r} = r_{\max} \mp |b_{0,r}|/2.5$. Subsequently, the fit is repeated. This is not optimised at all and the value of 2.5 is chosen mostly arbitrarily after the analysis of failures and the understanding that extreme cases should be avoided.

[6] The left and right limits of the fitted interval is set to $r_{\mathrm{Max}} \pm b_{0,r}/2.5$ before the fitting is repeated. If and only if this last fit is successful, an LFS sine with the current set of parameters is subtracted.

[7] In this chapter the $\chi^2_{\mathrm{Thres}}(n_{\mathrm{Fit}})$ are set to allow 5 % false positives. If a spectrum consists of 4,096 magnitude values (at positive frequencies) and approximately every fourth is a peak (Sec. 5.3), then there are around 50 subtractions in each spectrum if it consists only of noise. For signals containing different fundamental frequencies with several harmonics, this number can drastically increase. Assuming that 50 peaks, which will be successfully fitted, are equally distributed in a list of 1,000 peaks in total, then a restart is performed after every fit of one of the 50 successful fits, meaning there will be one late restart for every early restart. Thus, the average number of fits between two restarts will approximately lie at half of the complete number, namely 500. Consequently, for 50 restarts, the computational effort will be 25 times higher compared to the procedure without restarts.

the peak-width parameter (Sec. 4.3), but does not need to be precise.

A linear dependency of $|b_{0,r}|$ on the width of the interval that should be re-analysed, w^{re}, is assumed (in accordance with Fig. 4.3 (a)):[8]

$$w^{\mathrm{re}} = o^{\mathrm{re}} + s^{\mathrm{re}} \cdot |b_{0,r}|. \tag{6.1}$$

In order to find the margins of the range to be re-analysed, it is assumed that the value has to fall below the maximum divided by a certain factor f^{re} (fictitiously, irrespectively of the actual spectral background).[9] Systematically, the full width at a certain f^{re} (by analogy to full width at half maximum (FWHM)) is gained as a function of $|b_{0,r}|$ (the plots and fits are not shown here; the procedure is very similar to the ones used for the start value estimation, Sec. 4.3). It allows the derivation of the offset parameter:

$$o^{\mathrm{re}} = 1.803 \cdot \mathrm{Exp}\Big[0.7531 \cdot \log_{10}[f^{\mathrm{re}}]\Big] - 2.321 \tag{6.2}$$

and of the slope:

$$s^{\mathrm{re}} = 0.07373 \cdot \log_{10}[f^{\mathrm{re}}] + 0.7570. \tag{6.3}$$

All peaks located in the interval $i_{\max} \pm \mathrm{Round}[0.5 \cdot w^{\mathrm{re}}]$ which are still to be processed or have been processed unsuccessfully are erased from the list of (LFS) sine candidates. Within this interval, the new magnitude values are calculated and peaks are detected and added to the list. Finally the modified list is sorted by amplitude and processing continues with the strongest peak.

For all spectra analysed in this chapter, the factor is $f^{\mathrm{re}} = 10^4$.[10]

6.1.1.4 Reconstruction of the time-domain signal

As mentioned in Section 6.1, longer time intervals are analysed in this chapter, for this purpose sequences of spectra are processed. A longer time interval is apportioned into multiple short ones, according to the chosen number of samples per FFT (N). The application of the Hann-window function sets the first sample of each time interval zero before a FFT is performed; thus, after inverse FFT and even after the application of

---

[8] The deviations from linear behaviour for small $|b_{0,r}|$ (Fig. 4.3 (b)) are ignored here because this interval estimation may be imprecise.

[9] The complete algorithm proceeds without knowledge of parameters inherent in the data. This should not be changed for this small optimisation; therefore the estimation of a value for a parameter such as the general background of a spectrum is not introduced, even if it could somewhat optimise the length of the re-analysed interval, e.g. for low SNRs the interval being re-processed could be reduced because it is unlikely that peaks become valid in the vicinity of the peak if the band of frequencies is dominated by the underlying signal.

[10] Two examples: For $|b_{0,r}| = 0$, $w^{\mathrm{re}} = 35.40$, thus the range $[i_{\max} - 18;\ i_{\max} + 18]$ is re-analysed. $w^{\mathrm{re}}(|b_{0,r}| = 30) = 65.40$.

the inverted window function, this first value would remain zero.[11] If multiple intervals would be recombined, the result would show periodically missing samples. Furthermore, the window function decreases the weights for the outer-most values, giving the most weight to the middle. A particular reason for using considerable overlap is the trend of the errors (stemming from the notches after sine subtraction) to increase to the margins of the time interval (e.g. figures in Sec. 5.5). By merging spectra and suppressing their outermost values, this effect can be reduced strongly. In this chapter each single spectrum overlaps by 25 % with its precursor. Thus, in the sequence plots, the time shift between two beginnings of subsequent spectra is given by:

$$\Delta T_{\text{Spect}} = 0.75 \cdot N \cdot \Delta t. \tag{6.4}$$

If transformed back to the time domain, the overlapping parts are weighted in such a way that the amplitudes of the last spectrum decrease linearly and the amplitudes of the current spectrum increase in the same way over the time of overlap. Thus the preceding spectrum is faded out in the same way as the next spectrum is faded in, keeping the proportions right.

6.1.2 Real, measured data

Real, measured data are a composition of real signals with real environment background noise (and noise produced in the measurement system) as well as manipulations caused by the involved hardware and its transfer functions. Ideally, one tries to separate all these manipulators from each other and study their characteristics independently. For the purpose of this work, the background signals themselves are not evaluated in a way that, for example, the amplitude is used to draw conclusions about properties of its source; instead, if certain properties (namely periodic components) are given in the data, the data are manipulated and ideally, the given background is left as it is.

Important requirements are:

- the signal is sampled equidistantly,[12]
- the transfer function is independent from the frequency. Otherwise, the F_{Sum} approach could fail for $b_0 \neq 0\,\mathrm{Hz/s}$. It is assumed that the recorded value is proportional

---

[11] This is an issue only concerning the first value. The annulment of the window function for other values is unproblematic: For these numbers of samples per FFT, the calculation precision at every point is significantly higher than the range of weights resulting from the Hann-window function. Even at 8,192 samples the precision is several orders of magnitude higher than the quotient between the highest (1.0) and the lowest ($1.47 \cdot 10^{-7}$) non-zero value of the weight function – except for the first sample which will always be zero.

[12] In our measurement systems there is a slight drift of the time base, on the order of 10^{-5} relative, that does not matter over the time periods considered.

to the voltage at the ADC which itself is proportional to the actual physical quantity taken up by the respective sensor.[13]

6.1.3 Seismic and acoustic data

Even though the work is motivated by subtracting periodic noise from seismic signals, most of the following examples use acoustic data. It is much easier to find or generate periodic acoustic than seismic signals.[14] If acoustic signals couple to the ground, a significant amount of energy is reflected or absorbed causing the SNR to be considerably higher in acoustic data. Typically, compared to acoustic signals, seismic signals are complexer in the time domain (mainly because of reflections at soil-layer boundaries[15], additional seismic wave types[16] or, for surface waves in a layered medium, even a significant influence of dispersion); mainly, they show multiple arrivals of an event, caused by the multiple propagation paths and different propagation speeds of the wave types. However, the corresponding spectra remain relatively simple; the mentioned effects influence the spectral amplitudes and phases, but the frequencies stay the same.[17]

As described in section 5.6, the interference between the directly measured signal and signals propagating along indirect paths can be destructive or constructive, depending on the differences of their path and wave lengths. The self-interfered signal will show time dependent variations in its magnitude if either the relative path length or the frequency changes significantly within T; both cases are not covered by the algorithm.

The present approach works with all kinds of data, including the acoustic or seismic ones, recorded in our group. Because of the better SNR most of the evaluated signals shown in the following sections stem from acoustic measurements.

---

[13] To be precise: The transfer functions in principle have no influence on the fitting procedure, as long as their frequency dependency is insignificant within the peak width of a single peak. If a sine had a high frequency shift and the transfer functions would have a strong frequency dependency, then of course the fit quality would decrease because of a missed requirement: in this model the amplitude of the sine is expected to be constant within T. It will be argued that this requirement is most likely not fulfilled adequately for some situations (Sec. 6.2.2.3).

[14] One can use a sound card with a speaker and play a simple audio file. Beneath possible non-linearities in the transfer function of the hardware, a weak disadvantage of acoustic signals is the fluid propagation medium: the speed of sound (measured on the ground) can be time dependent (e.g. wind). Acoustic waves excite seismic waves if hitting surfaces – but with reduced amplitudes. The direct excitation of strong periodic seismic waves is more complicated; typically, special devices are operated, like vibrator trucks or smaller plate vibrators.

[15] The seismic-wave propagation depends on many factors, among others the kind, porosity and layering of the soil, the groundwater level etc. [40, Chap. 9]. Changes in the wave speeds between different layers, reflect and refract the wave.

[16] Compressional and shear waves, surface waves (Rayleigh, Love waves), [40, Chap. 2].

[17] Signals may become complicated if the interfering sines change their frequencies independently, e.g. if one propagation path hits a moving reflector (not moving exactly parallel to the source-sensor axis), it becomes Doppler-shifted and the superposed spectrum consists of doubled peaks, which can cause the algorithm to fail. A changing angle of incidence and fixed reflecting surfaces can cause the same problems (e.g. a geophone in layered soil and an overflight as signal source).

6.1.4 Number of samples per spectrum

The number of values forming a peak in the frequency domain increases quadratically with the number of samples of the Fourier transform: For a bigger number, the elapsed time T is longer, meaning that the end frequency has evolved farther away from the start frequency. In addition, the resolution in the frequency domain increases linearly with N, so more values are available in a given frequency interval.

As long as there are no significant changes of the frequency higher than to the first order, there are two arguments for a high number of samples: Firstly, the algorithm for broad peaks is to be tested with priority, therefore challenging conditions (with high values of $b_{0,r}$) are preferable. Secondly, the peaks have to be well separated; for this a suitable spectral resolution is required.

The precondition that the signal is sufficiently homogeneous usually is appropriately fulfilled if the time interval per spectrum is less than 1 s. Our standard sampling rate is 10 kHz, so it is reasonable to perform these evaluations with $N = 8,192$ samples.

6.1.5 False-positive rate

In the following evaluations 5 % false-positive fits are accepted (this means: in a spectrum of Gaussian white noise 5 % of all peaks are classified as originated by sines and subtracted, Sec. 5.3). As a consequence, many peaks will be subtracted (will be best visible in the plots of the fit results or the theoretical spectra, e.g. 6.2). Reasonable limits and conditions could be thought of for sorting out candidates for sines and to strongly reduce this percentage. Their implementation would result in more parameters that had to be described and motivated which would go beyond the scope of this thesis. Ideas are listed in Chapter 7. To demonstrate the performance of the fit algorithm this rate of 5 % false positives is accepted. Furthermore, the cursory analysis of the influence of sporadically subtracted erroneous (LFS) sines from data shows that the resulting modifications seem to be insignificant to non-periodic events in the data.[18]

6.2 Synthetic signals in a real environment

As a first step for the evaluation of real signals, sound files of (multiple) LFS sines are played via sound card and speaker. The main advantage is, that the input parameters are known and comparable with the fit results. For this purpose, a small procedure was

---

[18] We are not trained in analysing seismic wave forms. Details might get lost, but by visual inspection the worst case that happened is: a decrease in the order of a few percent of the peak-to-peak value in the time domain at the time of an event accompanied by small additional oscillations increasing to the margins of the time interval, see e.g. Fig. 5.12 (b) in Sec. 5.5. The small decrease of the peak amplitude in the time domain can hardly be seen. If multiple subtractions are performed within the frequency range of the (broadband) underlying signal the effect increases.

#	Start /s	End /s	Initial frequency /Hz	Initial phase /rad	Amplitude integer	Sweep duration /s	Sweep limit /Hz	Resulting b_0 $^{\mathrm{Hz}}/_{\mathrm{s}}$
1	0.0	110.0	150.0	0.0	$5 \cdot 10^5$	n/a	n/a	0.0
2	10.0	80.0	160.0	0.0	$5 \cdot 10^5$	n/a	n/a	0.0
3	20.0	90.0	180.0	0.0	$5 \cdot 10^5$	n/a	n/a	0.0
4	30.0	100.0	500.0	0.0	$5 \cdot 10^5$	n/a	n/a	0.0
5	0.0	110.0	1,000.0	0.0	$5 \cdot 10^5$	10.0	0.0	−100.0
6	50.0	110.0	2,000.0	0.0	$5 \cdot 10^5$	100.0	1,500.0	−5.0
7	20.0	110.0	500.0	0.0	$5 \cdot 10^5$	50.0	1,500.0	20.0
8	0.0	50.0	500.0	0.0	$5 \cdot 10^5$	50.0	700.0	4.0
9	20.0	60.0	1,000.0	0.0	$5 \cdot 10^5$	n/a	n/a	0.0

Table 6.1: Sine properties of the analysed sound file (`Sweep4.cmd`). The amplitude values are chosen to be high numbers to minimise discretisation effects and avoid noise production by strong amplification (the highest possible number is 2^{23}, this number should not be exceeded even if all sines sum up constructively). The real amplitude is determined by the volume setting of the hardware amplifier used which was adjusted subjectively to a quite high level which, on the contrary, was not too annoying for the environment. Important in this column would be the relative differences, but all amplitudes are the same. The ”sweep duration” is the duration until the LFS parameters are reset to their initial values in contrast to the duration in which this LFS sine is played (”Start” − ”End”). b_0 is not an input value but results from: (”Sweep limit” – ”Frequency”)/”Sweep duration”.

written for the `Eingabe` software which produces sound files in the RIFF/WAVE format. For the experiments described below, the sampling rate of the played files is 44,100 Hz with 24 bits per value. The measured signal of one of the files is analysed in the following and its input information is given in Table 6.1. The procedure was written in haste in the field after a day of measurements on the last evening of a measurement campaign in order to run the experiment the next morning. Two mistakes were made:

1. The sweep-duration parameter did not work: there are no resets of the frequency to its start value when the sweep-limit frequency is reached.[19]
2. There is no local time for each sine i.e. all sines propagate from the beginning of the sound file with the parameters given.[20]

These experiments could be repeated but, as the created file includes all properties of the intended file, the data are used here. The mistakes were described to allow a connection of the following plots with the input parameters shown in Table 6.1.

---

[19] E.g. sine #5 decreases from 1 kHz through 0 Hz to "negative" frequencies, in effect increasing for the next 100 s to more than 5 kHz. The measurement is done at 10 kHz with a low-pass filter at 3 kHz. That the amplitude does not decrease sharply at this frequency is a consequence of the not very steep filter characteristic. The ”reflection” at 5 kHz, the Nyquist frequency, is caused by aliasing.

[20] E.g. sine #7 should start after 20 s with 500 Hz and 0 phase. Instead, because of the mistake, at the time of its onset, its frequency increased already for 20 s according to the slope given by the sweep duration and the ν^{end} parameters. Thus, the start frequency is not the intended one.

As mentioned above, these sweeps are analysed with $N = 8{,}192$ samples per spectrum for two reasons: Firstly a good spectral resolution is required to separate the monofrequent sines with 150, 160 and 180 Hz (Table 6.1). Secondly, this analysis should demonstrate the behaviour of the fitting algorithm if confronted with broad peaks; the number of complex values used for a fit grows quadratically with N (Sec. 6.1.3). One instructive example: For 8,192 samples, T is 0.8192 s and $\Delta\nu = {}^{1}\!/_{T} = 1.22\,\mathrm{Hz}$. Sine #5 has a $b_0 = {}^{-100Hz}\!/_{-100s}$, in units of $\Delta\nu/T$ (Sec. 3.1.3) it is $b_{0,r} = -67.11$. For 1,024 samples with $T = 0.1024\,\mathrm{s}$ and $\Delta\nu = 9.77\,\mathrm{Hz}$ it was just $b_{0,r} = -1.05$. The first one represents a very broad peak, whereas the second one could even be fitted acceptably with the monofrequent approach.

6.2.1 The seismic data

The experiment was conducted near Münster (Westphalia) from the 13th to the 17th of May 2013.[21] The data processed in this section were measured by a geophone buried 15 cm under the grass of surface.[22]

Figure 6.1 shows a sequence of 194 magnitude spectra implying 120 s of data (time on the mantissa). The complete frequency range ($0 - 5{,}000\,\mathrm{Hz}$, 4,096 frequency values) is plotted on the ordinate; the density of spectral values is accordingly high; especially small peaks (horizontal lines if the frequency is constant), consisting of very few strong values, are barely visible. Nonetheless, it gives an overview of the complete processed data. The magnitudes of the spectral values of the soil velocity are given in the grey scale: With five orders of magnitude almost the full range is presented.[23] (a) demonstrates the original data. Bright lines stem from sines: The nine sines of the played sound file are visible as well as mains hum with all its harmonics at odd multiples of 50 Hz. (b) shows the same plot after (LFS) sines have been fitted and subtracted.

Figure 6.2 gives details on the fits. (a) is the sequence of the subtracted spectra. (b) is a different illustration: Each subtracted sine is represented by a circle (under the condition that its amplitude is at least 10^{-4} times the strongest of all amplitudes) at the mean frequency of the peak ($\nu_0 + 0.5 \cdot b_0/\Delta\nu$).[24] The colour codes stand for the different paths the fit procedure can take: Black circles indicate that the estimated peak width includes at least four complex values and the fit with the $\mathrm{F}_{\mathrm{Sum}}$ expression was successful. If the fit results in a $|b_{0,r}|$ much broader than expected, it is rerun with more complex values

---

[21] At the same experiment, aircraft signal were measured. For information on the measurement, see [41]. A more detailed publication by Mattes Liebsch is in preparation. Some more details related to aircraft measurements are given in Section 6.3.

[22] Vertical geophone #15 `Sensor Nederland SM-6`, eigenfrequency: 4.5 Hz, sensitivity: $\approx 26\,{}^{\mathrm{V}}\!/_{\mathrm{m/s}}$, factor of amplification: 100, connected to channel #21 of a 4-box combination of `Data Translation DT 9841` ADCs, sampling frequency 10 kHz, cut-off frequency 4.53 kHz.

[23] Within these five orders of magnitude all significant values are presented. Showing the full scale is not conducive: By chance arbitrarily small values can occur, reducing the resolution on a logarithmic scale of the grey scale likewise arbitrarily.

[24] Again, this limitation of visualised results is reasonable to focus on the strongest peaks with the highest impact on the signal.

(Sec. 6.1.1.2), this case is shown in purple. The other colours (explained in the figure margin) mark the different outcomes for narrow peaks (Sec. 6.1.1.1); in most cases the monofrequent approach ($\mathrm{F}_{\mathrm{Mono}}$) produces the best result.[25] The amplitude is given in the diameter (also here with logarithmic scaling), so bigger circles have a higher relevance.
One can see that many sines are subtracted. They mainly are aligned along straight horizontal lines, according to the mains hum. Figure 6.3 is a small cut-out and gives a detailed view of the found sines. At positions where lines cross each other the results tend to become worse or the algorithm even fails. Although the probability of a failure increases, the 550 Hz line shows that a crossing line does not necessarily make the algorithm fail (around 20 s both sines are subtracted in two stages, Sec. 6.1.1.3); on the other hand the fit for the same sine (at around 31 s) can fail even if no other lines are close.

6.2.1.1 Single-sine tracking

The list of fit results can be analysed and sets of parameters can be assigned to a certain evaluation sequence in order to get deeper insights respectively. Presently, this is done by hand – however, with the support of assistant suggestions.[26] Figure 6.4 shows two of the sequences of sines in separate plots. In order to get the frequency plot in a good resolution, the linear slope is subtracted by fitting a straight line to the mean frequencies. Its slope is in good agreement with, on the one hand, the b_0 values of each spectrum, on the other hand with the input parameters in Table 6.1. The time when a specific frequency is passed is not easily accessible because of the fast change with time and unknown time delays in the chain of signal production and measurement; therefore, the agreement between the actual input and fitted frequency is not evaluated. This effect is even stronger for the phase parameter.
In (a) two classes of outliers can be seen: First of all, there are two b_0 values close to zero, these are probably wrong picks: especially the third circle (at 05:47:22.5) seems to belong to the peak of sine #2,[27] which should have a constant frequency of 160.0 Hz. Another

---

[25] Because of the low χ^2_n threshold for $\mathrm{F}_{\mathrm{Sum}}$ as a result of one fit parameter more compared to $\mathrm{F}_{\mathrm{Mono}}$ (Sec. 6.1.1.1), green circles are very rare in general.

[26] A note for the software users: The procedure (`Extract Single Line (Seq)`, `Eingabe: Menu: 6.66.1`) allows the extraction of fit parameters for single peaks from the file containing all fit results. After one set of parameters is chosen for a certain spectrum, the position of the next peak is interpolated and the parameters of the best fitting set of the next spectrum is suggested. Additionally it shows the two next neighbours to both sides and allows further scrolling through all sets if the suggestion is not accepted. Returning to previous spectra is possible. If certain parameters (mean frequency, amplitude, b_0 or χ^2_n) fit, they are highlighted. Note that wrongly picked fit results typically have the lowest impact on the mean frequency – compared to other parameters – because the mean frequency itself is the basis for the suggestion of the next peak to pick. Other parameters (like b_0) can have strongly different values compared to their last pick; if the mean frequency of their peak matches the expected one, it will be suggested to the user if no better matching peak is available.

[27] The ochre colour indicates that it was originally proposed to be fitted with three complex values, meaning this peak is very narrow. The best result is gained after fitting four values (one is added to the right). The exact mean frequency of the corresponding fit result is 160.106 Hz which matches sine #2 (further fit results: $b_0 = 2.2661\,\mathrm{Hz/s}$, $\chi^2_n = 0.00516$).

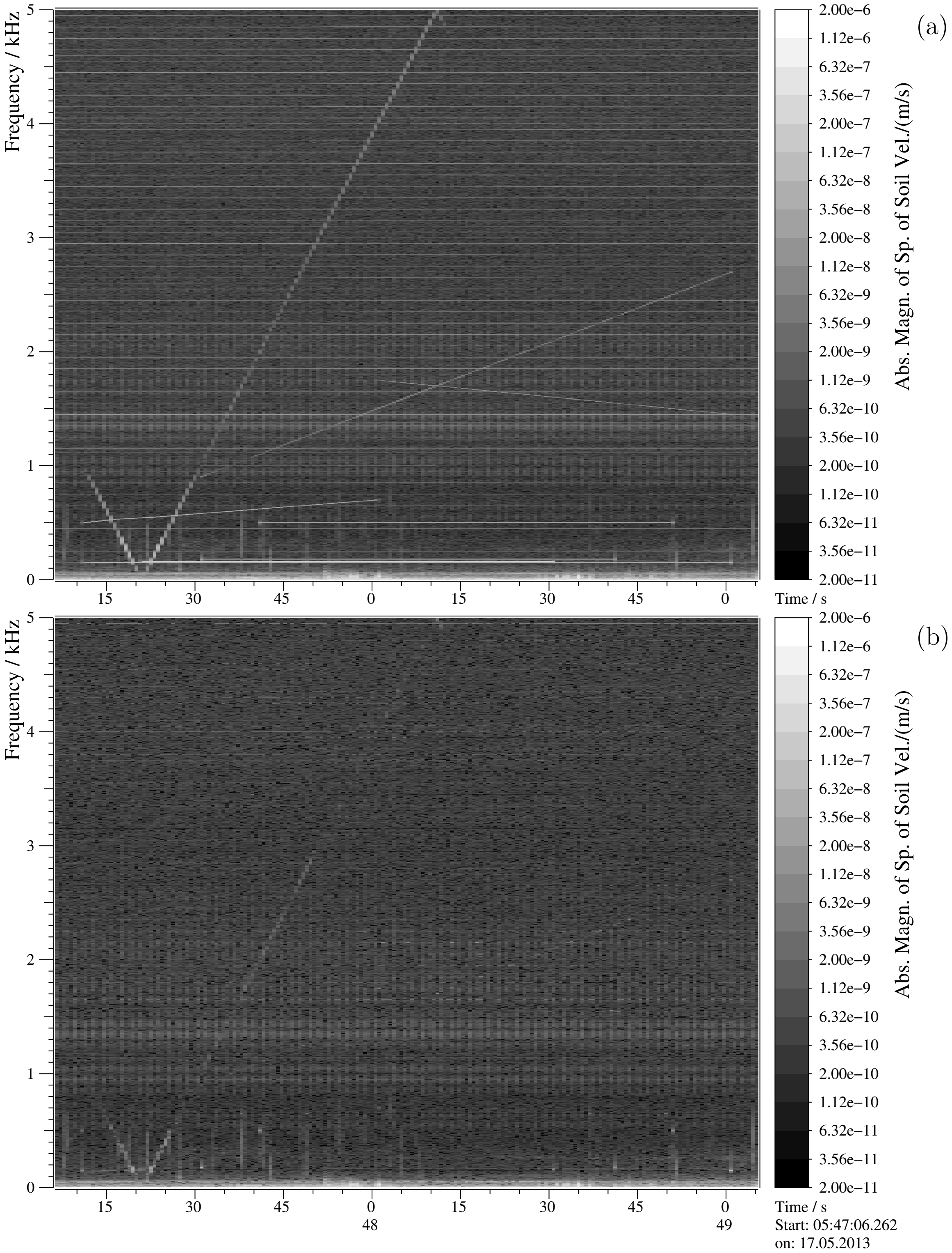

Figure 6.1: Seismically measured synthetic sines played via loudspeaker. To give an overview, the complete frequency interval over the complete time (universal time, coordinated (UTC)) over which this experiment was conducted is shown. LFS sines are visible as sloped lines. (a) before subtraction of peaks, (b) afterwards.

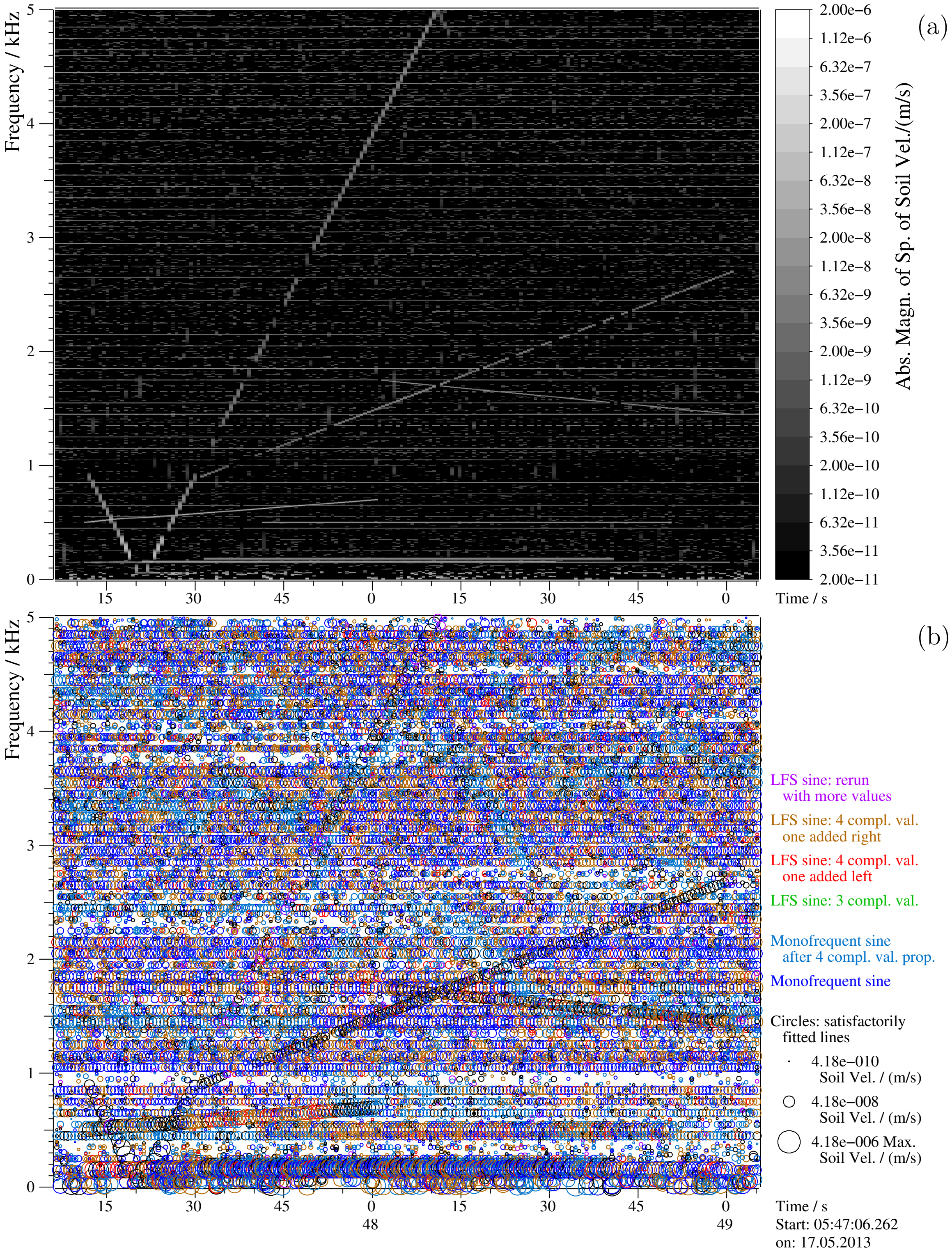

Figure 6.2: Additional spectrograms for Figure 6.1. (a) shows the subtracted spectra, (b) the amplitudes of the fitted sines and the types of fitting which led to the shown results. These plots show the whole range of the measurement; for better visibility a part of it is extracted in Figure 6.3.

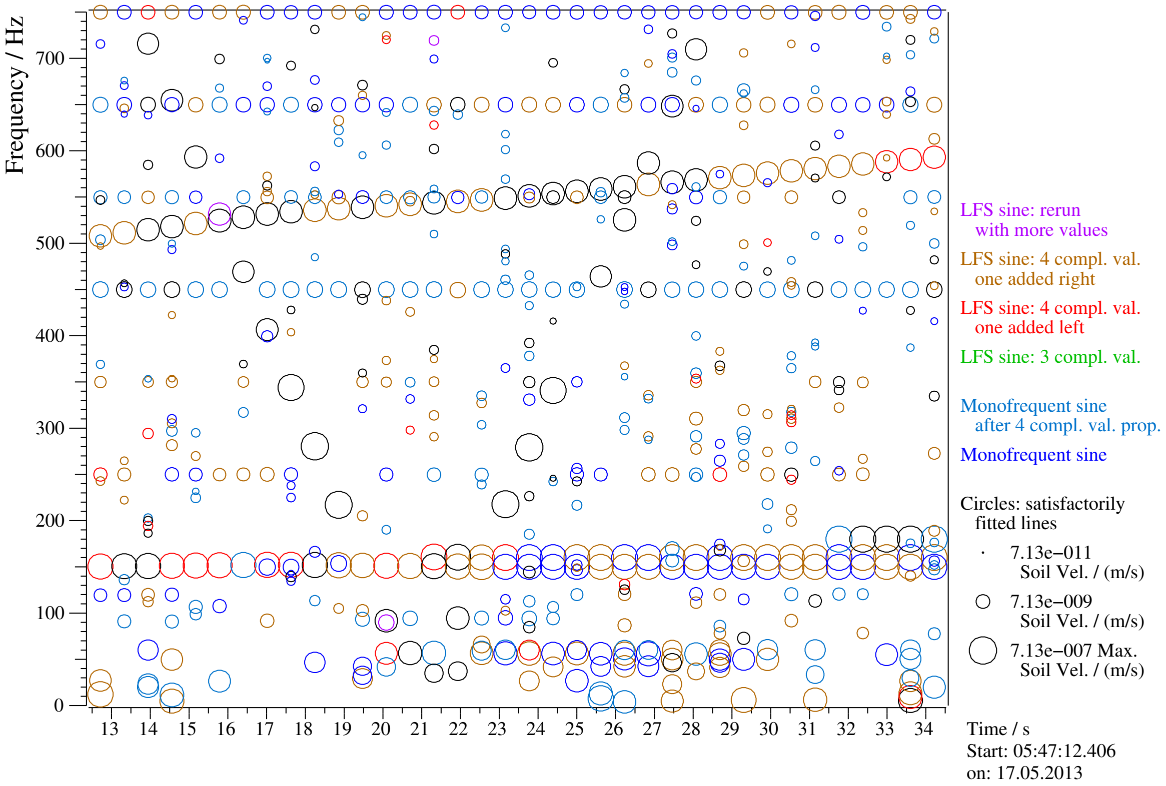

Figure 6.3: Small cut-out of Figure 6.2 (b). 50 Hz and odd multiples as well as the beginning of the monofrequent-sine triplet (150, 160 and 180 Hz, onsets at different times) show up as horizontal strings. Two lines with a slope are shown: One with a low positive slope starting with around 500 Hz and one with a strong negative slope which passes 0 Hz and continues with a positive slope, this one shows up as the black ”V”.

b_0 outlier is at (approx.) 05:47:42. It is fitted with $b_0 = -123.79\,\mathrm{Hz/s}$; here already the start value was wrong: $b_0^{\mathrm{Start}} = -100.48\,\mathrm{Hz/s}$. Obviously, the width was estimated fairly well but the procedure that determines the sign of b_0 failed. As described in Section 4.6.2, the sign is calculated from small, systematic deviations from a slope of π per $\Delta\nu$ in the phase spectrum. With a low probability the sign estimation can fail, and afterwards it is virtually impossible for the algorithm to get to the right values by iterating. It is interesting that even with this failure in the start values the algorithm ends at a point where the χ_n^2 value meets the threshold.[28]

It is not surprising that in (a) all fits were done to more than four complex values because of the big frequency shift per time which results in broad peaks (purple circles indicate a prior run with a lower peak width, Sec. 6.1.1.1). Whereas, in (b), the peaks are narrow and in many cases three values are proposed to be used for the fit. In this case the fit is repeated three more times with the linearly-changing frequency expression (Sec. 6.1.1.1): once with the same three values and a very strict $\chi^2_{\mathrm{Thres}}(n_{\mathrm{Fit}} = 3)$ and with one more value added to the left or the right. The colours of the circles show that, after comparing the four fit results, the $\mathrm{F}_{\mathrm{Sum}}$ expression outmatches the monofrequent expression by fit-result comparison in every spectrum, except for one. This makes sense as the sine changes linearly in time and an added value increases the χ_n^2 threshold. The mentioned single deviation (05:48:41) is fitted with the monofrequent approach and is not wrongly picked; its frequency is 1,563.49 Hz and therefore not very close to a harmonic of the mains hum. It is more likely that the underlying noise consists of just those values, which, by chance, superpose with the sine in such a way, that the $\mathrm{F}_{\mathrm{Mono}}$ approach, boosted by its lower threshold for χ_n^2, produces a better result than the $\mathrm{F}_{\mathrm{Sum}}$ approach.[29]

Inexplicable is the predomination of the right-hand-side added values in comparison to the left-hand-side added ones.[30]

---

[28] Fit details: 50 complex values are fitted, resulting in $\chi^2_{\mathrm{Thres}} = 0.642$. After 120 iterations it returns with: $\chi_n^2 = 0.329$. As the algorithm rarely gets to satisfactory results after reaching the limit of 120 iterations one should think about classifying its result under this condition as false (this has also been mentioned in Sec. 2.1.1).

[29] If cases like this appeared more often, the procedure ranking the results to compare the fits should be revised.

[30] Probably, this is a result by chance: For other sequences, this imbalance vanishes or shows the inverted direction (e.g. Fig. 6.17).

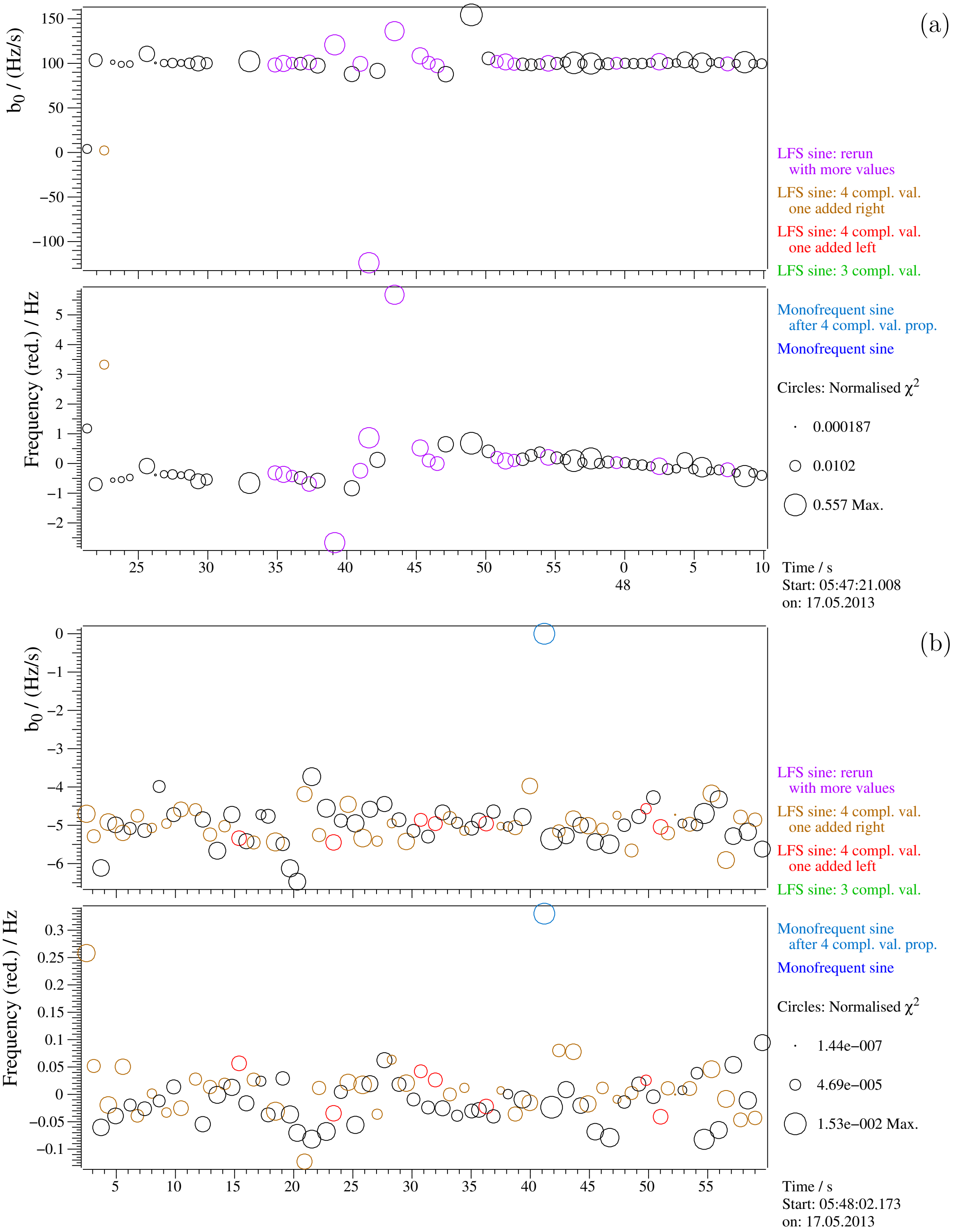

Figure 6.4: A pair of tracked sines, each with a plot of the fitted b_0 and one with the mean frequency (in order to get a good resolution, a linear progression is assumed and subtracted), different time intervals. Top: The sine with the strongest increase of the frequency (sine #5). Bottom: The sine with the negative b_0 (sine #6). The equations for the subtracted lines are: (a): $100.07\,{}^{\mathrm{Hz}}\!/\!{}_{\mathrm{s}} \cdot t + 33.81\,\mathrm{Hz}$. (b): $-5.0021\,{}^{\mathrm{Hz}}\!/\!{}_{\mathrm{s}} \cdot t + 1{,}742.78\,\mathrm{Hz}$. In contrast to the fits above, in plots like these, the circle radius gives the χ^2_n value. The smaller the circle, the better the fit.

6.2.2 The acoustic data

Analogously to the seismic signal of the last section (Sec. 6.2.1) a microphone signal measured 6.5 cm above ground is presented here.[31] This is the same measurement (at the same time, but a different channel of the ADC). Because the signal is produced acoustically by a speaker suspended by a crane and thus uncoupled from the ground and the SNR is much better than the one for the seismic sensors, consequently, the following figures show that the peaks in the spectrum are orders of magnitude above the underlying noise. This clarity makes this example appropriate for discussing additional effects, resulting in a series of supplementary plots and descriptions compared to the last section. Initially and in analogy to the seismic data, Figure 6.5 (a) demonstrates the sequence of spectra of the original data. Because of the good SNR, vertical lines are visible at the beginnings and ends of some (LFS) sines. These stem from spectra the periodic signals ends within the time interval T.[32] Figure 6.6 firstly shows the lines described in Table 6.1. Secondly, weak additional lines are visible which seem to be linked to the intended lines as they are most likely linear combinations of the main ones. The additional frequencies are probably produced by non-linearities in the speaker, the amplifier or even the digital-analogue converter (DAC) in the laptop computer used to play the RIFF/WAVE files. Thirdly, mains hum with low amplitude can be observed (best visible at frequencies of around $1,400 - 2,000$ Hz).

The horizontal lines are subtracted very successfully. Figure 6.6 indicates the same for the fastest linearly changing frequency, but a comparison with Figure 6.5 (b) makes clear that on the one hand the sines are fitted and subtracted successfully, but on the other hand not the complete power of the peak is subtracted (this phenomenon will be discussed in Sec. 6.2.2.3). The broadband excitations at the beginnings and ends of the sweeps remain in the signal which is reasonable as the algorithm is not designed to handle these cases. Because of their strong amplitude they also mask the underlying LFS-sine signals, preventing the fitting of other peaks. This phenomenon shows up in the dark vertical lines in Figure 6.6 (a).

6.2.2.1 Single sine tracking

Analogously to the tracked sines for the seismic data, the same two lines are presented for the acoustical measurement in Figure 6.7. For both lines every single sine is fitted

---

[31] Microphone `BK6`, `Brüel & Kjær 4198`, sensitivity: 0.0519 V/Pa, factor of amplification: 60, connected to channel #30 of the same 4-box combination of `Data Translation DT 9841` ADCs as for seismic measurement, sampling frequency 10 kHz, cut-off frequency 3.0 kHz.

[32] Ending a signal is like multiplying it with another, shorter rectangle (additional to the rectangle limiting the time interval to T). As shown in Section 2.3.2 the Fourier transform of a rectangle is a sinc function; its width (in the spectral domain) is determined by the length of the rectangle (in the time domain). The shorter the rectangle, the wider the sinc function that is convolved, often resulting in strong broadband excitation around the current frequency of the (LFS) sine. More information concerning this issue will be given in Section 6.2.2.3.

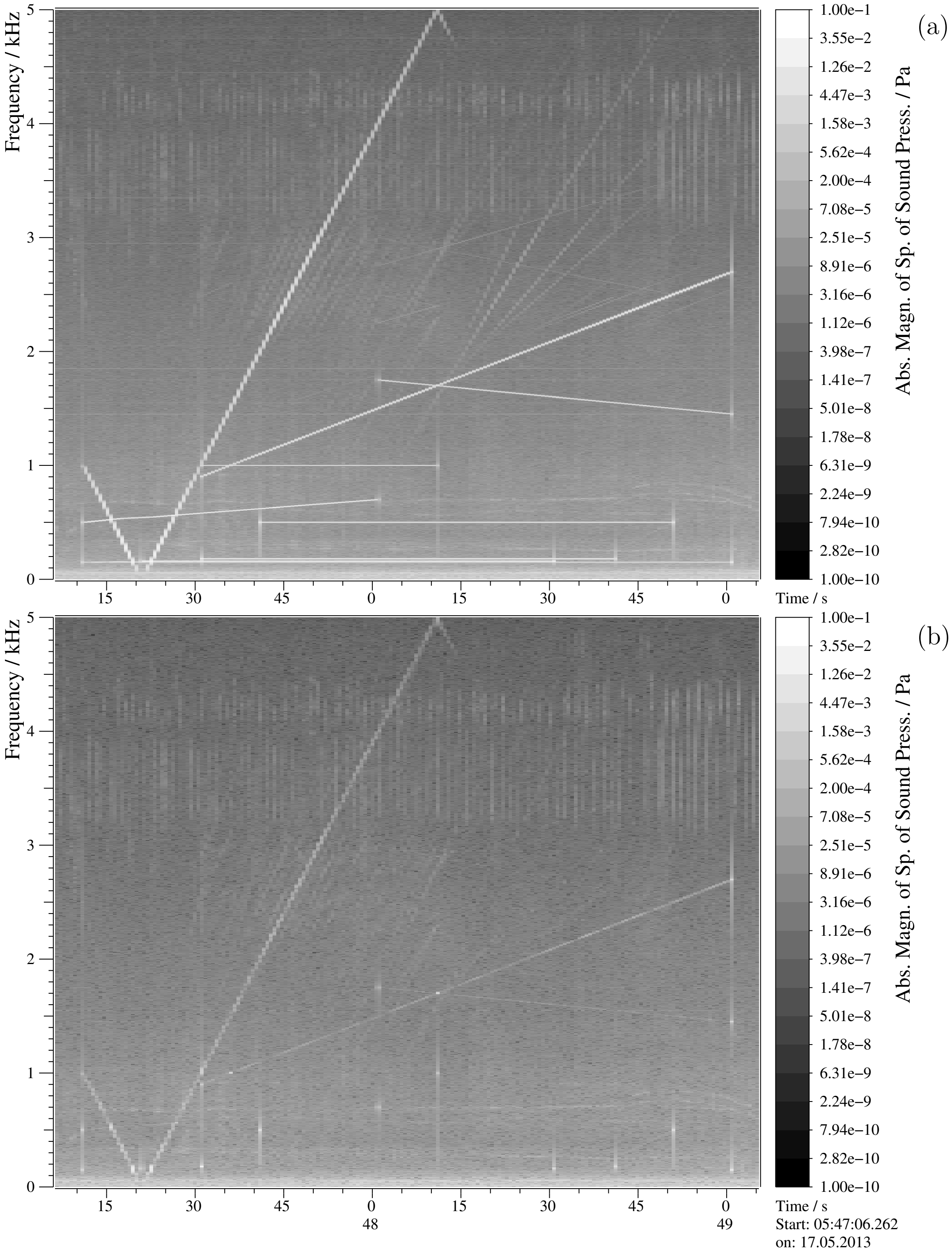

Figure 6.5: Acoustically measured synthetic sines played via loudspeaker (in analogy to Fig. 6.5). (a) shows the spectrum before subtraction of peaks, (b) afterwards.

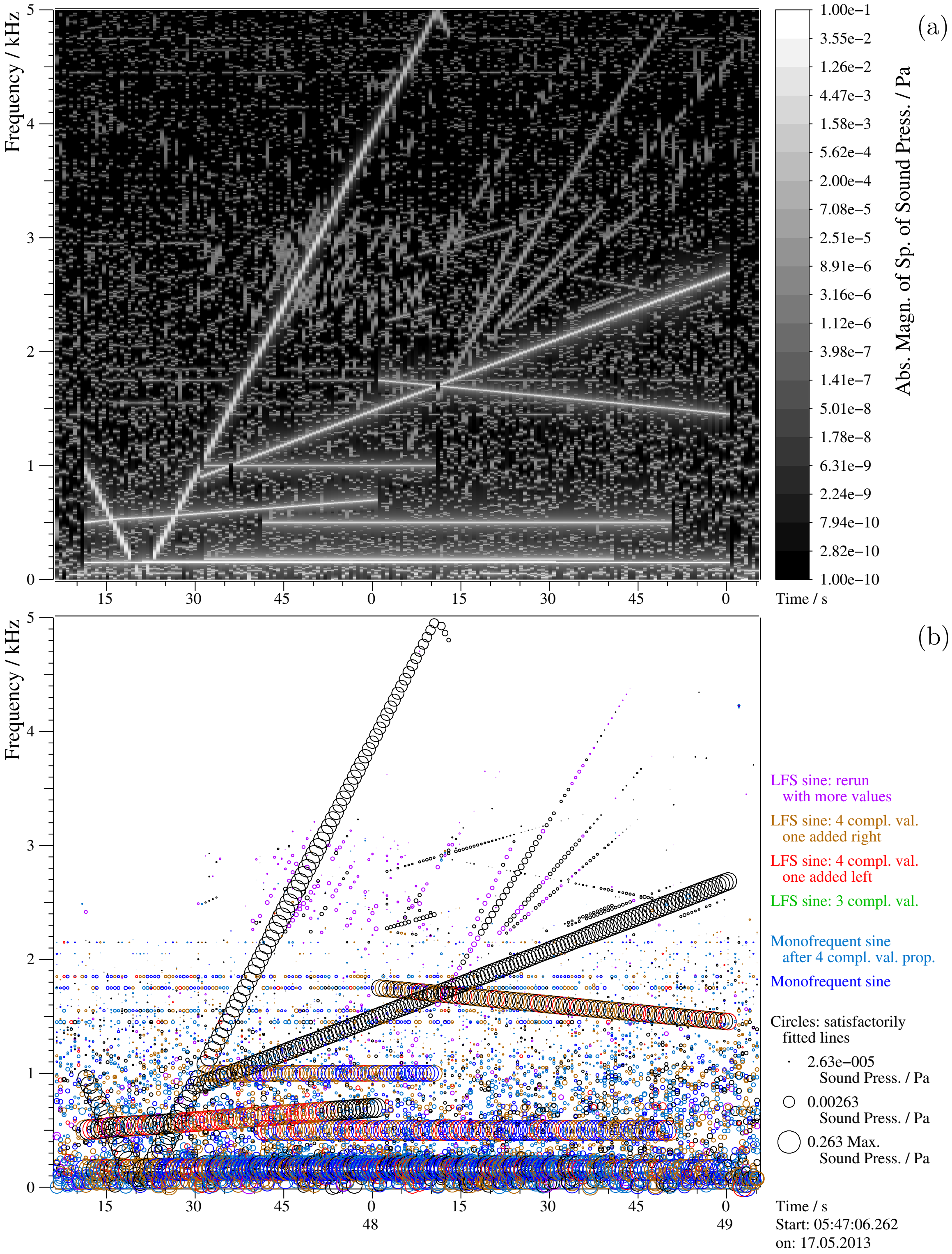

Figure 6.6: Additional spectrograms for Figure 6.5. (a) shows the sum of the subtracted spectra, (b) the amplitudes of the fitted (LFS) sines and the types of fitting which led to the shown results. In order to warrant transparency, the range of magnitudes in (b) is limited to four orders of magnitude which is much less than in figure (a) where considerably more results are shown.

	Sine #5		Sine #6	
	b_0 / (Hz/s)	$\nu_{\mathrm{Mean}}^{\mathrm{Red}}$ / Hz	b_0 / (Hz/s)	$\nu_{\mathrm{Mean}}^{\mathrm{Red}}$ / Hz
Seismic	100.07 ± 9.19*	0.000 ± 0.876*	-5.002 ± 0.452**	0.0000 ± 0.0485**
Acoustic	100.040 ± 0.344	0.0000 ± 0.0683	-5.0018 ± 0.0342	0.00000 ± 0.00625

Table 6.2: Summarised results of the acoustic and seismic peak tracking of the sines #5 and #6 (seismic: Fig. 6.4, acoustic: Fig. 6.7), with programmed b_0 of exactly 100.0 Hz/s and -5.0 Hz/s, respectively. Since for ν_{Mean} the linear progression is subtracted it is called $\nu_{\mathrm{Mean}}^{\mathrm{Red}}$ and varies around zero. The errors are the standard-deviation values. The peaks that are obviously wrongly picked are excluded here (* means one excluded peak, ** three excluded peaks) – they should not be included in a statistical evaluation as they do not represent the precision of the fit algorithm. In the seismic data the mains hum contributed significantly – its peaks are fitted successfully but do not belong to the LFS sine, whose peaks were intended to be tracked. These peaks are not an error of the picking suggestion algorithm because these peaks are at the right frequencies. It might be up to the user (or to an additional algorithm) to decide whether a peak belongs to the mains hum or to the tracked sine. In this case it would be simple to decide on the basis of b_0 – the discrimination between $b_0 \approx 100$ Hz/s and $b_0 \approx 0$ Hz/s was unproblematic – but for sines with low LFS or even monofrequent sines, additional parameters to classify the peak would be necessary. In order to avoid this, the peaks remain in the tracked sequence in this work, but are rejected for the statistical evaluation.

precisely and reliably. In comparison to the same tracked peaks in the seismic data (Fig. 6.4) no obvious outliers are picked or fits converged to secondary minima.

For signals of real sources with unknown emissions of noise, quantitative evaluations of the fitted parameters are difficult if not impossible. In contrast, the played sound files contain sines with at best linearly with the time changing frequencies. The mean frequency of the peaks, ν_{Mean}, should be constant after subtraction of a fitted straight line and the b_0 should be constant anyway. Table 6.2 gives measures for the deviation from the straight line respectively from the constant value. Obviously, fits in the acoustic data are significantly more precise. The ratio of standard-deviation values reaches from approximately 8 for $\nu_{\mathrm{Mean}}^{\mathrm{Red}}$ of sine #6 to more than 25 for b_0 of sine #5. It is presumed that the better SNR of the acoustic data is mainly responsible for this discrepancy.

6.2.2.2 RMS values in the time domain

RMS values were calculated in the time domain over intervals of 0.5 s.[33] Plots of these slowly sampled data give a measure for the progression of the power content. Figure

---

[33] Note that the measure RMS_Δ introduced in Section 5.2.1.1 is the RMS value of the difference between the underlying signal without (LFS) sine and the signal after addition, fitting and subtraction of an (LFS) sine in the time domain. For real signals this measure is not available and only the pure RMS value of a time-domain signal can be specified.

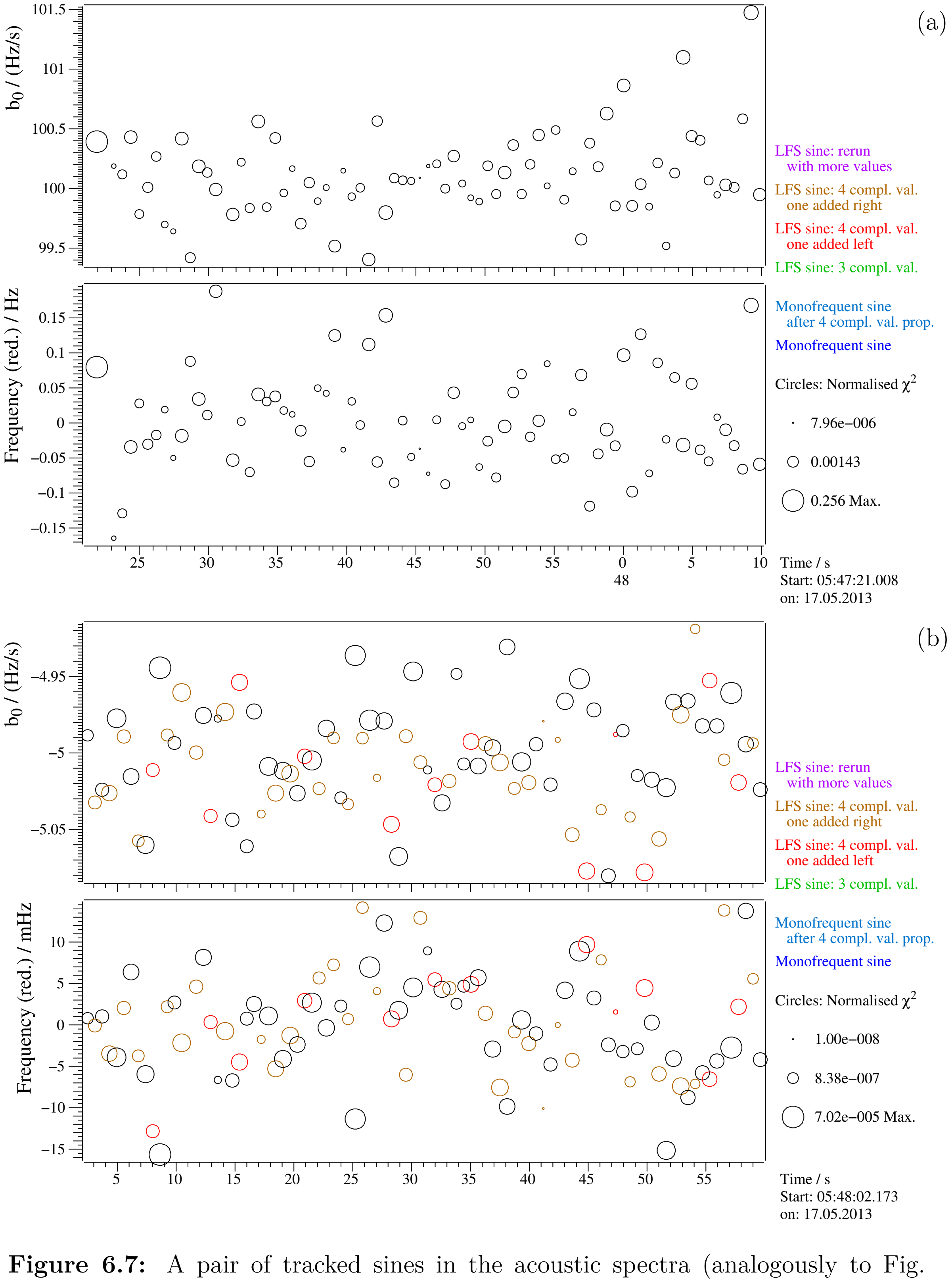

Figure 6.7: A pair of tracked sines in the acoustic spectra (analogously to Fig. 6.4), each with a plot of the fitted b_0 and one with the mean frequency after a linear progression is assumed and subtracted. The line equations are: (a): $100.04\,\mathrm{Hz/s}\cdot t + 34.32\,\mathrm{Hz}$. (b): $-5.0018\,\mathrm{Hz/s}\cdot t + 1{,}742.73\,\mathrm{Hz}$. The smaller the circle, the better the fit. For broad peaks the number of fitted values n_{Fit} is greater than 4, meaning that exclusively the $\mathrm{F}_{\mathrm{Sum}}$ approach is used, therefore only black circles are present in (a).

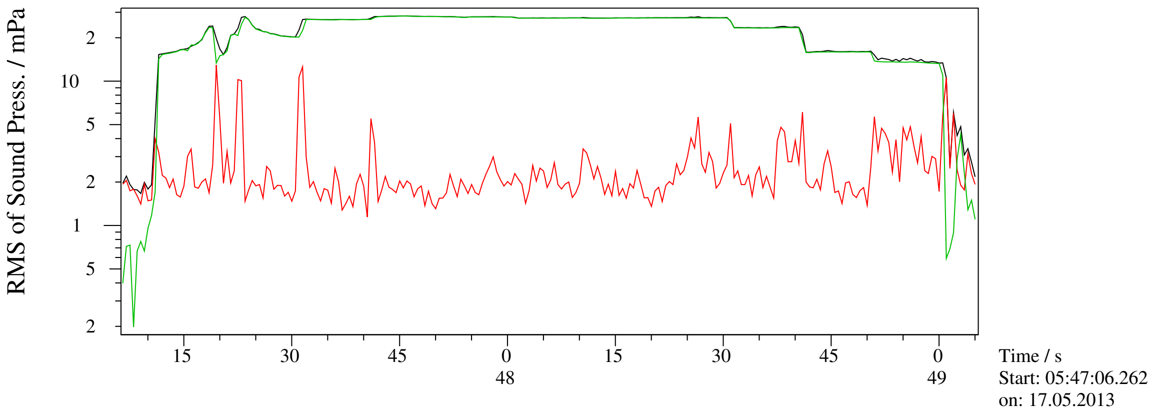

Figure 6.8: Time course of RMS values calculated from 0.5 s data intervals. During the sweeps the mean RMS value is reduced to the level of times with background noise only (first and last seconds in the shown interval). The spectra in which a single sine begins or ends, and thus this sine is not subtracted, show up as peaks. Colour codes: black: original signal, green: subtracted signal, red: signal after subtraction.

6.8 shows the three progressions: the original data (black), the sum of the subtracted (LFS) sines (green, gained from the inverse FFT of Fig. 6.6 (a)) and the processed data (red, corresponding to Fig. 6.5 (b)). The original curve shows steps as (LFS) sines are switched on or off. In addition, in some parts, the black curve shows a complex behaviour, which is likely to demonstrate a consequence of the characteristic of the speaker: in the interval of approximately 05:47:12 - 05:47:18 sine #5 decreases in frequency from 1 kHz. The RMS value increases slightly but more than linearly: the speaker seems to produce lower frequencies with higher efficiency. A kind of notch follows: typically the generated power of speakers collapses for very low frequencies, depending on the membrane size. In the following interval, the sine frequency increases again, which mirrors the described behaviour. However, an abrupt and lasting increase in the RMS amplitude is visible at 05:47:22: this stems from the onset of sine #2 (160 Hz). For frequencies well above 1 kHz, the speaker characteristic seems to decrease very slowly. After 05:47:30 the steps in the RMS amplitude can be used to identify onsets and ends of additional (LFS) sines.

The red line illustrates that in regions where no switching takes place, the processed data is approximately on the same background level as the data before and after the sound file is played, that is the (LFS) sines have been completely removed. Spikes occur at regions where at least one sine is not satisfactorily subtracted because one (LFS) sine, when switched on or off, does not last over the full time interval of one spectrum; this is analysed in Section 6.2.2.4. In this example the simulated periodic disturbances have been removed very well and the RMS amplitude is reduced by approximately one order of magnitude.

6.2.2.3 Imperfect peak subtraction

Figure 6.9 (a) shows the lower 1,500 Hz of a single spectrum (the 46th, starting at 05:47:33.00). This time period is chosen because here the played sound file contained relatively low frequencies, allowing a plot with a good resolution on the ν axis. All the sines of the audio file are fitted successfully and subtracted accordingly. The broad peak centred at $1,325.059\,\mathrm{Hz}$ is subtracted with a $\chi_n^2 = 5.1 \cdot 10^{-4}$ which is three orders of magnitude below its threshold.

By visual inspection, one can question this fit result: Although a reduction of 1.5 orders of magnitude has been achieved, the red curve is not as low as the surrounding. Could it be possible that the values for the fit parameters are not the optimal ones? Could it be possible that the start values make the algorithm run into secondary minima while minimising χ^2? If it were possible to find a set of parameters that – by subtraction of the corresponding sine – reduces the remaining spectral power more strongly than the fit result does, it would indicate that the algorithm has run into a secondary minimum. In order to analyse this issue, the LFS-sine parameters are systematically varied, the corresponding sines are subtracted and the remaining power in the frequency interval dominated by the peak, in this case $1,281\,\mathrm{Hz} - 1,373\,\mathrm{Hz}$, is determined.

Firstly, a reasonable step length for each parameter needs to be estimated. Since $\mathrm{F}_{\mathrm{Sum}}$ is proportional to A_0, this parameter can be determined independently from the other parameters and is even left out in this case; the value used for A_0 is the fitted one.[34] The most influential parameter on the curve progression is b_0, as it defines the curve progression of the phase spectrum (Fig. 3.8). Finally, ν_0 defines the position of the peak (Sec. 3.2.3).

If the fit algorithm runs into secondary minima, a combination of the latter two mentioned parameters should be the reason. To get an overview about the dependency strengths, one can set three of the parameters to their fit results and only vary the remaining one, in order to evaluate the spectral power after subtraction of an LFS sine with this set of parameters. Intersections through the four dimensional space and the variation parameters are given in Figure 6.10. If the steps between the values are chosen densely enough, the resulting curve is smooth. One can designate the values at which a threshold for the mean spectral magnitude in the interval of interest is passed, in this case it is a threshold for the mean of the magnitude values in the mentioned frequency range; it is reached at 1.5 times of the value gained by the set of fitted parameters. Combined with the demand that at least at two steps the values should be below this threshold, a rough estimation for the maximum step length for the variation of this parameter is possible. Table 6.3 shows these step

---

[34] The sum of squared magnitudes of differences of complex spectral values is to be minimised. In polar coordinates, for fixed magnitudes, each single difference becomes the smaller, the better their phases match. Therefore, the magnitude values, proportional to A_0, can be treated independently from the other parameters.

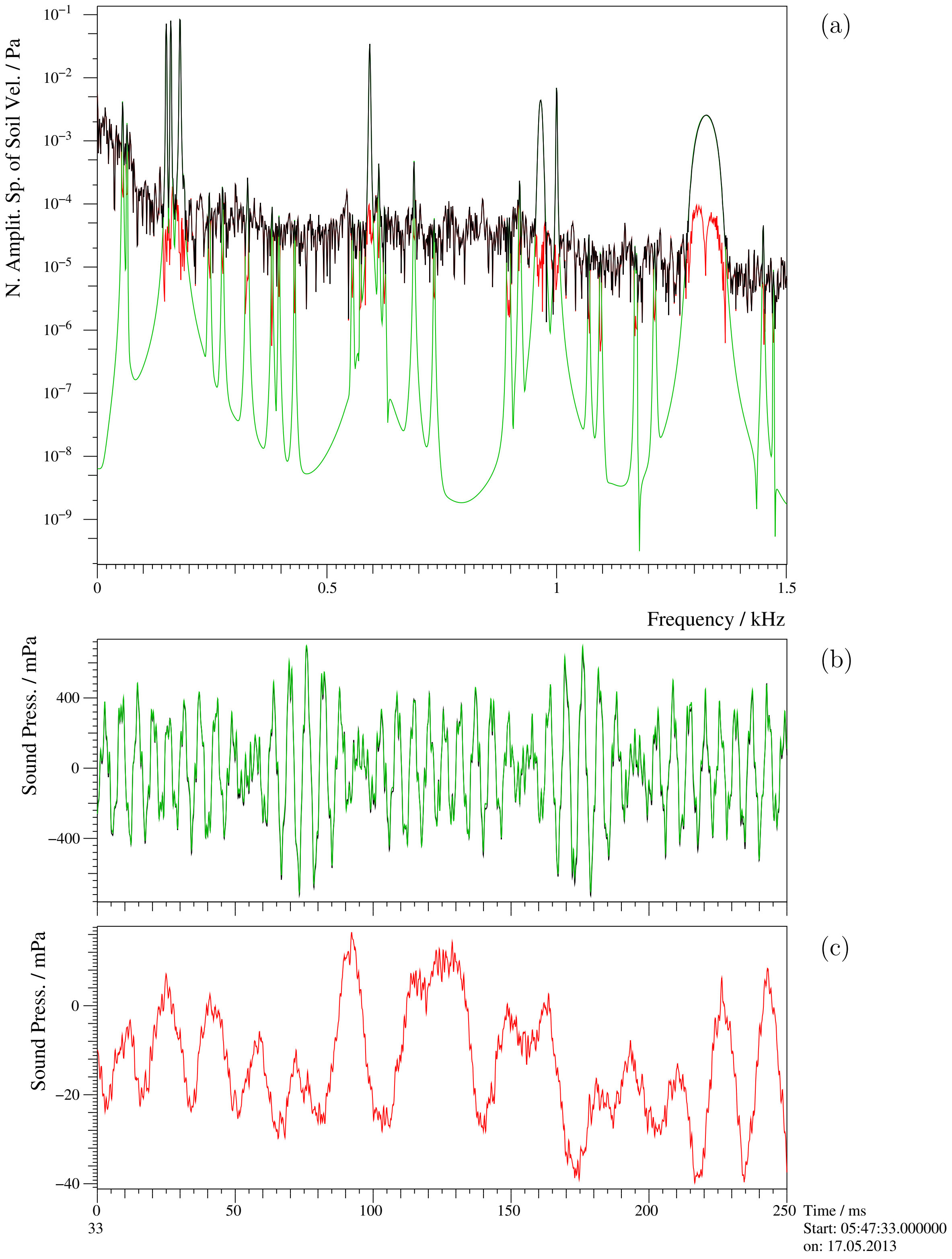

Figure 6.9: A typical small data interval of the acoustic measurement of the audio file. (a) shows a magnitude spectrum, (b) and (c) the time domain, the colour codes are: black: the original data, green: the subtracted signal, red: the result. In (b), the green line mostly masks the black one because the (LFS) sines are fitted very well.

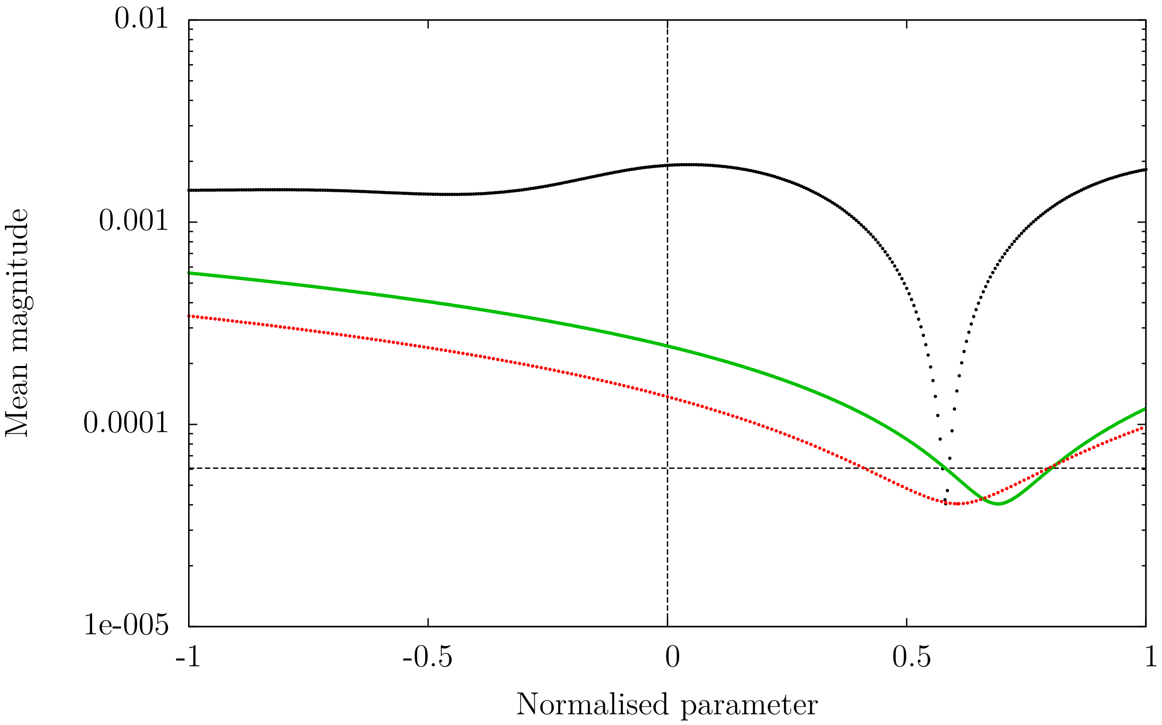

Parameter	Step length	Start	End	Fit result	Unit
$\Delta\nu$	0.01	1,283.0	1,285.0	1,284.1630	Hz
$\Delta\phi$	0.1	30.0	41.0	36.6659	°
Δb_0	0.001	99.5	100.0	99.8435	Hz/s

Figure 6.10: Intersections through the four-dimensional parameter space tested: three parameters are fixed at the fit optimums, one is varied: black: ν_0, green: b_0, red: ϕ_0. The step length and the start and end values are given in the table. Additionally, for each variation the exact fit result for the respective parameter is included, ensuring that the best result of the fit algorithm is part of every curve. The ordinate contains the mean magnitude value (of the spectral range: $1{,}281\,\mathrm{Hz} - 1{,}373\,\mathrm{Hz}$) after the subtraction of an LFS sine with the current set of parameters. In order to allow a combined graphic, the abscissa is normalised: between zero and one the range given by the start and end values is displayed. The curves are extended to the left by the same range (abscissa values -1 to 0) to demonstrate how the curves continue – especially in the case of b_0, where the values at the regular margins become constant or even decrease again; this plot demonstrates that no similar minimum is close. The horizontal line is at 1.5 times the value produced by the set of fitted parameters; it is used to determine a minimum step size for each of the three parameters (Tab. 6.3).

Parameter	Fit result	Step length	Start	End	Unit	No. steps
ΔA_0	0.025499	-	-	-	Pa	1
$\Delta\nu$	$1,284.1630$	0.04	$1,282.0$	$1,286.0$	Hz	102
$\Delta\phi$	36.6659	4.0	0.0	356.0	°	90
Δb_0	99.8435	0.1	99.7	100.3	$^{\mathrm{Hz}}/_{\mathrm{s}}$	8

Table 6.3: Combination information to subtract the broad peak in Figure 6.9 (a) without fitting. The values of the fit result are appended to the lists of values that are to be combined.

lengths, the parameter intervals and additionally the original fit results.

With given step lengths, the parameter intervals are critical because having long intervals strongly increases the number of combinations. Although the input is known (it is the sound file), this information can only be used partly – the precision of the hardware and software responsible for playing the file is unknown, therefore the current frequency can only be estimated and the phase is probably indeterminable at all. But, as the b_0 parameter should be constant in time, it can be strongly limited (Fig. 6.7 (a) shows that b_0 is fairly constant). ϕ_0 should include its complete range. ν_0 remains as a slightly unclear parameter, therefore the most values are used for this one.[35]

The mean magnitudes of a total of $73,440$ combinations are compared: The set of parameters, reducing the power best in this frequency interval, is exactly the fitted one. The only potential explanation I have for this result – that the best-fitting theoretical curve does not fully coincide with the real peak – is a slight frequency dependency of the transfer function between the sound file on the computer and the measured data that becomes the more relevant the higher $|b_{0,r}|$ is. A precise LFS sine is input to the sound card – but it seems to be changed after re-recording.[36] This does not seem to be a problem of the fit algorithm.

6.2.2.4 Abruptly ending (LFS) sines

Figure 6.11 illustrates the effect of hard transitions between presence and absence of signals. The spectrum (a) presents two broad peaks stemming from the convolution of the (LFS) sines with the DFT of the rectangle limiting the periodic signal to the time before (approx.) 05:49:01.[37] These cannot be handled by the fitting algorithm: fits finish

---

[35] If it should be the case, that the best set of parameters is not covered in this analysis, it is probably beyond the limits of the ν_0 parameter even though there is no indication if one plots or sorts the combination results.

[36] Where in the chain DAC – amplifier – speaker – sensor – ADC the distortion occurs is unclear. In Section 6.2.2.2 it was noted that the amplitude of the speaker decreases with increasing frequencies. This of course deforms the shape of the peak, distorts its symmetry and is likely to reduce the fit quality. However, this has not yet been analysed and is beyond the scope of this work.

[37] Sine #1 is visible in both spectra: Fig. 6.11 (a), where it is broadened by the convolution with an additional sinc function (additionally to the limiting the time interval for the spectrum), and Fig. 6.9 (a), where the peak is narrow as typical for monofrequent sines.

with a high χ_n^2, so the peaks remain in the signal.[38]

In the preceding spectra of the sequence all (LFS) sine signals are subtracted. In the following spectrum this signal is no longer present. Thus after inverse transformation to the time domain one expects a short interval in which the sweep signal is still present. This is shown in Figures (b) and (c). The ramp is a result of the linear fading of spectra after inverse transformation (Sec. 6.1.1.4). One can also observe that the time domain looks similar at both margins indicating that the (LFS) sines are subtracted without obvious changes of the data. Intervals like this cause the RMS values (Fig. 6.8) to show peaks.

---

[38] The $\chi_n^2/\chi_{\text{Thres}}^2(n_{\text{Fit}})$ ratios for the ending (LFS) sines are: sine #1: 7.02, sine #6: 6.30, sine #7: 1.29.

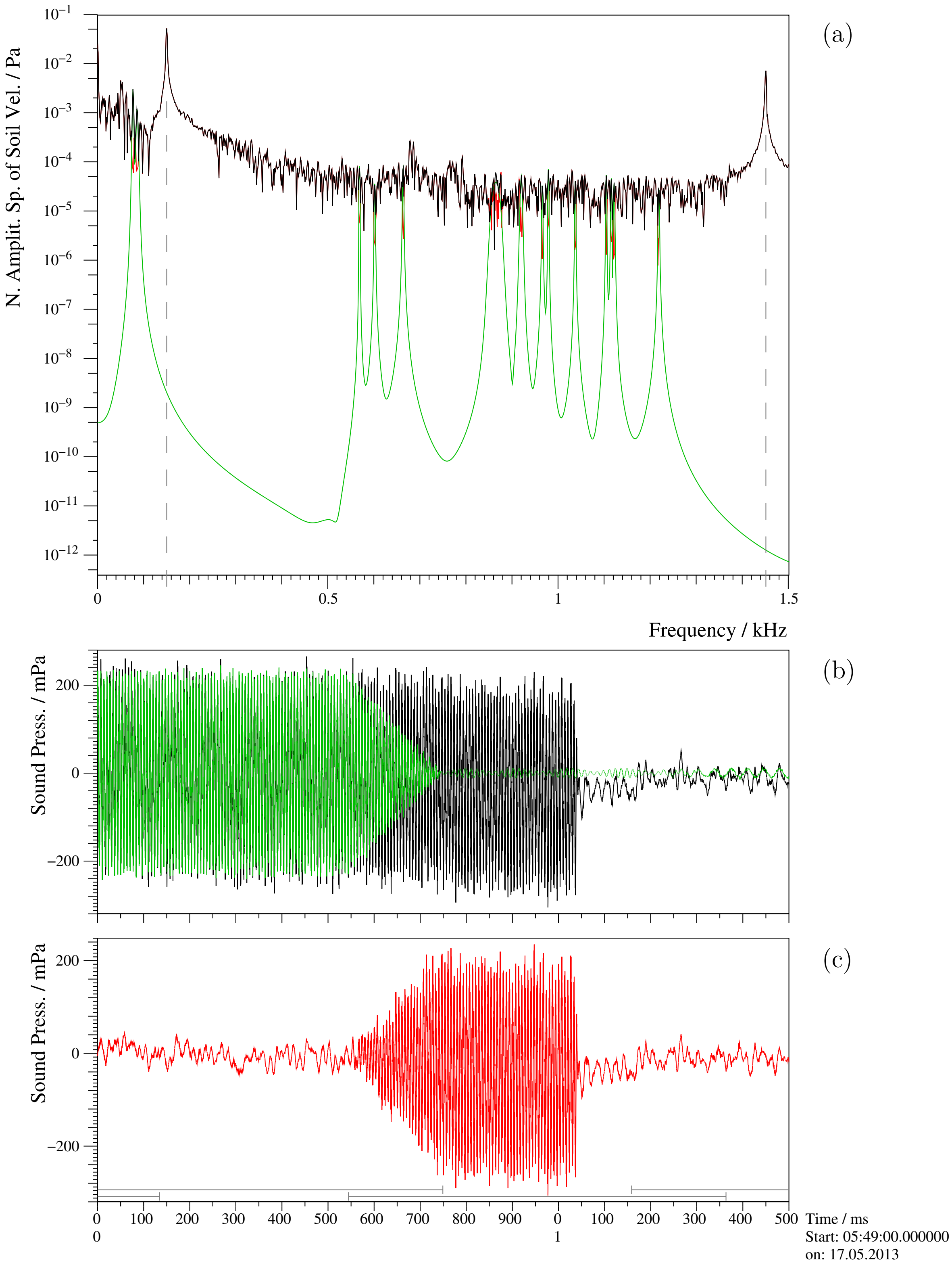

Figure 6.11: An analoguous structure but different time than in Figure 6.9: In this time interval three sines end simultaneously (at 150 Hz, 1,451 Hz and 2,697 Hz (not visible)). (b) and (c) show the transients between spectra in the time domain (grey bars indicate the intervals of single, overlapping spectra). At around 05:49:00.57 the inversely transformed data of the spectrum shown in (a) – in which all three sines are not subtracted (see also: Fig. 6.6 (a)) – fade in. Again the colour codes are: black: the original data, green: the sum of the subtracted sines, red: the result.

6.3 Single-engine propeller aircraft

One expects nuclear test explosions to be conducted in very rural areas with limited infrastructure. Main sources of anthropogenic noise could be: Traffic on through roads, aeroplanes and quarry blasts (the latter even for distances of hundreds of kilometres and probably far outside of the inspected area).[39] If an explosion should be conducted clandestinely, provisions could have been made. Related to this work, these could include construction or earth-moving sites and increased traffic of all kinds. Additional sources of noise might stem from the inspectors themselves: an area of up to 1,000 km^2 is to be covered with sensors which have to be set up and maintained on a daily basis. For these purposes off-road vehicles will be operated. Furthermore, different kinds of flights will be undertaken by helicopters and small aircraft e.g. for visual inspections of the destination area or airborne gamma spectroscopy and aeromagnetic field mapping [42].

Typically, small surveillance aircraft are propeller driven, producing primarily periodic noise; the same holds for helicopters. In this example the overflight of a single-engine propeller aircraft is processed.[40]

The signal was measured on the 16th of May 2013 at 10:56 UTC south-east of the airport Münster-Osnabrück,[41] Germany, with a Brüel & Kjær 4198 microphone.[42] The aircraft is a `PIPER PA-28R-180 Cherokee Arrow` [43] at an altitude of about 300 m.

Figure 6.12 gives an overview of the data and their processing results. First of all: These data seem to have strong contributions of low frequencies, showing up in the sequences as an irregular bright line for the smallest frequencies.[43] Most probably, gusting winds with fluctuations slower than $1\,\Delta\nu$ are responsible for the low-frequency contributions. Since the fitting procedure can handle any frequency without exceptions, even the direct current (DC) value could be fitted and subtracted. However, the start-value-estimation procedure is not capable of handling this case. Firstly, for small frequencies the problem becomes similar to the one of neighbouring sines because the peak at negative frequencies merges into the one at positive frequencies. Secondly, for very small frequencies (and in particular the DC value) the procedure would estimate wrong peak widths because it does not wrap to the other side of the data array (to negative frequencies), ending the peak

---

[39] Quarry blasts or the like produce pulsed signals whose shape can be similar to those of aftershock signals. The typical approach is to locate their origin and discard the corresponding time intervals from further investigations if the origin lies outside of the area of interest.

[40] Multiple-engine propeller aircraft have rotors with similar but typically most of the time slightly different revolution rates. Their signals could be used to analyse double peaks for instance – as this feature is not yet included, a single-engine propeller aircraft is chosen intentionally.

[41] IATA airport code: `FMO`, GPS coordinates of the measurement site: latitude: 52° 7′ 16″ N, longitude: 7° 36′ 16″ E, altitude: 105.8 m, located approximately 4 km from the end of and in line with the runway so aircraft passed nearly vertically above the sensors.

[42] Membrane height above ground: 6.5 cm. In this measurement, this sensor is connected to channel #32 of a 4-box combination of `Data Translation DT 9841` ADCs with: home-built amplifiers, sampling frequency 10 kHz, cut-off frequency 3 kHz.

[43] The microphone is specially suited for outdoor applications and low-frequency measurements.

at the first index (= 0 Hz). Such a peak is discarded from processing if the magnitude of the 0-Hz value is not smaller than 50 % of the maximal one. In particular, a DC peak will be discarded. If low-frequency peaks are successfully fitted and subtracted here, it means that the peak was centred at $1\,\Delta\nu$ at the very least. For these reasons most of the lowest-frequency peaks are not subtracted (best visible in the missing bright dots at the lower margin of the theoretical spectrogram in (b)). Their high magnitudes also explain the rare times with strong RMS-value reduction respectively the very low reduction at all other times (c).

Figure 6.13 shows details of one of the few cases when a peak at low frequencies is subtracted.[44] One harmonic series is marked – in all probability it belongs to the revolution rate of the propeller – here, peaks with an even index tend to be stronger. This indicates that a nearly symmetric state is reached in half of the time of one revolution, indicating that this aircraft is equipped with a two-blade propeller. Most of the strong peaks of the rotor series are subtracted, the remaining ones are low in magnitude or show an unusual shape.[45] (b) and (c) illustrate that most of the signal (including the strong, low-frequency variation) is subtracted.

---

[44] Fit details: After 46 iterations, the mean frequency is 1.77 Hz, $b_0 = 5.54\,\mathrm{Hz/s}$, $\chi^2_n = 1.64 \cdot 10^{-3}$ at $\chi^2_{\mathrm{Thres}}(n_{\mathrm{Fit}} = 4) = 8.61 \cdot 10^{-3}$.

[45] The peak at 328 Hz (multiple 18 of the fundamental frequency of 18.26 Hz) has two shoulders which could indicate that there are closely neighbouring sines (the higher one at 1/5 of maximum could have influenced the peak shape). The shape is also unusual for the peak at 438 Hz: it is too narrow at the top to be fitted successfully – even a monofrequent sine has three to four strong values caused by the convolution with the spectrum of the Hann window (Sec. 2.3.3 and 3.2.2); in addition, it seems too broad at its flanks.

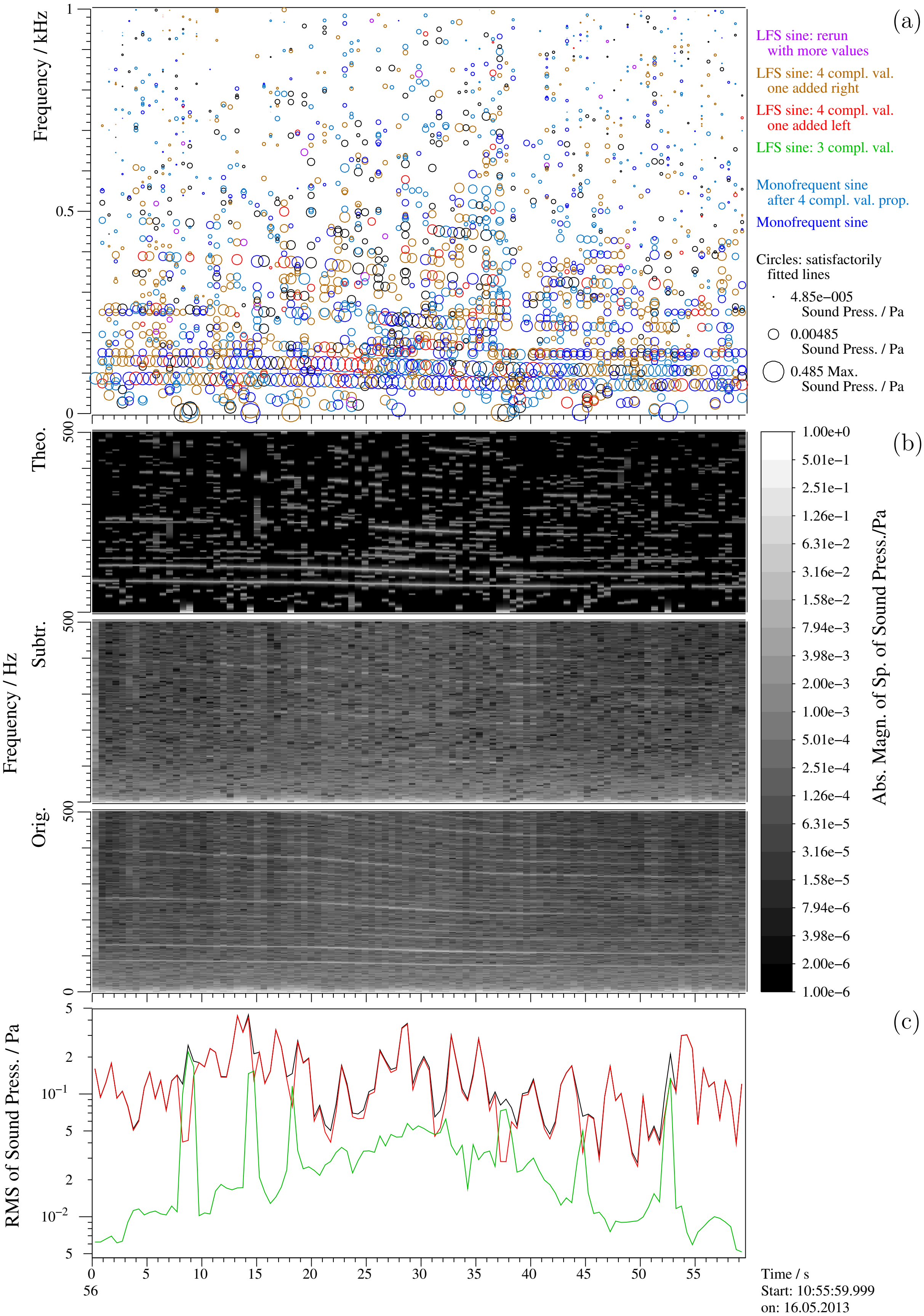

Figure 6.12: Evaluation of a propeller aircraft. The subplots are analogous to the former examples: (a) includes the subtracted peaks, (b) the three sequences of spectra: sum of subtracted sines, processed and original, (c) the corresponding RMS values (black: Original data, red: sum of subtracted sines, green: processed data).

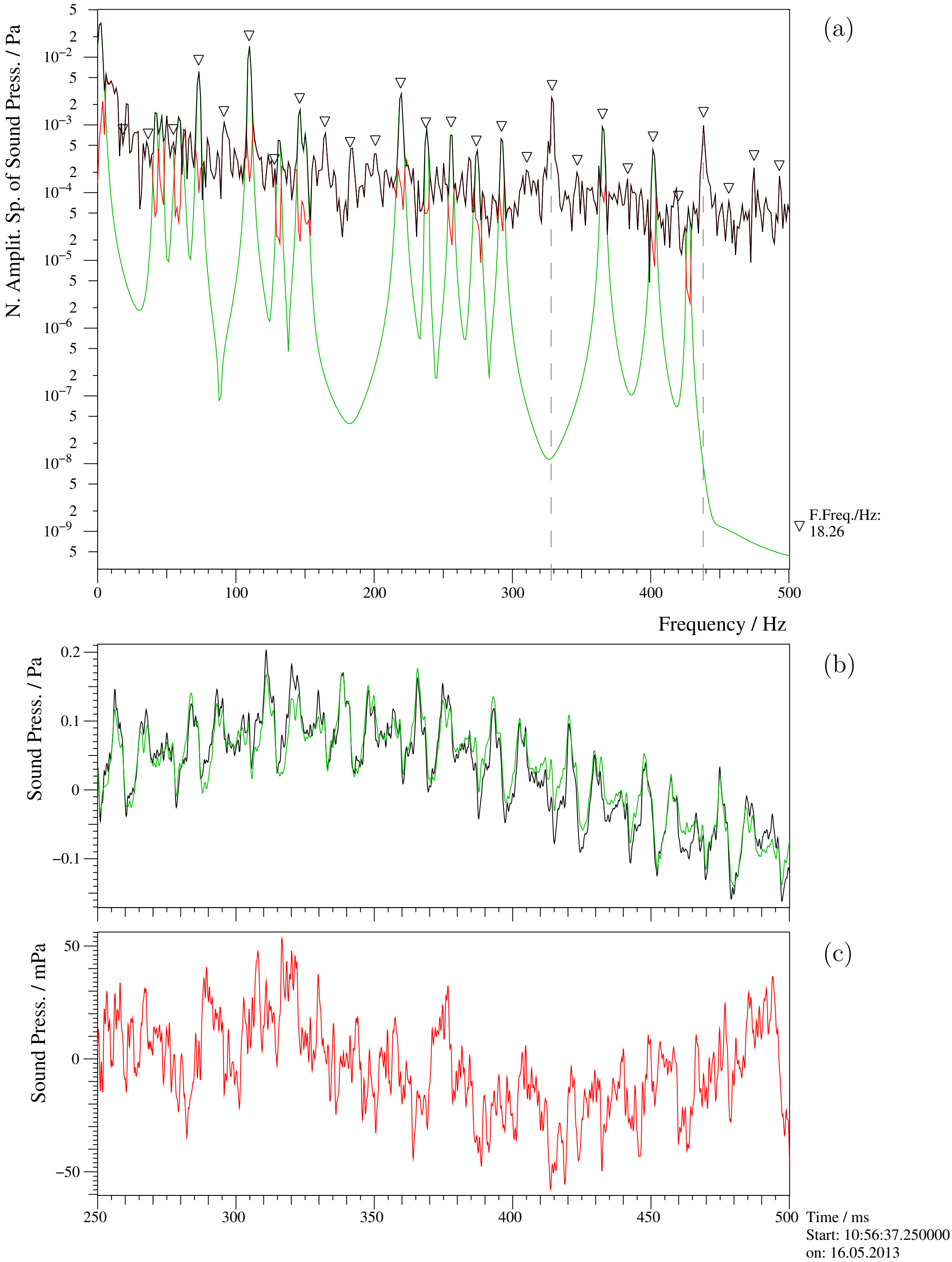

Figure 6.13: The data of a short time interval of Figure 6.12 at 10:56:37.25. (a) shows the lower frequencies of the 62th spectrum with one marked harmonic series, note the low-frequency fit centred at 1.77 Hz. The peaks mentioned in the main text (328 Hz and 438 Hz) are marked with vertical dashed lines. (b) and (c) present a small interval of the time domain. Colour codes: black: original data, green: sum of subtracted sines, red: processed data.

6.4 Main battle tank

We fortunately have access to seismic and acoustic data of passing military vehicles. These data had been measured between 1989 and 2001 by the Bochum Verification Project (BVP) which is continued as the Group Physics and Disarmament at TU Dortmund in which this work has been done. Ground vehicle noise and vibration are a second source of disturbing signals expectable during OSI. In particular on military ground tracked vehicles may be used. Compared to wheeled vehicles, tracked ones have an additional strong source of periodic noise: Beside the engine in general, the interlocking of the driven cogwheels into the track produces a second fundamental frequency and harmonics. And the rolling of the wheels over the track elements with corresponding variable forces to the ground produces seismic vibration at these frequencies directly.[46]

In Amersfoort (1992) the BVP together with several partner scientists from NATO and WTO countries measured the seismic and acoustic emissions of military vehicles. Here, an example of a `Leopard-1` tank driving with 11.161 m/s on a straight road (paved with smooth asphalt) is analysed at a distance of 11.78 m from the designated middle of the lane.[47] The acoustic spectra consist mainly of two fundamental frequencies and their respective harmonics, stemming from the exhaust and the track-drive. 4,096 samples corresponding to 0.5622 s are used for each spectrum as a compromise between spectral and time resolution.

Figure 6.14 gives an overview about the complete time interval that is analysed: (a) shows the (LFS) sines that are subtracted. One can see that the amplitudes are highest around 11:58:19. At this time the tank had passed the sensor. This matches the visible change of the Doppler shift: The horizontal lines progress like an negated arctangent, caused by the source during its linear trajectory moving towards, passing and moving away from the sensor. Since the tank signals are strongest at low frequencies and for the sake of clarity (b) shows the lower 500 Hz of the sequences of the spectra: before (bottom) and after subtraction (middle) of sines. Like before, the theoretical spectrum (top row) is the sum of the subtracted sines and the sum of the two top spectra is equal to the bottom one. (c) demonstrates the RMS values as a measure of the power in the data. Two times are marked by vertical lines: Here the factor for the reduction of power by sine subtraction is minimal and maximal, respectively. The sequence of theoretical spectra (b, top) is especially suitable for understanding the curve progression of the RMS values. When the former has many bright dots, much power is subtracted. The spectrum marked first (at 11:58:17.8) contains some of the strongest peaks even after the subtraction of sines,

---

[46] Wheeled vehicles can also produce a second series of peaks caused by a coarse the tyre profile, but with much lower amplitude [44], [23].

[47] The experiment is described and evaluated with regard to vehicle classification in [44]. File: `AME10215.DA6`, Microphone `BK3`, `Brüel & Kjæer 4188`, with preamplifier `2639`, height above ground: 20 cm, channel #13 ADC `Microstar DAP 2400/5`, sampling frequency 7,286 Hz, cut-off frequency 300 Hz.

$\nu_{\text{Mean}}/\text{Hz}$	$A_0/(\text{m}/\text{s})$	ν_0/Hz	$b_0/(\text{Hz}/\text{s})$	ϕ_0/rad	χ^2_n	χ^2_{Thres}	n_{Fit}	No. iterations
19.31	0.0346	10.46	31.47	3.275	0.025	0.029	6	70
217.24	0.0977	190.68	94.48	3.840	0.089	0.094	12	100

Table 6.4: Fit details for the two broad peaks visible in Figure 6.16 (a). Both peaks are close to rejection (χ^2_n close to their thresholds).

the spectrum and the corresponding time-domain interval are given in Figure 6.15. The spectrum with the strongest decrease of energy (at 11:58:22.75) is not the one with the most subtracted peaks but here most of the strongest peaks are subtracted (Fig. 6.16). This one is also interesting because of the subtraction of two broader peaks.[48] Based on the source of the signal one would not expect strong changes in the frequency, therefore both of these two peaks can be categorised as wrong positives; their fit results are given in Table 6.4.

Figure 6.17 tracks a single peak: whereas the change of Doppler shift is evident in the ν_0 plot, on the basis of b_0 the change of Doppler shift is not apparently visible. At the correct time two adjacent negative values indicate the right behaviour, but later on the spreading of the values is in the same order of magnitude. For the two picks, a consistency check is conducted: the LFS parameter are estimated by the differences between peak frequencies and the time between the two. The results are: $-2.18\,\text{Hs}/\text{s}$ and $-3.52\,\text{Hs}/\text{s}$; the corresponding values shown in the top figure are: $b_0 = -2.43\,\text{Hs}/\text{s}$ and $b_0 = -6.57\,\text{Hs}/\text{s}$.[49] This matches as roughly as the other b_0 values spread. For a comprehensive evaluation not enough values are available. The last set of parameters in the plots is probably wrongly picked, a gap should have been chosen instead.

Most of the strong peaks in the spectra are subtracted successfully but also many remain. Superpositions of harmonics of the two series occur which are likely to form peaks that cannot be separated and fitted with the expression for a single sine. Especially, the spectrum shown in Figure 6.15 contains peaks with no obvious distortion while having a strong magnitude. During this time, the tank is close to the sensor and the superposition conditions of different sources change most strongly. One can speculate whether this could be caused by the superposition of sources with the same frequency – this tank has two tracks and two exhausts. Changing the position of the tank changes the differences of lengths of the propagation paths between the sources and the sensor.

---

[48] Taking a very close look at the column of this spectrum (Fig. 6.14) shows the abnormal broadness of the two peaks.

[49] E.g. the difference between the red circles (11:58:18.5) is $-1.23\,\text{Hz}/\text{T}$, $T = 4{,}096/7{,}286\,\text{Hz}$, therefore it is $-2.18\,\text{Hs}/\text{s}$.

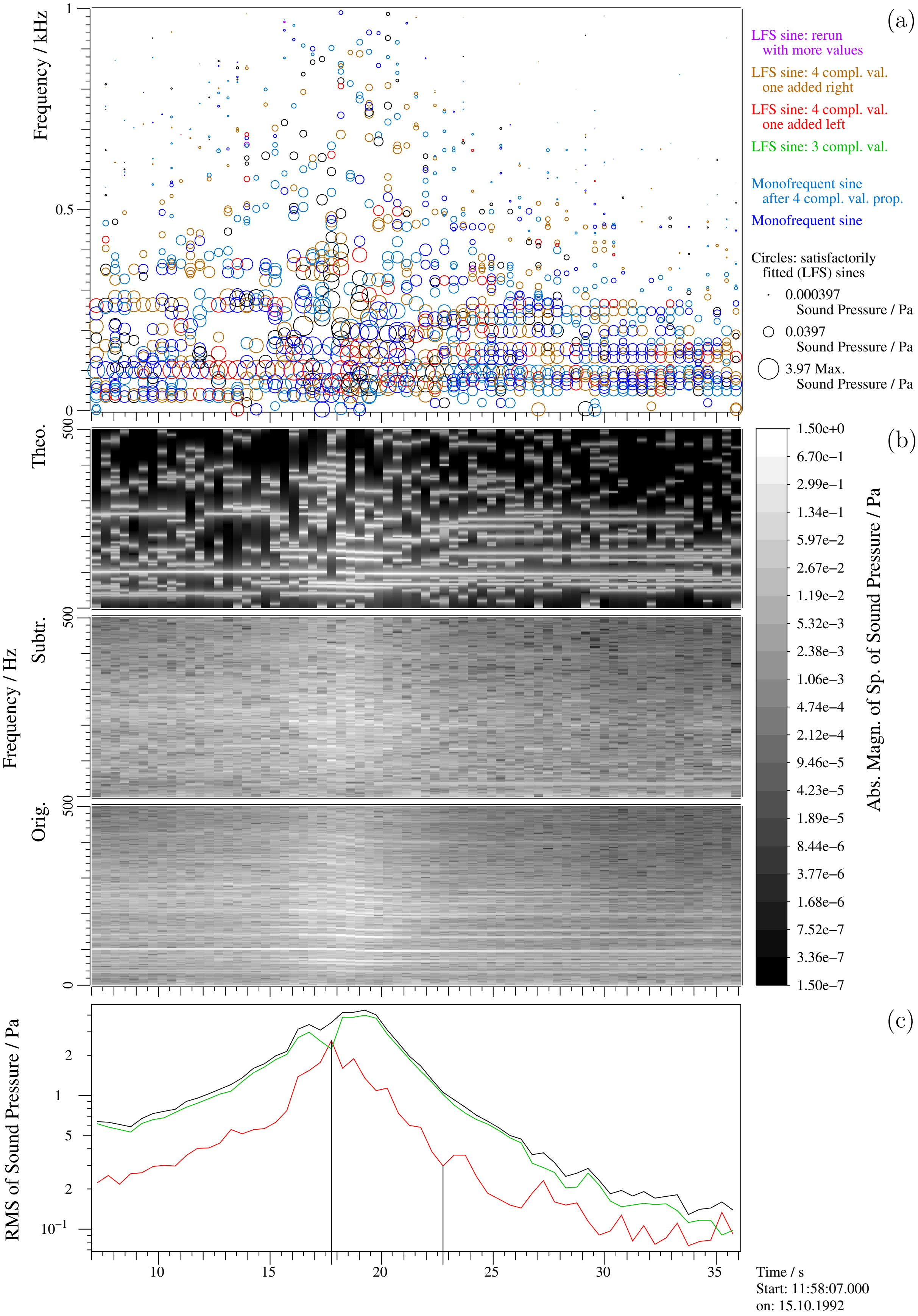

Figure 6.14: Evaluation of a tank passing a sensor. The subplots are analogous to the former examples: (a) includes the subtracted peaks, (b) the three sequences of spectra: sum of subtracted sines, processed and original, (c) the corresponding RMS values (black: original data, red: sum of subtracted sines, green: processed data).

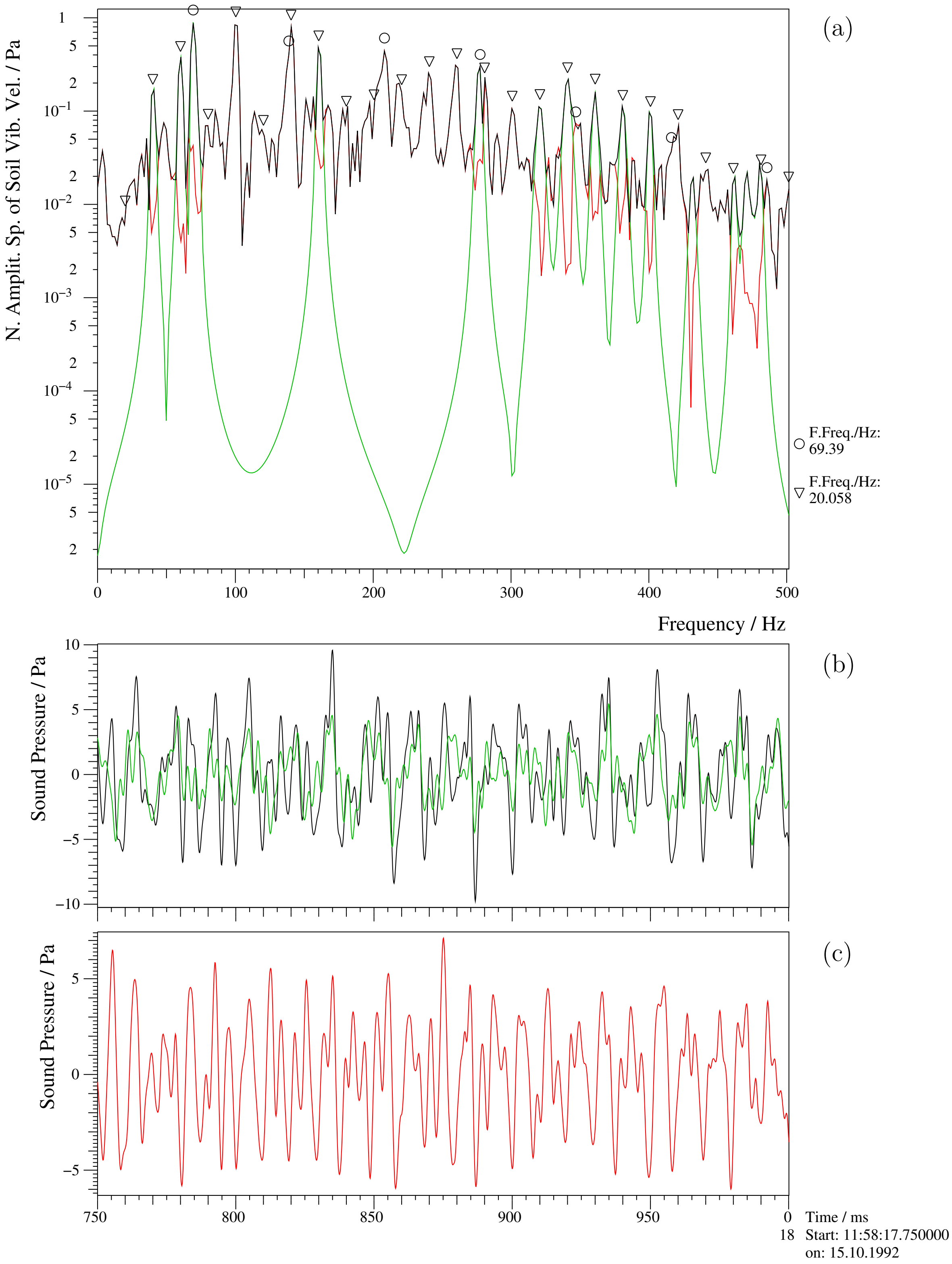

Figure 6.15: Example for a spectrum and the reconstructed time interval with the lowest reduction of energy (see Fig. 6.14 (c), at 17.75 s). (a): spectrum, (b): time domain of the original signal (black) and the sum of subtracted ones (green). (c): the remaining signal (red).

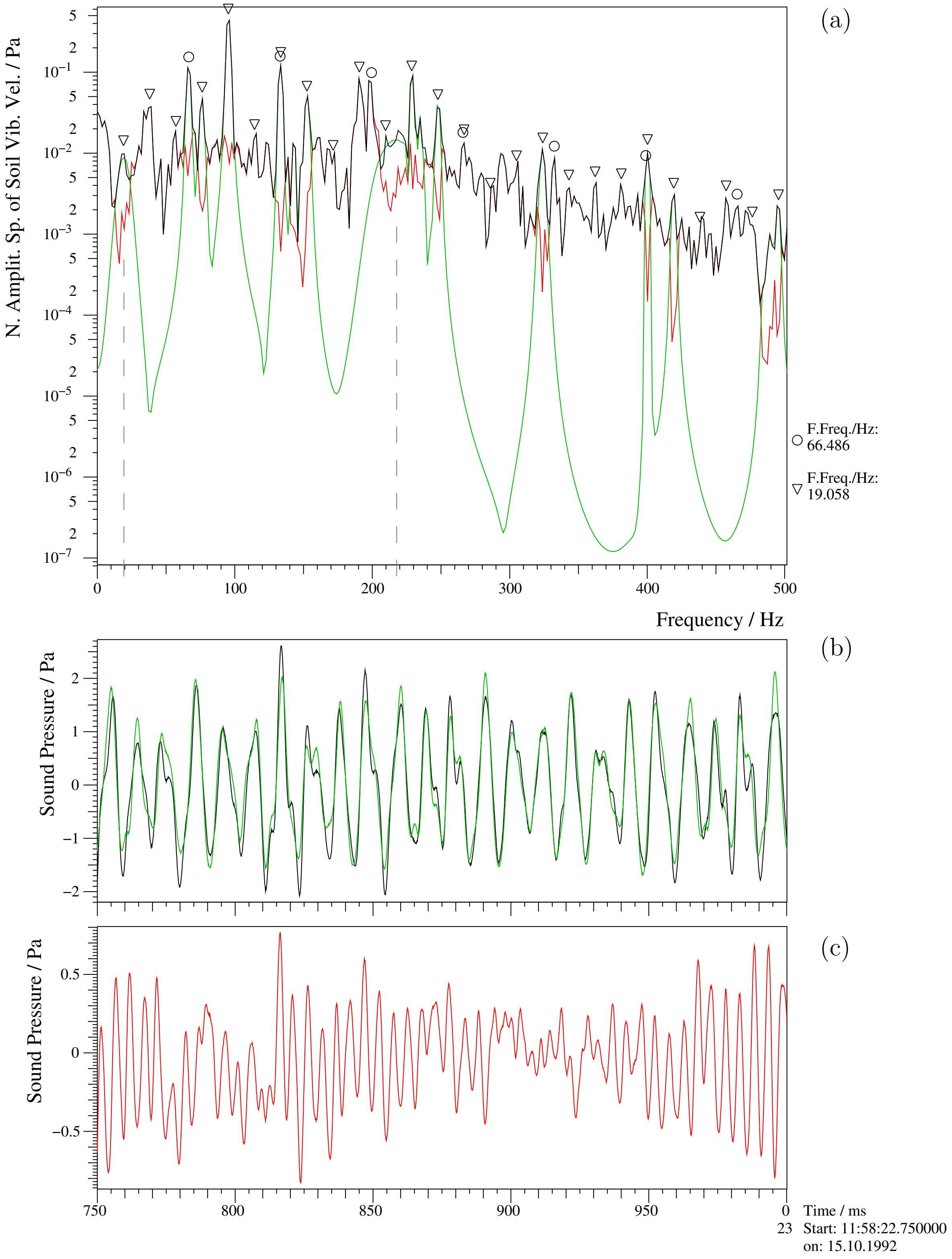

Figure 6.16: Another example for a spectrum and the reconstructed time interval (similar to Figure 6.15) with the strongest reduction of energy (see Fig. 6.14 (c), at 23.75 s). Colours as in Fig. 6.15. In (a), two exceedingly broad peaks are marked with dashed lines.

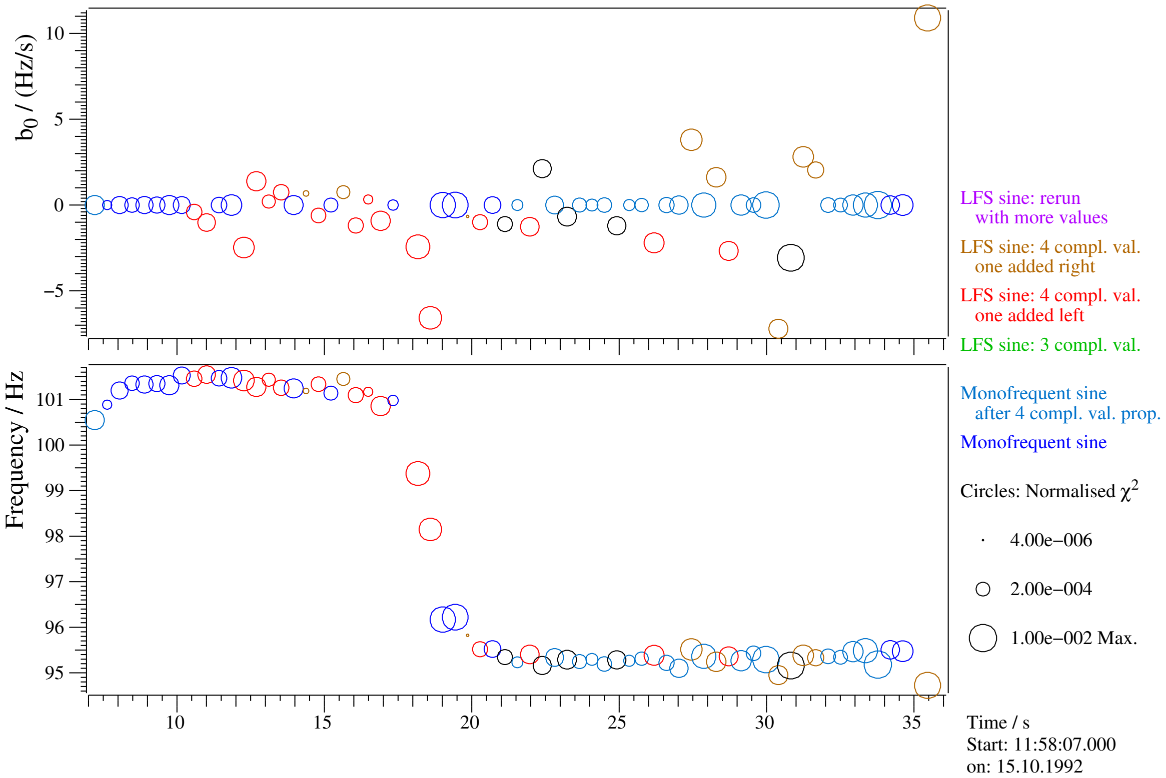

Figure 6.17: Similar to the sound file evaluation, a single peak is tracked. Top: b_0, bottom: Mean frequency. If no peak is found that is likely to belong to this tracked sequence or if the fit failed, there is no circle for the corresponding time.

6.5 Helicopters

During the last years we measured several helicopter signals.[50] Their spectra consist mainly of two strong harmonic series of sinusoids, stemming from the main and the tail rotor, respectively. At the beginning we thought that these two strong series make these signals ideal for performing periodic-noise suppression. This section introduces the challenge: The single peaks seem to be different from the ones of pure sinusoids producing worse fit results than for example the propeller aircraft. For the 5% false positives rate used in this chapter, the majority of fits fails at the corresponding threshold for χ_n^2. If one allows their subtraction anyway, the result serves its purpose and the peak is reduced significantly. An increase of the false-positive rate could reduce the periodic content successfully, but the impact on the underlying signals is unknown. This should be the subject of future research. An interesting question is: What are these peaks based upon? One example serves as a demonstration of the issue; this one is chosen because of a well observable course of events. Figure 6.18 gives an overview about data and the fit results of a helicopter mainly standing on its pad in approximately 20 m distance to the

---

[50] Published results of the processing of another helicopter signal can be found in [45]. The F$_{\text{Mono}}$ expression was applied exclusively. In order to get mainly successful fits even in times of frequency shifts, less data samples per seismic spectrum ($N = 1{,}024$) were used, resulting in blurred neighbouring peaks which remained in the spectra consequently.

sensor.[51] At around 11:44:57 the operation-revolution rate of the rotors is reached and the state remains stationary until it takes off at around 11:45:40. Subsequently, it climbs with increasing distance to the microphone close to the ground and thus frequencies are down-shifted.

The single spectrum in Figure 6.19 covers approximately 0.8 s at a time when the signal should be stationary. Nonetheless, at least two series of sines can be identified with very similar fundamental frequencies. Within the first harmonics, two respective frequencies are still close enough that the summed-up peak can be fitted by an LFS or a monofrequent sine within the threshold for χ^2_n. The more the frequencies split up, the more the peak shape changes and the worse the fit result becomes. If the signal consisted mainly of these two series, at some point the frequencies would diverge enough to fit them separately. But in these data, the spectrum at high frequencies fades into an unsteadily spiky, relatively flat progression (b). Concluding, spectra like these cannot be treated by the algorithm in its current form.

6.5.1 A brief first analysis

The investigation of these signals is beyond the scope of this work, however it may be interesting to understand how they are produced.

Typically helicopters have two strong series of sines, produced by the main and the tail rotor. Helpful is a typical revolution rate and the ratio between the two. For this type of helicopter at 100% the main rotor does 395 rpm (6.58 Hz) while the tail rotor does 3,584 rpm (59.7 Hz, marked in the spectra by red bars) [47]. Assuming that the main rotor blades are fully identical, theoretically, the fundamental frequency should be at four times the rotor revolution rate: $\nu_{\mathrm{main}} = 26.33\,\mathrm{Hz}$. Since the sequence of spectra (Fig. 6.18 (a)) shows intervals with literally no changes, longer (than the 0.8192 s for a single spectrum) time intervals can be used to generate high-resolution spectra: increasing the number of samples per FFT increases the spectral resolution, while averaging magnitude spectra statistically reduces the noise stemming from non-periodic contributions. Figure 6.20 is calculated with $N = 32,768$ samples and three averaged magnitude spectra overlapping by 50 % (the interval used is marked by a red bar in Figure 6.18 (a)). In (a) the revolution rate is marked ($^1/_4$ of the rotor blade frequency), the strong ratio of magnitudes between both indicate the high symmetry of the blades. The peaks produced by the main rotor broaden with increasing frequency. (b) shows the same spectrum but up to higher frequencies: the power of the single harmonics contribute to broader frequency bands, decreasing their

---

[51] Rescue helicopter `EC 135 D-HOFF` alias `Christoph 8`. Measured during an experiment mainly conducted to evaluate the coupling of acoustic signals to the ground. A description of the site and the measurements is given in [46]. UTC is used. Sensor: `Sennheiser KE-4-211-2` microphone, sampling frequency 10 kHz, sensitivity 10 $^{\mathrm{mV}}/_{\mathrm{Pa}}$, frequency range 20 Hz – 20 kHz, cut-off frequency 3 kHz. It is placed on the surface and assigned to channel #21 of a 3-box combination of `Data Translation DT 9841` ADCs.

magnitude. This is consistent with the visual observation in the sequence (Fig. 6.18 (a)) and the two series marked in black in Figure 6.19 and explains the fit results.

The `fenestron` tail rotor has irregular angles between its blades, so the fundamental frequency should be the same as the revolution rate. A corresponding series with low magnitude is marked in the spectra at multiples of roughly 60 Hz. Interestingly the tail rotor signal seems to be observable for a longer duration after the take-off indicating a strongly different directional characteristic. Additionally every second harmonic is stronger and the eighth is strong in particular. During this time, the fitting works better, although it is unclear if this is a result of the disappearance of the other lines or of the changed noise emission angle during the flight.

One can speculate about the reasons for two strong series with very similar frequencies. If both have the same stationary origin, they cannot be produced by the rotation of the blades.[52] If the double peaks result from the Doppler effect, a different source of their sounds must be assumed.[53]

---

[52] One could think of a locally moving medium with a different effective speed of sound compared to the system in which the measurement takes place. Since the sound is measured from the side, there are blades moving towards the sensor while others move away (and some pass orthogonally, without Doppler shift). However, the same number of blade-passes per time occurs at both sides, so the produced frequencies must be the same.

[53] Assuming the blades themselves would produce noise with a certain frequency (e.g. by vibration), this frequency could be changed by the Doppler effect produced by rotation for both directions – and for the continuous region in between. Besides, this additional source should produce another series of sines, since the revolution rate remains. It should be unlikely that these frequencies are very slightly different to integer multiples of each other what is observed here (the swashplate is no reasonable explanation as it should work with the same revolution frequency).

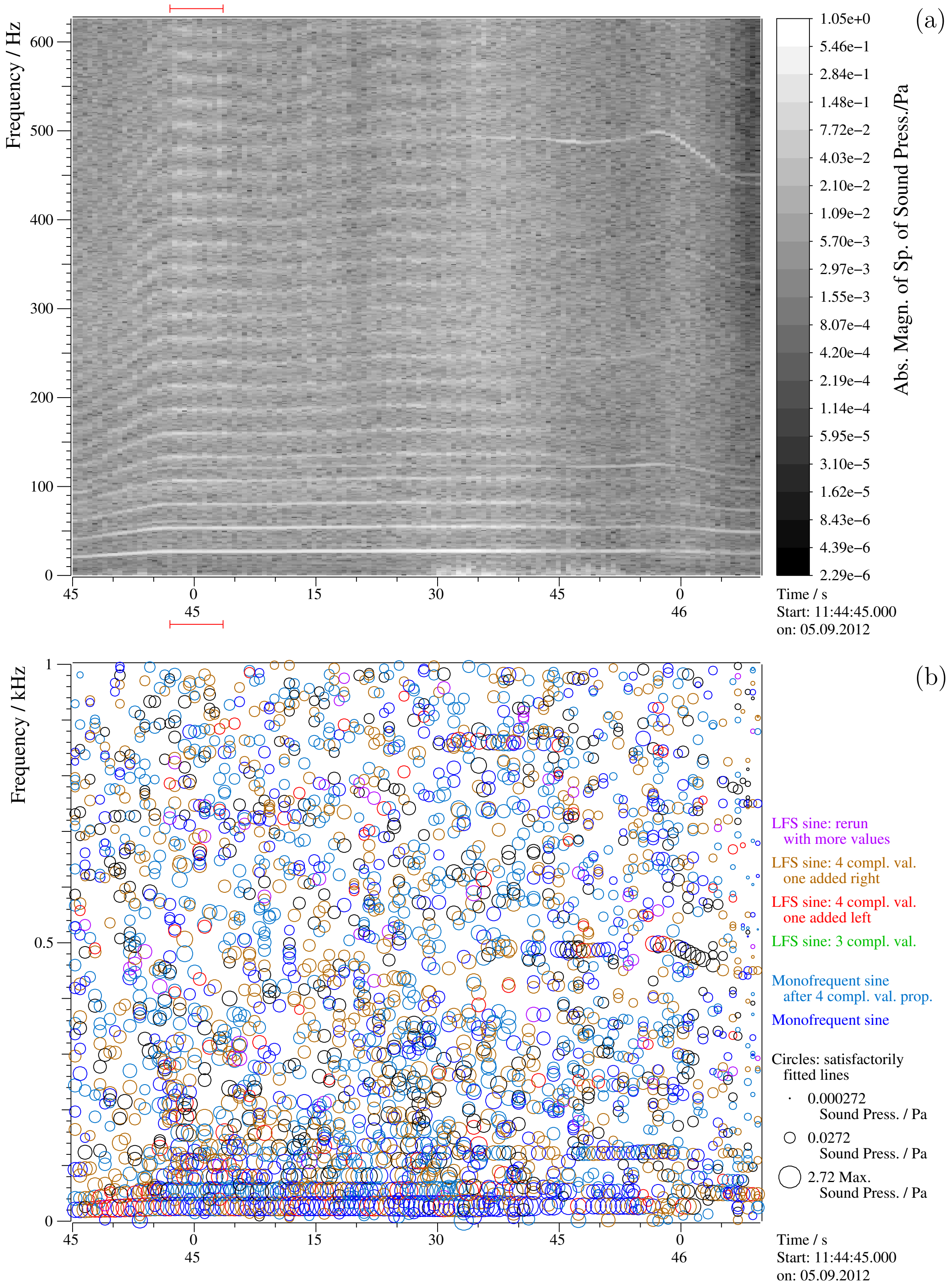

Figure 6.18: Sequence of spectra (8,192 samples per spectrum) of the signal of a helicopter which is most of the time stationary. (a) magnitude spectrum; the time interval covering the three averaged spectra for Figure 6.20 is marked in red. (b) demonstrates that very few sines are subtracted. The peaks within the lowest 50 Hz are fitted reliably, thinning out rapidly with in creasing frequency and already at 150 Hz peaks are subtracted only sporadically.

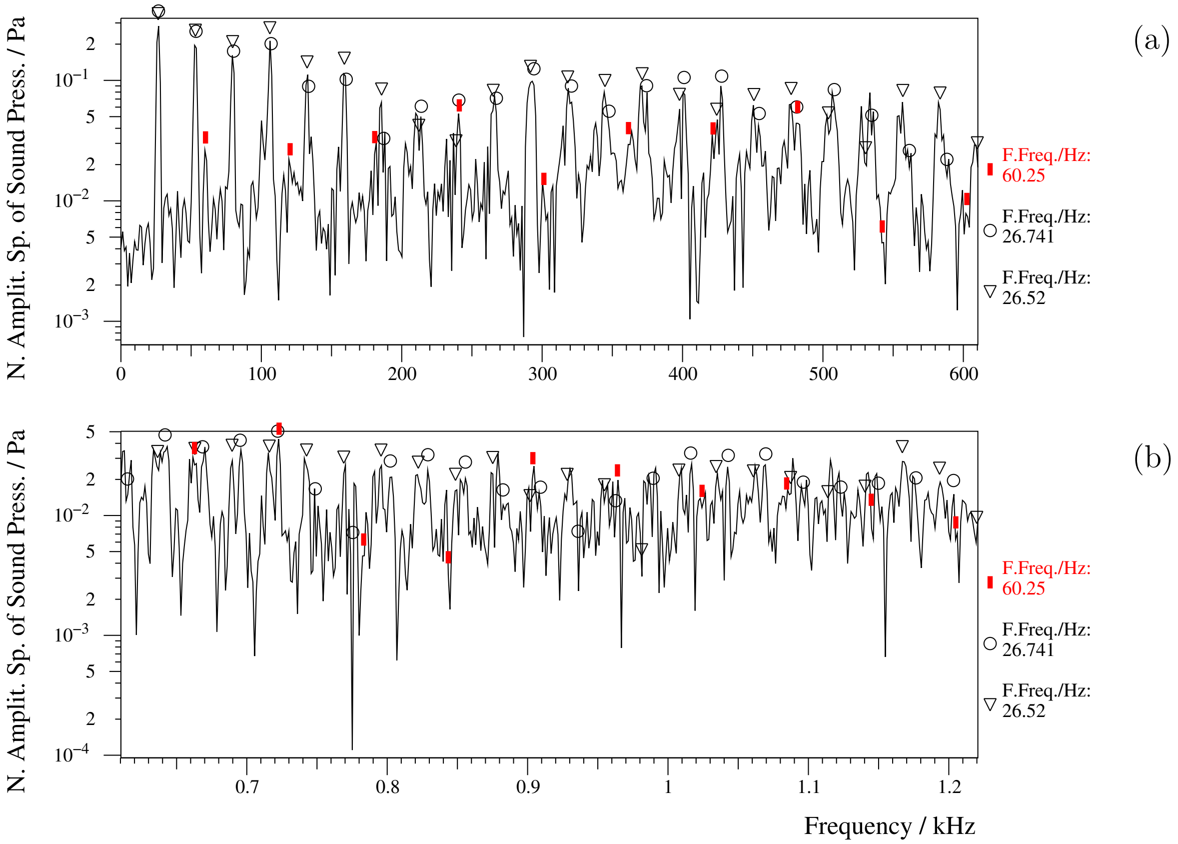

Figure 6.19: Single spectrum of Figure 6.18 (the 24th of 138, at 11:45:00, during stationarity). The first 500 magnitude values of are presented in (a), the following 500 values in (b). Three harmonic series are marked, the black ones have very close fundamental frequencies. One can see that the magnitude of the peaks decreases and they become broader with increasing frequency.

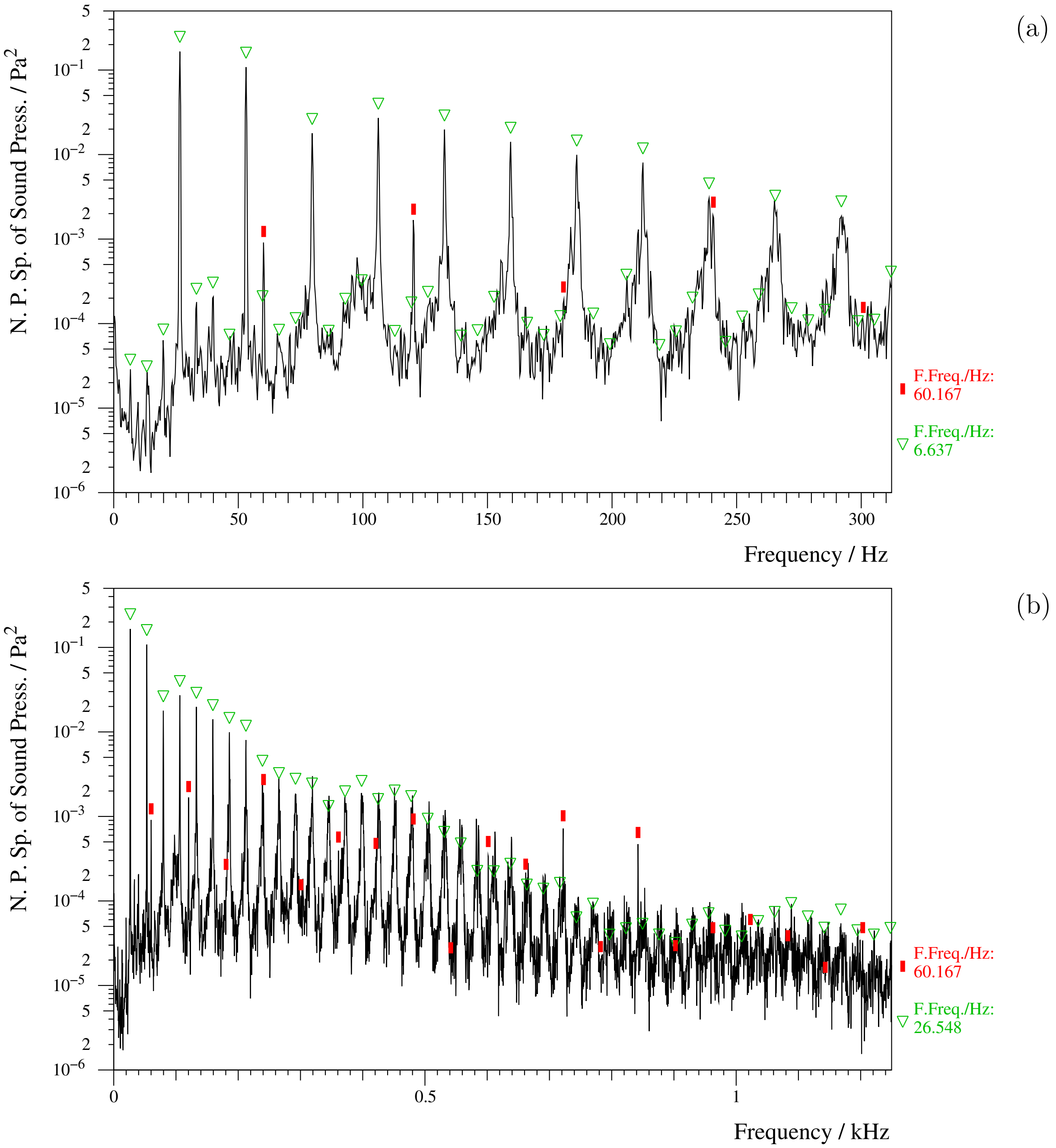

Figure 6.20: High-resolution, averaged spectrum of the helicopter; it is assumed that the signal was stationary during the time interval marked in Figure 6.18 when the helicopter was standing on its pad. Three overlapping (50 %) power spectra with 32,768 samples each are calculated and averaged. Here the fundamental frequency, equalling the revolution rate, is visible and its series is marked with green triangles. The symmetry between the four rotor blades is high, therefore mainly the quadrupled frequency and its integer multiples are present (marked in (b)) while the magnitude at the revolution rate and its non-quadruple harmonics is very low. Additionally, the tail rotor revolution rate series is marked in red.

6.6 Conclusion on real data applications

Synthetic sounds played by a computer and a speaker allow a comparison between the theoretical signal and the fit results, since the input parameters are known in principle.

Narrow peaks have been processed very successfully both for acoustic and seismic measurements, with the seismic data being strongly superposed with mains hum increasing the probability for a failed fit. The processed spectrum is reduced down to the background noise level, so that only a lower threshold for the reduction factor can be derived: it is at least three orders of magnitude. For narrow and monofrequent peaks – where the transfer function is constant – the factor might be principally unlimited, as indicated for synthetic superpositions in Section 5.5.

The broadest peaks analysed in this measurement correspond to $b_{0,r} = -67.11$ ($b_0 = -100.0\,{}^{\mathrm{Hz}}/_{\mathrm{s}}$), here the peak magnitudes are reduced by 1.5 orders of magnitude only. Perhaps a slight frequency dependency in the transfer function between played and recorded LFS-sine signals leads to deviations from the theoretical function for an LFS sine, thus decreasing the fit quality. Nonetheless, the RMS value of the signal is reduced by one order of magnitude down to the level of the background at times when no sounds were played.

The mean frequency and the LFS parameter of two sines – one with a strong linear frequency shift and one with a small one – have been tracked over several spectra for both, the acoustic and seismic signals. The fitted parameters are consistent with the theoretical ones, where the standard deviation for the acoustic signal is roughly one order of magnitude smaller than for the seismic signal. This is most probably a result of the sixfold better SNR.

For the signals of vehicles, the peaks have been too narrow to observe the deviations mentioned for broad peaks. All peaks that have been fitted successfully are reduced to the level of the background, but typically several smaller and sometimes even stronger peaks remain.

Real sources, which do not produce exclusively periodic noise, are not conducive to quantifying the fit performance, for instance by the ratio of RMS before and after processing. The optimal result is a complete removal of periodic components and simultaneously no manipulation of the non-periodic content. Since the ratio of the two is unknown, there is no quantitative measure for the degree of achieving the goal. However, one can use the RMS value to find out to what extent a signal is changed during processing.

If the data are dominated by (even single) strong peaks which remain in the data, the factor of RMS-value reduction will be small – independent of the number of successfully subtracted peaks. This phenomenon was strongly pronounced for the acoustic data of the propeller aircraft – here, the signals contain very low frequencies for which the start-value estimation fails. The reduction factor of the RMS amplitude ranges from insignificant to more than 5.

The acoustic data of a main battle tank have been processed successfully in general. Most of the highest peaks have been subtracted. Strong non-periodic contributions remain in the signal, however, so that the RMS amplitude of the signal was reduced by a factor of approximately 3.

If a peak shape does not match the one of a single (LFS) sine, the probability of a successful fit is small (even though sometimes by chance the χ_n^2-threshold requirement may be met) and thus, the chance of the peak remaining in the data is high. This was demonstrated for helicopter signals, where one can speculate about the reasons; by visual inspection of spectra it seems that at least two harmonic series with very similar fundamental frequencies dominate the spectrum.

The improvement of the procedure with regard to the evaluation of these insights is left for future work.

Chapter 7

Summary and conclusion

This work presents the derivation of an analytic expression for the discrete complex spectrum of a sine, the frequency of which can change with time linearly. The expression includes sampling, a limited duration and the Hann window function. With the first derivatives and well-estimated start parameters, the Levenberg-Marquardt algorithm is used to fit the parameters of such an LFS sine to single peaks in spectra. The $\mathrm{F}_{\mathrm{Sum}}$ expression can easily be implemented in typical programming languages. A major disadvantage for applications is the computation effort: on a single core of an `Intel i5` processor at 3.1 GHz the current implementation requires $0.5\,\mu$s per fitted value, per sample within the time interval of the spectrum and per iteration step. The processing time for a typical signal is on the order of days per minute of data.

Methods for the evaluation of the fit results are introduced by the systematic analysis of synthetic signals. The fit quality respectively the precision of the fitted parameters increases with decreasing noise to the point where the errors of the fit result are as small as the numeric precision, for example, 10^{-15} relative with double-precision variables. For certain ratios of acceptable false-positive fits to pure GWN, peak-width-dependent thresholds for the application to real data are gained.

In order to test the performance of the fitting procedure, artificial (LFS) sines are added to real signals that are non-periodic. It is demonstrated that sines with arbitrary parameters (including the amplitude, within the limits of the numerical precision) are fitted and subtracted successfully.

For completely real signals, the performance strongly depends on the data. We played sound files containing (LFS) sines with different parameters during our measurements and recorded the acoustic and seismic signals. Fits of narrow peaks have been very successfully both for acoustic and seismic measurements and the processed spectrum is reduced down to the background noise level. For the monofrequent case the peak magnitude is reduced by at least three orders of magnitude but the reduction factor might be principally unlimited, as indicated for synthetic superpositions. The broadest peak is reduced by 1.5 orders of magnitude only. Here, a slight frequency dependency in the transfer function between played and recorded LFS-sine signals may have led to deviations from the theoretical function for an LFS sine, thus decreasing the fit quality.

For real signals, all peaks which have been fitted successfully are reduced to the level of the background, but typically several smaller and sometimes even stronger peaks remain. Since the ratio of periodic to non-periodic noise is unknown, there is no quantitative measure for the degree of periodic-noise removal. However, one can use the RMS value to find out to what extent a signal is changed during processing.

On the basis of the acoustic signal of a propeller aircraft, the limitation of the current implementation of the algorithm regarding peaks at the very margins of a spectrum has been demonstrated. The acoustic data contain dominating low-frequency contributions which – in most instances – remain in the signal and thus lead to small factors of RMS-value reduction.

The acoustic data of a main battle tank have been processed successfully in general. Most of the highest peaks have been subtracted. The strong non-periodic contributions remain in the signal – fitting to the goal of the work. The RMS amplitude of the signal has been reduced by a factor of approximately 3.

The acoustic spectra of a helicopter signal recorded at close distance seem to contain peaks different from the ones of pure sinusoids. The processing results become worse for increasing frequencies of the harmonics as the divergence of the peaks increases. If a peak shape does not match the one of a single (LFS) sine, the probability of a successful fit is small (even though sometimes by chance the χ_n^2-threshold requirement may be met) and thus, the chance of the peak remaining in the data is high.

This work continues the field of research of the working group Physics and Disarmament at the chair Experimentelle Physik III of TU Dortmund. It was started in the 1990s in the frame of the BVP to find peaks and series of harmonics in power spectra with the objective of pattern recognition for vehicles [23]. This was the motivation to derive the expression of a monofrequent sine in the discrete spectrum; it was applied to the spectral magnitude. Later on, periodic noise was seen in a different context as a disturbance. In order to remove it by subtraction, the exact characterisation of the peaks in the complex spectrum is required. One task of my Diploma thesis was the improvement of the algorithm by inclusion of the phase parameter in the fit procedure [14, 39]. For signals of moving vehicles, it turned out that this approach was insufficient to handle cases when the frequency changes within the time used for one spectrum, often by the change of the Doppler shift when the sensor is passed. After the monofrequent expression, the next step is a linearly in the time shifting frequency; its derivation and evaluation is described in this work. Whether or not it will make sense to advance to higher orders is unknown, but it is doubtful whether it would be of great practical use.

The expression derived and applied in this work is an ideally adjusted filter for arbitrary

LFS sines. For synthetic signals it works very precisely and can reproduce signals on a level which is unattainable for notch filters. For all peaks that are not produced by pure (LFS) sines, the fit performance drops, sometimes strongly. This is impressively demonstrated for a helicopter signal measured at close distance. The peaks of other real sources are fitted and subtracted mainly successfully.

With regard to the primary motivation of this work, one can state that it is possible to reduce the periodic content of time-series data significantly. However, the signals of the vehicles analysed contain non-periodic components which remain in the signal – but retaining such components for the detection of weak impulsive events has been the goal. With the described procedure, noise of vehicles can be reduced but not completely removed. It will not allow the detection of smallest aftershock signals next to a busy motorway or the like. Nonetheless, it can increase the SNR.

In order to solve the problems that have been observed and to optimize and improve the procedure, several directions seem promising for future research:

- **Line tracking over several spectra**
  If it is obvious, that a lasting (LFS) sine is in the data, one could selectively increase (weaken) the χ^2 thresholds for very small frequency bands where the mean frequency of the sine is extrapolated in surrounding spectra. The processing of spectra should not be exclusively one by one but a progression to former and future times should be allowed as soon as a systematic behaviour is recognised. In this context it could even be possible to decrease the general threshold and therefore reduce false positives and false negatives in one approach simultaneously (this would extend the procedure of [21] to the LFS).

- **Searching for harmonics**
  The sources of the signals, in which periodic noise should be subtracted, typically consist of fundamental frequencies with several harmonics. Similar to the former item, one could think about weakening the threshold for members of series of sines. Cepstra (the inverse Fourier transform of the logarithm of the magnitude spectrum with logarithmically scaled frequency) could be used to get and track fundamental frequencies.

- **Fitting of neighbouring sines**
  The adaption of the fitting algorithm to include two (or even multiple) sines that contribute to one peak should not cause any problems at all. In contrast, estimating start values would be challenging. If runtime is not a big deal then systematic variations of the phases (similar to Sec. 4.9.3) could be a first approach.[1]

---

[1] First attempts for the case of two monofrequent sines were done by [36]. The fitting was performed

- **Simultaneous fit of multiple peaks**
  The magnitudes of peaks decrease monotonously to their sides but their influence on each other can still be significant even if the peaks are well separated and each fit is successful. In this work this fact has been met by processing the peaks in descending order of their magnitudes. This is reasonable but could be improved: close peaks could be merged to form a longer frequency band in which multiple peaks are fitted at once. The challenge of estimating start values is omitted if the fit results of the single peak fits are used. This approach would overcome the problem of mutual influences completely because the algorithm would fit the sum of (LFS) sines to all peaks instead of trying to fit a single (LFS) sine to one peak with superposed contributions from others. If fitting long intervals with many fit parameters will be unstable, the intervals could be limited artificially and only the innermost peaks could be subtracted. Then smaller overlapping intervals would be utilised in order to process long ones.

- **Threshold adjustment for very broad peaks**
  The threshold for χ^2_n should probably be adjusted for large numbers of complex values the $\mathrm{F}_{\mathrm{Sum}}$ is fitted to. At the moment the argument is: A certain amount of false positives in Gaussian white noise is acceptable. Because of a decreasing probability that a broad peak is found in noise, the threshold is weakened strongly with the number of values. With the meaning of the χ^2_n parameter in mind – it is the mean of squared relative deviations between given values and fitted ones – it could be reasonable to think about an absolute weakest threshold.

- **Improving start values**
  Even more effort could be put into the start-value estimation. Its benefit is to be determined since the current state works reliably with few exceptions and it is unlikely that the fit will not end up in the primary minimum. However, a higher accuracy could reduce computation effort and maybe further avoid exceptions. An easy improvement would be an iteration of the start-parameter determination mainly via the amplitude and peak width: The start parameters could be estimated in the described way and then used in a second run – the estimated amplitude would be an improved value compared to the magnitude value at i_{max} which is used to estimate the peak width. Subsequently, a more precise peak width could improve all further estimations since they depend on this value.

---

within the magnitude spectrum – in principle, this means the reduction of the set of fit parameters by the phase – and included an additional parameter for the relative phase difference between the two sines. This was necessary to address the fact that the peak shape strongly depends on the signs of the complex values of the summed sines. This approach was feasible because of the simple progression of the phases of the complex values of a monofrequent sine (Sec. 3.2.2). For broader peaks the slope of the phases depends on b_0 which makes this approach invalid.

Additionally, an approach to provide start values for peaks at very low frequencies ($\approx 1\,\Delta\nu$ down to zero) could be useful as they can strongly contribute.

- **Reducing computation effort**
  Many improvements could be worth an analysis. The maximum number of iterations for a single peak fit could be adjusted. The $\mathrm{F}_{\mathrm{Sum}}$ expression could be analysed with the aim to further reduce the number of summands. It could be possible that a reduction similar to the FFT is feasible (even though the roots of unity are not equally spaced around the unit circle in $\mathrm{F}_{\mathrm{Sum}}$). Additional criteria to reduce the number of sine candidates and thus the number of fit procedure calls could be implemented. Especially, a background criterion to reject peaks with a low amplitude should be promising if limited knowledge about the data to be processed is available (e.g. the mean spectral magnitude background during calm periods). With even more knowledge about the data, a threshold for the maximum peak width could avoid fits with high n_{Fit} (e.g. if only aircraft at high altitudes are expected, it can be assumed that no broad peaks will occur). Additionally, a more efficient FFT (with pre-set angular-function values for the used N) – could accelerate this part by a factor of at least 10; compared to the calculation effort for the fitting in the current implementation however, this improvement should be of minor benefit.

- **Higher orders of frequency shift**
  Cases occur in which the frequency of a sine changes with time more strongly than linearly. In Section A.2.2 it is argued that finite-sum expressions should exist also for higher orders of the frequency shift. For each additional order, an additional parameter would occur in the expression for a sine the frequency of which changes quadratically, cubically etc. with time. One can doubt whether a fit could be stable with real data, but this would need to be investigated.

Appendix A

Appendix

A.1 The $\mathrm{F}_{\mathrm{Erf}}$ approach – First applications and concluding words

A.1.1 Spectrum of an LFS sine limited by a rectangle for negative frequencies

This calculation can be done in analogy to the one in Section 2.4.1. Nonetheless, some signs are different, requiring the use of different symmetries compared to the approach described before.

$$\hat{\mathrm{S}}\mathrm{R}_{\mathrm{neg}}(\nu) = \frac{A_0}{2\mathrm{i}} \int_0^T -\cos\Big(-\pi b_0 t^2 - 2\pi(\nu_0+\nu)t - \phi_0\Big) - \mathrm{i}\sin\Big(-\pi b_0 t^2 - 2\pi(\nu_0+\nu)t - \phi_0\Big)\,\mathrm{d}t \tag{A.1}$$

$$\hat{\mathrm{S}}\mathrm{R}_{\mathrm{neg}}(\nu) = \frac{A_0}{2\mathrm{i}} \int_0^T -\cos\Big(\pi b_0 t^2 + 2\pi(\nu_0+\nu)t + \phi_0\Big) + \mathrm{i}\sin\Big(\pi b_0 t^2 + 2\pi(\nu_0+\nu)t + \phi_0\Big)\,\mathrm{d}t \tag{A.2}$$

With $a = \pi b_0$, $b = \pi(\nu_0+\nu)$, $c = \phi_0$

$$\hat{\mathrm{S}}\mathrm{R}_{\mathrm{neg}}(\nu) = \frac{A_0}{2\mathrm{i}} \int_0^T -\cos\Big(at^2 + 2bt + c\Big) + \mathrm{i}\sin\Big(at^2 + 2bt + c\Big)\,\mathrm{d}t \tag{A.3}$$

Use Equations 2.52 and 2.53

$$\begin{aligned}\hat{\mathrm{S}}\mathrm{R}_{\mathrm{neg}}(\nu) = &\frac{A_0}{2\mathrm{i}}\sqrt{\frac{\pi}{2a}}\Bigg(\\ &-\cos\left(\frac{b^2-ac}{a}\right)\mathrm{C}\left[\sqrt{\frac{2}{a\pi}}(ax+b)\right]_0^T - \sin\left(\frac{b^2-ac}{a}\right)\mathrm{S}\left[\sqrt{\frac{2}{a\pi}}(ax+b)\right]_0^T \\ &+\mathrm{i}\cos\left(\frac{b^2-ac}{a}\right)\mathrm{S}\left[\sqrt{\frac{2}{a\pi}}(ax+b)\right]_0^T - \mathrm{i}\sin\left(\frac{b^2-ac}{a}\right)\mathrm{C}\left[\sqrt{\frac{2}{a\pi}}(ax+b)\right]_0^T\Bigg)\end{aligned} \tag{A.4}$$

$$\begin{aligned}\hat{\mathrm{S}}\mathrm{R}_{\mathrm{neg}}(\nu) = &\frac{A_0}{2\mathrm{i}}\sqrt{\frac{\pi}{2a}}\Bigg(\\ &\cos\left(\frac{b^2-ac}{a}\right)\left(-\mathrm{C}\left[\sqrt{\frac{2}{a\pi}}(aT+b)\right]+\mathrm{C}\left[\sqrt{\frac{2}{a\pi}}b\right]+\mathrm{iS}\left[\sqrt{\frac{2}{a\pi}}(aT+b)\right]-\mathrm{iS}\left[\sqrt{\frac{2}{a\pi}}b\right]\right) \\ &+\sin\left(\frac{b^2-ac}{a}\right)\left(-\mathrm{S}\left[\sqrt{\frac{2}{a\pi}}(aT+b)\right]+\mathrm{S}\left[\sqrt{\frac{2}{a\pi}}b\right]-\mathrm{iC}\left[\sqrt{\frac{2}{a\pi}}(ax+b)\right]+\mathrm{iC}\left[\sqrt{\frac{2}{a\pi}}b\right]\right)\Bigg)\end{aligned} \tag{A.5}$$

Symmetry relation (Abramowitz 1964: Equation 7.3.18):

$$\mathrm{C}[\mathrm{i}z] = \mathrm{iC}[z], \mathrm{S}[\mathrm{i}z] = -\mathrm{iS}[z] \tag{A.6}$$

$$\begin{aligned}\hat{\mathrm{S}}\mathrm{R}_{\mathrm{neg}}(\nu) = &\frac{A_0}{2\mathrm{i}}\sqrt{\frac{\pi}{2a}}\Bigg(\\ &\cos\left(\frac{b^2-ac}{a}\right)\left(\mathrm{i}\left\langle\mathrm{C}\left[\mathrm{i}\sqrt{\frac{2}{a\pi}}(aT+b)\right]+\mathrm{iS}\left[\mathrm{i}\sqrt{\frac{2}{a\pi}}(aT+b)\right]\right\rangle-\mathrm{i}\left\langle\mathrm{C}\left[\mathrm{i}\sqrt{\frac{2}{a\pi}}b\right]+\mathrm{iS}\left[\mathrm{i}\sqrt{\frac{2}{a\pi}}b\right]\right\rangle\right) \\ &+\sin\left(\frac{b^2-ac}{a}\right)\left(-\mathrm{iS}\left[\mathrm{i}\sqrt{\frac{2}{a\pi}}(aT+b)\right]-\mathrm{C}\left[\mathrm{i}\sqrt{\frac{2}{a\pi}}(ax+b)\right]+\mathrm{iS}\left[\mathrm{i}\sqrt{\frac{2}{a\pi}}b\right]+\mathrm{C}\left[\mathrm{i}\sqrt{\frac{2}{a\pi}}b\right]\right)\Bigg)\end{aligned} \tag{A.7}$$

With Equation 2.56

$$\begin{aligned}\hat{\mathrm{S}}\mathrm{R}_{\mathrm{neg}}(\nu) = &\frac{A_0}{2\mathrm{i}}\sqrt{\frac{\pi}{2a}}\Bigg(\\ &\mathrm{i}\cos\left(\frac{b^2-ac}{a}\right)\left(\frac{1+\mathrm{i}}{2}\mathrm{Erf}\left[\frac{\sqrt{\pi}}{2}(1-\mathrm{i})\,\mathrm{i}\sqrt{\frac{2}{a\pi}}(aT+b)\right]-\frac{1+\mathrm{i}}{2}\mathrm{Erf}\left[\frac{\sqrt{\pi}}{2}(1-\mathrm{i})\,\mathrm{i}\sqrt{\frac{2}{a\pi}}b\right]\right) \\ &+\sin\left(\frac{b^2-ac}{a}\right)\left(-\frac{1+\mathrm{i}}{2}\mathrm{Erf}\left[\frac{\sqrt{\pi}}{2}(1-\mathrm{i})\,\mathrm{i}\sqrt{\frac{2}{a\pi}}(aT+b)\right]+\frac{1+\mathrm{i}}{2}\mathrm{Erf}\left[\frac{\sqrt{\pi}}{2}(1-\mathrm{i})\,\mathrm{i}\sqrt{\frac{2}{a\pi}}b\right]\right)\Bigg)\end{aligned} \tag{A.8}$$

The cosine and sine expressions can be combined to one exponential expression:

$$\hat{\mathrm{S}}\mathrm{R}_{\mathrm{neg}}(\nu) = \frac{A_0}{2\mathrm{i}}\sqrt{\frac{\pi}{2a}}\frac{1+\mathrm{i}}{2}\mathrm{e}^{\mathrm{i}\frac{b^2-ac}{a}}\mathrm{i}\left(\mathrm{Erf}\left[\mathrm{i}\,(1-\mathrm{i})\,\sqrt{\frac{1}{2a}}\,(aT+b)\right]-\mathrm{Erf}\left[\mathrm{i}\,(1-\mathrm{i})\,\sqrt{\frac{1}{2a}}b\right]\right) \tag{A.9}$$

With:

$$\mathrm{Erfi}(z) = -\mathrm{i}\mathrm{Erf}(\mathrm{i}z) \tag{A.10}$$

$$\hat{\mathrm{S}}\mathrm{R}_{\mathrm{neg}}(\nu) = -\frac{A_0}{2\mathrm{i}}\sqrt{\frac{\pi}{2a}}\frac{1+\mathrm{i}}{2}\mathrm{e}^{\mathrm{i}\frac{b^2-ac}{a}}\left(\mathrm{Erfi}\left[(1-\mathrm{i})\,\sqrt{\frac{1}{2a}}\,(aT+b)\right]-\mathrm{Erfi}\left[(1-\mathrm{i})\,\sqrt{\frac{1}{2a}}b\right]\right) \tag{A.11}$$

Undo substitutes:

$$\begin{aligned}\hat{\mathrm{S}}\mathrm{R}_{\mathrm{neg}}(\nu) =& -\frac{A_0}{2\mathrm{i}}\sqrt{\frac{\pi}{2\pi b_0}}\frac{1+\mathrm{i}}{2}\mathrm{e}^{\mathrm{i}\frac{\pi(\nu_0+\nu)^2-b_0\phi_0}{b_0}}\\ &\left(\mathrm{Erfi}\left[(1-\mathrm{i})\,\sqrt{\frac{1}{2\pi b_0}}\,(\pi b_0T+\pi(\nu_0+\nu))\right]-\mathrm{Erfi}\left[(1-\mathrm{i})\,\sqrt{\frac{1}{2\pi b_0}}\pi(\nu_0+\nu)\right]\right)\end{aligned} \tag{A.12}$$

$$\begin{aligned}\hat{\mathrm{S}}\mathrm{R}_{\mathrm{neg}}(\nu) =& -\frac{A_0}{4}\sqrt{\frac{1}{2b_0}}\,(1-\mathrm{i})\,\mathrm{e}^{\frac{\mathrm{i}\pi(\nu_0+\nu)^2}{b_0}-\mathrm{i}\phi_0}\\ &\left(\mathrm{Erfi}\left[(1-\mathrm{i})\,\sqrt{\frac{\pi}{2b_0}}\,(b_0T+\nu_0+\nu)\right]-\mathrm{Erfi}\left[(1-\mathrm{i})\,\sqrt{\frac{\pi}{2b_0}}(\nu_0+\nu)\right]\right)\end{aligned} \tag{A.13}$$

A.1.2 Proof of symmetry

The expression for a peak which is located at positive frequencies must be equal to the expression for a peak which is located at negative frequencies with negated signs for all LFS sine parameters and vice versa (Sec. 2.3.1.1):

$$\begin{aligned}\hat{\mathrm{S}}\mathrm{R}_{\mathrm{neg}}\left(-A_0,-\nu_0,-\phi_0,-b_0,T,\Delta t,\nu\right) =& -\frac{-A_0}{4}\sqrt{\frac{1}{-2b_0}}\,(1-\mathrm{i})\,\mathrm{e}^{\frac{\mathrm{i}\pi(-\nu_0+\nu)^2}{-b_0}+\mathrm{i}\phi_0}\\ &\left(\mathrm{Erfi}\left[(1-\mathrm{i})\,\sqrt{\frac{\pi}{-2b_0}}\,(-b_0T-\nu_0+\nu)\right]-\mathrm{Erfi}\left[(1-\mathrm{i})\,\sqrt{\frac{\pi}{-2b_0}}(-\nu_0+\nu)\right]\right)\end{aligned} \tag{A.14}$$

$$\begin{aligned}\hat{\mathrm{S}}\mathrm{R}_{\mathrm{neg}}\left(-A_0,-\nu_0,-\phi_0,-b_0,T,\Delta t,\nu\right) =& \frac{A_0}{4}\sqrt{-\frac{1}{2b_0}}\,(1-\mathrm{i})\,\mathrm{e}^{\frac{-\mathrm{i}\pi(\nu_0-\nu)^2}{b_0}+\mathrm{i}\phi_0}\\ &\left(\mathrm{Erfi}\left[-(1-\mathrm{i})\,\sqrt{-\frac{\pi}{2b_0}}\,(b_0T+\nu_0-\nu)\right]-\mathrm{Erfi}\left[-(1-\mathrm{i})\,\sqrt{-\frac{\pi}{2b_0}}(\nu_0-\nu)\right]\right)\end{aligned} \tag{A.15}$$

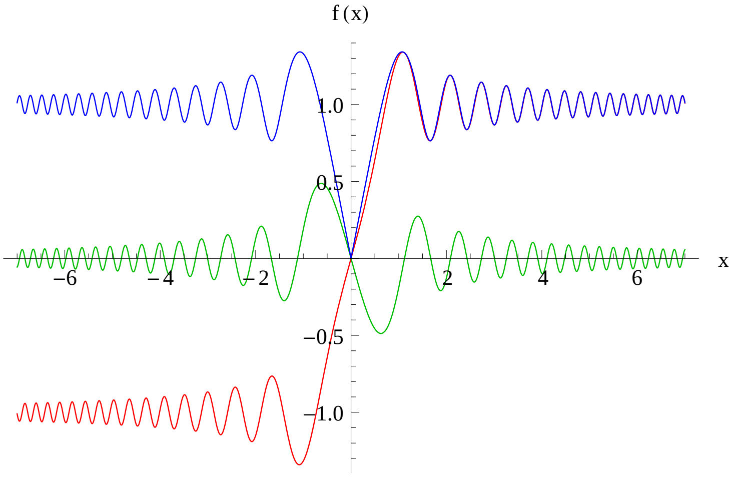

Figure A.1: Plots of the complex error function along a line through zero with slope −1 in the complex plane. Red: $\mathrm{f}(x)=\mathrm{Re}\Big[\mathrm{Erf}[(1-\mathrm{i})x]\Big]$, green: $\mathrm{f}(x)=\mathrm{Im}\Big[\mathrm{Erf}[(1-\mathrm{i})x]\Big]$, blue: $\mathrm{f}(x)=\mathrm{Abs}\Big[\mathrm{Erf}[(1-\mathrm{i})x]\Big]$.

With Equation A.10:

$$\hat{\mathrm{S}}\mathrm{R}_{\mathrm{neg}}\left(-A_0,-\nu_0,-\phi_0,-b_0,T,\Delta t,\nu\right)=\mathrm{i}\frac{A_0}{4}\sqrt{\frac{1}{2b_0}}\left(1-\mathrm{i}\right)\mathrm{e}^{\frac{-\mathrm{i}\pi(\nu_0-\nu)^2}{b_0}+\mathrm{i}\phi_0}$$
$$\left(-\mathrm{iErf}\left[-\mathrm{i}\left(1-\mathrm{i}\right)\mathrm{i}\sqrt{\frac{\pi}{2b_0}}\left(b_0T+\nu_0-\nu\right)\right]+\mathrm{iErf}\left[-\mathrm{i}\left(1-\mathrm{i}\right)\mathrm{i}\sqrt{\frac{\pi}{2b_0}}\left(\nu_0-\nu\right)\right]\right) \tag{A.16}$$

$$\hat{\mathrm{S}}\mathrm{R}_{\mathrm{neg}}\left(-A_0,-\nu_0,-\phi_0,-b_0,T,\Delta t,\nu\right)=\frac{A_0}{4}\sqrt{\frac{1}{2b_0}}\left(1-\mathrm{i}\right)\mathrm{e}^{\frac{-\mathrm{i}\pi(\nu_0-\nu)^2}{b_0}+\mathrm{i}\phi_0}$$
$$\left(\mathrm{Erf}\left[\left(1-\mathrm{i}\right)\sqrt{\frac{\pi}{2b_0}}\left(b_0T+\nu_0-\nu\right)\right]-\mathrm{Erf}\left[\left(1-\mathrm{i}\right)\sqrt{\frac{\pi}{2b_0}}\left(\nu_0-\nu\right)\right]\right) \tag{A.17}$$
$$=\hat{\mathrm{S}}\mathrm{R}_{\mathrm{pos}}\left(\quad A_0,\quad \nu_0,\quad \phi_0,\quad b_0,T,\Delta t,\nu\right)$$

Figure A.1 illustrates the curve progression of the error function.

A.1.3 Next neighbours

Without inclusion of the Dirac comb, $\mathrm{F}_{\mathrm{Erf}}$ consists of two peaks (at negative and positve frequencies) and converges monotonously to zero. The spectrum is incomplete with regard to the tails of peaks located at periodically repeating positions on the frequency scale ($n\cdot N\cdot\Delta\nu$, $n\in\mathbb{N}$, Fig. 2.3). The Dirac comb is impractical to implement in software, but an arbitrary number of repetitions is elementary, with the disadvantage of increasing computation effort. The actual number of repetitions increases with an increasing demand for precision. Furthermore, it is essential to understand the influences of the spectral and LFS sine parameters on the strength of the tails of peak in repeated spectra.

1. The influence of b_0: Firstly, the bigger the $|b_{0,r}|$ the slower the amplitude decreases to the sides (Fig. 4.3 (a)). Secondly, the smaller the $|b_{0,r}|$ the more does the theoretical centre frequency of a peak (r_{Max}) with respect to the raster of discrete frequencies (Eq. 4.14) influence the amplitude decrease (Fig. 4.3 (b)).

2. The influence of the peak position: Due to the monotonous convergence, in general, one can say that the peak is the more influenced by neighbouring peaks the closer the peaks are (the less discrete spectral values lie between them) – this depends on the location of the peak within the complete range of discrete spectral values (in comparison to the effect described above) and is a small scale influence from one peak to the closest peak of the ”next spectrum” (the next repetition according to the Dirac comb). The closer this neighbouring peak is, the farther the second next one will be.[1]

3. The influence of N: Adding more and more neighbours will decrease the influence on the position of the peak in a single spectrum (3^{rd} item) but a long scale influence will remain: In every spectrum there are exactly two peaks, counting this as one unit, then the next unit is exactly N points away – that means that the smaller the N is, the more neighbours must be taken into account to reach a certain precision if all the other parameters remain unchanged. In other words: The less points a single spectrum consists of the closer the neighbouring spectra are and the stronger their influence is because the amount of points between the peaks is less.[2]

For the following consideration two aspects need to be taken into account:

- The function $\mathrm{F}_{\mathrm{Erf}}$ includes exactly the two peaks of a single spectrum: One at negative and one at positive frequencies.
- The fitting is done to the peak in the positive frequencies.

The mean frequency determines the location of the peak within the $N/2$ values of the positive spectrum. $\mathrm{F}_{\mathrm{Erf}}$ considers all peaks located within the spectral range $[-\nu_{\mathrm{Nyquist}};\nu_{\mathrm{Nyquist}}]$. The bigger the frequency is, the closer the peak gets to the peak in the neighbouring spectrum to the right which is not considered. This means that (depending on the N) the mean frequency of a peak decides if this influence is small

---

[1] Each spectrum consists of two peaks (at positive and negative frequencies), the bigger the mean frequency is, the more the peaks move outwards (towards $\pm\nu_{\mathrm{Nyquist}}$). The more outwards the peaks are, the closer they are with regards to the closest peak within the next repetition of the spectrum (due to the Dirac comb) and the bigger the distance to the second closest peak becomes. To include the complete Dirac comb: Increasing ν_0 decreases the distance to every odd multiple peak and increases the distance to every even multiple peak.

[2] Interestingly, with respect to the computation effort, this is inverse to the $\mathrm{F}_{\mathrm{Sum}}$ approach: The calculation of $\mathrm{F}_{\mathrm{Sum}}$ is proportional to N, but here, the bigger the N, the less repetitions of spectra need to be taken into account to achieve a certain precision (actually, it is inverse proportional).

(small frequencies) or disastrous high (if the frequency is close to ν_{Nyquist}). This asymmetry comes mainly from the fact that for small frequencies the influence of the peak at negative frequencies increases – but it is already included in F_{Erf}. In contrast, for high frequencies the real data are influenced strongly by the peak of the next neighbour to the right whereas the theoretical function does not contain this influence. That means that adding the neighbouring spectrum to the right is by far the most important improvement and a solution of the 2nd effect in the list of dependencies. This is done by:

$$\mathrm{F}^{1}_{\text{Erf}}(\nu) = \mathrm{F}_{\text{Erf}}(\nu) + \mathrm{F}_{\text{Erf}}(\nu - N\Delta\nu) \tag{A.18}$$

$\mathrm{F}^{1}_{\text{Erf}}(\nu)$ (Eq. A.18) considers all peaks within the frequencies range: $[-\nu_{\text{Nyquist}}, 3\cdot\nu_{\text{Nyquist}}]$. That means that with $\mathrm{F}^{1}_{\text{Erf}}(\nu)$ at least $N/2$ spectral values form a kind of buffer to the next non-considered peak.[3] The next step is to add a repetition to the left (smaller than $-\nu_{\text{Nyquist}}$), restoring the asymmetry in considered peaks; it makes sense to use an odd number of neighbours to improve the theoretical function (the 3rd item). E.g. the next improvement is:

$$\mathrm{F}^{3}_{\text{Erf}}(\nu) = \mathrm{F}^{1}_{\text{Erf}}(\nu) + \mathrm{F}_{\text{Erf}}(\nu - 2N\Delta\nu) + \mathrm{F}_{\text{Erf}}(\nu + N\Delta\nu) \tag{A.19}$$

In general:

$$\mathrm{F}^{n}_{\text{Erf}}(\nu) = \mathrm{F}^{n-2}_{\text{Erf}}(\nu) + \mathrm{F}_{\text{Erf}}(\nu - (n-1)N\Delta\nu) + \mathrm{F}_{\text{Erf}}(\nu + (n-2)N\Delta\nu) \tag{A.20}$$

The 1st item in the list of dependencies concern the individual parameters b_0 and ν_0 and therefore are not considerable in advance (except the expected signals are known).

In a series of plots the some examples for fits with different numbers of considered peaks are given. For reasons of compatibletly, the parameters used here are the same as in Figure 5.4. Figure A.2 illustrates the fit result if one "spectrum" is added behind the ν_{Nyquist}: $\mathrm{F}^{1}_{\text{Erf}}$ (Eq. A.18).[4] Figure A.3 shows the same for $\mathrm{F}^{31}_{\text{Erf}}$. Naturally the start parameters are the same in both examples.

A.1.4 The error-function approach for small LFS parameters

The implemented F_{Erf} expression becomes invalid for $|b_{0,r}| \to 0$ (Eq. 2.63). Figure A.4 shows how the fit algorithm behaves if the signal consists of a pure, monofrequent sine.

---

[3] To be exact: For the fitting, there is one peak to the left (at least $N/2$ points) and even two peaks (at least N points) to the right that are considered. For the subtraction both peaks (at negative and positive frequencies) are edited so here is one peak (at least $N/2$ points) to each side taken into account.

[4] The start values are different to the ones for the F_{Sum} approach. This analysis has been done at an earlier stage of the software. The start value estimation was typically more precise for pure LFS sine spectra but much more susceptible to superposed signals in general.

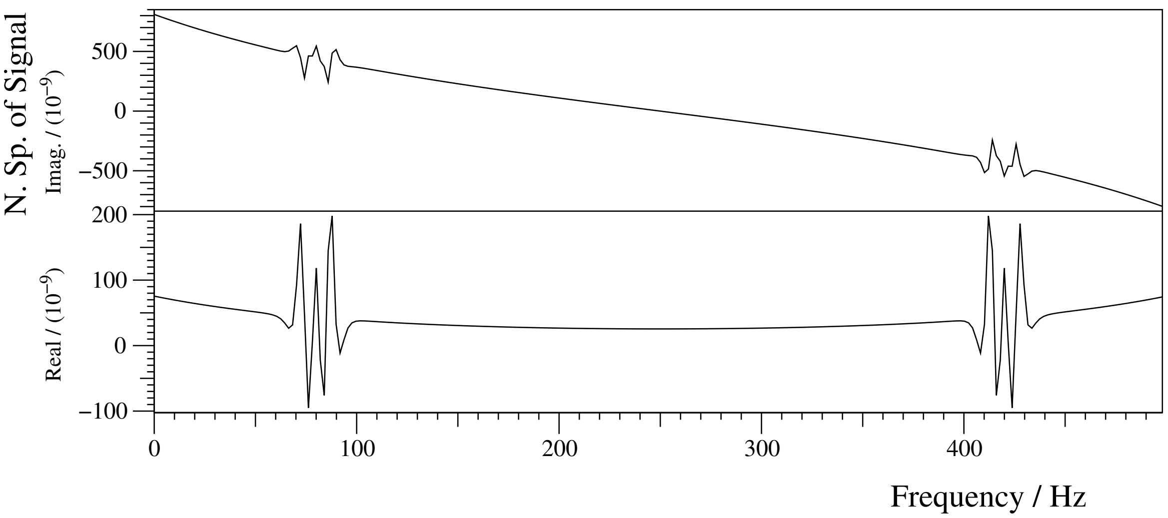

	ν_0 / Hz	b_0 / (Hz/s)	ϕ_0 / °	A_0
Input:	70.1	40.1	160.1	100.0
Start:	70.00523189	40.51867734	171.9325300	100.219671694
Fit:	70.09999989	40.10000042	160.1000046	100.000000074

Figure A.2: Real and imaginary part of the LFS sine spectrum after fit and subtraction of the approximated error-function expression with one next neighbour (F^1_{Erf}, Eq. A.18). $N = 256$, $\Delta\nu = 1.0\,\text{Hz}$. Number of iterations: 37, $\chi^2 = 4.95 \cdot 10^{-14}$, sample rate: 500.0 Hz, so behind the Nyquist frequency (250.0 Hz) the negative frequencies are shown.

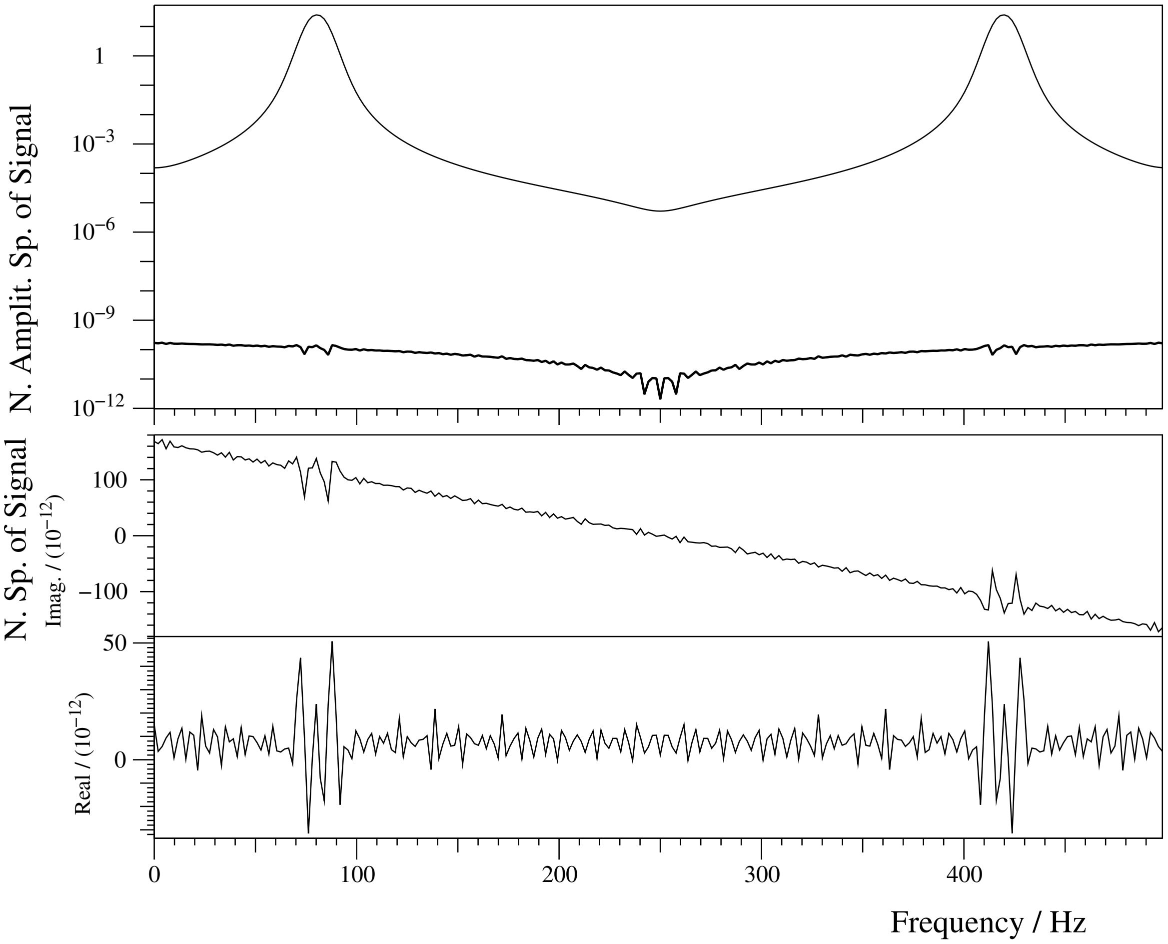

	ν_0 / Hz	b_0 / (Hz/s)	ϕ_0 / °	A_0
Input:	70.1	40.1	160.1	100.0
Start:	70.00523189167	40.51867733762	171.9325300261	100.2196716935
Fit:	70.099999999972	40.10000000011	160.1000000012	100.000000000024

Figure A.3: Similar content to Figure A.2: Real and imaginary part of the LFS sine spectrum after fit and subtraction of the approximated error-function expression with 31 next neighbours ($F^3_{\mathrm{Erf}}1$, Eq. A.20 with $n = 31$). $N = 256$, $\Delta\nu = 1.0\,\mathrm{Hz}$. Number of iterations: 47, $\chi^2_n = 3.29 \cdot 10^{-21}$, sample rate: 500 Hz.

The parameters of the sine are chosen in such a way, that no spectral leakage occurs.[5] Therefore, the basic $\mathrm{F}_{\mathrm{Erf}}$ function (without additional summands to compensate for the omitted Dirac comb) is sufficient. Consequently, the subtraction leaves the peak at negative frequencies basically unchanged.[6] For the subtraction of a spectrum with the fitted parameters, the magnitude of the peak is reduced only by five orders of magnitude (compared to the example given in Fig. A.3 this is a bad result, in particular because one would expect it to be better because no next neighbours are needed). The magnitude of the values around the peak is increased by orders of magnitude compared to the original spectrum. On the one hand, this parameter set should work perfectly because no leakage comes from any other peak, on the other hand fitting has to fail because $\mathrm{F}_{\mathrm{Erf}}$ in its implemented form is invalid for $|b_{0,r}| \to 0$. Additionally, the figure includes the difference spectra if subtractions are done without fitting but with given parameters. Except for b_0, the parameters are chosen to be exactly the ones that are used to generate the spectrum. It is reasonable that the smaller b_0 gets, the better the result becomes. But for $b_{0,r} < 10^{-7}$, the result becomes worse because of numerical errors. For even smaller values of $b_{0,r}$ the decrease of peak amplitude becomes as small as two orders of magnitude with simultaneous increase of the rest of the spectrum to the same level. For $b_{0,r} < 10^{-14}$, strange rectangles limiting the regions of strong magnitude increase occur. From $b_{0,r} = 10^{-17}$ on, the result is as good as the numerical precision allows. This varying behaviour is not investigated any further. It needs to be noted that the fit result is likely to become erratic where the numerical problems begin. For applications one should switch to a series expansion or the $\mathrm{F}_{\mathrm{Mono}}$ approach before $b_{0,r}$ is as low as 10^{-7}.

A.1.5 Brief conclusion

The values calculated with the $\mathrm{F}_{\mathrm{Erf}}$ approach are not exact but can reach an ever increasing precision with adding more and more neighbours (in real instances this is limited by the numerical precision of the floating point type implementation). This approach needs less computation effort for big N (no summing up N elements); for most cases in real data $\mathrm{F}^{1}_{\mathrm{Erf}}(\nu)$ should be precisely enough. That is why this way is presented here although the exact calculation is shown afterwards. One disadvantage is the divergence for $b_0 \to 0$; a threshold could be set to switch to the monofrequent approach (Eq. 2.29) where necessary.

---

[5] Except for three points for each of the peaks at positive and negative frequencies the magnitude should be exact zero – for floating-point variables with double precision after performing an FFT with $N = 128$ samples, around 10^{-14} is a realistic magnitude for "zero".

[6] The $\mathrm{F}_{\mathrm{Erf}}$ function includes the negative frequencies at the mathematically correct location: Left from the positive ones (Sec. A.1.3). As usual, the array holding the FFT data arranges the negative frequencies behind the positive ones. So internally a complete spectrum is in the index range of $[0; N-1]$. If the algorithm calculates the negative frequencies, it inserts large values for the frequency instead of negative ones. This fact does not matter with respect to the other approaches ($\mathrm{F}_{\mathrm{Mono}}$ and $\mathrm{F}_{\mathrm{Sum}}$) as they are periodically. For the $\mathrm{F}_{\mathrm{Erf}}$ approach the effect is typically cancelled by adding odd numbers of "additional spectra" to the $\mathrm{F}_{\mathrm{Erf}}$ (Sec. A.1.3)

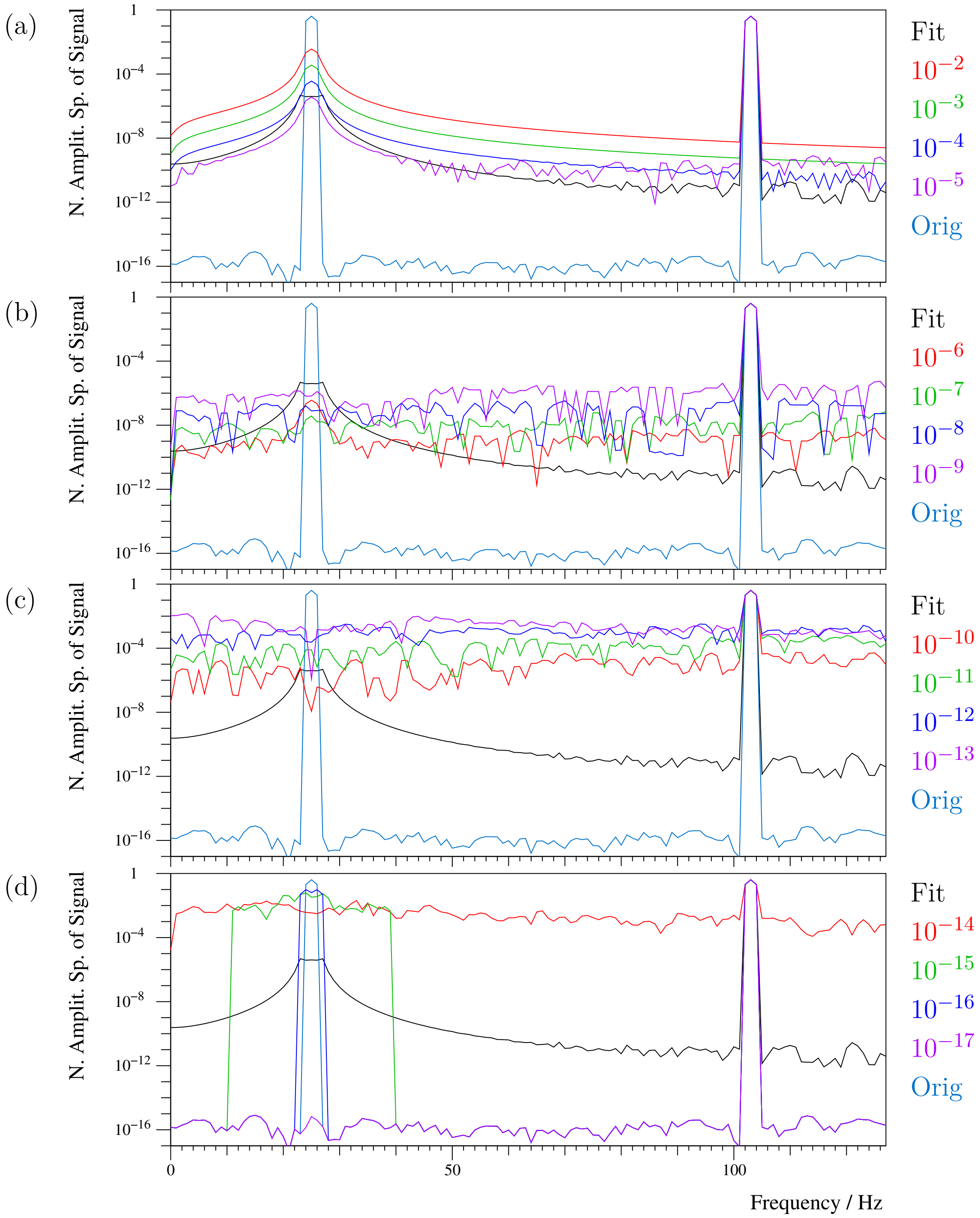

	ν_0 / Hz	b_0 / ($^{\mathrm{Hz}}/_{\mathrm{s}}$)	ϕ_0 / °	A_0
Input:	25.0	0.0	0.0	1.0
Start:	25.54574	−1.09149	−49.914	1.0136550984
Fit:	25.00012	−0.00024	359.990	1.0000000009

Figure A.4: The spectrum of a monofrequent sine with its frequency (ν_0) on the raster of discrete frequencies and the same after the $\mathrm{F_{Erf}}$ with different parameters is subtracted ($N = 128$, $\Delta\nu = 1.0\,\mathrm{Hz}$, thus the value of b_0 equals the one of $b_{0,r}$). Two curves are contained in all plots: the FFT of the monofrequent sine before (light blue) and after (black) the fitted spectrum is subtracted. The other, coloured curves show this difference for the $\mathrm{F_{Erf}}$ function with the exact values for the input parameters: A_0, ν_0 and ϕ_0, but with different b_0 – its values are given at the right margin. Further fit details: number of iterations: 74, $\chi^2_n = 9.23 \cdot 10^{-11}$.

A.2 Sum approach for the monofrequent sine

As a check for consistency, Equation 2.84 (rectangle and Dirac comb) is convolved with Equation 2.11 (monofrequent sine):

$$\begin{aligned}\mathrm{SRD}(\nu) &= \mathrm{RD}(\nu) * \mathrm{S}(\nu)\\ &= \left[\frac{1}{2}\left(1+\mathrm{e}^{-\mathrm{i}2\pi N\nu\Delta t}+2\sum_{k=1}^{N-1}\mathrm{e}^{-\mathrm{i}2\pi k\nu\Delta t}\right)\right] * \left[\mathrm{i}\frac{A_0}{2}\left(\delta(\nu+\nu_0)\mathrm{e}^{-\mathrm{i}\phi_0}-\delta(\nu-\nu_0)\mathrm{e}^{\mathrm{i}\phi_0}\right)\right],\end{aligned} \tag{A.21}$$

leading to:

$$\begin{aligned}\mathrm{SRD}(\nu) = \mathrm{i}\frac{A_0}{4}\Bigg(&\mathrm{e}^{-\mathrm{i}\phi_0}\left(1+\mathrm{e}^{-\mathrm{i}2\pi N(\nu+\nu_0)\Delta t}+2\sum_{k=1}^{N-1}\mathrm{e}^{-\mathrm{i}2\pi k(\nu+\nu_0)\Delta t}\right)\\ &-\mathrm{e}^{\mathrm{i}\phi_0}\left(1+\mathrm{e}^{-\mathrm{i}2\pi N(\nu-\nu_0)\Delta t}+2\sum_{k=1}^{N-1}\mathrm{e}^{-\mathrm{i}2\pi k(\nu-\nu_0)\Delta t}\right)\Bigg).\end{aligned} \tag{A.22}$$

The second half of this equation represents the peak centred at positive frequencies. This is the same as the limit of Equation 2.97 for $b_0 \to 0$:

$$\hat{\mathrm{S}}\mathrm{RD}_{\mathrm{pos}} \overset{b_0\to 0}{=} -\mathrm{i}\frac{1}{4}\cdot A_0\mathrm{e}^{\mathrm{i}\phi_0}\left(1+2\sum_{k=1}^{N-1}\mathrm{e}^{\mathrm{i}\pi k\Delta t(-2\nu+2\nu_0)}+\mathrm{e}^{\mathrm{i}\pi N\Delta t(-2\nu+2\nu_0)}\right) \tag{A.23}$$

$$= -\mathrm{i}\frac{1}{4}\cdot A_0\mathrm{e}^{\mathrm{i}\phi_0}\left(1+\mathrm{e}^{-\mathrm{i}2\pi N(\nu-\nu_0)\Delta t}+2\sum_{k=1}^{N-1}\mathrm{e}^{-\mathrm{i}2\pi k(\nu-\nu_0)\Delta t}\right). \tag{A.24}$$

This means that it does not matter whether one takes the LFS sine with a time-shifting rate equal to zero or directly uses the monofrequent sine.

A.2.1 Additional observation

$$\mathrm{SRD}_{\mathrm{pos}}(\nu) = -\mathrm{i}\frac{1}{4}\cdot A_0\mathrm{e}^{\mathrm{i}\phi_0}\left(1+\mathrm{e}^{-\mathrm{i}2\pi N(\nu-\nu_0)\Delta t}+2\sum_{k=1}^{N-1}\mathrm{e}^{-\mathrm{i}2\pi k(\nu-\nu_0)\Delta t}\right) \tag{A.25}$$

$$\mathrm{SRD}_{\mathrm{pos}}(\nu) = -\mathrm{i}\frac{1}{4}\cdot A_0\mathrm{e}^{\mathrm{i}\phi_0}\left(\sum_{k=1}^{N}\mathrm{e}^{-\mathrm{i}2\pi(k-1)(\nu-\nu_0)\Delta t}+\sum_{k=1}^{N}\mathrm{e}^{-\mathrm{i}2\pi k(\nu-\nu_0)\Delta t}\right) \tag{A.26}$$

With $\Delta t = \frac{1}{N\Delta\nu}$

$$\mathrm{SRD}_{\mathrm{pos}}(\nu) = -\mathrm{i}\frac{1}{4}\cdot A_0\mathrm{e}^{\mathrm{i}\phi_0}\left(\sum_{k=1}^{N}\underbrace{\mathrm{e}^{\mathrm{i}2\pi\frac{k-1}{N}\frac{\nu_0}{\Delta\nu}}}_{q_k}\cdot\mathrm{e}^{-\mathrm{i}2\pi\frac{k-1}{N}\frac{\nu}{\Delta\nu}}+\sum_{k=1}^{N}\mathrm{e}^{\mathrm{i}2\pi\frac{k}{N}\frac{\nu_0}{\Delta\nu}}\cdot\mathrm{e}^{-\mathrm{i}2\pi\frac{k}{N}\frac{\nu}{\Delta\nu}}\right) \tag{A.27}$$

For integer values of $\nu/\Delta\nu$, the sum expression can be written as the DFT of $q_k = \mathrm{e}^{\mathrm{i}2\pi\frac{k-1}{N}\frac{\nu_0}{\Delta\nu}}$ which is itself rotated equidistantly on the unity circle and only depends on the frequency of the input sine.

A.2.2 Interpretation of the sum result

Theoretically an expression like this has to exist because:

- The result has be be periodic because of the Dirac comb.

→ The result must be expressible by sinusoidal functions (resp. exponential functions with imaginary exponents) with frequencies of this periodicity and integer multiples.

- Because the time domain is discretised, the information between two data samples is neglected, which means that the absolute information is limited to N complex values.

- By Fourier theory this can be expressed by N values (coefficients of an orthogonal set of functions) in the spectral domain.[7]

→ No matter how complex the function in the time domain is, there should always be a sum expression consisting of up to N independent sinusoids (e.g. $N/2$ sines and $N/2$ cosines) in the frequency domain being able to represent that function. The difficulty seems to be the determination of the Fourier coefficients.

A.2.3 Comparing the expressions

Two different expressions for the monofrequent $\mathrm{RDS}_{\mathrm{pos}}(\nu)$ expressions have been derived. Equation A.24 with a finite sum and Equation 2.27 with a product of trigonometric functions, both are equalised and their coefficients are reduced:

$$\mathrm{i}\left(1+\mathrm{e}^{-\mathrm{i}2\pi N(\nu-\nu_0)\Delta t}+2\sum_{k=1}^{N-1}\mathrm{e}^{-\mathrm{i}2\pi k(\nu-\nu_0)\Delta t}\right)=\left(1-\mathrm{e}^{-2\mathrm{i}\pi N(\nu-\nu_0)\Delta t}\right)\cdot\cot\left(\pi\Delta t(\nu-\nu_0)\right). \tag{A.28}$$

The substitution: $x = \pi\Delta t\,(\nu-\nu_0)$ can be used in all arguments. Furthermore and similar to Equation 2.26 the following identities are used:

$$1+\mathrm{e}^{-\mathrm{i}2Nx} = 2\cos(Nx)\mathrm{e}^{-\mathrm{i}Nx} \qquad \text{and} \qquad 1-\mathrm{e}^{-\mathrm{i}2Nx} = \mathrm{i}2\sin(Nx)\mathrm{e}^{-\mathrm{i}Nx} \tag{A.29}$$

$$\cos(Nx)+\mathrm{e}^{\mathrm{i}Nx}\sum_{k=1}^{N-1}\mathrm{e}^{-\mathrm{i}2kx} = \sin(Nx)\cdot\cot(x) \tag{A.30}$$

---

[7] Rather it is expressed by N complex values but with redundant information (the negative frequencies can be gained by utilisation of symmetry relations, Sec. 2.3.1.1).

$$\sum_{k=1}^{N-1} \mathrm{e}^{\mathrm{i}(-2kx+Nx)} = \sin(Nx) \cdot \cot(x) - \cos(Nx) \tag{A.31}$$

This should be valid for $N \geq 2$. Therefore this equation provides an infinite number of trigonometric identities which in parts I have never seen somewhere. Of course it is quite special, nonetheless it might help at some point. With Euler's equation (Eq. 2.7) it becomes:

$$\sum_{k=1}^{N-1} \cos(-2kx+Nx) + \mathrm{i} \sum_{k=1}^{N-1} \sin(-2kx+Nx) = \sin(Nx) \cdot \cot(x) - \cos(Nx). \tag{A.32}$$

This can be divided into real and imaginary part.

A.2.3.1 Imaginary part

$$\sum_{k=1}^{N-1} \sin(-2kx+Nx) = 0 \tag{A.33}$$

This basic equation means that the summation of pairs of sines with inverted signs is zero.

A.2.3.2 Real part

$$\sum_{k=1}^{N-1} \cos(-2kx+Nx) = \sin(Nx) \cdot \cot(x) - \cos(Nx) \tag{A.34}$$

I have no demonstrative description for this equation but checked its correctness for $N \leq 4$.

A.2.4 Further formulations

$$\sum_{k=1}^{N-1} \mathrm{e}^{-\mathrm{i}2kx} = \frac{\sin(Nx) \cdot \cot(x) - \cos(Nx)}{\mathrm{e}^{\mathrm{i}Nx}} \tag{A.35}$$

$$\sum_{k=1}^{N-1} \cos(-2kx) + \mathrm{i} \sum_{k=1}^{N-1} \sin(-2kx) = \Big(\sin(Nx) \cdot \cot(x) - \cos(Nx)\Big) \cdot \Big(\cos(-Nx) + \mathrm{i}\sin(-Nx)\Big) \tag{A.36}$$

A.2.4.1 Real part

$$\sum_{k=1}^{N-1} \cos(-2kx) = \Big(\sin(Nx) \cdot \cot\big(x\big) - \cos(Nx)\Big) \cdot \cos(-Nx) \tag{A.37}$$

$$\sum_{k=1}^{N-1} \cos(2kx) = \sin(Nx) \cdot \cos(Nx) \cdot \cot(x) - \cos^2(Nx) \tag{A.38}$$

leading to:

$$\sum_{k=1}^{N-1} \cos(2kx) = \cos^2(Nx) \cdot (\tan(Nx) \cdot \cot(x) - 1), \tag{A.39}$$

or:

$$\sum_{k=1}^{N-1} \cos(2kx) = \cos^2(Nx) \cdot \left(\frac{\sin(Nx)}{\cos(Nx)} \frac{\cos(x)}{\sin(x)} - 1 \right), \tag{A.40}$$

or:

$$\sum_{k=1}^{N-1} \cos(2kx) = \frac{1}{2} \sin(2Nx) \frac{\cos(x)}{\sin(x)} - \cos^2(Nx). \tag{A.41}$$

A.2.4.2 Imaginary part

$$\sum_{k=1}^{N-1} \sin(-2kx) = \Big(\sin(Nx) \cdot \cot(x) - \cos(Nx)\Big) \cdot \sin(-Nx) \tag{A.42}$$

$$\sum_{k=1}^{N-1} \sin(2kx) = \sin^2(Nx) \cdot \cot(x) - \cos(Nx) \cdot \sin(Nx) \tag{A.43}$$

$$\sum_{k=1}^{N-1} \sin(2kx) = \frac{1}{2}(1 - \cos(2Nx)) \cdot \cot(x) - \frac{1}{2} \sin(2Nx) \tag{A.44}$$

One could use: $\cot(\frac{x}{2}) = \frac{\sin(x)}{1-\cos(x)}$; $y = 2x$, then some kind of symmetry occurs:

$$2 \sum_{k=1}^{N-1} \sin(ky) = \sin(y) \left(\frac{1 - \cos(Ny)}{1 - \cos(y)} - \frac{\sin(Ny)}{\sin(y)} \right). \tag{A.45}$$

A.3 The thresholds for χ_n^2 for the monofrequent approach

The $\mathrm{F}_{\mathrm{Mono}}$ expression (Eq. 2.29) has one parameter less than the $\mathrm{F}_{\mathrm{Sum}}$ one (Eq. 2.95). Therefore, if the data consist only of noise, the probability for a fit producing a χ_n^2 below a certain value is lower than for the $\mathrm{F}_{\mathrm{Sum}}$. Accepting the same rate of false-positives, the threshold must be adapted.

For the sake of consistency the same spectra are used as for the LFS sine (Sec. 5.3): 320 spectra with 128 samples, 40 with 1,024 and 5 with 8,192. 15,580 local maxima are evaluated by discretising χ_n^2 into intervals, counting their frequencies, summing them up from zero to the current χ_n^2 value and dividing each value by the total number. This is shown in Figure A.5. The following thresholds for false positives are extracted:

1%	0.0035584
2%	0.0060959
5%	0.0117342

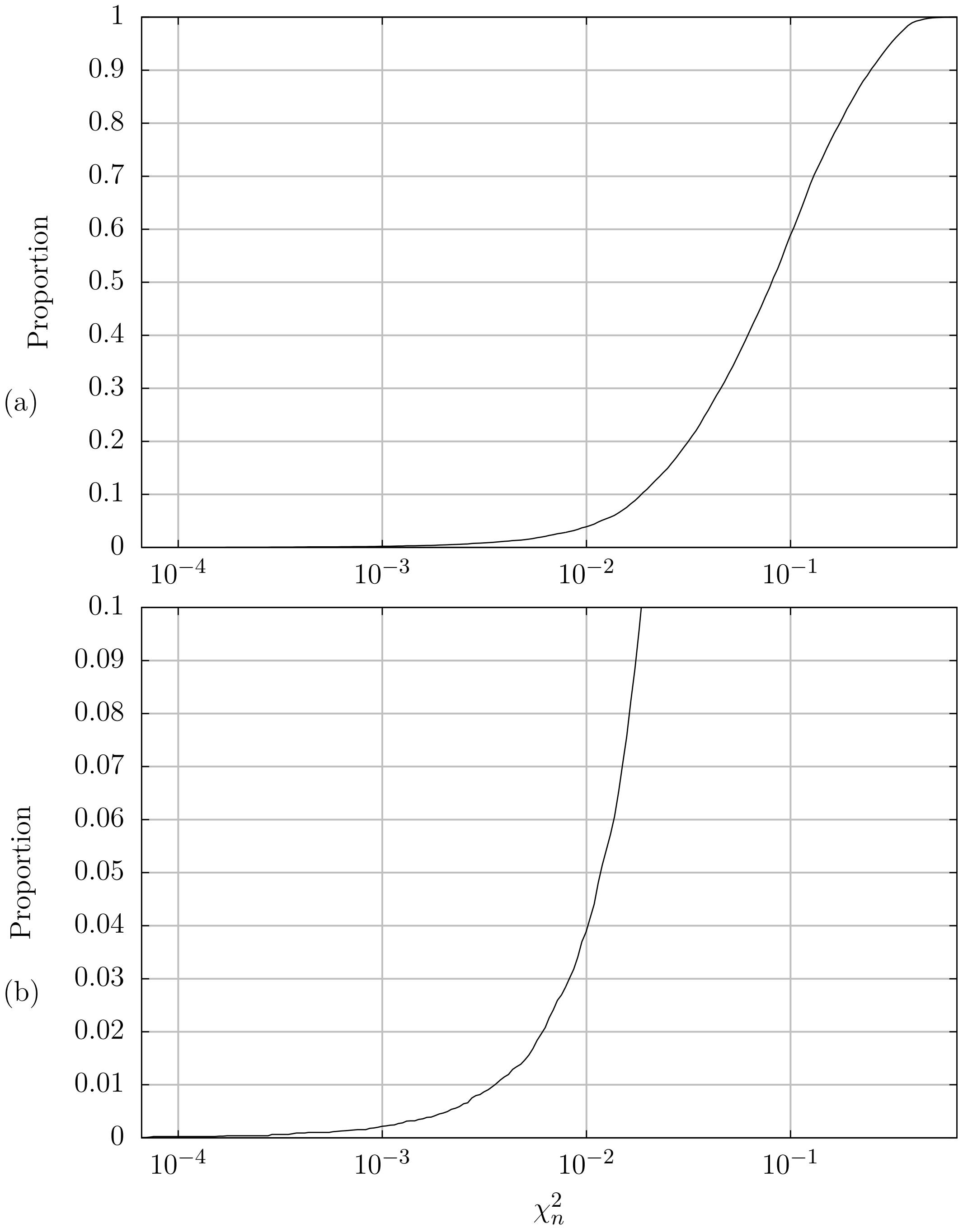

Figure A.5: These plots are generated analogously to the ones in Figure 5.6: The ordinate shows the proportion of fits within spectra consisting of pure GWN with regard to their χ_n^2. (a) full scale, (b) zoomed in to the lowest 10 %.

A.4 Computer run time

The run time of the fitting algorithm is approximately proportional to:

- the number n_{Fit} of complex values the function is fitted to,
- the number of iterations,
- N (for $\mathrm{F}_{\mathrm{Sum}}$).

In order to measure the duration of the fit, the system time is gained before and after the fitting. The difference is divided by the three proportionalities, which should result in a constant value. Two facts should be mentioned: Firstly, there are some calculations that are done exactly once for each fit (like the start-value estimation) and act like an offset to the number of iterations; this is not taken into account here. Secondly, the utilized `GetSystemTimeAsFileTime()` function provided by Microsoft returns quantised values with step lengths depending on the operating system. The computer used here is an `Intel i5-3450` (3.10 Ghz, 64 bit, 4 GB RAM, 64 bit `Windows 7 Enterprise`); the minimal time resolution is $15.6\,\mu$s. This quantisation effects the result most strongly if the fit duration is short which mainly occurs for small N. Here it even occurs that the same time is returned before and after the fitting, therefore the difference appears as zero. In the same way as in Section 5.3 (but with different seeds) spectra of GWN were produced and the fitting algorithm passed through the local maxima in the magnitude spectrum. Figure A.6 contains the resulting durations. This evaluation is done without the systematic phase variation for the start value estimation of ϕ_0 (Sec. 4.9.3), otherwise the time for the calculations done once per fit would increase significantly. The mean normalised time is $0.5\,\mu$s. Deductively, the time that is required to fit one peak can be estimated by the product: $0.5\,\mu\mathrm{s} \times n \times \mathrm{no.\ iterations} \times N$. One example for the propeller aircraft: the mean number of complex values used per peak is 10.36; the mean number of iterations is 89.33, $N = 8,192$. Thus the mean time to process a single peak is 3.8 s. With 1,360 peak fits per spectrum, it takes 1.4 h to process one spectrum. 96 spectra are in the sequence, meaning that the processing of 1.0 min of input aircraft data takes 5.7 d of computation time on a single core of that PC. This estimated duration fits to the real run time of several days.

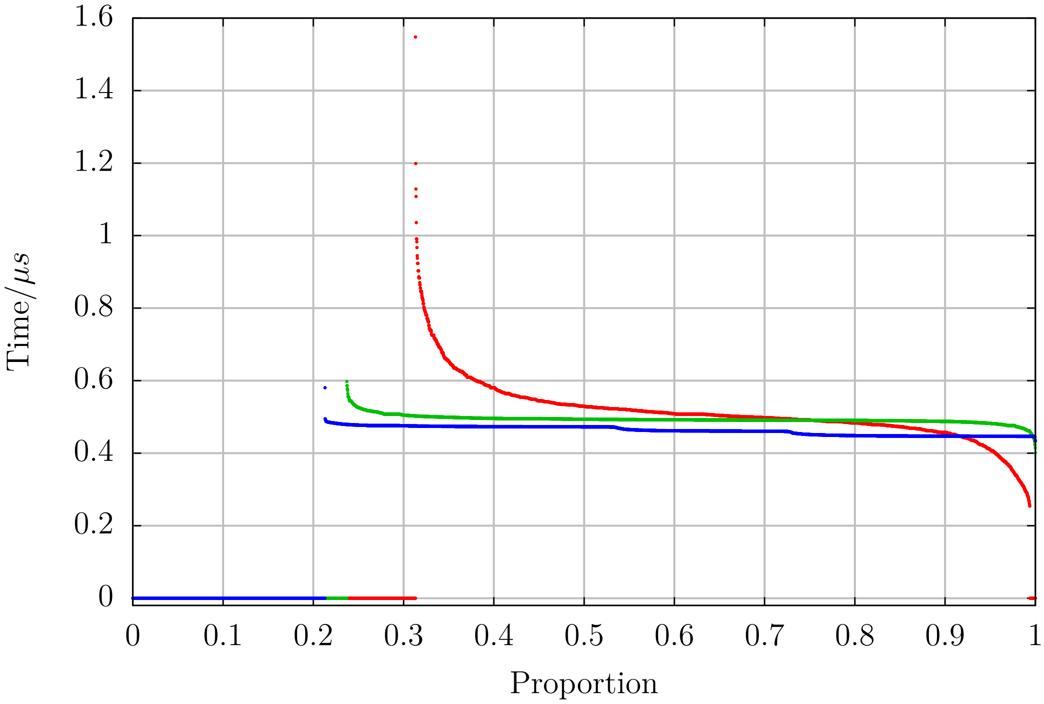

Figure A.6: Time used to fit one peak, divided by the proportionalities described in the text, segmented by the number of FFT samples, red: $N = 128$ (4,989 peaks), green: $N = 1,024$ (5,267 peaks) and blue: $N = 8,192$ (5,315 peaks). The abscissa shows the share of the peaks that take the respective duration. The increases and decreases are mainly produced by the quantisation of the utilized operating-system function. Because N contributes strongly, the variations decrease with increasing N. Zeroes occur either if the start value estimation failed (left), or if the duration is actually zero by quantisation (right).

A.5 Major extensions added to our software

A.5.1 Evaluation

- **Software porting** The `Pascal` program `Eval6`[8] developed by the BVP was ported into `C/C++` (in large parts already as part of my diploma thesis). Because of the continuous growing of the program there was a need to restructure the code, switch to object-oriented programming (still in progress) and avoid simple global variables.

- **Command file – recording**
  For the existing mode of running the program using input from a command (`.CMD`) file instead of input from the console a command (CMD)-record mode was implemented. Every input given via console can be saved in a ASCII file (including comments to every line) allowing the user to redo the same or – after editing the file – a modified operation without further input.

- **Command file – metaprogramming layer**
  Parameters can be set and used within a command file. Parameters can hold multiple entries such as value ranges, random numbers, strings or the files of a specified directory; they can also depend on each other. If parameters with multiple entries are given, the evaluation is repeated with all combinations of entries.

- **Command file – plot raster**
  When marking a series and its harmonics in the plot of a spectrum it is recorded when the CMD-record mode is active.

- **Fit-result files**
  A container type is used to save the arbitrary numbers of fit results in arbitrary numbers of spectra (this is the basis for plots like Fig. 6.2 (b)).

- **Single sine tracking**
  Support for the user to extract a single sequence of fits (see footnote in Sec. 6.2.1.1).

A.5.2 Measurement

- **Measurement program**
  A measurement program addressing the `Data Translation` systems was developed in `C/C++`, in part on the basis of the existing `Pascal` program `Mess6`.

- **Long measurement files**
  Recent measurements ran over longer time periods and the events were to be classified in a global context (e.g. for the Gorleben experiments the times of blasts, at the

---

[8] The basic structure of the software is described in [48] at 1994 levels.

airport the overflights of the planes). The preambles now contain the microseconds since January 1, 1970 00:00 hours UTC.

Measurements can cover many gigabytes of data, saved in blocks of 512 MB each; the evaluation program now is able to handle any measurement length and provides all services across data file borders throughout the measurement.

- **Data recording software (in strong collaboration with Jürgen Altmann)**
  New ADC converters (`DT 9841`) were bought and run during the measurements. The four independent devices can be synchronised to the same clock. Programs for input and transfer for the signal processors were written using `Texas Instruments Code Composer`. The basic concept for the software could be ported from `Pascal` code. For programming the communication via USB with the analog-digital systems a library provided by `DATA Translation` was available.

- **Converters for different file types**
  In order to evaluate data of other than our measurements, conversions were needed for files with a different byte order, ASCII- or compressed files into our binary format with its header.

A.5.3 Visualisation

- **Absolute time labels**
  All time axis can be set to UTC.

- **Compression of data for sequences of spectra**
  In order to find periodic content in large measurements (in parts up to 180 sensors and two weeks of measurement), multiple sequences can be plotted in one figure, additionally the number of displayed dots can be reduced drastically by combining values [49].

A.5.4 Algorithm

- **Error-function for complex values**
  This is needed for the implementation of the F_{Erf} approach.

- **Sequence-of-spectra processing**
  The procedure described in this work was implemented. This includes: the start value estimation; the F_{Sum}, F_{Erf} and F_{Mono} expressions, their derivatives and, as the case may be, Taylor expansions; the criteria for fit result evaluation; the reconstruction of the time-domain signal.

- **FIR filter kernels**
  A procedure to apply FIR filter kernels was already developed in the former `Eval6` program, this was ported into `C/C++`. A procedure was added to create FIR filter kernels of practically all combinations of low, and high passes (and thus band and notch filters) based on instructions given in [50].

- **Function generator**
  A function generator was implemented to create artificial time-domain files for analysis purposes with pre- and postambles (`*.dm6`) and audio files (uncompressed `*.wav`) to be played at experiments to excite acoustic waves.

Bibliography

[1] National Research Council. *Research required to support comprehensive nuclear test ban treaty monitoring*. National Academy Press, Washington and DC (1997). URL `http://site.ebrary.com/lib/academiccompletetitles/home.action` 4

[2] Committee on International Security and Arms Control. Technical issues related to the CTBT. Technical report, Committee on Technical Issues Related to Ratification of the Comprehensive Nuclear Test Ban Treaty, National Academy of Sciences, Policy and Global Affairs (2002). 6

[3] CTBT. `http://www.un.org/disarmament/WMD/Nuclear/CTBT.shtml`. Accessed: 2014-06-28. 1.1.2

[4] CTBT - status of signature and ratification. `http://www.ctbto.org/the-treaty/status-of-signature-and-ratification`. Accessed: 2014-06-28. 7

[5] armscontrol.org - National Academy of Sciences issued Technical Issues Related to the Comprehensive Nuclear Test Ban Treaty. `https://www.armscontrol.org/print/1110`. Accessed: 2014-06-29. 8

[6] A. Giuntini, V. Materni, S. Chiappini, R. Carluccio, R. Console, M. Chiappini. Travel-time source specific station correction improves location accuracy. Poster (T1-P61) presented at Science and Technology 2013 Conference, Vienna (2009).
URL `http://www.ctbto.org/fileadmin/snt2013/posters/T1-P61.pdf` 1.1.2

[7] Matjaz Prah, *Overview of CTBT On-Site Inspections*, CTBTO. `http://ctbtcourse.files.wordpress.com/2010/10/lecture_13_-ic_osi_matjaz_prah_14102010.pdf`. Accessed: 2014-06-29. 1.1.2

[8] Zhenfu Li, *On-Site Inspection*, CTBTO. `http://www.ctbto.org/fileadmin/user_upload/pdf/ISS_Publication/OSI_41-46.pdf`. Accessed: 2014-06-29. 1.1.2

[9] CTBTO - Have You Seen a Cavity. `http://education.ctbto.org/moodle/pluginfile.php/5605/mod_forum/attachment/476/MELAMUD%20-%20Have%20you%20seen%20a%20cavity.pdf`. Accessed: 2014-06-28. 9

[10] A. Belyashov, V. Suvorov *Studying of upper cross-section of Une area at Semipalatinsk test site according to seismic data (for OSI purposes)*, CTBTO - T3-P116, 2013. `http://www.ctbto.org/fileadmin/snt2013/posters/T3-P116.pdf`. Accessed: 2014-06-28. 9

[11] E. O. Brigham. *The Fast Fourier Transform.* Prentice-Hall, Inc., Englewood Cliffs, NJ, USA (1974). 1.1.3, 1.3.2.1, 2.1, 2.2, 4.8

[12] M. Liebsch, J. Altmann. *Acoustic-Seismic Coupling in Porous Ground - Measurements and Analysis for OSI Support.* Poster presented at Science And Technology (SNT 2013) Conference, Vienna, 17-21 June (2013). `http://www.ctbto.org/fileadmin/snt2013/posters/T3-P7.pdf`. 1.1.3

[13] J. Altmann. Acoustic Signals of Tracked Vehicles - Evaluations in the Spectral and Time Domain for Co-operative Verification of Disarmament and Peace-keeping Agreements (unpublished). Technical report, Ruhr-Universität Bochum (1999). 1.1.5, 1.3.2.1

[14] F. Gorschlüter. *Messung, Erkennung und Unterdrückung periodischer akustischer und seismischer Störsignale.* Diploma thesis, Technische Universität Dortmund (2009). 1.1.5, 7

[15] S. Krey, U. Ligges, F. Leisch. Music and timbre segmentation by recursive constrained K-means clustering. *Computational Statistics* **29**(1-2, SI), 37 (2014). doi:10.1007/s00180-012-0358-5. 11

[16] D. Ruppert. *Statistics and Data Analysis for Financial Engineering.* Springer (2011). 1.3.1

[17] A. P. Hatzes. The radial velocity detection of earth-mass planets in the presence of activity noise: The case of alpha centauri bb. *Astrophysical Journal* **770**(2) (2013). doi:10.1088/0004-637X/770/2/133. 1.3.2

[18] D. G. Manolakis, S. M. Kogon, V. K. Ingle. *Statistical and adaptive signal processing: spectral estimation, signal modeling, adaptive filtering and array processing.* Artech House Signal Processing Library. Artech House, Boston (2005). URL `http://opac.inria.fr/record=b1105860` 1.3.2, 1.3.2.1, 1.3.2.2, 18, 3.1.2

[19] Z. Leonowicz. *Parametric methods for time-frequency analysis of electric signals.* Politechnika Wrocławska, Wroclaw University of Technology, Poland (2006). 13, 17, 1.3.2.2

[20] P. Stoica, R. L. Moses. *Spectral Analysis of Signals.* Prentice Hall (2005). 1.3.2.1

[21] J. O. Smith, X. Serra. Parshl: An analysis/synthesis program for non-harmonic sounds based on a sinusoidal representation. *Proceedings of the International Computer Music Conference (ICMC-87, Tokyo)* (1987). 1.3.2.1, 7

[22] B. Bischl, U. Ligges, C. Weihs. Frequency estimation by DFT interpolation: a comparison of methods. Technical Report // Sonderforschungsbereich 475, Komplexitätsreduktion in Multivariaten Datenstrukturen, Universität Dortmund 2009,06, Technische Universität Dortmund, Dortmund (2009).
URL `http://hdl.handle.net/10419/36600` 1.3.2.1

[23] J. Altmann, S. Linev, A. Weiss. Acoustic-seismic detection and classification of military vehicles – developing tools for disarmament and peace-keeping. *Applied Acoustics* **63**(10), 1085 (2002). doi:10.1016/S0003-682X(02)00021-X. 1.3.2.1, 46, 7

[24] M. Gasior, J. L. Gonzalez. Improving FFT frequency measurement resolution by parabolic and gaussian interpolation. Technical Report AB-Note-2004-021 BDI, CERN - AB Division (2004). 1.3.2.1

[25] J. C. Brown, M. S. Puckette. A high resolution fundamental frequency determination based on phase changes of the Fourier transform. *The Journal of the Acoustical Society of America* **94**(2), 662 (1993). 1.3.2.1

[26] B. Babadi, E. N. Brown. A review of multitaper spectral analysis. *IEEE Transactions on Biomedical Engineering* **61**(5, SI), 1555 (2014). doi:10.1109/TBME.2014.2311996. 1.3.2.1, 1.3.2.2

[27] T. BRONEZ. On the performance advantage of multitaper spectral-analysis. *IEEE Transactions on Signal Processing* **40**(12), 2941 (1992). doi:10.1109/78.175738. 1.3.2.1

[28] S. Rossignol, P. Desain, H. Honing. State-of-the-art in fundamental frequency tracking. In *Proceedings of the Workshop on Current Research Directions in Computer Music*, pp. 244–254 (2001). 1.3.2.1

[29] P. Naidu. *Modern Spectrum Analysis of Time Series: Fast Algorithms and Error Control Techniques*. Taylor & Francis (1995).
URL `http://books.google.de/books?id=6Tx8gK2l-ewC` 1.3.2.2

[30] W. H. Press, S. A. Teukolsky, W. T. Vetterling, B. P. Flannery. *Numerical recipes in Pascal: the art of scientific computing*. Cambridge University Press, 1st edition (1989). 2.1, 2.1.1, 3.1.1, 2

[31] E. O. Brigham. *The Fast Fourier Transform and Its Applications*. Prentice-Hall, Inc., Upper Saddle River, NJ, USA (1988). 2.1, 2.3.4

[32] Y. Katznelson. *An Introduction to Harmonic Analysis*. Dover Publications Inc., New York (1976).
URL http://opac.inria.fr/record=b1077889 2.3.6

[33] I. Bronštejn, K. Semendjaev, G. Musiol, Mühlig. *Taschenbuch der Mathematik*. Verlag Harri Deutsch, 5th edition (2001). 2.3.7.1, 2.4.2.2, 7

[34] M. Abramowitz, I. A. Stegun. *Handbook of Mathematical Functions: with Formulas, Graphs, and Mathematical Tables*. Dover Publications, tenth printing, december 1972, with corrections edition (1964). 2.4.1, 2.4.1, 2.4.1, 2.4.1, 2.4.1, 2.4.2.1, 2.4.2.1

[35] Least squares regression for quadratic curve fitting. http://www.codeproject.com/Articles/63170/Least-Squares-Regression-for-Quadratic-Curve-Fitti. Accessed: 2014-01-20. 5

[36] J. Altmann. Two sine fit, as implemented in the `Eval6` program. Oral communication. 11, 1

[37] M. Bischoff, A. Cete, R. Fritschen, T. Meier. Coal mining induced seismicity in the Ruhr Area, Germany. *Pure Appl. Geophys.* **167**, 63 (2010). 5.5

[38] F. Gorschlüter, J. Altmann. *Subtraction of Periodic Disturbances in Seismic Aftershock Recordings*. Poster presented at Science and Technology (SnT2013) Conference, Vienna, 17-21 June (2013). Available from http://www.ctbto.org/fileadmin/snt2013/posters/T3-P103.pdf (17. Sep. 2014). 14

[39] F. Gorschlüter, J. Altmann. Suppression of periodic disturbances in seismic aftershock recordings for better localisation of underground explosions. *Pure and Applied Geophysics* **171**(3-5), 561 (2014). doi:10.1007/s00024-012-0617-y. 5.6, 7

[40] H. Militzer, F. Weber. *Angewandte Geophysik*. Number Bd. 3 in Angewandte Geophysik. Akademie-Verlag Berlin (1987). 15, 16

[41] C. Waldera. *Dämpfung einer akustischen Abschirmung und Einblick in ihren Einfluss auf seismische Messungen*. Bachelor thesis, Technische Universität Dortmund (2013). 21

[42] CTBTO – Airborne Technique Skills. http://www.ctbto.org/press-centre/highlights/2013/honing-airborne-technique-skills/. Accessed: 2014-08-04. 6.3

[43] SKYbrary – P28R. http://www.skybrary.aero/index.php/P28R. Accessed: 2014-08-04. 6.3

[44] J. ALTMANN. Acoustic and Seismic Signals of Heavy Military Vehicles for Co-operative Verification. *Journal of Sound and Vibration* **273**, 713 (2004). 46, 47

[45] F. GORSCHLÜTER, J. ALTMANN. *Removal of Periodic Disturbing Noise – Supporting the Monitoring for Seismic Aftershocks During On-Site Inspections of the CTBTO.* Poster presented at European Geosciences Union General Assembly, Vienna, 22-27 April (2012). 50

[46] J. KNOOP. *Akustisch-seismische Kopplung bei Hubschrauberanregung.* Master thesis, Technische Universität Dortmund (2013). 51

[47] EC 135 – Revolution rates. `http://www.ntsb.gov/aviationquery/brief2.aspx?ev_id=20001211X11617&ntsbno=NYC99FA032&akey=1`. Accessed: 2014-08-10. 6.5.1

[48] J. ALTMANN, S. BROSIG. MESS6/EVAL6 - A Versatile Program for Measuring and Evaluating Multiple Sensor Signals. Technical report, Ruhr-Universität Bochum (1994). 8

[49] F. GORSCHLÜTER, J. ALTMANN. *Removing Periodic Noise: Improved Procedures.* Poster presented at Science and Technology (SnT2011) Conference, Vienna, 8-10 June (2011). Available from `http://www.ctbto.org/fileadmin/user_upload/SandT_2011/posters/T4-P29%20F_Gorschluter%20Removing%20periodic%20noises%20-%20improved%20procedures.pdf` (17. Sep. 2014). A.5.3

[50] S. W. SMITH. *The Scientist and Engineer's Guide to Digital Signal Processing.* California Technical Publishing, San Diego, CA, USA (1997). A.5.4

Acknowledgement

First of all I would like to thank Dr. Jürgen Altmann, who gave me the opportunity to work in this interesting field of study and who shared and continues to share so much knowledge with his staff and the students and who was always available for discussion and prompt to answer questions.

Secondly I would like to thank Prof. Dr. Thomas Weis for being immediately responsive with great personal interest to my request of him being the second examiner of this work.

I am utmost grateful to Prof. Dr. Dieter Suter for having accepted Mr. Altmann's group as an annex to his chair of experimental physics III, thus providing us with an official status at the Technical University of Dortmund, a research facility and infrastructure for efficient investigation and work.

I would like to thank the volunteers at the Research Association for Science, Disarmament and International Security (FONAS), who work towards connecting (mainly) physicists engaged in disarmament and international security by organising regular meetings and relaying the scientists' results of research to decision-makers in politics.

I also wish to thank the German Foundation for Peace Research (DSF) for providing main financial support. Equally, I wish to thank the CTBTO for the intriguing joint venture and the invitations to conferences, which offered me great insight into the many realms, which it combines. Monika Bischoff and Sebastian Wehling-Benatelli (Institute of Geology, Mineralogy and Geophysics; Ruhr-Universität Bochum) contributed to this work by administering measurement data, which is used to review the methods applied in this work on the basis of real data.

Furthermore I would like to express my gratitude to my family and friends, who, despite my increasing neglect of social life, stood by me with patience and renouncement. Notably Björn Zelinski, Sebastian Knoche and Claudia Breit helped me constructively with discussions, imparting knowledge on software details or regarding mathematical terms from different perspectives.